Dissertations, Theses, and Masters Projects   Theses, Dissertations, & Master Projects

2008

Controls on Erodibility in a Partially Mixed Estuary, York River, Virginia

Patrick J. Dickhudt
College of William and Mary - Virginia Institute of Marine Science

Controls on Erodibility in a Partially Mixed Estuary: York River, Virginia

---

A Thesis

Presented to

The Faculty of the School of Marine Science

The College of William and Mary

In partial fulfillment

of the requirements for the degree of

Master of Science

---

by

Patrick J. Dickhudt

2008

Approval Sheet

This thesis is submitted in partial fulfillment of the

requirements for the degree of

Master of Science

July 2008
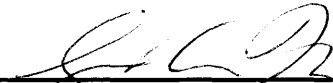
Patrick J. Dickhudt
_____
Patrick J. Dickhudt
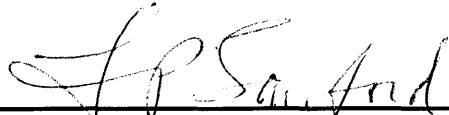

Academic Committee Members

_____
Dr. Carl T. Friedrichs
Advisor

_____
Dr. Steven A. Kuehl

_____
Dr. Linda C. Schaffner

_____
Dr. Lawrence P. Sanford
University of Maryland
Center for Environmental Science
Horn Point Laboratory
Cambridge, MD

Table of Contents

iv

Acknowledgments

List of Tables

vi

List of Figures

Abstract

A time-series of erodibility measurements and physical and biological sediment properties was used to evaluate spatial and temporal variability in cohesive bed erodibility and controls on erodibility in the York River estuary, VA. Two sites near Clay Bank displayed dramatic seasonal variations in bed erodibility while a third near Gloucester Point displayed a more consistent level of low erodibility. Total bed solids fraction and cohesive sediment grain size were not correlated with bed erodibility. The surficial sediments were characteristically composed of 2% to 50% sand supported in a mud matrix. The total solids fraction of the bed was shown to be a function of sand fraction, complicating its use as a measure of bed consolidation. The solids fraction of the mud matrix was calculated to evaluate changes in consolidation independent of sand content. An evaluation of data from multiple studies available in the literature demonstrated that when a large range of data was considered, the solids fraction of the mud matrix provided a better correlation to erodibility than did the total solids fraction. However, the range in solids fraction of the mud matrix in York River sediments was quite small and no significant relationship was found locally between this parameter and bed erodibility.

Common proxies for bioadhesion including colloidal carbohydrate concentration, extracellular polymeric substance concentration, and organic content were measured to evaluate the influence of biostabilization on bed erodibility. In contrast to the results of many published works studying erodibility on mudflats, these bioadhesion proxies did not exhibit systematic variation in either space or time and were not correlated to bed erodibility. The seasonal timing of erodibility maxima and presence of laminations during periods of highest erodibility indicated that bioturbation was not responsible for increases in erodibility during the winter and spring at Clay Bank. Although not quantified in this study, anecdotal evidence from sediment cores and seabed camera images suggest that biological reworking and repackaging may alter bed cohesivity and structure potentially influencing the relationship between erodibility and bed solids fraction.

Periods of rapid deposition, as indicated by the presence of thick sequences of laminated sediments, suggest that periodic sediment flux convergence processes are responsible for the observed seasonal cycle in bed erodibility at Clay Bank. High bed erodibility was associated with rapid deposition in the likely presence of the mid-estuary turbidity maximum while low erodibility was associated with sediment bypassing and decreased deposition in the absence of a local turbidity maximum. Finally, a consistent, low erodibility condition was observed at the Gloucester Point site for the majority of the study period and at Clay Bank in the summer and fall. A comparison of these data to other published data from the Chesapeake Bay indicated that the low erodibility background state may be characteristic of an "equilibrium" bed condition often present in many regions of the Chesapeake Bay. In the absence of recent, rapid deposition, the data set presented from the York River reasonably characterizes both the range and the profile information of the bed critical erosion stress for mid-depth, muddy regions in other similar estuaries.

Controls on Erodibility in a Partially Mixed Estuary: York River, Virginia

Chapter 1

Introduction

1 Introduction

Understanding the transport and fate of cohesive sediments is of great importance in coastal waters. In net depositional areas, such as most estuaries, fine sediments rapidly fill in navigation channels resulting in the need for repeated dredging operations to maintain navigable waterways. Additionally, cohesive sediment deposition can alter benthic communities influencing local ecology (Thrush et al., 2003; Lohrer et al., 2004) and altering sediment-water exchange processes. When suspended in the water column, cohesive sediments attenuate light, limiting primary productivity, and often degrading the health of ecosystems (e.g. Dennison et al., 1993; Jassby et al., 2002). In particular, high turbidity, likely attributed to suspended cohesive sediments, has been implicated as a primary factor hindering the recovery of sea grasses in the Chesapeake Bay, Florida Bay, and many other systems (e.g. Dennison et al., 1993; Hall et al., 1999; Koch, 2001). Additionally, many contaminants including, PCBs, dioxins, and heavy metals adsorb to cohesive sediments (e.g. Valette-Silver et al., 1996; Chapman and Wang, 1999). The fate and distribution of these contaminants are directly linked to fine sediment dynamics.

While the dynamics of cohesive sediments have been studied for decades, in both the seabed and the water column, significant uncertainties remain in virtually every aspect of their transport and fate. This project focuses on the thin veneer of sediment on the surface of the seabed that is actively and regularly resuspended and deposited by tidal

currents. Of particular interest are the seabed properties that control the erodibility of this active surface layer.

The erodibility of the seabed is quantified in terms of the critical shear stress necessary to initiate movement of particles. Near the surface of the seabed, the critical stress increases rapidly with depth into the seabed (Parchure and Mehta, 1985; Piedra-Cueva and Mory, 2001; Sanford and Maa, 2001). As critical stress rapidly increases, the properties of the seabed responsible for controlling critical stress must also exhibit a corresponding gradient. In terms of erodibility, a number of physical variables have been investigated including water content, temperature, salinity, mineralogy, and grain size (e.g. Kandiah, 1974; Kelly and Gularte, 1981; Parchure and Mehta, 1985; Roberts et al., 1998). Additionally, it is recognized that in highly productive environments such as estuaries and mudflats, benthic biota may play a significant role in influencing seabed erodibility both by destabilizing the bed through their burrowing and feeding activities (expressed as an increase in water content) and stabilizing the bed with sticky secretions (e.g. Widdows et al., 2000; Black et al., 2002; Tolhurst et al., 2002; Widdows and Brinsley, 2002).

This work focused on cohesive bed erodibility in the York River estuary, VA, USA. Close proximity to the Virginia Institute of Marine Science made the York River a convenient field area, while extensive previous works characterizing the hydrodynamics, benthic biology, and sediment transport processes of this system provided an excellent framework to build upon. Three sites on the York River were sampled monthly to bi-

monthly over a 19-month period to provide a range in cohesive sediment erodibility and bed conditions as well as investigate spatial and temporal variations in bed erodibility. The results of this effort are presented in the following chapters. Chapter Two investigates variations in the physical properties of the bed sediment and their relationship to bed erodibility. Chapter Three evaluates seasonal and spatial variations in bed erodibility and addresses the dominant processes resulting in the observed variability.

Chapter Two presents the results of a 14-month time-series of bed erodibility measurements and numerous related physical bed properties. Bed erodibility at two sites in the Clay Bank region of the York River was observed to vary dramatically over the course of the time-series. A third site, near Gloucester Point, VA generally exhibited a consistent and low level of erodibility over the 14-month period.

Other published works have reported that the solids fraction of cohesive sediments was a representative measure of the degree of consolidation of the bed with erodibility decreasing with increasing solids fraction. The work presented in Chapter Two demonstrated that the solids fraction of the top centimeter of the bed was quite variable but not related to the erodibility of the bed. The observed variations in solids fraction were shown to be a function of the sand fraction of the bed with solids fraction increasing with sand fraction. Sand fraction was found to vary between 2% and 50% indicating a cohesive bed with sand grains supported by a mud matrix. As the sand in the bed was characteristically fine, the critical stress for erosion of the sand was similar to and generally less than that observed for mud.

It was proposed in Chapter Two that for cohesive beds with varying sand fraction, solids fraction was not a good measure of the degree of consolidation of the bed as related to erodibility. Instead, the solids fraction of the mud matrix was calculated to represent the degree of consolidation of the cohesive portion of the bed responsible for controlling erodibility. However, data from the York River indicated no relationship between bed erodibility and solids fraction of the mud matrix. Published results from the literature were surveyed to evaluate the relationship between solids fraction and erodibility and solids fraction of the mud matrix and erodibility in a range of settings. The results from this study in the York River were included with seven published works, greatly expanding the range in data relative to that from the York River alone. The resulting comparisons demonstrated a weak positive relationship (R^2=0.16) between solids fraction and the initial critical stress for erosion. Impressively, this comparison provided a strong relationship (R^2=0.68) between solids fraction of the mud matrix and initial critical stress indicating that across a range of environments the solids fraction of the mud matrix was a better measure of the degree of bed consolidation than total solids fraction. Comparing the data from the York River to other published data indicated that the range in solids fraction of the mud matrix observed in the York was quite small. It was concluded that the range in solids fraction of the mud matrix in the York River was sufficiently small that its relationship to erodibility was likely overwhelmed by other factors.

Chapter Two has been submitted for publication as a manuscript co-authored by Carl T. Friedrichs and Lawrence P. Sanford.

Chapter Three provides a detailed investigation of the observed spatial and temporal variability in bed erodibility as well as evaluates the relative contributions of physical and biological influences on bed erodibility. A strong seasonal cycle in erodibility was observed at two sites in the Clay Bank region of the York River with consistent low erodibility in the summer and fall and elevated erodibility in the winter and spring. A third site, near Gloucester Point, VA had consistently low erodibility at a level similar to that found in the Clay Bank region in summer and fall.

Colloidal carbohydrate concentration and extracellular polymeric substance (EPS) concentration have proven to be proxies for bioadhesion in mudflat environments where biofilms are prevalent on the sediment surface. However, at the three sites sampled in the York River, little light reached the sediment surface and biofilms have not been observed. Measurements of colloidal carbohydrates and EPS from sediment samples collected in coordination with the samples from this study indicated that colloidal carbohydrate and EPS concentrations were relatively consistent in space and time and were not correlated to the observed variations in erodibility. Additionally, while no measures of biodestabilization were presented, the seasonal timing and presence of laminated sediments during the period of highest erodibility indicated that biodestabilization could not explain the elevated erodibility in the winter and spring.

While biostabilization and biodestabilization were not clearly linked to the observed variations in bed erodibility, it is hypothesized in Chapter Three that biological modifications to surficial sediments may confound the expected relationships between bulk measures of sediment consolidation and bed erodibility. Pelletization may alter the cohesivity of sediments as well as the fabric of the seabed, effectively altering the relationship between solids fraction of the mud matrix and bed erodibility. Additionally, burrowing activities may introduce heterogeneity into the seabed resulting in high values for bulk measures of solids fraction of the mud matrix that do not represent the true consolidation state of the bed on the small scale relevant to surface erosion.

Previous studies have characterized the Clay Bank region as physically dominated with high suspended sediment concentrations resulting from an ephemeral secondary turbidity maximum (STM). These studies demonstrated that the presence of an STM in the Clay Bank region was associated with elevated river flow enhancing stratification and particle trapping. The associated convergent sediment transport periodically resulted in high suspended sediment concentrations in the region. The coincidence of high river flow, low salinity, and high erodibility presented in Chapter Three indicates that this process translates to the sediment bed with convergent sediment transport resulting in enhanced erodibility. Further, thick laminated sequences observed in digital X-radiographs, revealed that greater than 15 centimeters of sediment was deposited between November 2006 and April 2007. This rate of deposition greatly exceeded the long-term

accumulation rate of this region indicating an ephemeral deposit likely migrating with the STM.

Erodibility data from the York River was compared to other published results from the Chesapeake Bay. The York River data was split into three categories, low erodibility, transitional, and high erodibility based on the level of erodibility and seasonal timing. A striking similarity was found in both the ranges and mean conditions of the York River low erodibility data, representing nearly all measurements at the Gloucester Point site as well as the Clay Bank sites in the summer and fall of 2006 and 2007, and published data from Baltimore Harbor, MD and the upper portion of the Chesapeake Bay main-stem. Conversely, the transitional and high erodibility cases from the York River were found almost entirely at the Clay Bank sites and fell well outside the range of the data from Baltimore Harbor and the upper-Chesapeake main-stem. This comparison suggests a common state of "low" erodibility in many muddy areas in the Chesapeake Bay outside of turbidity maximum zones. This low erodibility condition likely represents an equilibrium state resulting from a balance between physical resuspension and consolidation and biological reworking and repackaging. Overall, the cumulative York River data set provides a range in bed erodibility characterizing and contrasting mid-depth muddy regions both inside and outside of turbidity maximum zones.

Chapter Three will be submitted for publication as a manuscript co-authored by Carl T. Friedrichs, Linda C. Schaffner, Lawrence P. Sanford, and Robert J. Diaz. Measurements of colloidal carbohydrate and EPS presented in Chapter Three were

provided by Dr. Schaffner. Sediment images presented in Chapter Three were provided

by Dr. Diaz.

Chapter 2

Mud matrix solids fraction and bed erodibility in the York River, USA, and other muddy environments[1]

[1] Dickhudt, P.J., Friedrichs, C.T., and Sanford, L.P., in review. Mud matrix solids fraction and bed erodibility in the York River, USA, and other muddy environments. P. Le Hir, ed., Nearshore and Estuarine Cohesive Sediment Transport Processes, Elsevier Press.

2   Mud matrix solids fraction and bed erodibility in the York River, USA, and other muddy environments

Abstract

A 14-month time series of sediment cores from the bed of the York River estuary, Chesapeake Bay, USA, were sampled with a Gust erosion microcosm and further analyzed to evaluate variability in a variety of physical bed properties. Variation in sediment solids volume fraction did not relate to variability in bed erodibility. However, solids volume fraction was found to be highly dependent on the sand fraction of the bed. The solids volume fraction of the mud matrix was calculated to evaluate changes in bed compaction not related to the sand fraction of the bed. The range of variability in solids volume fraction of the mud matrix was found to be significantly less than the variability of the total solids volume fraction. Reevaluation of erodibility data from the literature combined with that from this study revealed a strong correlation between solids volume fraction of the mud matrix and the initial critical stress for erosion when a large range in sand fraction and solids volume fraction were included. These results suggest that compaction within the cohesive portion of the bed is better related to erodibility than compaction of the bed as a whole (mud and sand). The poor correlation found within the

York River data alone likely resulted from the relatively small range observed in the solids volume fraction of the mud matrix.

2.1 Introduction

Sediment erodibility is generally quantified as the erosion rate or mass of sediment available for erosion at a given stress applied to the bed. While bed erodibility can be measured by a number of *in situ* or laboratory devices (McNeil et al., 1996; Gust and Mueller, 1997; Tolhurst et al., 2000; Widdows et al., 2007), it is typically time consuming and expensive. As a result, it is often impractical to resolve bed erodibility at adequate temporal or spatial scales. To improve resolution and understand the controlling factors causing changes in erodibility, it is desirable to relate the erosion rate and/or the critical stress for erosion to the properties of the deposited sediments that can be more easily measured at sufficient spatial and temporal scales.

When working with non-cohesive sediments, the critical stress for erosion is controlled by the gravitational resistance to motion and is a relatively simple and known function of grain size (Shields, 1936). Cohesive sediments on the other hand are notably more complicated. Cohesive sediments form weak inter-particle bonds the strength of which are a function of both the fluid properties (e.g., salinity, temperature) (Kelley and Gularte, 1981; Parchure and Mehta, 1985; Lau, 1994) and bed properties (e.g., fine fraction grain size, porosity, mineralogy) (Kandiah, 1974; Roberts et al., 1998; Torfs et al., 2001). As muddy seabeds are commonly found in biologically productive areas, the

relationship between the physical properties of the bed and fluid and erodibility are often further modified by a variety of biological influences (e.g., bioturbation, pelletization, EPS) (Widdows et al., 2000; Black, 2002; Andersen et al., 2005; and many others) that can act to either enhance or reduce erodibility.

Sediment bulk density (a term functionally interchangeable with dry density, porosity, solids fraction, and water content) is a common physical bed property linked to erodibility. Laboratory studies have shown a clear relationship between sediment bulk density and erodibility when other physical properties of the sediment are controlled (particularly grain size and mineralogy; Jepsen et al., 1997; Roberts et al., 1998) and in the absence (to the extent it is possible) of biological influence. As the bulk density increases, cohesive sediment grains are more tightly packed, enhancing the inter-particle bonds and increasing the critical stress for erosion. However, in natural sediments this relationship has often proven difficult to resolve (Houwing, 1999; Riethmueller et al., 2000; Mahatma, 2004; Tolhurst et al., 2006; Stevens et al., 2007). While this may be largely due to biological influences, variations in sediment grain size and mineralogy may also obscure this relationship.

Laboratory studies have shown clear variations in the cohesive strength of different clay minerals (Kandiah, 1974; Torfs et al., 2001). When evaluating erodibility in different geographical regions, the mineralogy of the seabed may vary due to different source materials. Within a given region on the other hand, mineralogy may be effectively constant or vary slowly over distances on the order of hundreds of kilometers. Within the

Chesapeake Bay for instance, Feuillet and Fleischer (1980) found the mineralogy of the seabed to vary only gradually along the estuarine gradient. In this case, both the freshwater reaches and Atlantic Ocean provided sediments that mixed within the James River estuary. The relative proportion of marine and freshwater source minerals were controlled by estuarine circulation. This suggests that at a particular site, and likely for a particular region, mineralogical composition will be effectively constant and will not be responsible for temporal or relatively small-scale (10s of kilometers) spatial variations in bed erodibility.

In most muddy coastal environments, the seabed is a mixture of non-cohesive (sand) and cohesive (mud) sediment. As a result, the erodibility of a cohesive bed may be modified by the presence of sand in the bed. While a few studies have addressed this problem, there is still no clear relationship to explain the modification in critical shear stress resulting from the presence of sand in the bed. In a laboratory study, Torfs et al. (2001) measured the critical stress for erosion of artificial and natural sediments of a constant bulk density but with varying sand versus mud fraction. As mud fraction increased above 3-13%, the bed began to behave cohesively, and the critical stress for erosion increased as a function of increasing mud fraction of the bed. A related study by Panagiotopoulos et al. (1997) using estuarine mud mixed with quartz sand showed that as mud fraction increased from 0-50%, the critical stress for erosion also increased. Similar to the results of Torfs et al. (2001), the bed began to behave cohesively at a mud fraction

15

of 11%-14%. In Panagiotopoulos et al. (1997), bulk density was not held constant, and

they noted that as the mud fraction increased, the bulk density decreased.

Similar to Panagiotopoulos et al. (1997), a number of other researchers have noted

that as sand fraction increases, bulk density also increases. Flemming and Delafontaine

(2000) and Riethmueller (2000) found a positive relationship between water content and

mud fraction, which Flemming and Delafontaine (2000) approximated as a power law

function with site specific coefficients. Mahatma (2004) also found water content to vary

with mud fraction and proposed that changes in mud fraction must be accounted for if

water content is to be used as a proxy for bed compaction. To evaluate changes in the

degree of compaction between sites or temporally at a given site, Mahatma (2004)

derived a generalized relationship between mud fraction and water content using data

from four of six sites. The ratio of the actual water content to that predicted from this

relationship gives the normalized water content. Values of normalized water content less

than 100% indicate more compacted sediments while values more that 100% indicate less

compacted sediments.

Rather than using a site-specific empirical relationship, Sanford (2008)

represented the influence of sand on sediment solids fraction using a simple analytical

relationship of the form

$$\phi_{stot} = \frac{1}{f_s + \frac{1 - f_s}{\phi_{sm}}} \qquad\qquad \text{(Eq. 1)}$$

where:

ϕ_{stot}= bed solids volume fraction = volume solids / volume total

ϕ_{sm}= solids volume fraction of mud matrix = volume mud / (volume mud plus water matrix)

f_s= mass fraction of sand per mass total solids

This approach treats the bed as a mixture of sand and mud-water matrix. The sand with a bulk density of 2650 kg m^{-3} is suspended in the mud and water matrix of lower bulk density. As the sand fraction is increased, lower density mud matrix material is displaced by higher density sand, raising the bulk density (or solids fraction) of the bed. At a sand fraction of zero, $\phi_{stot} = \phi_{sm}$.

2.2 Methods

2.2.1 Study Site

The field component of this study was conducted on the York River estuary, a subestuary of the Chesapeake Bay, USA. Although its mean tidal range is only about 80 cm, the York River is characterized by strong tidal currents reaching magnitudes of ~1m s^{-1} at the surface during spring tide (Schaffner et al., 2001). Three sites were chosen in the York River to provide variation in erodibility and associated bed properties (Figure 2-1). Two sites were chosen near Clay Bank, about 30 km from the mouth of the York in a region characterized by strong tidal currents, an ephemeral secondary estuarine turbidity

maximum, and suspended sediment concentrations often reaching 100s of mg l^{-1} (Lin and Kuo, 2001). The strong physical processes at this site make it a generally unfavorable environment for benthic biota, leading to a depauperate benthic community (Schaffner et al., 2001). One site at Clay Bank was located on the flank of the main channel at ~11 m depth (CC), while the other site was about 1 km away in a secondary channel at ~6 m depth (CS). The third site, near Gloucester Point (GP) is located about 10 km from the mouth of the York at a depth of ~8 m. Relative to the Clay Bank sites, the Gloucester Point site experiences less physical disturbance to the seabed and lower suspended sediment concentrations (10s of mg l^{-1}), leading to more favorable conditions for benthic communities and potentially less physical dominance in sediment transport processes (Schaffner et al., 2001).

2.2.2 Sampling

Each of the three sites was sampled monthly to bimonthly from April 2006 to July 2007. The dates and times of sampling were determined primarily for logistical reasons, and sampling took place randomly with respect to tidal phase and spring/neap cycle. Whenever possible, the three sites were sampled on consecutive days and following the same phase of the tide.

Each time a site was visited, two cores were collected for erodibility measurements, three slabs were collected for digital X-radiography, and sediment samples sliced at 1-cm intervals were collected to be analyzed for water content,
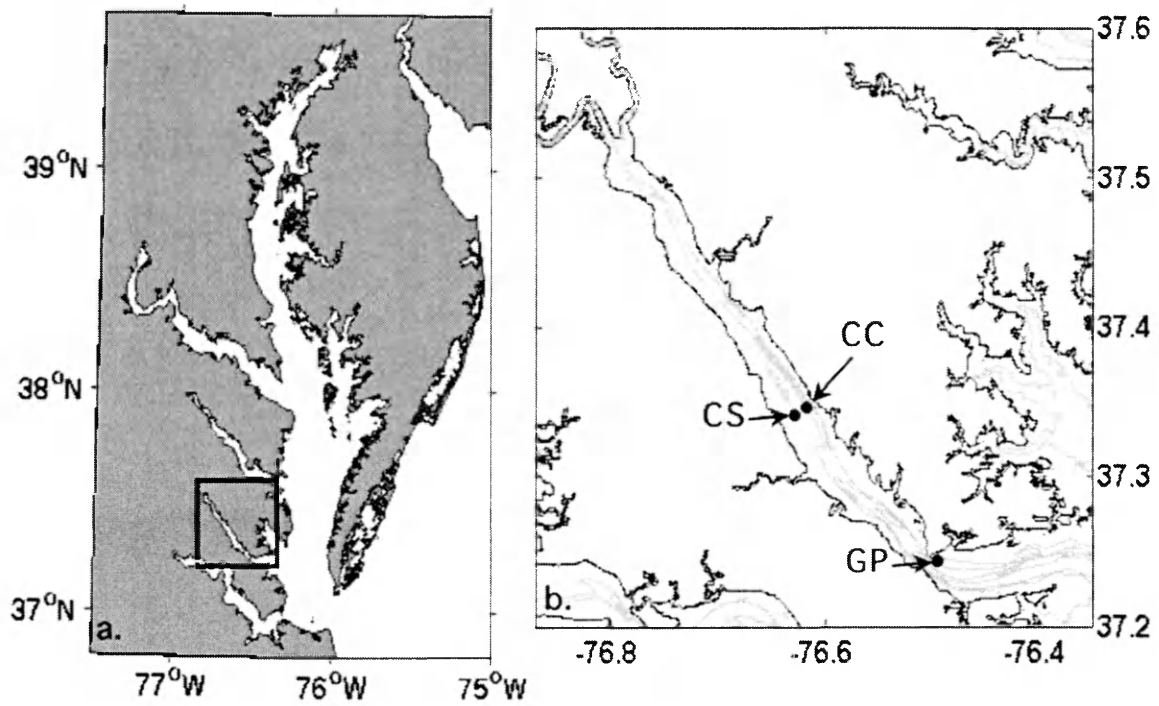
Figure 2- 1 a. Map of Chesapeake Bay, USA. **b.** Map of York River estuary. Circles represent locations of study sites. GP is Gloucester Point site, CC is Clay Bank channel site, and CS is Clay Bank secondary channel site.

clay/silt/sand fraction, and organic content. All sediment samples were sub-sampled from an Ocean Instruments Gomex box corer (surface area 625 cm^2) deployed from a small vessel (~8 m) on anchor at or near slack tide. To minimize errors associated with core collection and sub-sampling, particular attention was paid to preservation of the sediment-water interface. Due to the soft nature of these sediments, the weight of the corer allowed sufficient penetration (~20-40 cm). As a result, the Gomex could be slowly lowered to the seabed, allowed to penetrate, and then slowly retrieved. Lids on the box corer, which automatically closed following penetration, prevented sloshing of the water overlying the sediment sample, further minimizing disturbance of the sediment-water interface. Box cores and sub-cores with turbid water overlying the sediment surface were assumed to be disturbed and were rejected. Due to the number of sub-samples collected and the relatively small size of the box corer, numerous box cores were collected from each site. As a result of collecting numerous cores while swinging on anchor, all results likely incorporate spatial variation within a radius of roughly 15 to 25 m.

2.2.3 Erodibility Measurements

Seabed erodibility was measured with a dual core Gust erosion microcosm system constructed at the University of Maryland Center for Environmental Science – Horn Point Laboratory. This device uses a rotating disc with central suction to impose a nearly uniform shear stress on the surface of a 10 cm sediment core (Gust and Mueller,

1997). The individual erosion heads were calibrated in the lab of Dr. Gust using hot film anemometry.

Cores chosen for erosion testing were carefully selected to ensure uniform, level surfaces and minimal disturbance of the sediment-water interface. After collection, cores were carefully transported to the Virginia Institute of Marine Science, located adjacent to the GP site on the banks of the York River. Erodibility tests were generally underway within about two hours of core collection to minimize consolidation effects. Erodibility measurements consisted of a sequence of seven steps of approximately 20-min duration, each with a consecutively increasing stress (0.01 Pa, 0.05 Pa, 0.1 Pa, 0.2 Pa, 0.3 Pa, 0.45 Pa, 0.6 Pa) applied to the sediment surface.

Each erodibility measurement included two cores from a given site eroded simultaneously. Surface water, collected from the sampling site, was circulated through the cores, generating the radial component of the applied bed stress, and flushing suspended sediment from the core. The effluent containing eroded sediment was then passed through a Hach 2100AN turbidimeter equipped with a flow-through cell and collected. The sediment-laden effluent was filtered using 0.7-μm GFF filters to determine the total mass of sediment eroded during each step and to calibrate the turbidimeters. The product of the calibrated turbidimeter data and the flow rate of water circulated through the cores provided a time series of erosion rate. Additionally, the filtrate from each step provided the actual mass eroded during each step, the sum of all steps providing the total mass eroded during the experiment.

21

Results were analyzed with the erosion formulation of Sanford and Maa (2001). This erosion formulation uses a linear erosion rate expression and allows for depth-varying critical stress and "erosion rate constant." The initial critical shear stress, final critical shear stress, erosion rate constant (M), and the initial erosion rate (E_0) were calculated for each step. For each step, E_0 was calculated as the erosion rate at time $t = 0$ from an exponential fit to the erosion rate time series. The erosion rate constant M was calculated using this value of E_0.

2.2.4 Determination of Physical Bed Properties

Samples for sediment water content, sand/silt/clay fraction, and organic content were collected from cores sub-sampled from the Gomex box corer while on anchor and simultaneous to collecting cores for erosion with the Gust erosion microcosm. These sub-cores where then sliced at 1-cm intervals and saved for analysis. Whenever possible, two X-ray slabs were also sliced at 1-cm intervals after being X-rayed providing a total of three samples and allowing estimation of the standard error for each of these physical properties of the bed.

Sediment water content was determined using standard wet weight/dry weight analysis. By assuming the density of water to be 1015 kg m^{-3} and the density of sediment to be 2650 kg m^{-3} the solids volume fraction was calculated from the water content. Sand fraction was measured by sieving sediments with a 63-μm mesh sieve. The sand fraction was calculated as the mass of sand per mass dry weight of sediment. The size

distribution of the sand fraction was determined using a Rapid Sediment Analyzer. Percentages of silt and clay were determined by standard pipette method for each of the three sites over the entire 14-month period. Prior to the pipette test, a dispersant was added and samples were placed in a sonicator bath to disaggregate the sample.

2.3 Results

2.3.1 Erodibility

Erodibility measurements conducted with the Gust Microcosm system produced profiles of the critical shear stress for erosion and erosion rate. The results of erodibility measurements conducted on 60 cores (20 from each site) are presented here. With the exception of a small amount of sediment eroded at a low shear stress in some cores, erosion was entirely Type 1 depth-limited erosion. As a result, we used the critical shear stress for erosion to evaluate sediment erodibility. As comparing 60 critical shear stress profiles would be overly complicated and potentially confusing, these data have been simplified and are presented as the total erodible mass at a shear stress of 0.4 Pa. This is similar to the results presented in Widdows et al. (2000), where erodibility data were presented as the total mass eroded at a given current velocity. A critical shear stress of 0.4 Pa was chosen as this represents a typical tidal maximum shear stress within the York River system. Additionally, a relatively large mass of sediment (1 - 8 mm of depth) was eroded from the bed at this stress. As these results are compared to the properties

23
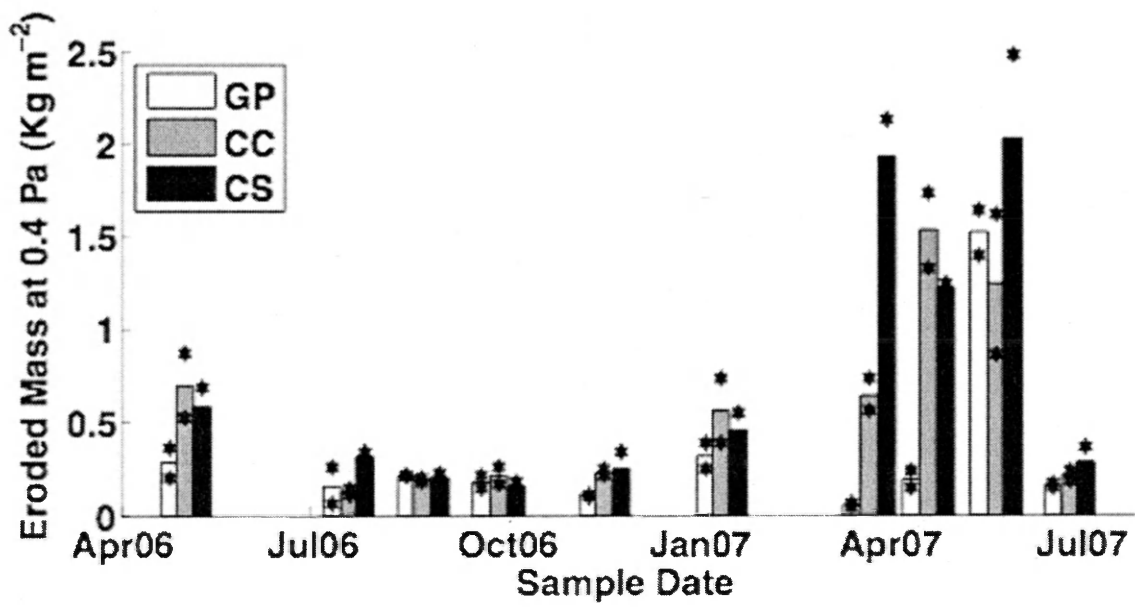
Figure 2- 2 Time series of eroded mass at 0.4 Pa at three sites on York River, VA. Bars represent mean eroded mass of two cores eroded. Stars represent mass eroded from each individual core.

(e.g., solids fraction and sand fraction) of the top centimeter of the bed, it is desirable to have erodibility data and bed property data represent the same material as much as possible. This is in contrast to measuring the initial critical shear stress, as is common, in which case the material eroded likely represents less than the top millimeter of sediment. Resolution of bed properties at this scale was not feasible, so a larger scale of erosion was chosen.

The erodibility results are summarized in Figure 2-2. As only two replicate measurements were performed each time a site was sampled, it was not possible to evaluate statistical significance associated with these measurements. To illustrate the amount of variation between replicates, the results of each replicate core are presented as stars in Figure 2-2, while the average of both cores is presented as the bars in this plot.

In all cores eroded, the initiation of motion occurred at an applied stress of 0.05 Pa or 0.1 Pa. Erosion behavior was typical of depth-limited erosion in this type of stepwise measurement. A spike in erosion rate occurred at the beginning of a step followed by an exponential decay in erosion rate throughout the step. While erosion rate had decreased significantly by the end of each step, it was not uncommon for erosion to continue until the end of a 20-minute step, particularly at the higher applied stresses. The erodible mass at 0.4 Pa was found to vary by roughly an order of magnitude at all sites (Figure 2-2). A total erodible mass at 0.4 Pa of ~ 0.2 kg m^{-2} was typical in cases of low erodibility, representing about 1 mm of sediment eroded from the seabed. An erodible

mass of $1.5 - 2$ kg m^{-2} was representative of periods of high erodibility, corresponding to about 8 mm of sediment eroded from the seabed.

2.3.2 Erodibility and Solids Volume Fraction

The results of a 14-month time series of total solids (sand + mud) volume fraction (ϕ_{stot}) for each of the three sites are presented in Figure 2-3a. Three samples for ϕ_{stot} were collected each time a site was sampled. The mean ϕ_{stot} ranged from 0.08 to 0.18, and the error bars in Figure 2-3a represent two times the standard error associated with these data. The GP and CS sites displayed the largest variation in ϕ_{stot}, and both covered approximately the entire range. The CC site showed less variation and tended to have lower values of ϕ_{stot} than either the GP or CS site. The large error bars in Figure 2-3a illustrate a high degree of variability on a relatively small spatial scale (10s of meters associated with core collection on anchor). Additionally, the approximately month-to-month variation at a given site suggests this property of the bed can vary significantly on relatively short time scales.

No significant correlation was found between the eroded mass at 0.4 Pa and ϕ_{stot} of the top cm of the bed (Table 2-1). Cases of low erodibility ~0.2 kg m^{-2} spanned the entire range of ϕ_{stot}, suggesting that large changes in ϕ_{stot} can result in virtually no change in bed erodibility. While it would be expected that the highest erodibility would coincide with the lowest values of ϕ_{stot}, the observed correlation was opposite (i.e., positive; Table 2-1), and the cases of highest erodibility fell toward the middle of the range of ϕ_{stot}.
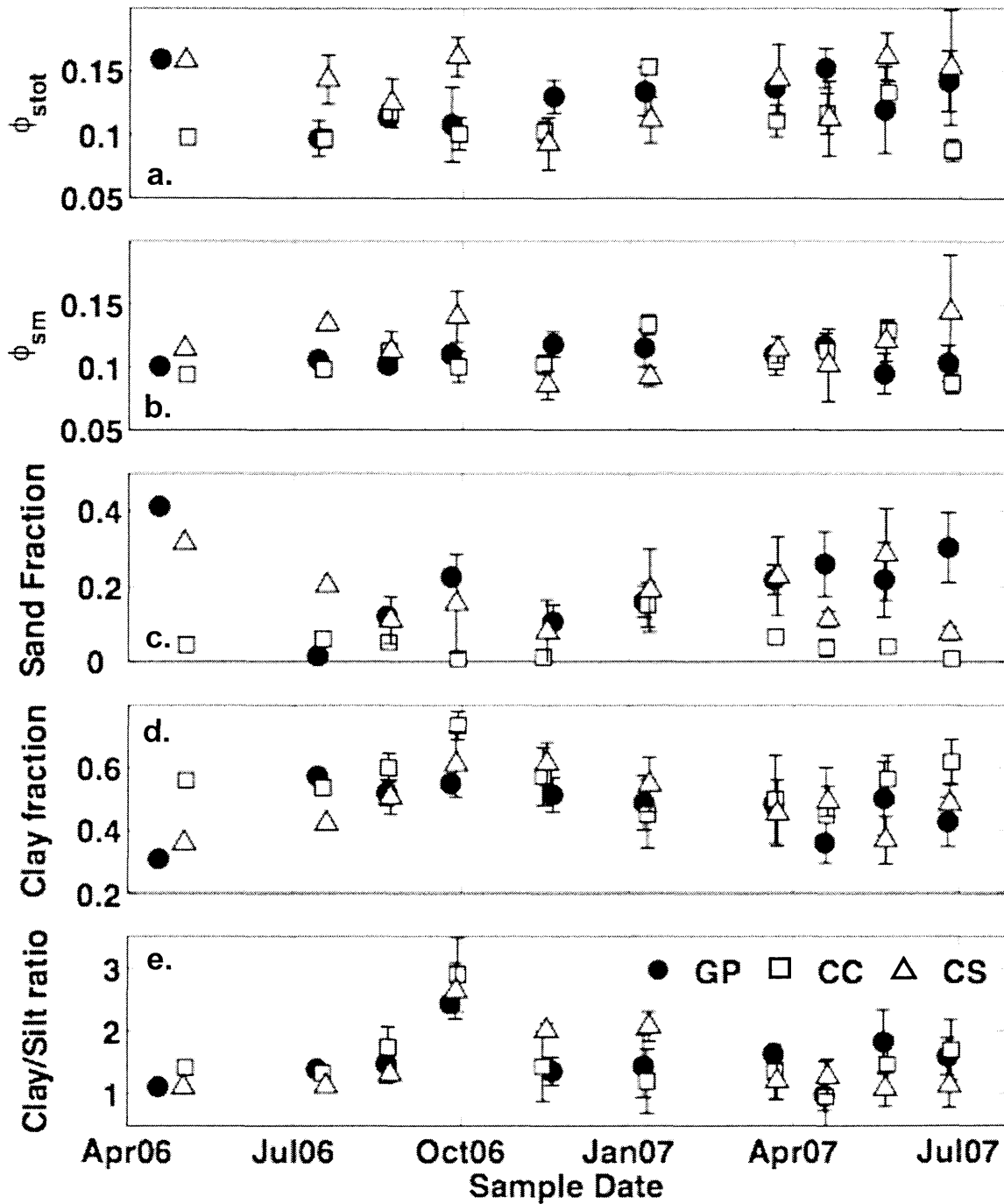
Figure 2- 3 Time series of properties of upper cm of bed: **a.** total solids (sand + mud) volume fraction (ϕ_{stot}), **b.** solids volume fraction of mud matrix (ϕ_{sm}), **c.** sand fraction of total solids, **d.** clay fraction, **e.** clay : silt ratio. In each case, error bars represent two standard errors.

	Eroded Mass @ 0.4 Pa	ϕ_{stot}	ϕ_{sm}	Sand Fraction	Clay Fraction
ϕ_{stot}	0.1906^a				
ϕ_{sm}	0.0667^a	0.8116^b**			
Sand Fraction	0.1306^a	0.6395^b**	0.0785^b		
Clay Fraction	-0.2909^a	-0.6007^b**	-0.2720^b**	-0.6769^b**	
Clay:Silt ratio	-0.3106^a*	-0.3041^b**	-0.2521^b**	-0.1895^b	-0.7992^b**

Table 2- 1 R-values of Pearson's correlation test amongst erodibility and bed property data. [a] indicates n=30. [b] indicates n=72. * indicates significant at p<0.10, ** at p<0.05.

2.3.3 Solids Volume Fraction, Sand Fraction, and Solids Volume Fraction Mud Matrix

Similar to ϕ_{stot}, a large variation in sand fraction was found both within a given site and between sites (Figure 2-3c). The GP and CS sites exhibited the largest range in sand fraction, varying between 0.02 and 0.42, while the CC site typically had less sand, ranging between 0.02 and 0.15. In all cases, the sand fraction was sufficiently small that the bed was a mud-dominated cohesive mixture supported by a mud matrix. The sand at all sites was typically very fine to fine sand with a D50 of between 100 and 150 μm. The D90 of the sand size distribution was almost always less that 250 μm.

Consistent with the results of Panagiotopoulos et al. (1997), Flemming and Delafontaine (2000), Paterson et al. (2000), Riethmueller (2000), and Mahatma (2004), ϕ_{stot} was found to increase with increasing sand fraction of the bed (Table 2-1; Figure 2-4). Additionally, the analytical relationship (Eq. 1) between sand fraction and solids volume fraction presented in Sanford (2008) was tested, the results of which are also presented in Figure 2-4. Similar to Flemming and Delafontaine (2000) and Mahatma (2004), a constant state of consolidation was assumed regardless of sand fraction to prepare Figure 2-4. This was implemented by assigning a constant value of 0.11 to the solids volume fraction of the mud matrix (ϕ_{sm}).
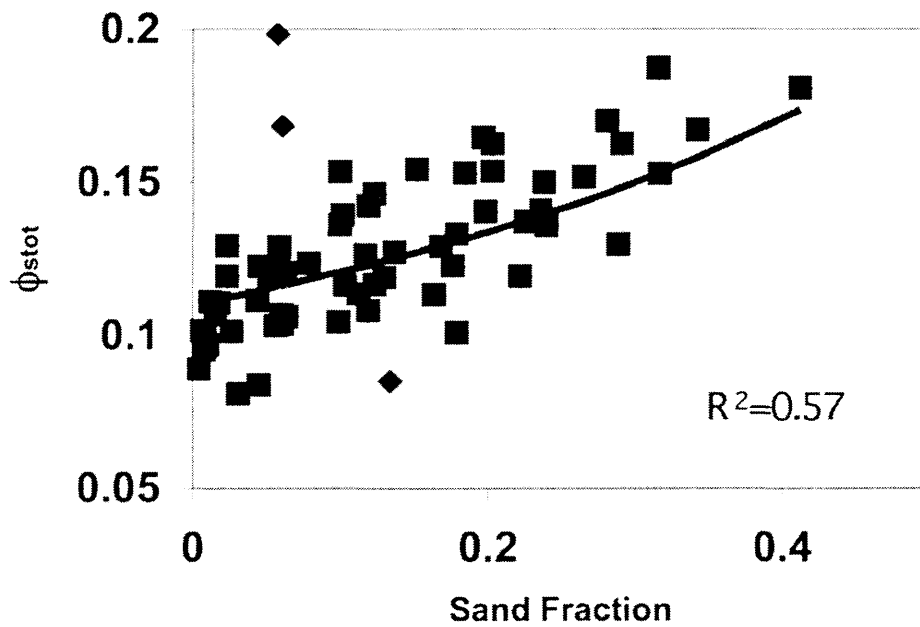
Figure 2- 4 Total solids volume fraction (ϕ_{stot}) of the upper cm of bed as a function of the sand fraction of total solids. Solid line represents relationship from Eq. 1 with ϕ_{sm} = 0.11. Diamonds represent outliers not included in R^2 calculation.

Clearly there is a good relationship between the data presented in Figure 2-4 and

Eq. 1 when ϕ_{sm} is assumed to be constant. Even more useful, however, if sand fraction

and ϕ_{stot} are known, Eq. 1 can be rearranged to

$$\phi_{sm} = \frac{\phi_{stot} - f_s \phi_{stot}}{1 - f_s \phi_{stot}} \qquad \text{(Eq. 2)}$$

and used to calculate ϕ_{sm}. Doing so eliminates the necessity of assuming a constant state

of consolidation with varying sand fraction.

2.3.4 Erodibility and Solids Volume Fraction Mud Matrix

The solids volume fraction of the mud matrix (ϕ_{sm}) was calculated using Eq. 2 for

the top 1 cm of sediment from each of the three sites over the 14-month period sampled.

This time series of ϕ_{sm} is presented in Figure 2-3b. The range of ϕ_{sm} for all three sites

(excluding one data point) is 0.085 – 0.145, about half that of the range in ϕ_{stot} (Figure 2-

3a). The range in ϕ_{sm} was similar for all sites, eliminating the distinction between the CC

site and the other two sites, and suggesting that much of the between site variation in ϕ_{stot}

was a result of variation in sand fraction between sites. The standard errors associated

with ϕ_{sm} (Figure 2-3b) are also considerably diminished in comparison to ϕ_{stot} (Figure 2-

3a) suggesting that much of the variability observed within a site was a result of local

variation in the sand fraction of the bed. Figure 2-5 further emphasizes that consideration

of ϕ_{sm} in place of ϕ_{stot} significantly reduces variability between sites as well as down
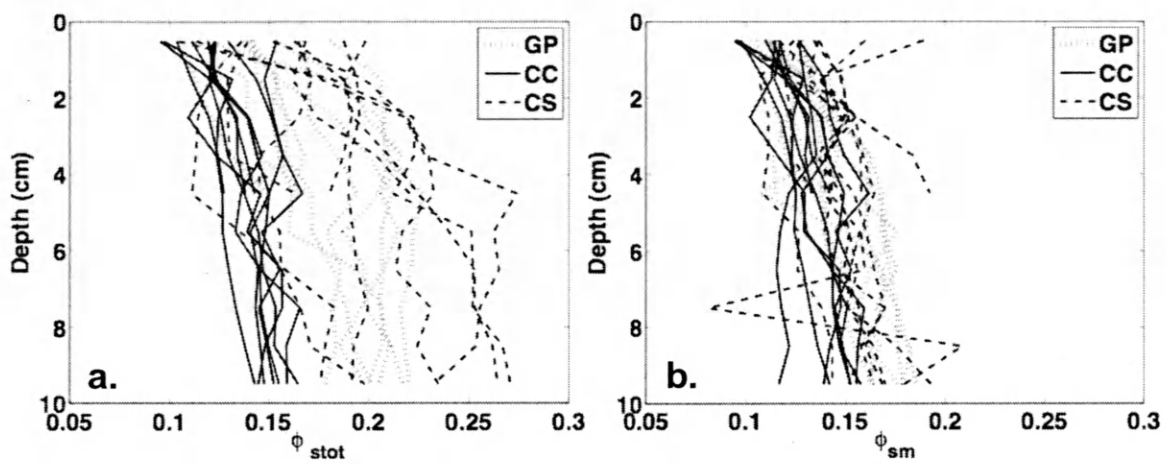
Figure 2- 5 a. Depth profiles of ϕ_{stot} collected over a 14-month period at each of the three York River sites. **b.** Depth profiles of ϕ_{sm} collected over a 14-month period at each of the three York River sites. ϕ_{sm} was calculated using data from Fig. 2-5a and sand fraction profiles.

cores. The overall standard deviation of ϕ_{sm} for all samples from all sites is only 0.021, whereas the standard deviation of ϕ_{stot} for all samples is 0.040.

Similar to the comparison of ϕ_{stot} to eroded mass, there was no correlation between ϕ_{sm} and the eroded mass at 0.4 Pa (Table 2-1). While eroded mass varied by roughly an order of magnitude, there was no clear distinction in ϕ_{sm} between periods of high and low erodibility. In fact, values of ϕ_{sm} for periods of low erodibility ranged from 0.085 to 0.145, representing the entire range observed in ϕ_{sm} data.

2.3.5 Fine Fraction Grain Size

The fraction of silt and clay in York River sediments was quite variable between sites and over the course of the 14-month sampling period. A time-series of clay fraction from each site is presented in figure 2-3d. While the observed clay fraction ranged from 0.30 to 0.76, the correlation between sand fraction and clay fraction reported in Table 2-1 indicates that much of the variation in clay fraction results from variations in sand fraction. Similarly, the correlation between clay fraction and ϕ_{stot} (Table 2-1) results from the correlation of clay fraction to sand fraction and the dependence of ϕ_{stot} on sand fraction.

The ratio of the clay fraction to silt fraction was determined and presented in Figure 2-3e to evaluate changes in fine fraction grain size not resulting from variations in

33

sand fraction. Results from pipette analysis indicated that the clay to silt ratio was variable over the 14-month period, with a mean clay to silt ratio of approximately 1.5 (Figure 2-3e). While there was no significant correlation between clay fraction and eroded mass, a significant, negative correlation ($p<0.10$; Table 2-1) was found between the eroded mass at 0.4 Pa and the clay to silt ratio. This suggests that periods of higher erodibility coincided with siltier, less cohesive bed sediments. However, a negative correlation, significant at $p<0.05$, was also found between the clay to silt ratio and ϕ_{sm}. This may indicate that an increase in the clay to silt ratio both inhibited consolidation and increased cohesivity, resulting in two counteracting influences on erodibility.

2.4 Discussion

2.4.1 Limitations of ϕ_{stot}

The erodibility of muddy beds is largely a function of inter-particle cohesion. As the bed becomes more compacted, the degree of inter-particle cohesion will increase, presumably resulting in decreased erodibility. The magnitude of ϕ_{stot} of the bed is assumed to reasonably represent the degree of compaction of the bed and, thus, is often compared to measures of erodibility. Numerous studies in both laboratory and natural environments have compared ϕ_{stot} of the bed to erodibility with varying results. While some studies have shown a strong relationship between erodibility and ϕ_{stot} (Amos et al., 1997; Jepsen et al., 1997; Roberts et al., 1998), it has been equally as common to find

34

little (Riethmueller et al., 2000) or no relationship (Houwing, 1999; Mahatma, 2004; Tolhurst et al., 2006; Stevens et al., 2007).

While both ϕ_{stot} and erodibility were found to be variable in this study, no clear relationship was found between the two. However, we and others (Flemming and Delafontaine, 2000; Panagiotopoulos et al., 1997; Paterson et al., 2000; Riethmueller, 2000; and Mahatma, 2004) have illustrated that ϕ_{stot} is highly dependent on the sand fraction of the bed. The relationship shown in Eq 2. and data shown in Figure 2-4 clearly illustrate that the addition of sand to the bed results in an increase in ϕ_{stot}. As ϕ_{stot} is assumed to be an estimate of the degree of compaction of the bed and, thus, inter-particle cohesion, it stands to reason that the addition of sand to the bed may complicate this assumption. In the simplest sense, comparing ϕ_{stot} to erodibility for mixed mud/sand beds of varying sand fraction assumes that mud and sand are equally cohesive. As this is known to not be true, it becomes apparent that an increase in ϕ_{stot} resulting from increasing sand fraction should not result in the same decrease in erodibility as would be expected for a similar increase in ϕ_{stot} in a bed composed entirely of mud. This distinction may explain the lack of correlation between erodibility and ϕ_{stot} found in many studies.

2.4.2 Removing the Effect of Sand on Solids Fraction

Flemming and Delafontaine (2000) and Mahatma (2004) recognized the influence of sand fraction on ϕ_{stot} and attempted to account for it by deriving empirical relationships between the two. Flemming and Delafontaine (2000) found the relationship to be site

specific and developed site-specific relationships to account for changes in ϕ_{stot} with sand fraction. Mahatma (2004) used data from four of six sites to derive an empirical relationship and used this relationship to normalize data from all sites. This "normalized water content" was used to compare the degree of consolidation. While strong relationships were shown in both cases, this approach requires the assumption that the true degree of compaction does not vary with sand fraction. While this assumption may be correct, deriving site-specific relationships makes comparison between sites difficult, while normalizing data is only possible when all sites exhibit a similar degree of compaction.

Rather than deriving empirical relationships between ϕ_{stot} and sand fraction, we propose the analytical solution given in Eq. 2. This solution derives the solids volume fraction of the mud matrix (ϕ_{sm}) supporting the bed and is independent of variation in sand fraction. Further, Eq. 2 eliminates the necessity of deriving site-specific relationships and effectively normalizes solids fraction data without making the assumption that ϕ_{sm} does not vary with sand fraction. Calculating ϕ_{sm} from ϕ_{stot} and sand fraction provides a way of comparing erodibility to the degree of compaction of the muddy matrix supporting the bed. While eliminating the apparent increase in compaction and cohesion associated with the addition of sand, this approach (as well as that of Mahatma, 2004) makes the assumption that the sand fraction of the bed has no influence on bed erodibility. At first glance, this assumption appears to be contradicted by the results of Torfs et al. (2001).

36

2.4.3 Re-evaluating the results of Torfs et al. (2001)

A laboratory study presented in Torfs et al. (2001) shows a clear increase in the critical stress for erosion with increasing mud fraction or, conversely, that as sand fraction increases, the critical stress for erosion decreases. However, Torfs et al. (2001) maintained a constant bulk density while varying the mud fraction. As was shown here and by others (Flemming and Delafontaine, 2000; Riethmueller, 2000; and Mahatma, 2004), as sand fraction increases, bulk density (or ϕ_{stot}) also increases. Conversely, from Eq. 2 it is apparent that maintaining a constant bulk density while increasing sand fraction must also cause a decrease in ϕ_{sm}. Thus the relationship shown in Torfs et al. (2001) illustrating a decrease in critical shear stress with increasing sand fraction also represents a decrease in critical shear stress with decreasing ϕ_{sm}.

Equation 2 predicts a monotonic negative relationship between sand fraction and ϕ_{sm} for sediments of a constant bulk density that approaches linearity as ϕ_{sm}, ϕ_{stot}, and f_s decrease. Thus, reevaluating the data of Torfs et al. (2001) in terms of both sand fraction and ϕ_{sm}, and including only data with a sand fraction of 0.96 or less, demonstrates that either sand fraction or ϕ_{sm} can be used to predict the initial critical stress for erosion equally well (Figures 2-6a and 2-6b). A power law regression between ϕ_{sm} and critical stress for montmorillonite and for a combination of kaolinite and natural mud yield R^2 values of 0.740 and 0.794, both of which are significant at $p<0.05$. While the resulting relationships between ϕ_{sm} and critical stress are dependent on sediment type, it allows a

single type of equation (i.e., critical stress versus ϕ_{sm}) to represent the data, rather than requiring both a relationship between bulk density and critical stress and a relationship between sand fraction and critical stress.

Similar to the reevaluated results of Torfs et al. (2001), the results of this study also suggest that sand fraction does not have an appreciable influence on the relationship between ϕ_{sm} and erodibility. The CC and CS sites both exhibited similar patterns in erodibility including both the amount of material eroded and the seasonal timing of major changes in erodibility. Additionally, these two sites had very similar values of ϕ_{sm}, both exhibiting a small and similar range. However, the sand fraction was generally quite different between these sites. Sand fraction at the CC site ranged from 0.02 to 0.15 while the CS site was always sandier ranging between 0.08 and 0.32. Despite differences in sand fraction of as much as 0.30, the two sites displayed similar erodibility.

While neither this study nor that of Torfs et al. (2001) was designed to evaluate the influence of sand fraction on erodibility for a specific value of ϕ_{sm}, this new approach could easily be evaluated with controlled laboratory experiments. It should also be noted that this approach is only appropriate for sand that erodes at critical shear stresses similar to those of the supporting mud matrix. If coarser sand with higher critical stress was present, the eroded mud mass might be limited by bed armoring (Wiberg et al., 1994) as opposed to consolidation of the mud matrix, which would confound interpretation of the
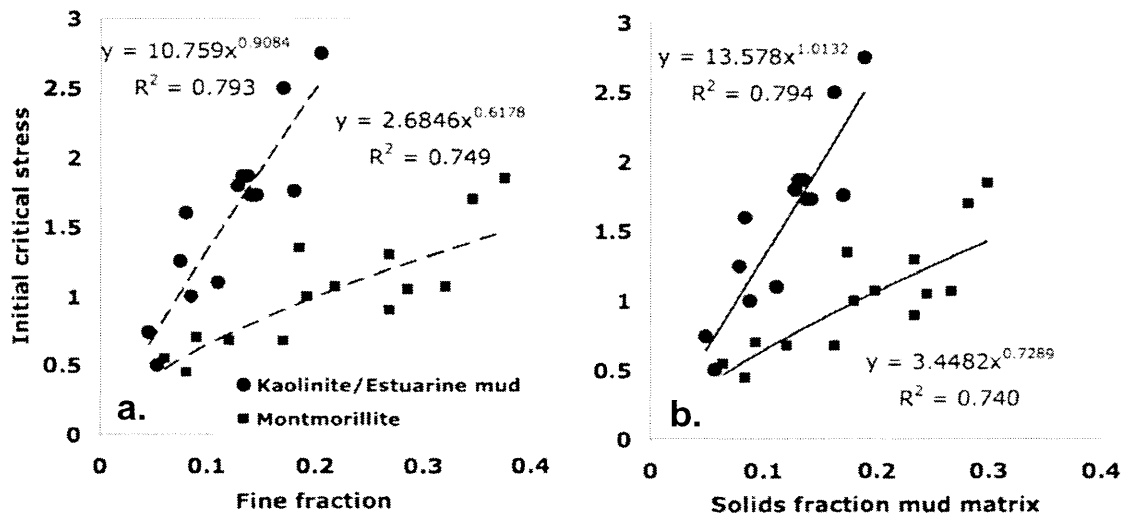
Figure 2- 6 a. Initial critical stress for erosion as a function of fine fraction for a mixed mud/sand bed. Results re-plotted from Torfs et al. (2001). **b.** Initial critical stress for erosion as a function of solids fraction mud matrix. Reevaluated results from Torfs et al. (2001). Solids fraction mud matrix was calculated from bulk density and sand fraction using Equation 2.

results. As the sand present in our study was about 120 μm in diameter, the critical stress

for erosion of the sand was about 0.1 Pa, similar to that of the eroded mud.

2.4.4 Relationship Between Erodibility and ϕ_{sm} over a broader range

While the results of this study did not reveal a significant relationship between

erodibility and ϕ_{sm}, we still believe this approach to be promising. To further evaluate its

potential, a literature search was performed in an attempt to apply this relationship to a

greater range of data from mud matrix supported mixed mud/sand beds. ϕ_{sm} could only be

calculated from published data that included both sand fraction and ϕ_{stot} (or bulk density,

water content, etc.), greatly limiting the previous work that could be included in this

comparison. As the initial critical stress for erosion proved to be the most common

measure of erodibility included in these published works, the results of this study were

also presented in this form. The erodibility measurements presented in this study were

originally designed to measure profiles of the critical stress for erosion with depth into

the seabed. As a result, the initial critical stress was not well resolved. For every core

eroded, initiation of motion occurred at an applied stress of either 0.05 Pa or 0.1 Pa, and

these data are presented accordingly in Figure 2-7.

The results of nine published works were found to include information on sand

fraction, ϕ_{stot}, and critical stress for the initiation of motion and were considered for this

comparison. Of these nine, Torfs et al. (2001) and Kamphius and Hall (1983) proved to

be outliers in that the values of critical stress presented were an order of magnitude or more higher for a given value of ϕ_{sm} and were thus excluded. As there are no accepted standards for measuring erodibility or interpreting erodibility results (Sanford, 2006), the relatively high critical stress values presented in these papers may represent differences in the definition of initial critical stress, erosion device behavior, calibration, or data analysis techniques. Data from the remaining seven and this study (Table 2-2) were included in Figure 2-7. Critical stress data with sand fractions greater than 90% were excluded from these results as the work of Panagiotopoulus et al. (1997) and Torfs et al. (2001) demonstrated that sediment with sand fraction greater than approximately 90% did not behave cohesively. The remaining data represent a wide range of sand fraction (2 - 90%), ϕ_{stot} (0.08 − 0.5), and ϕ_{sm} (0.06 − 0.39).

Figure 2-7a presents a comparison of ϕ_{stot} to the initial critical stress for erosion. While there is a weakly significant positive relationship overall ($R^2 = 0.16$), some of the individual data sets showed a negative relationship, while others show no relationship at all. In contrast, the comparison of ϕ_{sm} to initial critical stress in Figure 2-7b provides a much stronger and consistently positive relationship. Given the number of devices used and likely inconsistencies in identification of initial critical stress, there is a surprisingly strong relationship between ϕ_{sm} and initial critical stress ($R^2 = 0.68$). This suggests that, provided a sufficient range in ϕ_{sm}, it may be possible to identify a characteristic relationship between ϕ_{sm} and initial critical stress.

41
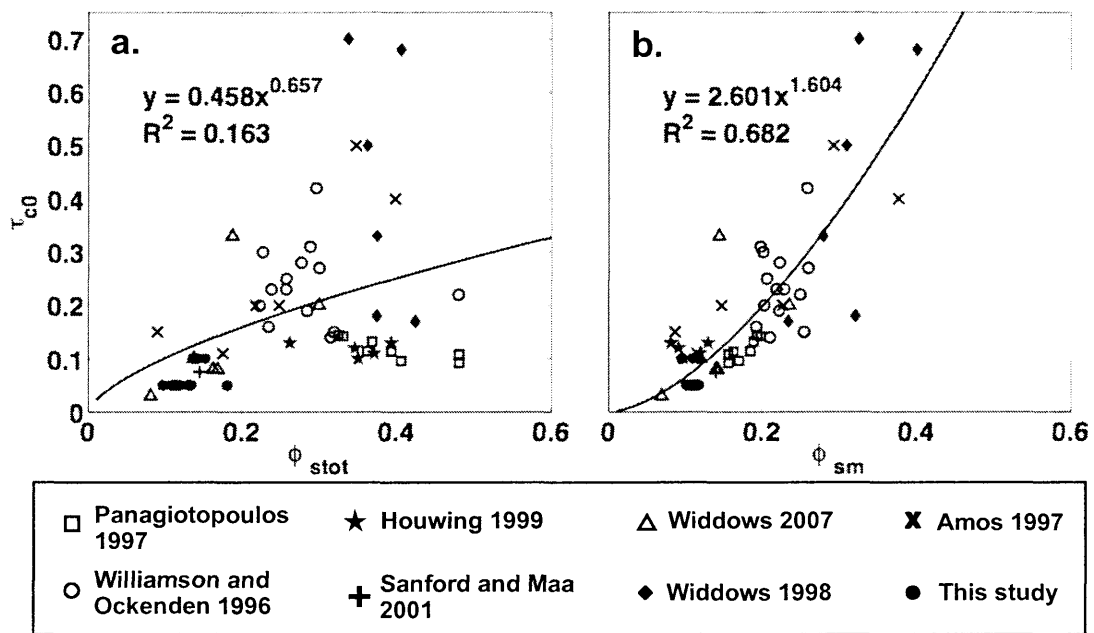
Figure 2- 7 Critical stress for initiation of erosion (τ_{c0}) from this study and a number of published works (see Table 2-2), as a function of **a.** total solids volume fraction (ϕ_{stot}) and **b.** solids volume fraction of mud matrix (ϕ_{sm}).

Reference	Location	Sediment Source	Instrument
Panagiotopoulos et al. (1997)	Laboratory - remoulded	Natural estuarine mud	Recirculating Flume
Williamson and Ockenden (1996)	*In situ*	Intertidal mudflat- Blue Anchor Bay	ISIS - bell
Houwing (1999)	*In situ*	Intertidal mudflat- Dutch Wadden Sea	ISEF – *in situ* flume
Sanford and Maa (2001)	*In situ*	Chesapeake Bay	Sea Carousel
Widdows et al. (2007)	*In situ*	Intertidal mudflat- multiple sites	*In situ* flume
Widdows et al. (1998)	*In situ*	Intertidal mudflat- Humber Estuary	*In situ* mini-flume (flume also similar results but not shown)
Amos et al. (1997)	*In situ*	Fraser River Delta	Sea Carousel
This study	*Ex situ* – undisturbed cores	Subtidal -York River, Chesapeake Bay	Gust microcosm

Table 2- 2 Sources and relevant information for data included in Figure 2-7.

However, the scatter about the fit between critical stress and ϕ_{sm} in Figure 2-7b is still considerable, and if considering a subset of these data with a relatively small range in ϕ_{sm} (0.2 to 0.25 for instance), ϕ_{sm} may be a relatively poor predictor of initial critical stress. This suggests that when the range in ϕ_{sm} is small, other factors may overwhelm this relationship. Consistent with this, the relatively small range in ϕ_{sm} shown in Figures 2-3b and 2-5 may explain the lack of relationship found in this study. It seems likely that a similar parallel may be drawn to other bed properties commonly related to erodibility in natural sediments. For example, studies that have found a clear and strong relationship between biological parameters and erodibility, such as colloidal carbohydrate concentration (Lucas et al., 2003) or macrofauna abundances (Widdows et al., 2000; Andersen et al., 2005), typically include a large range in these biological parameters, often spanning orders of magnitude.

The relatively small range in ϕ_{sm} and the lack of a relationship between ϕ_{sm} and erodibility in this study suggest that seasonal changes in ϕ_{sm} are not responsible for the observed variability in bed erodibility at the three York River sites included in this study. In a highly productive environment such as the Chesapeake Bay, it seems likely that biologically induced changes in cohesion may be largely responsible for the observed variation in bed erodibility. Analysis of seasonal variations in the concentration and composition of organic matter at each of the sites visited in this study is ongoing. We also plan to further analyze the significance of clay versus silt fraction as a potential control on erodibility using a Multisizer 3 Coulter Counter. Nonetheless, ϕ_{sm} may still be

44

the dominant variable distinguishing our York River data as a whole from the erodibility results from the other systems in Figure 2-7b.

2.5 Conclusions

Seabed erodibility at three mid-depth muddy sites within the York River was found to be highly variable over a 14-month time period. The eroded mass at 0.4 Pa varied by an order of magnitude, ranging from about 0.2 kg m^{-2} to 2.0 kg m^{-2}. The total solids volume (sand plus mud) fraction (ϕ_{stot}) of the top centimeter of sediment also varied extensively but was not significantly related to observed changes in erodibility. Consistent with the findings of other studies, variations in ϕ_{stot} were largely a function of the sand fraction of the bed. The analytical relationship between ϕ_{stot}, sand fraction, and solids volume fraction of the mud matrix alone (ϕ_{sm}) provided in Sanford (2008) was shown to reasonably represent observed changes in ϕ_{stot}. Further, this relationship was modified to allow determination of ϕ_{sm} provided ϕ_{stot} and sand fraction were known.

The variability of ϕ_{sm} was found to be significantly less than the variability of ϕ_{stot}, a finding consistent with the inference that changes in ϕ_{stot} driven by sand fraction do not control erodibility in muddy environments. Although the York River data presented in this study demonstrated no clear relationship between ϕ_{sm} and erodibility, we believe this to be a result of the small range in ϕ_{sm} observed at the three sites included in this study. In spite of a lack of correlation within the surficial sediments at selected sites in the York

River, we believe ϕ_{sm} to be a better parameter to relate to erodibility than ϕ_{stot}. Relating ϕ_{sm} to erodibility eliminates apparent increases in compaction resulting from the addition of sand to a muddy bed.

Including available published data from other systems when evaluating the relationship between ϕ_{sm} and initial critical stress for erosion effectively increased the range in observed ϕ_{sm} and revealed a surprisingly strong correlation across eight of ten studies considered, including the York. Furthermore, the correlation with ϕ_{sm} was significantly stronger than that between ϕ_{stot} and initial critical shear stress. This suggests that across a range of settings it may be advantageous to use ϕ_{sm} as a proxy for the initial critical stress for erosion. However it is also apparent that other influences may result in significant deviations from this general relationship, including fine fraction grain size, mineralogy, biological influences, and other effects.

Chapter 3

Seasonal and spatial variation in cohesive sediment erodibility the York
River estuary: physical deposition versus biological reworking[2]

3   Seasonal and spatial variation in cohesive sediment erodibility in the York River estuary: physical deposition versus biological reworking

Abstract

Sediment erodibility was measured at three sites on the York River estuary monthly to bimonthly from April 2006 through October 2007. Erodibility at the three sites was similar during the summer and fall. One site near Gloucester Point maintained this level of erodibility greater than 90% of the time while the two sites in the more physically dominated Clay Bank region exhibited a consistent and pronounced increase in erodibility in the late winter and spring. Weak to non-existent correlations between bed erodibility, solids volume fraction, and surficial concentrations of organic matter, colloidal carbohydrate, and extracellular polymeric substances, were not sufficient to explain the observed seasonal pattern at Clay Bank. Digital X-radiographs revealed thick sequences (10 – 20+ cm) of laminated sediments at the surface at Clay Bank coincident with the period of highest erodibility and more biologically reworked sediment during the rest of the year, suggesting that periodic rapid deposition introduced new sediment that was seasonally easy to erode. The finding that seasonal deposition influenced erodibility in the Clay Bank region is consistent with previous results indicating the occasional

presence of a secondary turbidity maximum. Comparison of the biologically reworked, but still "low" erodibility condition in the York to other published Chesapeake Bay erodibility data revealed a consistent critical shear stress range and profile, suggesting this equilibrium critical stress profile may be representative of other similar estuarine environments in the absence of rapid deposition. At relatively low stresses and in the absence of rapid deposition, we speculate that burrowing and/or pelletization may play a role in maintaining high equilibrium bulk water content without reducing the strength of the surface of the seabed.

3.1 Introduction

Cohesive sediments in marine and coastal environments are responsible for degrading water quality, influencing the cycling and availability of particle bound contaminants, and filling in navigable waterways. In spite of their significance to coastal environments, there are still major gaps in our understanding of many of the fundamental processes governing cohesive sediment transport and deposition. In particular, seabed erodibility, which facilitates sediment exchange between the bed and water column, is under-resolved in field studies and is often treated as a tuning parameter in numerical models.

The predominant physical influences on the erodibility of muddy sediments are the degree of consolidation and the distribution of grain sizes making up the bed. (e.g., Kandiah, 1974; Jepson et al., 1997; Roberts et al., 1998). The critical stress for the

initiation of motion of a pure sand bed increases with grain size and is independent of time. Inter-particle bonds in abiotic, cohesive beds result in a very different relationship, with critical stress for erosion increasing with decreasing grain size and increasing consolidation time. Laboratory studies have shown that even at mud to sand ratios as low as 0.05 to 0.2, a mixed bed begins to act as a cohesive bed (Panagiotopoulos et al., 1997; Torfs et al., 2001). Thus, even for a bed with a relatively small mud fraction, the degree of consolidation of the bed, often represented as bulk density or solids fraction, can play an important role in determining bed erodibility. In the absence of biological effects, the degree of consolidation of the bed is largely a function of the deposition rate and consolidation time (Parchure and Mehta, 1985; Jepsen et al., 1997; Roberts et al., 1998; Sanford, 2008). As a result, spatial or temporal variations in deposition may greatly affect local patterns in bed erodibility.

In shallow environments, sufficient light reaches the seabed that biofilms are common. In this setting, biological influences have generally been characterized as biostabilizing or biodestabilizing, acting to respectively decrease or increase sediment erodibility. Biofilms on mudflats, often quantified by measuring chlorophyll-a (Chl-a) or extracellular polymeric substances (EPS), are secreted by benthic diatoms and have been shown to stabilize the seabed and decrease sediment erodibility (Andersen, 2001; de Brouwer et al., 2005). On mudflats, Chl-a and EPS levels often vary seasonally with minima in winter and maxima in late spring and early summer (de Brouwer et al., 2000; Widdows et al., 2004). Potentially counteracting biostabilizing influences, the feeding

and bioturbation rates of benthic organisms also reach a maximum during the warmer months, which has been shown to result in a seasonal maximum in biodestabilization (de Brouwer et al., 2000; Widdows et al., 2000; Andersen, 2001). In a deeper water, estuarine environment such as the Chesapeake Bay, benthic communities and their influence on the estuarine seabed can vary significantly over space and time due to variations in salinity, hydrodynamic processes, and sediment dynamics (Schaffner et al., 1987a; Schaffner et al., 2001). In either mudflat or deeper water, estuarine settings, the net biological influence on erodibility may represent the integration of numerous biostabilizing and destabilizing influences each of which may be variable in space and time.

Measurements of cohesive sediment erodibility in coastal and marine environments are typically costly and time consuming (Sanford, 2006). As a result, seabed erodibility is often poorly resolved in both space and time. While numerous exceptions do exist (e.g., Sanford and Maa, 2001; Maa and Kim, 2002; Stevens et al., 2007), cohesive bed erodibility studies which attempt to systematically resolve seasonal and spatial gradients have most often been conducted in mudflat environments. Fewer published works address temporal and spatial variations of erodibility in deeper, turbid environments were little light reaches the seabed. As the stabilizing effects of biofilms are likely to be less well developed in these environments it is difficult to draw parallels as to the dominant influences on seabed erodibility.

The goal of this work was to evaluate variation in seabed erodibility over several seasons in a cohesive estuarine environment and gain insight into the dominant physical
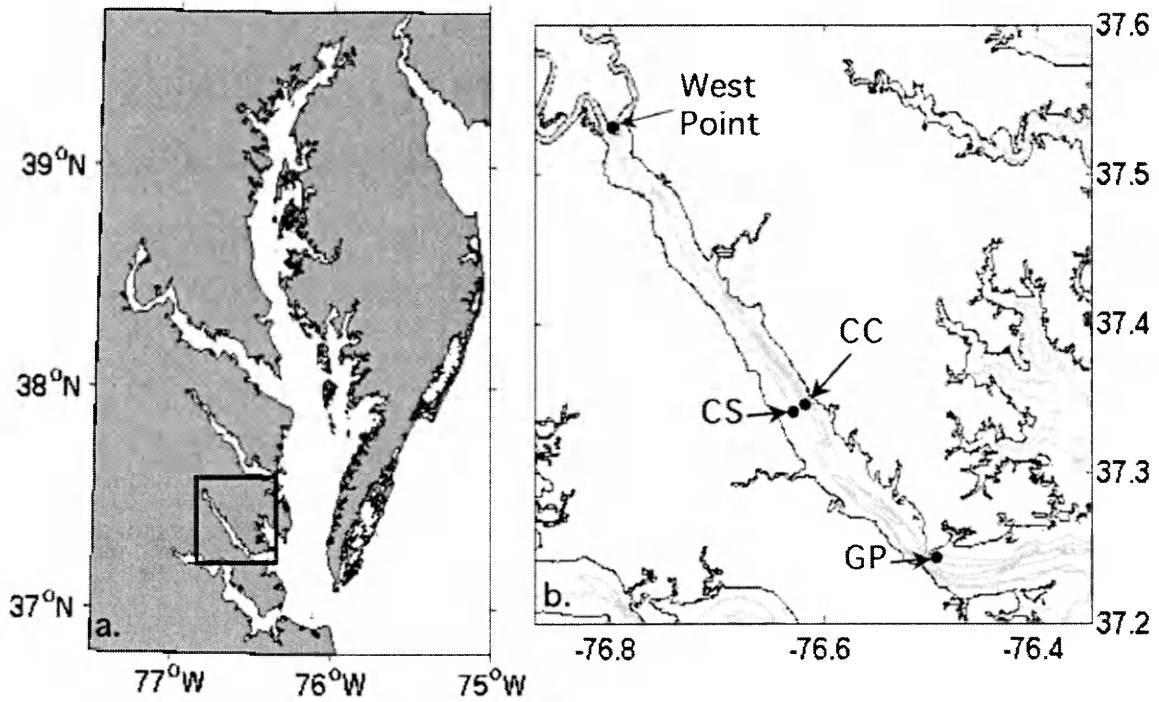
Figure 3- 1 a. Map of Chesapeake Bay, USA. Black box indicates region included in Figure 3-1b. **b.** Map of York River estuary including sampling station locations. GP = Gloucester Point station, CC = Clay Bank channel station, CS = Clay Bank secondary channel station.

and biological processes influencing these variations. Following a description of our field site, methodology, and main results, our findings are discussed in terms of the dominant seasonal cycle and the main differences between the more biologically and physically influenced regions of the estuary. Next we discuss the impact of key biological and physical interactions with regard to equilibrium and disequilibrium bed conditions. Finally, we close with a conceptual model for the dominant controls on spatially and temporally evolving bed erodibility in the York River estuary.

3.2 Regional Setting

This study was conducted on the York River estuary, a sub-estuary of the Chesapeake Bay, USA (Figure 3-1). The York River, with a mean tidal range of about 80 cm, is classified as a microtidal estuary. However, this system is tidally energetic with strong tidal currents reaching magnitudes of ~ 1m s^{-1} at the surface during spring tide (Schaffner et al., 2001) and capable of resuspending large amounts of sediment (Friedrichs et al., 2000). Sediment supply to the York River is a combination of riverine input (~55%), shoreline erosion (~12%), and influx from the Chesapeake Bay main stem (~33%; Nichols, 1991). However, the ratio of annually introduced sediment to internally recycled sediment is small. Based on ^{210}Pb accumulation rates, mixing depths, and sediment supply, Dellapenna et al. (1998, 2003) estimated the sediment residence time prior to burial to be about 70 to 200 years.

A persistent estuarine turbidity maximum (ETM) has been reported just upstream of West Point in both the Pamunkey and Mattaponi Rivers, the York's main tributaries. Additionally, an ephemeral secondary turbidity maximum (STM) has been reported in the Clay Bank region, about 25 km from the York River mouth (Lin and Kuo, 2001). Near bottom suspended sediment concentrations in the STM commonly exceed 100 mg l^{-1} at slack tide (Lin and Kuo, 2001) and may reach concentrations as high as 2 g l^{-1} during strong tidal currents (Friedrichs et al., 2000). Using ^{7}Be as a tracer for recently deposited sediment, Romine (2004) observed a muddy deposit migrating with the location of the Pamunkey River ETM suggesting a mobile pool of cohesive sediment actively transported in association with evolving hydrodynamic conditions.

Radioisotope geochronology, used in previous studies in this region, has indicated an active seabed with physical reworking depths of as much as 1 meter (Dellapenna et al., 1998; Kniskern and Kuehl, 2003). Additionally, stair-stepped ^{210}Pb profiles and X-radiographs with laminated sequences, bioturbated sequences, and hiatal surfaces suggest a history of active erosion and deposition (Schaffner et al., 1987b; Dellapenna et al., 1998; Kniskern and Kuehl, 2003). However, the mechanism and time-scale associated with deep physical mixing and erosion and deposition "events" remain unclear. Severe fetch limitation results in waves seldom exceeding heights of 0.5 m and periods of 2 to 3 seconds (Vandever, 2007). In this weak wave climate, cohesive sediment resuspension is dominated by tidal currents (Boon, 1996). However, suspended sediment stratification has been observed to limit tidal resuspension (Friedrichs et al., 2000) at concentrations on

54

the order of 2 g l^{-1} indicating a limit to direct resuspension by tidal currents on the order of 1 to 2 centimeters.

With regards to benthic biology, Schaffner et al. (2001) reported a strong estuarine gradient in ecological diversity from the ETM region of the York into the main stem of the Chesapeake Bay. Both the ETM and STM regions were characterized by strong tides, high suspended sediment concentrations, and evidence of physical bed reworking which resulted in unfavorable conditions for benthic biota. The resulting benthic community in these regions were typically impoverished and consisted of predominantly short lived, shallow dwelling, opportunistic species. In contrast, the main stem of the Chesapeake Bay had weaker tides, the occasional influence of local wind waves, and lower suspended sediment concentrations. The resulting benthic community was diverse, longer lived, and capable of higher bioturbation rates than those found in the ETM and STM regions of the middle to upper York.

Three sites were chosen in the York River (Figure 3-1) to provide variation in erodibility and the associated physical and biologic influences. Two of these sites were located near Clay Bank, about 25 km from the York River mouth, with a typical salinity of 10 to 20 ppt. This region is commonly occupied by a STM and is characterized by strong tidal currents and high suspended sediment concentrations (100s of mg l^{-1}). It falls toward the physically dominated end of the biologic gradient described by Schaffner et al. (2001). One site at Clay Bank was located on the flank of the main channel at ~ 11 m depth (CC), while the other site was about one kilometer away in a secondary channel at

~6 m depth (CS). A third site was chosen near Gloucester Point (GP), about 10 km from the York River mouth and at a depth of 8 m and typical salinity of 13 to 23 ppt. Suspended sediment concentrations near Gloucester Point (10s of mg l^{-1}) are typically much less than those found at Clay Bank. This site falls between the physically and biologically dominated end members of the estuarine gradient described by Schaffner et al. (2001). Conditions are generally more favorable for benthic fauna down-estuary of the Clay Bank region and potentially result in less physical dominance in sediment transport processes at the GP site.

3.3 Materials and Methods

3.3.1 Sampling

Three sites in the York River were sampled monthly to bimonthly from April 2006 through October 2007 (Table 3-1). The dates and times of sampling were determined primarily by logistical concerns and to coincide with slack tide. As a result, sampling took place randomly with respect to tidal phase (ebb/flood) and the spring/neap cycle. Whenever possible, the three sites were sampled on consecutive days.

All sediments were collected from a small vessel (~8 meters), on anchor, at or near slack tide, with an Ocean Instruments Gomex box corer (surface area 625 cm^2). Individual samples were sub-sampled from the box corer. Each time a site was visited, two cores were collected for erodibility measurements, three cores were collected for

digital X-radiography, and numerous (12-24) samples of the top 5 mm of sediment were collected for analysis of organic components. Due to the large number of samples required and relatively small size of the box corer, numerous box cores were collected while swinging on anchor. As a result, all data presented here likely incorporated spatial variation within a radius of roughly 15 to 25 m at each site.

Due to the interest of this study in the surface of the seabed and easily eroded material, particular attention was paid to minimize disturbance of the sediment-water interface during core collection and sub-sampling. The soft nature of these sediments allowed collection of 20 to 40 cm long box cores using only the weight of the corer. As a result, the Gomex could be slowly lowered to the seabed, allowed to penetrate under its own weight, and then slowly retrieved. Lids on top of the box corer automatically closed upon retrieval, preventing agitation to the sediment surface due to sloshing of the overlying water. Box cores and sub-cores with turbid water (exceeding the ambient conditions) overlying the sediment surface were assumed to be disturbed and were rejected.

3.3.2 Erodibility measurements

Seabed erodibility was measured with a dual core Gust erosion microcosm system. This device uses a rotating disc with central suction to impose a nearly uniform

57

Site	G P	C C	C S
Sample Date	4/18/06	5/3/06	5/2/06
	7/14/06	7/17/06	7/19/06
	8/21/06	8/22/06	8/23/06
	9/25/06	9/29/06	9/28/06
	11/20/06	11/15/06	11/17/06
	1/9/07	1/11/07	1/12/07
	3/21/07	3/22/07	3/23/07
	4/18/07	4/19/07	4/20/07
	5/21/07	5/23/07	5/22/07
	6/25/07	6/27/07	6/26/07
	8/10/07	8/8/07	8/9/07
	10/16/07	10/15/07	10/17/07

Table 3- 1 Sampling dates for erodibility measurements at the three York River sites. GP = Gloucester Point, CC= Clay Bank channel, and CS=Clay Bank secondary channel.

shear stress on the surface of two 10 cm diameter sediment cores (Gust and Mueller, 1997). Cores chosen for erosion testing were carefully selected to ensure uniform, level surfaces and minimal disturbance of the sediment-water interface. After collection, cores were carefully transported to the Virginia Institute of Marine Science located on the York River adjacent to the GP site. Erodibility measurements were generally underway within about two hours of core collection to minimize consolidation effects.

Erodibility measurements consisted of a sequence of seven steps of approximately 20-min duration, each with a consecutively increasing applied shear stress (0.01 Pa, 0.05 Pa, 0.1 Pa, 0.2 Pa, 0.3 Pa, 0.45 Pa, 0.6 Pa) applied to the sediment surface. Each erodibility measurement included two cores from a given site eroded simultaneously. Results were analyzed with the erosion formulation of Sanford and Maa (2001). For a more detailed description of these erodibility measurements see Chapter 2 of this thesis.

Sediment laden effluent from the Gust microcosm system was collected and then filtered with 0.7 μm GF/F filters. After being dried and weighed to determine total suspended solids, these filters were muffled at 550 degrees Celsius to determine the loss on ignition organic content for each applied stress step of each core eroded.

3.3.3 Digital X-radiography

Slabs for digital X-radiography measuring ~12 cm in width, 2.5 cm thick, and 10 to 20 cm in length were sub-sampled from the Gomex box corer. Upon returning to

VIMS, digital X-radiographs of the slabs were collected with a coupled X-ray generator and Paxscan 4030R Amorphous Silicon Digital X-ray detector system. This system was connected to a desktop computer providing nearly instantaneous high quality X-ray images. The grayscale of digital X-radiographs was indicative of the relative density of the sediment. X-ray negatives are presented here where lighter shades of gray indicate higher density while darker shades indicate lower density. Images were adjusted to optimize contrast and aid in identification of sedimentary structures. As a result, in this paper grayscale levels vary between images and the relative grayscale are not compared between images to evaluate changes in bed density.

3.3.4 Solids volume fraction mud matrix

Solids volume fraction of the mud matrix (ϕ_{sm}), averaged over the top centimeter of the bed, was calculated from measurements of the total solids volume fraction (ϕ_{stot}) and the sand fraction (f_s). Sediment water content was determined by standard wet weight/dry weight analysis. Total solids volume fraction (ϕ_{stot}) was calculated from the water content by assuming the density of water to be 1015 kg m^{-3} and the density of solids to be 2650 kg m^{-3}. Sand fraction was determined by sieving sediments with a 63 μm sieve with the sand fraction equal to the mass of sand (retained on sieve) per total mass dry weight sediment. Following the method described in Chapter 2, solids volume fraction of the mud matrix (ϕ_{sm}) was calculated as
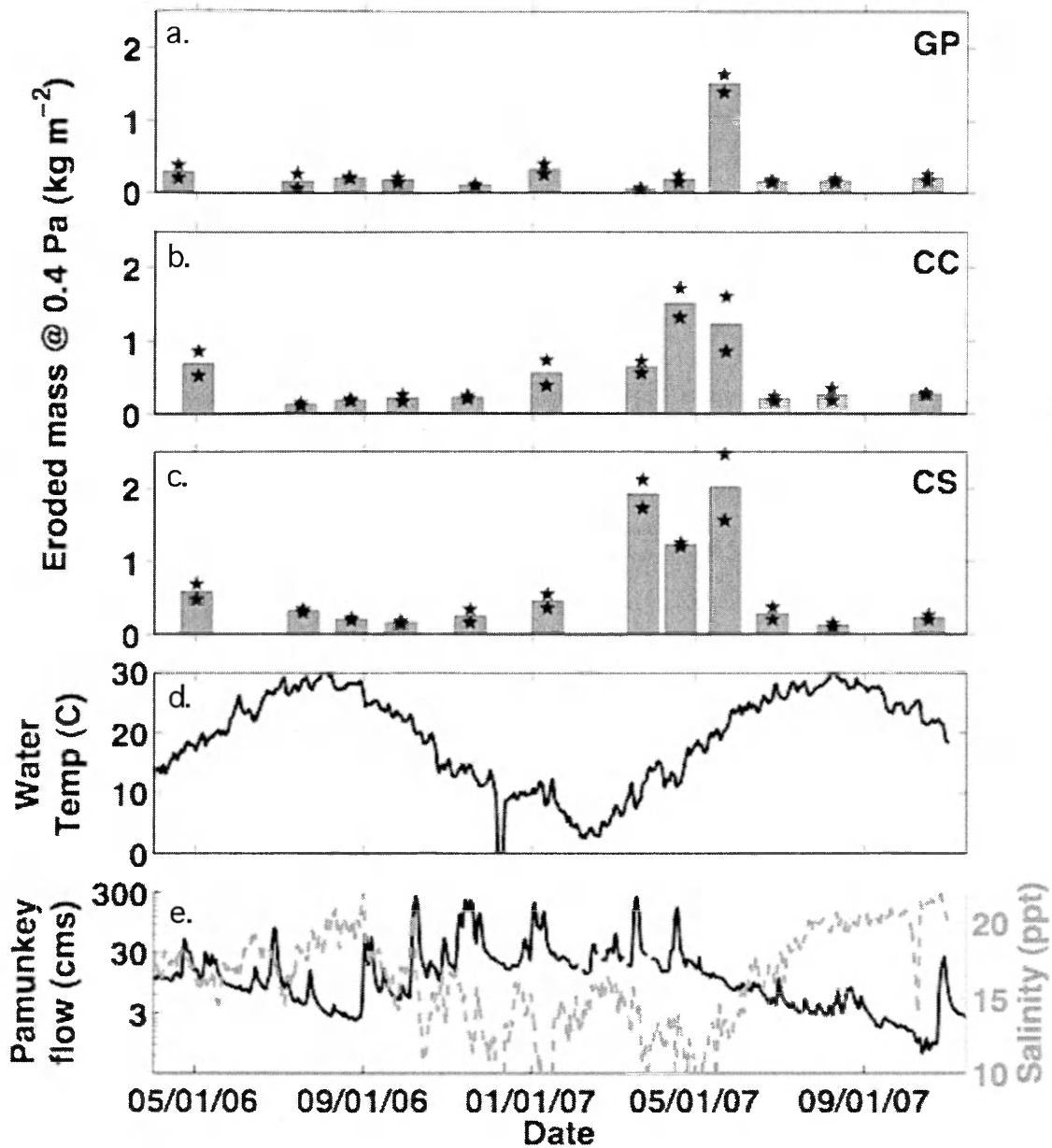
Figure 3- 2 Time series of eroded mass at 0.4 Pa at **a.** Gloucester Point (GP) site, **b.** Clay Bank channel (CC) site, **c.** Clay Bank secondary channel (CS) site. Stars are values for each of the two individual cores eroded; bars indicate the mean value. **d.** Time-series of water temperature in the York River estuary near Clay Bank. Data from Virginia Estuarine and Coastal Observing System (VECOS, http://www2.vims.edu/vecos). **e.** Time-series of Pamunkey River flow (solid black line) measured at Hanover, VA. Data

from USGS Water Data website at *http://waterdata.usgs.gov/nwis*. Time-series of York River salinity (dashed gray line) near Clay Bank. Data from Virginia Estuarine and Coastal Observing System (VECOS, http://www2.vims.edu/vecos).

$$\phi_{sm} = \frac{\phi_{stot} - f_s\phi_{stot}}{1 - f_s\phi_{stot}}.$$ (Eq. 1)

3.3.5 Colloidal Carbohydrates and EPS

Colloidal carbohydrate and extracellular polymeric substance (EPS)

concentrations were determined by Dr. Schaffner's lab. Sediment samples were collected

for analysis from multiple box cores using 5 ml syringes. Twelve to twenty-four sediment

samples were collected from the top 5 mm of sediment each time a site was visited.

Sediment colloidal carbohydrate concentrations were determined following the

methodology described in Underwood et al. (1995). Sediment EPS concentrations were

determined following the methodology described in Smith and Underwood (1998, 2000).

3.3.6 Other environmental data

River flow data for the Pamunkey River at Hanover, VA was acquired from the

USGS Water Data website at *http://waterdata.usgs.gov/nwis*. Water temperature and

salinity data near Clay Bank were acquired from the Virginia Estuarine and Coastal

Observing System (VECOS) website at http://www2.vims.edu/vecos. These data were

collected near the seabed in about 1.5 meters of water on the northeast shoal of the York

River just outside the main channel.

3.4 Results

3.4.1 Erodibility

Erodibility measurements from the Gust microcosm system were analyzed using the erosion formula of Sanford and Maa (2001) to produce profiles of the critical stress for erosion vs. eroded mass. Rather than compare the 72 critical stress profiles derived in this study, these data have been simplified and presented as the total eroded mass at 0.4 Pa in Figures 3-2a, 3-2b, and 3-2c. 0.4 Pa was chosen as this integrates the results of the majority of an erodibility measurement and represents the typical maximum tidal shear stress in the York River (Scully and Friedrichs, 2003).

The two sites in the Clay Bank region (CC and CS) exhibited a similar and pronounced seasonal cycle in erodibility (Figures 3-2b and 3-2c). The lowest erodibility was found in the summer and fall. These sites had a relatively low level of erodibility from July 2006 through November 2006 and from July 2007 through October 2007. Erodibility was quite consistent during these periods, ranging from 0.10 to 0.32 kg m^{-2} at 0.4 Pa. The combined data from both sites over these two periods of low erodibility had a mean eroded mass at 0.4 Pa of 0.22 kg m^{-2} with a standard deviation of 0.074 (data from 28 eroded cores).

In contrast, the highest levels of erodibility were found in the late winter and spring. The CC site in April and May 2007 and the CS site in March, April, and May

2007 had eroded mass at 0.4 Pa ranging from ~1.2 to 2.0 kg m^{-2} representing a five to eight fold increase over the observed conditions of the previous summer and fall. Moderate erodibility (~0.5 to 0.7 kg m^{-2} at 0.4 Pa) observed in January 2007 at CS and January and March 2007 at CC appear to represent transitional periods, as erodibility had increased from the summer/fall low erodibility condition but had not yet reached the very high erodibility observed in the spring. Similar erodibility at both sites in May 2006 may be another transitional period. In this case, erodibility may have been decreasing from a period of higher erodibility prior to the onset of this time series.

Erodibility at the GP site (Figure 3-2a) was generally low and did not exhibit the pronounced seasonal pattern found at the two Clay Bank sites. Excluding May 2007, the eroded mass at 0.4 Pa at GP ranged from 0.05 to 0.32 kg m^{-2} with a mean eroded mass of 0.18 kg m^{-2} and standard deviation of 0.089 (data from 22 eroded cores). Interestingly, the range in eroded mass and mean eroded mass found at GP nearly year-round was quite similar to that measured at the Clay Bank sites in the summer and fall of 2006 and 2007. The exception to this was May 2007, when the eroded mass at 0.4 Pa at GP was considerably elevated relative to all other data from this site. The eroded mass increased by roughly an order of magnitude from 0.19 kg m^{-2} in April to 1.62 kg m^{-2} in May and then decreased again to 0.16 kg m^{-2} in June. In contrast to the Clay Bank sites, there did not appear to be any transitional period of increasing or decreasing erodibility at GP, suggesting that the increased erodibility in May 2007 may have been short lived.
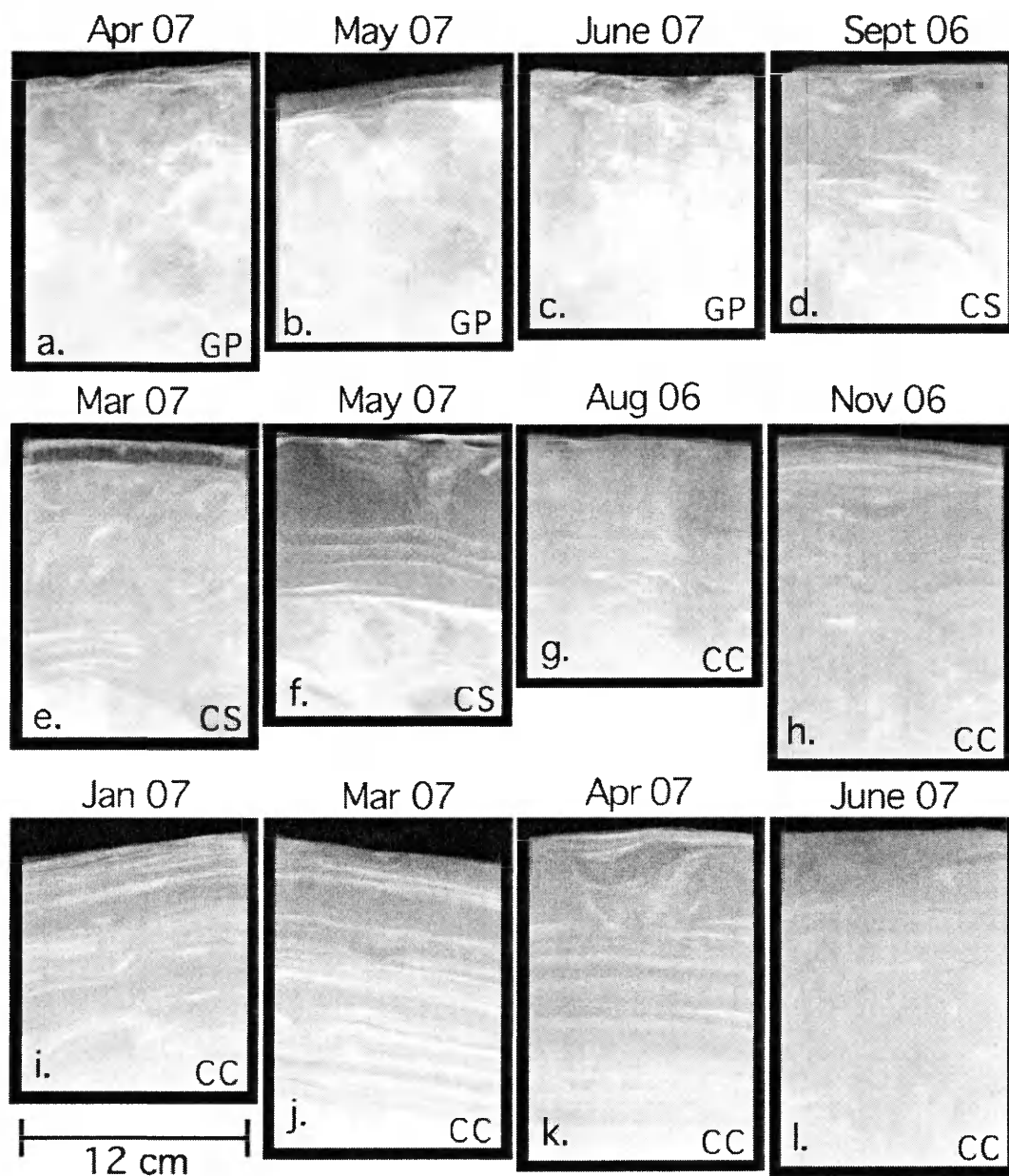
Figure 3- 3 Digital X-radiograph negative images from the York River, VA. Month and
year of sample collection is indicated above each X-radiograph. Site associated with
each sample is located in lower right hand corner of each image. GP = Gloucester Point,
CS = Clay Bank secondary channel, and CC = Clay Bank channel.

3.4.2 Digital X-radiography

Digital X-radiographs were collected coincident with cores for erodibility measurements to provide insight into the condition of the seabed and the relative influence of biological and physical processes operating on the seabed. The presence of laminated bedding highlighted times when physical processes dominated bioturbation due to either a lack of abundant bioturbators or rapid deposition and/or reworking overwhelming the ability of benthic biota to mix the seabed. Mixed or mottled sediments were indicative of times with either very active bioturbation or low rates of sediment deposition (Schaffner et al., 1987b).

Digital X-radiographs from the GP site (Figures 3-3a, 3-3b, 3-3c) reveal little temporal variability in the structure of the seabed. Sediments from this site appeared moderately bioturbated when compared to other published results from the Chesapeake Bay main stem and York River (Schaffner et al., 2001; Dellapenna et al., 1998). Fine scale laminations were rare but occasionally observed in the top 3-5 cm of the bed. Coincident with a substantial increase in erodibility in May 2007, a 1 to 2 cm thick layer of more X-ray transparent material was present in May 2007 (Figure 3-3b) but not observed in April or June 2007 (Figures 3-3a and 3-3c), suggesting recent deposition of an ephemeral, thin layer of highly erodible material.

Similar to the GP site, digital X-radiographs from the CS site often appear mixed with few laminations (Figure 3-3d). However, a more uniform surface layer, occasionally

containing thin laminations and ranging in thickness from 1 to 15 cm thick, was occasionally observed (Figures 3-3e and 3-3f). This layer was most distinct in March, April, and May 2007.

Digital X-radiographs from the CC site revealed the most dramatic seasonal variability in bed structure. From May through September 2006 the bed appeared mottled and relatively featureless (Figure 3-3g). In November, a surface layer, approximately 2 cm thick and containing many fine laminations appeared (Figure 3-3h). Similar fine laminations were then observed in January 2007 (Figure 3-3i) down to a depth of about 10 cm. By March and April 2007, the laminations spanned the entire length of the X-ray cores ($\sim$15 – 18 cm) with many thick laminations ($\sim$1 cm) observed throughout (Figures 3-3j and 3-3k). In May 2007 only traces of laminations remained and by June 2007 laminations were absent from X-radiographs and the cores appeared generally mottled and featureless once again (Figure 3-3l).

3.4.3 Solids fraction, sand fraction, and organic fraction

Total solids fraction (ϕ_{stot}), solids fraction of the mud matrix (ϕ_{sm}), and sand fraction (f_s) were determined for sediments from the top centimeter of the bed to evaluate the degree of consolidation of the bed and its relationship to erodibility. Based on the results presented in Chapter 2, ϕ_{sm} is expected to be the most direct proxy for erodibility among these variables. Including the data from all three York River sites, ϕ_{sm} ranged from about 0.08 to 0.14 (Figure 3-4a) suggesting poorly consolidated sediments. No
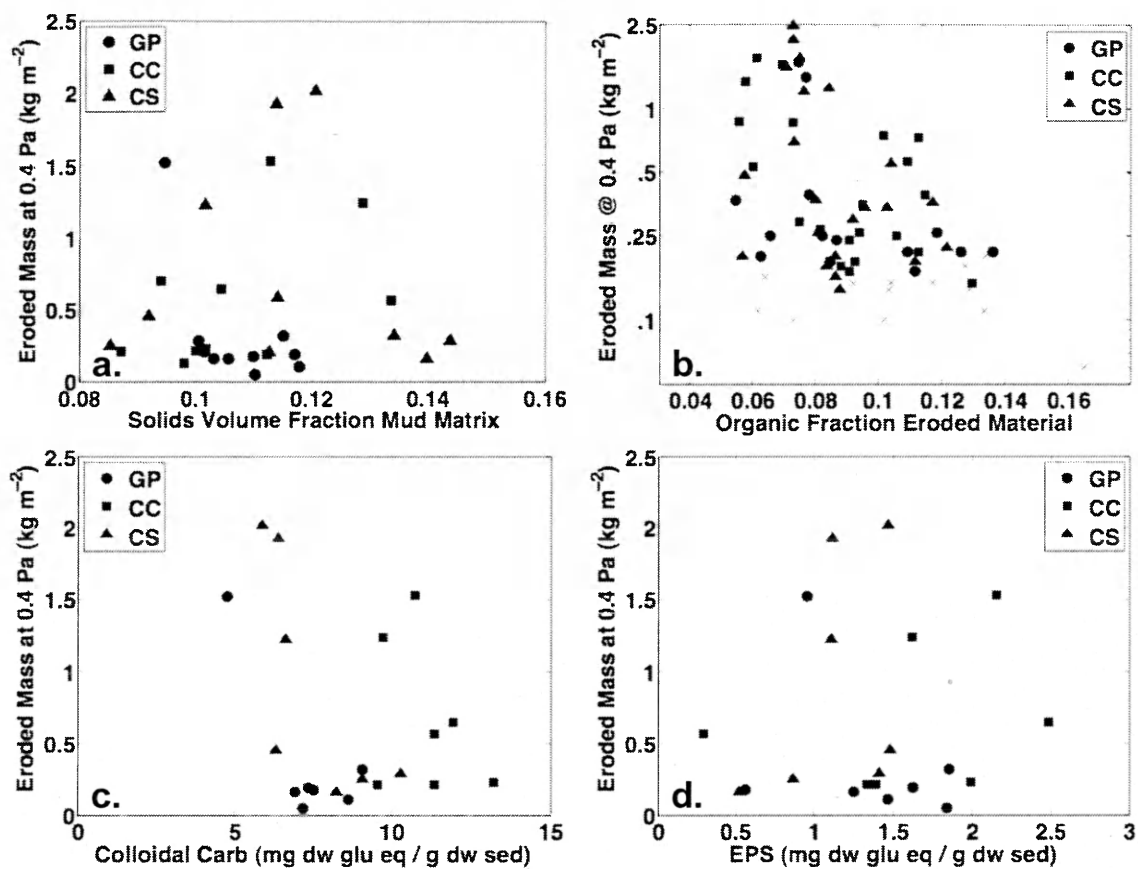
Figure 3- 4 Eroded mass at 0.4 Pa as a function of: **a.** solids volume fraction mud matrix of top centimeter of bed (modified from Chapter 2), **b.** organic fraction of eroded material, from the first 0.3 kg m^{-2} eroded, **c.** colloidal carbohydrate concentration, **d.** extracellular polymeric substance (EPS) concentration. Units in c. and d. are milligrams dry weight glucose equivalents per gram dry weight sediment. X's in b indicate cores in which less than 0.3 kg m^{-2} total sediment was eroded during erosion measurement. EPS and colloidal carbohydrate data provided by Dr. Schaffner's lab.

significant correlation was found between the eroded mass at 0.4 Pa and ϕ_{sm}, ϕ_{stot}, or f_s

(Table 3-2; see also Chapter 2). Values of ϕ_{sm} during periods of low erodibility spanned

the entire range, while ϕ_{sm} associated with periods of highest erodibility fell roughly in

the middle of the range.

The organic fraction (by weight) of the eroded sediment was determined by loss

on ignition for each applied stress step of each core eroded. There was a tendency for the

material eroded at lower stresses to be enriched in organic matter relative to the material

eroded at higher stresses. The organic fraction at an applied stress of 0.05 Pa was often

0.2 or greater although the total mass of material eroded was generally quite small at this

low applied stress. In general, the organic fraction decreased with depth into the bed (as

measured by eroded mass) and the total organic fraction decreased with total mass

eroded. An aim of this study was to evaluate the influence of organic material on

erodibility, making it necessary to prevent biasing of the organic fraction by its

correlation with the total mass eroded. To do so, we always analyzed the same portion of

the upper seabed for organic matter to allow comparison of the same mass depth interval

of sediment.

The organic fraction of eroded sediment as shown in Figure 3-4b represents the

organic fraction of the first 0.3 kg m^{-2} of sediment eroded from each core. A weak but

statistically significant (p<0.01) negative correlation was found between the eroded mass

at 0.4 Pa and the organic fraction of eroded material to a mass depth of 0.3 kg m^{-2} (Figure

		ϕ_{stot}	ϕ_{sm}	f_s	Organic fraction eroded sediment	Colloidal Carbohydrate	EPS
Eroded mass @ 0.4 Pa	R	0.191	0.0667	0.131	-0.445	-0.341	0.0526
	p	.313	0.726	0.492	<0.01	0.130	0.821
	# samples	30	30	30	57	21	21
	Time interval	4/06 – 6/07	4/06 – 6/07	4/06 – 6/07	4/06 – 10/07	9/06 – 6/07	9/06 – 6/07

Table 3- 2 Correlation table relating eroded mass at 0.4 Pa to selected measured sediment properties. R is Pearson's rho. p is p-value. # of samples refers to the number of samples used to determine R. For ϕ_{stot}, ϕ_{sm}, f_s, colloidal carbohydrates, and EPS, this represents the number of mean values of each property that was related to eroded mass. For organic fraction eroded sediment, this value represents the number of eroded cores included in this comparison.

3-4b and Table 3-2). However, with a R value of only -0.445 this relationship only

explained 20% of the variance in the data, indicating that either an increase in organic

content plays a relatively small role in increasing cohesion in the bed or that organic

content may be a tracer varying in concert with some other factor influencing bed

cohesion.

3.4.4 Colloidal carbohydrates and extracellular polymeric substances

The concentrations of colloidal carbohydrates and extracellular polymeric

substances (EPS) were measured as a proxy for biostabilization by benthic and/or particle

associated organisms. In contrast to the erodibility results and digital X-radiograph

comparisons, EPS concentrations were relatively similar for all three sites (Figure 3-4d).

Colloidal carbohydrate concentrations tended to be higher at CC than the other two sites

(Figure 3-4c). Including all three sites, colloidal carbohydrates concentration varied by

about a factor of 3, ranging from about 4 to 13 milligrams dry weight glucose equivalents

per gram dry weight sediment (mg dw glu eq / g dw sed). EPS concentration varied by

approximately an order of magnitude, ranging between 0.3 and 2.5 mg dw glu eq / g dw

sed. However, the majority of samples fell within a smaller range, with approximately

two-thirds of the samples having colloidal carbohydrates concentrations of 5 to 10 mg dw

glu eq / g dw sed and EPS concentrations of 1 to 2 mg dw glu eq / g dw sed. There were

no apparent seasonal variations in colloidal carbohydrate or EPS concentrations.

Comparison of colloidal carbohydrates and EPS concentrations and eroded mass at 0.4 Pa

revealed no significant correlation (Figure 3-4c and 3-4d and Table 3-2).

3.5 Discussion

3.5.1 Seasonal cycle in erodibility: The role of biology versus deposition

Two sites (CS and CC) located in the Clay Bank region of the York River estuary

exhibited a pronounced seasonal cycle in seabed erodibility (Figure 3-2). Both CS and

CC had consistent and relatively low erodibility in the summer and fall of 2006 and 2007

and elevated erodibility in the late winter and spring of 2007. CS and CC also exhibited

what appear to be transitional periods of moderate and presumably increasing erodibility

prior to the periods of highest erodibility found in late winter and spring of 2007. Similar

levels of moderate erodibility in May 2006 may represent a transitional period of

decreasing erodibility after a period of elevated erodibility prior to the onset of sampling.

Further evidence suggesting this may be a recurring seasonal pattern was presented in

Maa and Kim (2002). They presented results of erodibility measurements conducted

with a Sea Carousel in the Clay Bank region about 4 kilometers up-estuary from the CS

site (also in the secondary channel) in winter, spring, summer, and fall of 1995. They

found the lowest critical stress for initiation of motion and by far the highest erosion rate

to occur in May. In fact, their reported erosion rates in May were 80 to 400 times what

they reported for summer and winter.

With respect to biological influences on erodibility, it would be expected that the magnitude of bioturbation would be in phase with seasonal variations in water temperature (Bender and Davis, 1984; Gerino et al., 1998). Thus, we expected a bioturbation maximum when water temperature was high (Figure 3-2d) resulting in enhanced erodibility in summer and fall (Widdows et al., 2000; de Brouwer et al., 2000; Andersen, 2001). Contrary to this, the highest measured erodibility occurred in the late winter and spring when the water temperature was low. Further indication that bioturbation was not the cause of elevated erodibility was found in the X-radiograph images from CC (Figures 3-3j and 3-3k) depicting strongly laminated sediments coincident with periods of highest erodibility and indicating a seabed sculpted by physical processes with relatively little disruption by bioturbators.

Potentially counteracting the influence of biodestabilization, biostabilizing influences can bind sediment together and decrease erodibility. In mudflat environments, where biofilms are common, colloidal carbohydrate and extracellular polymeric substance concentrations have proven to be proxies for bioadhesion (Paterson et al., 2000; Widdows et al., 2004). In these settings, erodibility has been negatively correlated to colloidal carbohydrate and/or EPS concentrations. However, it was not clear that similar results should be expected at depths of 5 - 12 meters in the Chesapeake Bay, an environment where little light reaches the seabed and that lacks the diatom mats found on tidal mudflats.

74

Contrasting the results from mudflat settings, colloidal carbohydrate and EPS concentrations sampled at the GP and Clay Bank sites did not correlate well to variations in bed erodibility (Figures 3-4c and 3-4d and Table 3-2). This suggests that either biostabilization was not responsible for variations in bed erodibility or that colloidal carbohydrates and EPS were not the appropriate measure of biostabilization in this environment. Further, colloidal carbohydrate and EPS concentrations at our sites were relatively consistent in both space and time. This indicates that while EPS was a potential and likely influence on sediment cohesivity in the York River, it did not vary significantly and thus did little to influence seasonal and spatial variations in bed erodibility.

Previous studies in the York River have indicated that the Clay Bank region is generally physically dominated, with strong tidal currents, high suspended sediment concentrations (Lin and Kuo, 2001), records of erosion and deposition in the seabed (Dellapenna et al., 1998) and a depauperate benthic community dominated by short lived opportunistic species (Schaffner et al., 2001). Lin and Kuo (2001) found this region to be seasonally occupied by an ephemeral secondary turbidity maximum (STM), the location of which was related to river flow and salinity. Their results demonstrated that in the Clay Bank region, high suspended sediment concentrations associated with a STM occurred in winter and/or spring following periods of elevated river flow, decreased salinity, and increased stratification (Figure 3-5). While the present study did not include hydrographic surveys documenting the location of the STM, the very high seabed
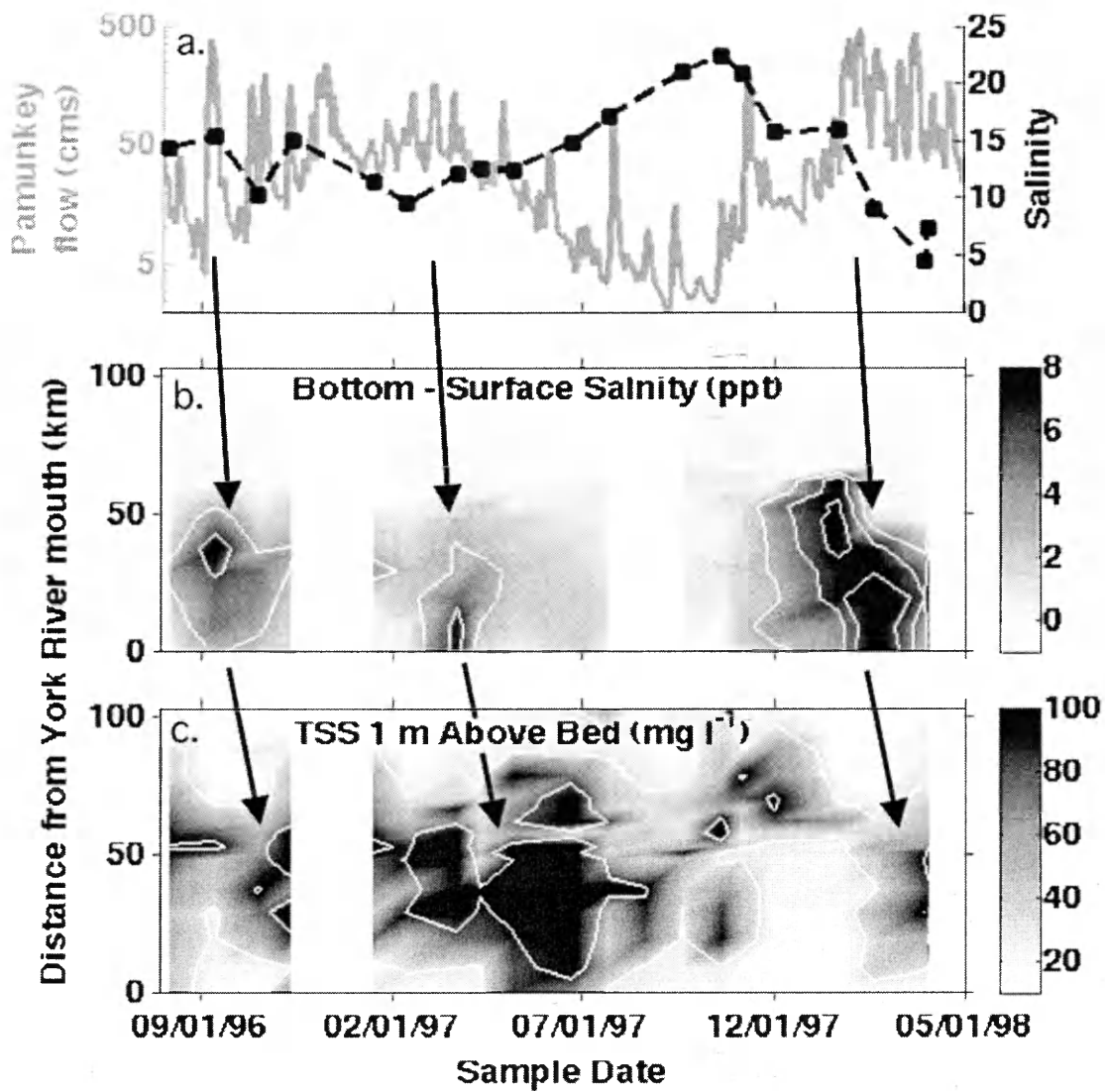
Figure 3- 5 a. Time-series of Pamunkey River flow (solid gray line) measured at Hanover, VA, and depth-averaged salinity (dashed black line) in the York River near Clay Bank. Squares indicate timing of surveys from Lin and Kuo (2001). **b.** Time-series of bottom – surface salinity along York River. **c.** Time-series of near bottom total suspended solids (TSS) along York River. In Figures b and c, Gloucester Point, Clay Bank and West Point are ~ 10, 25 and 55 km from the York River mouth, respectively. Arrows highlight time-lags between episodes of high river flow, salinity stratification, and high sediment concentration in the Clay Bank region. River flow data from USGS Water Data website at *http://waterdata.usgs.gov/nwis*. All other data from Lin and Kuo (2001).

76

erodibility which we observed seasonally in the Clay Bank region also followed high

river discharge and low salinity (see Figure 3-2), and we conclude that high erodibility

was most likely associated with the seasonal STM.

While relatively low levels of erodibility were observed near the onset of high

river flow conditions in November, it is expected that there should be some lag period

while conditions favorable for convergent sediment transport develop, and sufficient

convergence occurs to result in a large increase in bed erodibility. The gradual increase

in erodibility at Clay Bank from November through March (Figures 3-2b and 3-2c)

indicates this process may occur on a time scale of months. Additionally, the lack of a

similarly clear seasonal pattern at GP (Figure 3-2a), outside the region where the STM

has normally been observed, further supports this to be the process causing seasonal

increases in erodibility at Clay Bank. Finally, the deposition of a thick sequence of

laminated sediments at CC, beginning in November 2007 and reaching a thickness of

greater than 15 cm in March and April 2007 (Figure 3-3h - 3-3k), indicates periodic rapid

deposition in this area. The deposition of more than 15 cm of sediment in about 6 months

greatly exceeds the long-term accumulation rate in this area of about 0.2 cm yr^{-1}

(Dellapenna et al., 1998), indicating the deposit itself may be ephemeral, presumably

migrating seasonally with the location of the STM. Further indication of periodic rapid

deposition occurring near Clay Bank in the spring was presented in Kniskern and Kuehl

(2003) who found thick laminated sequences in the surface sediments of the Clay Bank

region in March through May of 1999. Additionally, they found the depth of maximum ^{137}Cs penetration to increase by about 20 cm from February to April of 1999.

3.5.2 Limited spatial variation in erodibility: Indications of a background equilibrium condition

Our measurements from the York River (Figure 3-1), as well as comparison to other published works, provide insight on spatial variation in bed erodibility in the York River estuary and Chesapeake Bay. Small-scale variation on the order of meters to tens of meters was evaluated by comparing erodibility at a given site from duplicate cores during a single sampling period and from multiple cores at a given site during extended periods of relatively constant bed erodibility. Variation on the order of a kilometer was evaluated by comparing the two Clay Bank sites, while variation over 10s to hundreds of kilometers was addressed by comparing the results from the Clay Bank sites to the GP site as well as to other published data from the Chesapeake Bay.

Cores were collected for erodibility measurements while swinging on anchor, and no two erodibility cores were collected from the same box core. Consequently, the variation in results from a given site and sampling period incorporate spatial variation on the order of meters to tens of meters, providing an indication of relatively small-scale variation in bed erodibility. As some of this variation may be due to core collection and handling, this comparison may overestimate small-scale variations. For individual pairs of cores run simultaneously, the eroded mass at 0.4 Pa had an average deviation of only

9% from the mean. On many occasions, the two cores are nearly identical, indicating consistency in the sampling and measurement procedure and negligible small-scale spatial variation. Additionally, the regular occurrence of a consistent level of relatively low erodibility (for example August, September, November 2006 at CC) suggests that even spatial variations associated with attempting to re-occupy a given site (~50 to 100 meters) have minor effects on the measured erodibility.

Comparing the time-series data from the two Clay Bank sites indicates that even on a spatial scale of kilometers there may not be substantial variability in bed erodibility within a given environment (in this case mid-depth and muddy). The two Clay Bank sites were approximately 1 kilometer apart and at different depths (6 m vs. 11 m). Despite this, both sites exhibited quite similar behavior both in terms of the mass of sediment eroded and the timing of seasonal changes in bed erodibility (Figures 3-2b and 3-2c). Only upon comparing the results from the Clay Bank sites to GP were large spatial differences in bed erodibility occasionally observed. GP did not exhibit the seasonal pattern found at Clay Bank and five of the twelve times sampled, eroded mass at the Clay Bank sites was two to ten times that at GP. However, during the remaining seven times each site was sampled, all between the months of June and November in both 2006 and 2007, the eroded mass was quite similar for all three sites.

Erodibility was quite consistent for nearly half of each year, on a spatial scale of tens of kilometers along the axis of the estuary, and at depths ranging from about 6 to 11 meters. Impressively, combining all the GP data (except for May 2007) with
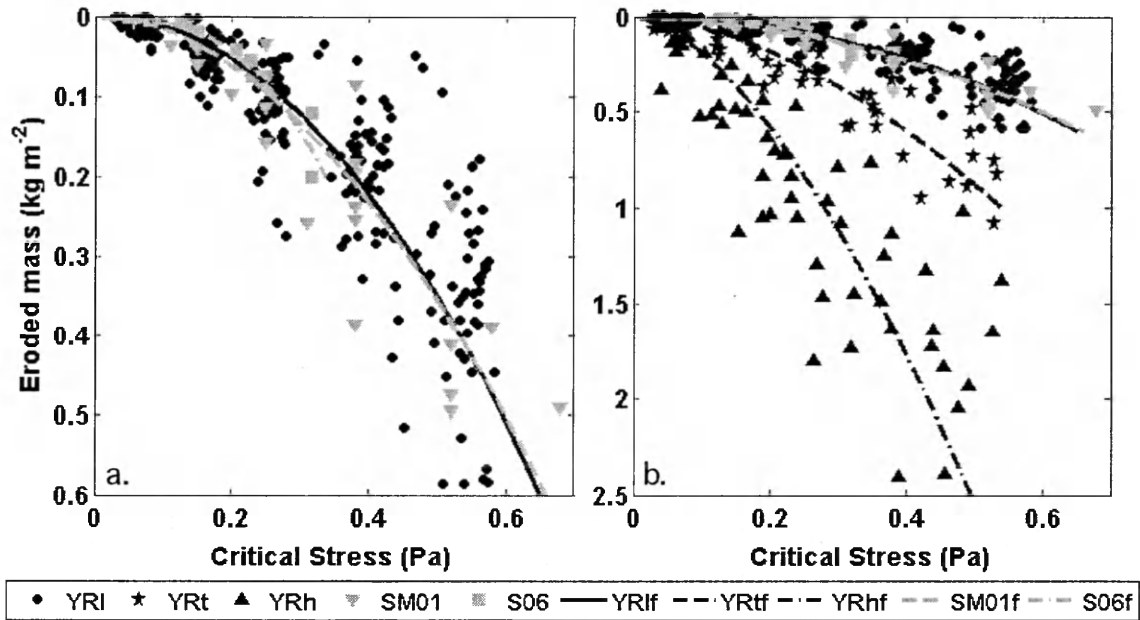
Figure 3- 6 Profile of critical stress for erosion versus eroded mass including: **a.** data and power law best fits from Sanford and Maa (2001), Sanford (2006), and York River "low" erodibility periods, **b.** data from Figure 3-6a as well as York River "transitional" and "high" erodibility data and power law best fits. YRl = York River low erodibility, YRt = York River transitional erodibility, YRh = York River high erodibility, SM01 = Sanford and Maa (2001), S06 = Sanford (2006), YRlf = fit to YRl, YRtf = fit to YRt, YRhf = fit to YRh, SM01f = fit to SM01, and S06f = fit to S06.

data from both Clay Bank sites from July, August, September, and November of 2006

and June, August, and October of 2007 yielded a mean eroded mass at 0.4 Pa of 0.21 kg

m^{-2} with a standard deviation of only 0.082. This included 50 of the 72 total cores eroded

and indicated a surprisingly consistent level of erodibility within the York River much of

the time. This may represent an equilibrium background condition characteristic of mid-

depth muddy sites in this system provided the absence of recent deposition.

The results of several other published erodibility measurements from elsewhere in

the Chesapeake Bay region are quite similar to the results presented here from the York

River estuary. Sanford and Maa (2001) presented the results of erodibility measurements

conducted with a Sea Carousel at four sites in Baltimore Harbor, MD. Additionally,

Sanford (2006) presented erodibility measurements conducted with a Gust microcosm

system from one site in the main stem of the upper Chesapeake Bay. Data from the

present study representing the "low" erodibility condition as discussed in the previous

paragraph are presented along with data from Sanford and Maa (2001) and Sanford

(2006) in Figure 3-6a. Best fit power law regressions in the form of $\tau_c = am^b$, where $\tau_c =$

critical stress for erosion, m=cumulative eroded mass, and a and b are coefficients, were

applied to the Sanford and Maa (2001), and Sanford (2006), and York River data (Figure

3-6; Table 3-3). Interestingly, the range and best-fit power law regression for the four

Baltimore Harbor sites from Sanford and Maa (2001) were nearly identical to the range

and a best-fit power law regression for the "low" erodibility condition presented in this

study. Additionally, the data from the upper-Chesapeake Bay main stem site presented in

Sanford (2006) fell roughly in the middle of the range of data from both the York River and Baltimore Harbor.

Figure 3-6b contains the data presented in Figure 3-6a as well as the higher erodibility data from the York River. The entire York River data set displayed in Figure 3-6b was grouped into 3 categories based on erodibility. Low erodibility cases had a mean eroded mass at 0.4 Pa of less than 0.4 kg m^{-2}, transitional cases had a mean eroded mass at 0.4 Pa of 0.4 to 0.8 kg m^{-2}, and high erodibility cases had a mean eroded mass at 0.4 Pa of greater than 0.8 kg m^{-2}. All periods in the transitional group were from the CC or CS sites and immediately preceded an extended period of either low or high erodibility. Clearly, the largest variations in bed erodibility were observed seasonally at Clay Bank, indicating that turbidity maximum zones may experience seasonal changes in sediment flux convergence resulting in a dynamic seabed and highly variable bed erodibility. Additionally, it appears that muddy areas outside turbidity maximum zones generally exhibit a somewhat consistent level of bed erodibility in both space and time. The data presented in Figure 3-6a and relationship in Table 3-3 (for either Sanford and Maa (2001) or York River low erodibility cases) may be a good approximation of the range and mean of this apparently common equilibrium condition of bed erodibility in muddy areas of moderate depth in the Chesapeake Bay.

Name	a	b	R^2	# of samples
Sanford and Maa (2001)	0.862	0.526	0.88	6
Sanford (2006)	0.590	0.349	0.95	2
York River (low erodibility)	0.832	0.486	0.87	50
York River (transitional)	0.540	0.590	0.91	10
York River (High erodibility)	0.280	0.620	0.84	12

Table 3- 3 Power law fit parameters relating critical stress for erosion to eroded mass. Fit was in the form $\tau_c = am^b$, where τ_c = critical stress for erosion (Pa) and m = cumulative eroded mass (kg m^{-2}). For Sanford and Maa (2001), # of samples represents the number of individual deployments of the VIMS Sea Carousel. For the remaining data, # of samples represents the number of individual cores eroded with a Gust erosion microcosm.

3.5.3 Erodibility and biological impact on solids fraction

We can safely conclude that the seasonal pattern in bed erodibility observed in the Clay Bank region of the York River estuary was ultimately due to temporal and spatial variability in convergent sediment transport processes. However, neither this study nor a related work (see chapter 2) was able to relate changes in erodibility in the York River to bulk physical or biological properties of the bed (Figure 3-4). For the most part, colloidal carbohydrates and EPS proved to be consistent spatially and temporally, suggesting that while these proxies for bioadhesion may still have influenced the overall cohesivity of the bed, they did so more-or-less evenly over the duration and areal extent of our study. Thus, it does not appear that standard biochemical proxies for bioadhesion were primarily responsible for the observed variations in bed erodibility.

Bulk geophysical proxies for bed cohesion / consolidation in the York River estuary (e.g., water content, sand fraction) likewise did not correlate sensibly with bed erodibility (also see Chapter 2). Particularly interesting was the relative consistency in the bulk solids fraction of the mud matrix (ϕ_{sm}) in the York River seabed in time and space. In contrast, when the range was expanded by including data from seven diverse cohesive environments, ϕ_{sm} was shown in Chapter 2 to resolve changes in the bed consolidation state much better than the total solids fraction (ϕ_{stot}), since ϕ_{stot} is often confounded by changes in sand fraction. In the York River, however, even during periods of rapid deposition and high erodibility, there was not a resolvable decrease in

ϕ_{sm}. This indicates either a change in cohesivity unrelated to ϕ_{sm}, or that bulk ϕ_{sm} as determined from slices of the top centimeter of sediment was not sufficient to resolve millimeter-scale changes in bed consolidation responsible for changes in erodibility.

The observed variations in erodibility must be reflected in some property of the sediment bed. A possible explanation may be the degree of pelletization of the sediment by biota. Previous studies in the region have observed fecal pellets to represent an important component of spatially varying surficial sediments (Schaffner et al, 1987b; Schaffner et al., 2001) and of suspensions tending to remain near the seabed (Wright et al., 1997). Off the coast of Peru, Reimers (1982) similarly observed changes in the fabric near the surface of the seabed to be associated with the presence of pelletized sediment. Anecdotal observations of eroded material and sediment core surfaces from this study in the York River estuary indicated that pelletized sediment can represent a large fraction of the surficial sediments and eroded material (Figure 3-7). Ongoing observations are focusing on the distribution and nature of these pellets. During periods of low erodibility, dense, fast-settling pellets appeared to dominate the eroded material. Conversely, during periods of higher erodibility, suspensions within the Gust microcosm appeared to be composed primarily of finer material. In the York River estuary, pelletization represents a significant repackaging of muddy sediment, potentially altering the cohesion of the surficial seabed during periods of elevated activity by benthic biota and modifying the relationship between ϕ_{sm} and erodibility.

The presence of burrows may be another factor altering the structure of the seabed. However, the net effect of burrows on bulk geophysical measures is not entirely clear. For example, Jones and Jago (1993) found that the presence of burrows in sandy sediment altered seabed structure as indicated by geophysical measures but was not reflected in bulk measures of sediment porosity from sediment samples. Conversely, Rowden et al. (1998) found a positive correlation between the abundance of burrowers and the bulk water content of cohesive sediment. But Murray et al. (2002) point out that some burrowers may increase the shear strength of freshly deposited cohesive sediment by increasing permeability and, thus, hastening dewatering. Images from a benthic camera deployed across the sediment-water interface (Figure 3-8a) in the York River estuary near Gloucester Point in March 2008 revealed heterogeneity in the seabed resulting from burrows. Although we recognize that glass barriers may cause burrowers to congregate, burrowing still represents a potential mechanism for altering the seabed structure and confounding the expected relationship between ϕ_{sm} and bed erodibility.

In a physically dominated seabed the structure of the bed is overwhelmed by depositional processes, often resulting in a laterally homogenous bed as illustrated in Figure 3-8b. In this case, the total solids fraction as measured by a bulk sediment sample (ϕ_t) is equal to the solids fraction of the sediment matrix (ϕ_1), and ϕ_t accurately portrays the microstructure and degree of consolidation of the bed. Conversely, in a biologically altered seabed, burrows and/or pellets may introduce heterogeneity into the bed,

86
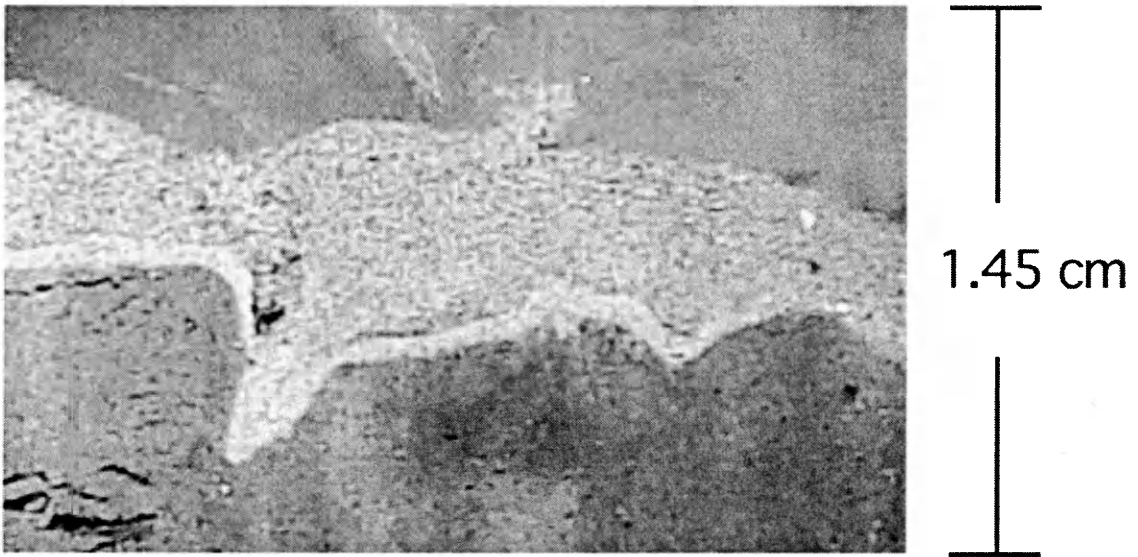
Figure 3- 7 Image from sediment profile camera illustrating highly pelletized surficial sediments. Image collected near Gloucester Point in May 2008 following methods of Diaz and Cutter (2001). Camera pixel size is ~69 μm. Sediment image provided by Dr. Diaz.
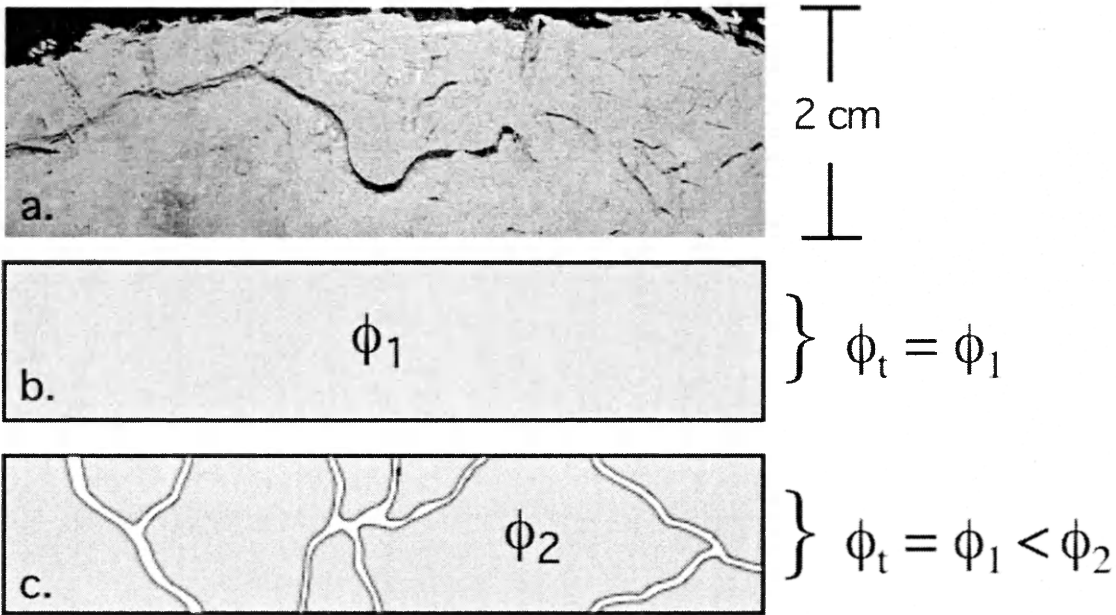
Figure 3- 8 a. Image from sediment profile camera illustrating abundance of burrows in surficial sediments, collected near Gloucester Point in March 2008. Conceptual images depicting: **b.** homogeneity in a physically dominated seabed, **c.** heterogeneous seabed containing burrows. ϕ_t = bulk solids volume fraction, ϕ_1 = solids volume fraction of sediment matrix, and ϕ_2 = solids volume fraction of sediment matrix. Sediment image provided by Dr. Diaz.

complicating the validity of bulk measures of solids fraction such as the centimeter-thick

sediment slices used in this study. The solids fraction of a burrowed bed is illustrated

conceptually in Figure 3-8c. In this case, the idealized bed is composed of a non-

burrowed sediment matrix (average solids fraction = ϕ_2) and numerous dissecting

burrows (solids fraction = 0). A mixture such as this may have an apparent solids

fraction, as measured by a bulk sediment sample, nearly equal to the physically

dominated case ($\phi_t \approx \phi_1$). However, in this case, the solids fraction of the sediment matrix

would have to be greater than in the physically dominated bed ($\phi_2 > \phi_1$).

In the presence of burrows or pellets, the relationship between the solids fraction

of the sediment matrix found between voids (ϕ_2) and the solids fraction of the bulk

sediment sample (ϕ_t) can be represented by

$$\phi_2 = \frac{\phi_t}{1 - \phi_v} \qquad \text{(Eq. 2)}$$

where ϕ_v is the volume fraction of voids (burrows or space between pellets). If the

concentration of voids increases, but ϕ_t as measured by bulk sediment samples remains

nearly constant, then ϕ_2, representing either the solids fraction of the matrix between

burrows (Figure 3-8c) or the solids fraction of pellets, must have increased. Equation 2

indicates that in a bed composed of 10% burrows, for example, ϕ_2 will be about 11%

greater than ϕ_t. If ϕ_2 is actually the more accurate representation of surficial erodibility,

then the lower value provided by the bulk solids fraction may mask the true relationship

between the fine-scale solids fraction and the critical erosion stress. Figure 3-9 highlights
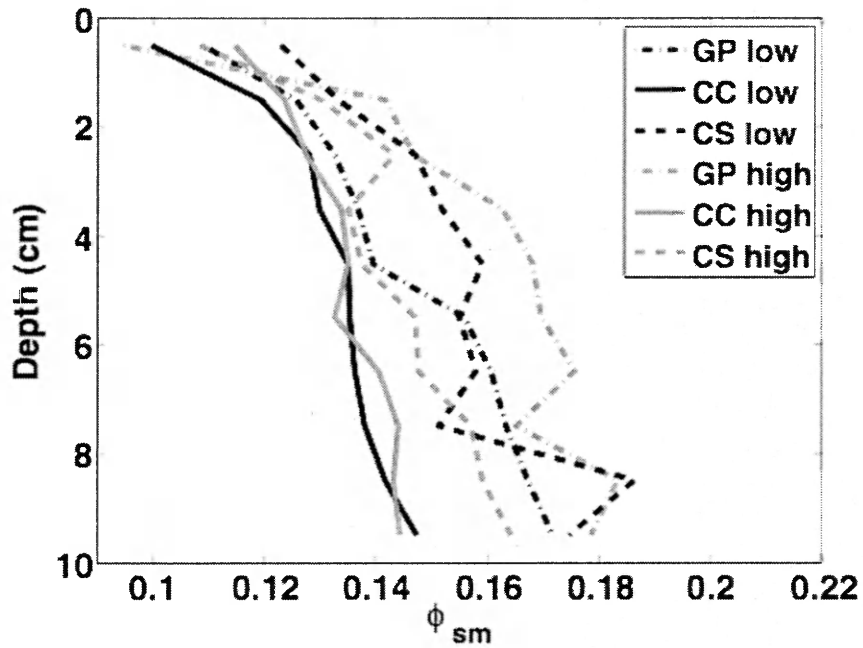
Figure 3- 9 Depth profiles of bulk solids volume fraction of the mud matrix from each of the three sites in the York River. Data was grouped and averaged by erodibility. Profiles named "low" indicate samples collected when eroded mass at 0.4 Pa was less than 0.4 kg m^{-2}. Profiles named "high" indicate samples collected when eroded mass at 0.4 Pa was greater than 0.4 kg m^{-2}.

how small the mean differences are in the bulk solids fraction among cores collected in the York River estuary. The differences in the unsampled microstructure-scale solids fraction (which accounts for the presence or absence of burrows or density of pellets) may have been significantly larger.

Since the Gust erosion microcosm quantifies small-scale surface erosion associated with typical resuspension by individual tidal cycles, controls on our resulting measurements of erodibility are likely dominated by microstructure-scale bed properties. We believe that as a result, the 1-cm core slices used in this study may have been too large to resolve changes in bed consolidation on scales small enough to explain the observed variations in bed erodibility. It is therefore likely that changes in seabed structure associated with biologic pelletization and/or burrowing confounded the observed relationship between ϕ_{sm} and erodibility. It is important to note that while we believe the microstructure scale may be dominant in controlling surface erosion, it is not clear how this translates to larger scales of erosion. For instance, the presence of burrows likely weakens the bed and enhances erodibility when considering erosion on the scale of several centimeters. In such a case, it is likely that the heterogeneity associated with burrows may provide a tendency for mass erosion rather than surface erosion.

3.6 Conceptual model and conclusions

The combined results of this and previous studies of the York River estuary suggest an active system with dynamic and variable sediment transport processes. A

91

After period of high river flow

20 ‰   15 ‰   10 ‰   5 ‰   0 ‰

Gloucester Point   Clay Bank   West Point

After period of low river flow   Near bed sediment flux

Salinity isohalines   20 ‰   15 ‰   10 ‰   5 ‰   0 ‰

Pelletized sediment   Low suspended sediment concentrations   High suspended sediment concentrations

Fines and/or flocs

Laminated seabed

Mottled seabed
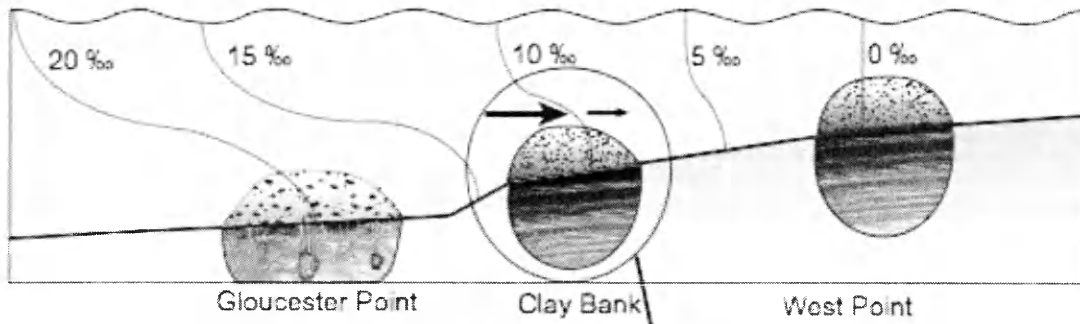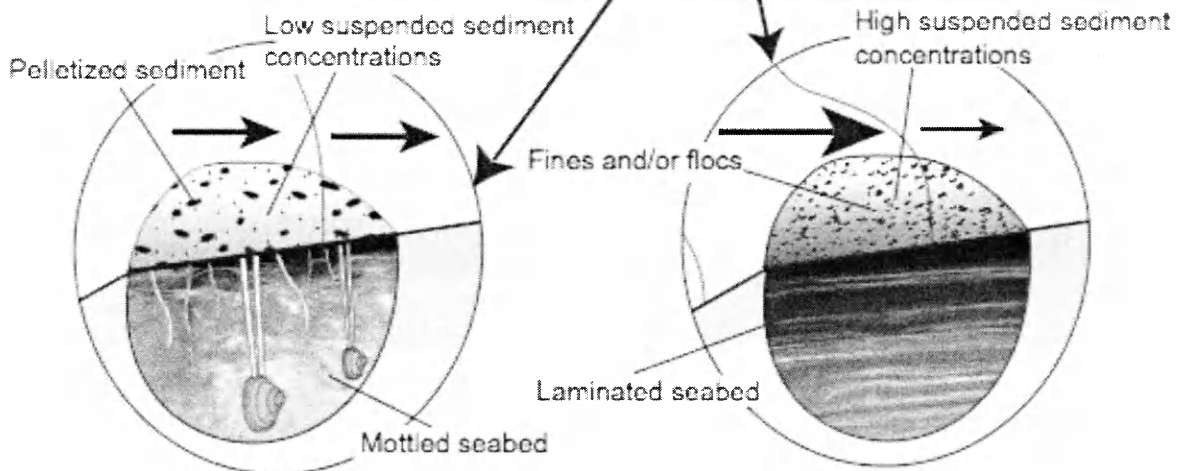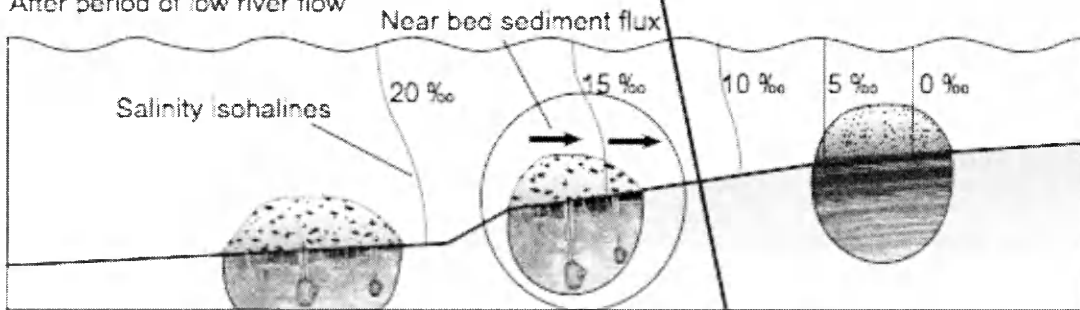
-After low river flow

-Little or no stratification

-No sediment flux convergence

-No STM

-Low erodibility

-After high river flow

-Stratified

-Sediment flux convergence

-STM

-High erodibility

92

Figure 3- 10 Conceptual diagram depicting sediment transport processes in the York River estuary. Symbols courtesy of the Integration and Application Network (ian.umces.edu/symbols/), University of Maryland Center for Environmental Science.

persistent estuarine turbidity maximum is located near the limit of salt just up-estuary

from West Point. Following periods of high river flow, a secondary turbidity maximum

(STM) tends to form in the middle estuary near Clay Bank (Figure 3-10). The STM is

found near a transition from stratification in the lower estuary to more mixed-conditions

up-river, triggered in part by a localized along-estuary decrease in channel depth (Lin and

Kuo, 2001). The transition in stratification favors a convergence in up-estuary near-bed

sediment flux due to resulting spatial gradients in tidal asymmetries and gravitational

circulation.

The presence of the STM near Clay Bank results in high suspended sediment

concentrations dominated by fines and flocs, rapid deposition of an ephemeral deposit

10's of centimeters thick, a physically dominated seabed, and high bed erodibility (Figure

3-10). The lower estuary, including our Gloucester Point site, lies outside of the region

typically occupied by the STM. The result at Gloucester Point is lower suspended

sediment concentrations, highly pelletized surficial sediment, a more actively burrowed

seabed, and low erodibility throughout the year. After an extended period of low river

flow, stratification throughout the estuary breaks down, and the STM either moves up-

estuary or dissipates, resulting in a period of divergent sediment transport and/or

sediment bypassing. During this period, the conditions near Clay Bank more closely

resemble Gloucester Point, with lower suspended sediment concentrations, increasingly

pelletized sediment, more intense bioturbation near the sediment water interface, and

lower erodibility (Figure 3-10).

A similar spatial gradient with regards to suspended particle properties was observed by Fugate and Friedrichs (2003). At Clay Bank in May 2000, Fugate and Friedrichs (2003) documented relatively high concentrations (up to 230 mg l^{-1}) of fragile suspended flocs that settled at 0.6 mm s^{-1}. At a biologically dominated site in the adjacent Chesapeake Bay, they observed lower concentrations (up to 75 mg l^{-1}) of resilient suspended pellets that settled at 1.3 mm s^{-1}.

The largest scale variations in bed erodibility appear to be mainly a function of physical processes facilitating periodic sediment flux convergence and rapid deposition of easily erodible material. The commonly observed condition of "low" erodibility likely represents a more biologically influenced bed with "low" erodibility resulting from a dynamic equilibrium between (i) physical resuspension and consolidation and (ii) biological reworking and repackaging. This "equilibrium" magnitude and range of erodibility was observed throughout most of the year at both Clay Bank and Gloucester Point and also in historical data from other Chesapeake Bay sites, suggesting the low erodibility, biologically mediated scenario may be broadly representative of other cohesive estuarine environments in the absence of rapid deposition.

Standard geophysical and biochemical proxies for consolidation and bioadhesion provided no explanation for the observed variations in bed erodibility. The surprising lack of systematic variation in observed colloidal carbohydrate and EPS concentrations suggests that the forms of biostabilization highlighted in erodibility studies in inter-tidal areas may not translate to an estuarine environment where little light reaches the seabed.

The lack of correlation between erodibility and the bulk solids fraction of the mud matrix suggests that the presence of biologic structures may have confounded the expected relationship. In physically dominated cases, a laterally homogeneous bed may allow bulk samples to adequately reflect the relevant microstructure. In contrast, the presence of burrows may cause the bulk solids fraction to be lower than the solids fraction of the millimeter-scale surficial sediment most relevant to erosion by moderate strength tidal currents.

Chapter 4

Conclusions and Future Work

4   Conclusions and Future Work

A time-series of bed erodibility and physical and biological properties of the surficial sediment was used to evaluate seasonal and spatial scales of variability in bed erodibility and the associated bed properties. Erodibility was found to vary substantially in both time and space but this variation was not clearly correlated to the measured properties of the bed.

Chapter 2 specifically focused on relating key physical bed properties to bed erodibility. The total solids fraction of the bed, commonly measured to represent the degree of consolidation of a cohesive sediment bed, was not correlated to bed erodibility. However, a strong correlation between bed sand fraction and total solids fraction indicated that variation in bed solids fraction was largely a function of sand fraction. This suggested that total solids fraction may not be an ideal proxy for bed consolidation and its relationship to cohesive sediment erodibility may be complicated by variations in sand fraction.

To better represent the degree of consolidation of the muddy matrix supporting the bed, an analytical relationship from Sanford (2008) was used to calculate the solids fraction of the mud matrix. This metric of consolidation did not correlate to the observed variations in bed erodibility in the York River. However, when the range was expanded using other published data, the solids fraction of the mud matrix demonstrated a strong

correlation to the initial critical stress for erosion for a range of environments. This suggests that while this approach is valid, the range of solids fraction of the mud matrix at our sites in the York was insufficient to adequately evaluate this parameter as a proxy for consolidation and develop a relationship between solids fraction of the mud matrix and the critical stress for erosion.

The small range in surficial solids fraction of the mud matrix in the York River estuary could be expanded considerably by eroding deeper into the bed. To more adequately assess using the solids fraction of the mud matrix as a proxy for bed consolidation, future work should include larger scales of erosion not possible with the Gust erosion microcosm device used in this study.

Chapter 3 focused on the strong seasonal cycle in erodibility at the Clay Bank sites and contrasted the results from Clay Bank to those at the more biologically influenced Gloucester Point site.

Traditional measures of biostabilization on mudflats were not correlated to variations in bed erodibility. Additionally, observations of seabed structure from digital X-radiographs indicated that bioturbation was not responsible for the elevated erodibility measured at Clay Bank in the winter and spring. However, observations from an *in situ* seabed camera indicated an abundance of burrows and anecdotal observations from sediment cores often indicated highly pelletized sediment. This and previous works (e.g., Schaffner et al., 1987b; Wright et al., 1997; Schaffner et al., 2001) suggest that biological

reworking and repackaging may have significantly altered particle and seabed properties relevant to sediment erodibility but their influence was not directly resolved in this study.

Future work should attempt to quantify these likely biological influences on bed geophysical properties and erodibility. The abundance of pellets can be directly measured in association with measures of bed erodibility. In the presence of burrows, measuring bed solids fraction at a sufficiently small scale presents challenges but may be possible by decreasing the individual sample volume with a greater number of smaller bulk samples or by using probes, such as a resistivity probe.

The highly variable bed erodibility condition measured near Clay Bank is in agreement with previous studies in this area describing dynamic sediment transport processes associated with an ephemeral secondary turbidity maximum (STM). An extended period of high river discharge in the winter and spring resulted in the development of a STM near Clay Bank that caused rapid deposition and high bed erodibility. This was followed by an extended period of low river discharge in which stratification broke down and the STM was absent resulting in low erodibility. The Gloucester Point site, outside of the region occupied by the STM, was considerably less dynamic than the Clay Bank sites. Bed erodibility near Gloucester Point was typically low and consistent throughout the year.

This work studying bed erodibility in the York River could be complimented with hydrographic surveys measuring salinity and total suspended solids. Along-channel profiles of these parameters could provide insight on time scales and specific conditions

for development of the high erodibility condition as well as the distribution of sediment during the low erodibility condition. It remains unclear whether the sediment associated with high erodibility near Clay Bank in the winter and/or spring simply moves up-estuary, possibly to the primary estuarine turbidity maximum near West Point, or in the absence of particle trapping near Clay Bank, is distributed throughout the upper estuary.

A comparison of bed erodibility measurements from the York River to historical data from other sites in the Chesapeake Bay showed remarkable similarities. Critical stress versus eroded mass profiles from the frequently observed "low" erodibility condition in the York River were in agreement with similar measurements from Baltimore Harbor, MD and the upper-Chesapeake Bay main stem. Due to a paucity of data, bed erodibility is often used as a tuning parameter in numerical models. However, these data suggest that it may be possible to characterize erodibility over similar, relatively large areas, making it possible to constrain this parameter to a reasonable range even with a limited data set.

The findings of this study were complimented by the contributions of past researchers in the York River estuary. Combining the findings of this study with previous work in this setting provides a conceptual model of sediment transport processes in the York River estuary. A persistent estuarine turbidity maximum is found near West Point associated with the limit of salt. Following an extended period of low river discharge, minimal stratification in the rest of the estuary results in sediment bypassing near Clay Bank, relatively low suspended sediment concentrations, a low rate of sediment

deposition, and low bed erodibility. These conditions are favorable for benthic organisms resulting in a bioturbated seabed and pelletized suspended sediments. Following a period of high river discharge, stratification develops in the Clay Bank region facilitating strong sediment flux convergence, high suspended sediment concentrations, rapid deposition, and high bed erodibility. These conditions are generally unfavorable for benthic organisms. As a result, physical processes dominate, the seabed is laminated, and suspensions are composed primarily of fines and flocs. Down estuary of Clay Bank, conditions remain similar to periods of low river discharge with low suspended sediment concentrations consisting of pelletized sediments and low bed erodibility.

Appendix I

Station Log

Site	Site #	Date	Latitude (N)	Longitude (W)	Depth (meters)	Start time (EST)	Stop time (EST)
GP	3905	4/18/06	37 14.655'	76 29.885'	8.23	8:30	10:30
GP	3911	7/14/06	37 14.671'	76 29.919'	5.49	7:30	9:30
GP	3914	8/21/06	37 14.671'	76 29.903'	7.32	8:10	10:45
GP	3918	9/25/06	37 14.669'	76 29.914'	7.01	6:10	8:40
GP	3924	11/20/06	37 14.661'	76 29.899'	7.92	9:50	12:40
GP	3925	1/9/07	37 14.666'	76 29.909'	6.71	8:35	10:30
GP	3928	3/21/07	37 14.656'	76 29.923'	7.92	9:10	13:20
GP	3931	4/18/07	37 14.662'	76 29.930'	7.92	8:00	11:55
GP	3937	5/21/07	37 14.659'	76 29.882'	7.01	7:30	11:00
GP	3940	6/25/07	37 14.668'	76 29.907'	7.62	5:50	8:30
GP	3945	8/10/07	37 14.667'	76 29.905'		6:50	9:05
GP	3947	10/16/07	37 14.675'	76 29.877'	6.40	6:30	9:30

Site	Site #	Date	Latitude (N)	Longitude (W)	Depth (meters)	Start time (EST)	Stop time (EST)
CBC	3908	5/3/06	37 20.836'	76 36.969'	11.28	9:30	11:30
CBC	3912	7/17/06	37 20.816'	76 36.952'	10.06	9:25	12:20
CBC	3916	8/22/06	37 20.848'	76 36.979'	11.28	8:45	11:30
CBC	3921	9/29/06	37 20.830'	76 36.947'	11.58	9:05	12:15
CBC	3922	11/15/06	37 20.848'	76 36.953'	12.50	7:20	9:40
CBC	3926	1/11/07	37 20.850'	76 36.959'	10.97	10:30	13:30
CBC	3929	3/22/07	37 20.826'	76 36.955'	10.36	6:25	9:10
CBC	3932	4/19/07	37 20.844'	76 36.990'	10.67	9:50	13:40
CBC	3939	5/23/07	37 20.831'	76 36.958'	10.67	9:05	12:55
CBC	3942	6/27/07	37 20.837'	76 36.967'	10.97	6:45	9:20
CBC	3943	8/8/07	37 20.855'	76 36.969'	11.28	5:55	8:15
CBC	3946	10/15/07	37 20.829'	76 36.950'	10.36	7:00	10:15

Site	Site #	Date	Latitude (N)	Longitude (W)	Depth (meters)	Start time (EST)	Stop time (EST)
CBS	3907	5/2/06	37 20.452'	76 37.459'	6.10	8:00	10:20
CBS	3913	7/19/06	37 20.435'	76 37.484'	5.79	6:30	8:30
CBS	3917	8/23/06	37 20.424'	76 37.624'	5.79	9:15	12:45
CBS	3920	9/28/06	37 20.484'	76 37.488'	5.97	8:20	12:20
CBS	3923	11/17/06	37 20.467'	76 37.481'	6.71	8:30	11:05
CBS	3927	1/12/07	37 20.439'	76 37.449'	5.79	10:20	12:55

CBS	3930	3/23/07	37 20.449'	76 37.456'	5.49	6:45	10:15
CBS	3933	4/20/07	37 20.487'	76 37.508'	6.10	9:55	13:35
CBS	3938	5/22/07	37 20.455'	76 37.477'	5.49	8:00	10:15
CBS	3941	6/26/07	37 20.499'	76 37.494'	6.10	6:35	10:20
CBS	3944	8/9/07	37 20.487'	76 37.520'	6.10	6:30	8:50
CBS	3948	10/17/07	37 20.451'	76 37.486'	5.49	7:40	9:40

Appendix II

Physical sediment data from top centimeter of seabed

Explanation of Appendix II data table headings

Site # – Site number. CHSD lab consectutive station number. See appendix I for location information

Sample – Sample identifier. If none given, sample was specifically for determination of physical sediment properties. If identifier contains "x", sample was X-ray slab subsampled for sediment property analysis after being X-rayed.

Min Depth – Minimum depth. Depth from sediment surface of top of extruded and sliced sediment subsample.

Max Depth – Maximum depth. Depth from sediment surface of bottom of extruded and sliced sediment subsample.

Clay – Clay fraction. Mass of clay per mass total sediment as determined by pipette test grain sizing. Clay fraction defined as sediment with diameter of < 4 μm.

Silt – Silt fraction. Mass of silt per mass total sediment as determined by pipette test grain sizing. Silt fraction defined as sediment with diameter of > 4 μm and < 63 μm.

Sand –Sand fraction. Mass of sand per mass total sediment as determined by retention on a 63 μm sieve.

ϕ_{stot} – Solids volume fraction. Water content determined by wet weight / dry weight analysis. ϕ_{stot} determined water content by assuming density of solids to be 2650 kg m^{-2} and density of water to be 1015 kg m^{-2}.

ϕ_{sm} – Solids volume fraction of mud matrix. Determined from ϕ_{stot} and sand fraction using Equation 2 from Chapter 2.

Organic – Organic fraction. Mass organic matter per mass total sediment. Determined by loss on ignition after drying sediment.

Site #	Sample	Site Name	Date	Min Depth	Max Depth	Clay	Silt	Sand	ϕ_{stot}	ϕ_{sm}	Organic
S3905		GP	04/18/2006	0	1	0.310	0.278	0.412	0.160	0.100	0.056
S3907		CBS	05/02/2006	0	1	0.360	0.325	0.316	0.158	0.114	0.061
S3908		CBC	05/03/2006	0	1	0.560	0.395	0.045	0.098	0.094	0.086
S3911		GP	07/14/2006	0	1	0.573	0.411	0.016	0.107	0.106	0.100
S3911	2x	GP	07/14/2006	0	1	NaN	NaN	NaN	0.083	NaN	NaN
S3911	9x	GP	07/14/2006	0	1	NaN	NaN	NaN	0.100	NaN	NaN
S3912		CBC	07/17/2006	0	1	0.536	0.403	0.061	0.104	0.098	0.096
S3912	5x	CBC	07/17/2006	0	1	NaN	NaN	NaN	0.093	NaN	NaN
S3912	8x	CBC	07/17/2006	0	1	NaN	NaN	NaN	0.093	NaN	NaN
S3913		CBS	07/19/2006	0	1	0.422	0.375	0.203	0.163	0.134	0.072
S3913	2x	CBS	07/19/2006	0	1	NaN	NaN	NaN	0.137	NaN	NaN
S3913	4x	CBS	07/19/2006	0	1	NaN	NaN	NaN	0.131	NaN	NaN
S3914		GP	08/21/2006	0	1	0.479	0.408	0.113	0.114	0.102	0.086
S3914	1x	GP	08/21/2006	0	1	0.549	0.332	0.119	0.108	0.097	NaN
S3914	3x	GP	08/21/2006	0	1	0.529	0.330	0.130	0.119	0.105	NaN
S3916		CBC	08/22/2006	0	1	0.605	0.342	0.052	0.119	0.114	0.087
S3916	8x	CBC	08/22/2006	0	1	0.556	0.385	0.058	0.122	0.116	NaN
S3916	9x	CBC	08/22/2006	0	1	0.637	0.318	0.044	0.111	0.107	NaN
S3917		CBS	08/23/2006	0	1	0.511	0.387	0.102	0.140	0.127	0.080
S3917	6x	CBS	08/23/2006	0	1	0.456	0.375	0.169	0.129	0.110	NaN

Site #	Sample	Site Name	Date	Min Depth	Max Depth	Clay	Silt	Sand	ϕ_{stot}	ϕ_{sm}	Organic
S3917	7x	CBS	08/23/2006	0	1	0.550	0.389	0.061	0.107	0.101	NaN
S3918		GP	09/25/2006	0	1	0.549	0.225	0.225	0.137	0.110	0.069
S3918	3x	GP	09/25/2006	0	1	NaN	NaN	NaN	0.092	NaN	NaN
S3918	4x	GP	09/25/2006	0	1	NaN	NaN	NaN	0.094	NaN	NaN
S3920		CBS	09/28/2006	0	1	0.704	0.235	0.061	0.169	0.160	0.058
S3920	1x	CBS	09/28/2006	0	1	0.605	0.272	0.123	0.146	0.131	NaN
S3920	3x	CBS	09/28/2006	0	1	0.523	0.196	0.281	0.170	0.129	NaN
S3921		CBC	09/29/2006	0	1	0.689	0.298	0.012	0.111	0.110	0.087
S3921	1x	CBC	09/29/2006	0	1	0.760	0.233	0.007	0.102	0.101	NaN
S3921	6x	CBC	09/29/2006	0	1	0.754	0.242	0.004	0.089	0.089	NaN
S3922		CBC	11/15/2006	0	1	0.654	0.336	0.010	0.097	0.096	0.097
S3922	1x	CBC	11/15/2006	0	1	0.566	0.416	0.018	0.111	0.109	NaN
S3922	3x	CBC	11/15/2006	0	1	0.496	0.496	0.009	0.100	0.100	NaN
S3923		CBS	11/17/2006	0	1	0.549	0.286	0.164	0.113	0.097	0.082
S3923	1x	CBS	11/17/2006	0	1	0.657	0.312	0.031	0.081	0.079	NaN
S3923	6x	CBS	11/17/2006	0	1	0.637	0.318	0.045	0.084	0.080	NaN
S3924		GP	11/20/2006	0	1	0.527	0.353	0.119	0.143	0.128	0.078
S3924	1x	GP	11/20/2006	0	1	0.553	0.384	0.063	0.120	0.114	NaN
S3924	9x	GP	11/20/2006	0	1	0.460	0.403	0.137	0.127	0.112	NaN
S3925		GP	01/09/2007	0	1	0.523	0.293	0.184	0.153	0.129	0.074

Site #	Sample	Site Name	Date	Min Depth	Max Depth	Clay	Silt	Sand	ϕ_{stot}	ϕ_{sm}	Organic
S3925	4x	GP	01/09/2007	0	1	0.539	0.343	0.118	0.126	0.113	NaN
S3925	7x	GP	01/09/2007	0	1	0.402	0.422	0.177	0.123	0.103	NaN
S3926		CBC	01/11/2007	0	1	0.473	0.324	0.203	0.154	0.127	0.070
S3926	3x	CBC	01/11/2007	0	1	0.532	0.368	0.100	0.154	0.140	NaN
S3926	4x	CBC	01/11/2007	0	1	0.348	0.500	0.152	0.154	0.134	NaN
S3927		CBS	01/12/2007	0	1	0.608	0.292	0.099	0.104	0.095	0.090
S3927	7ax	CBS	01/12/2007	0	1	0.569	0.252	0.179	0.101	0.084	NaN
S3927	7bx	CBS	01/12/2007	0	1	0.463	0.249	0.288	0.130	0.096	NaN
S3928		GP	03/21/2007	0	1	0.468	0.296	0.236	0.141	0.111	0.073
S3928	6x	GP	03/21/2007	0	1	0.471	0.289	0.240	0.136	0.107	NaN
S3928	8x	GP	03/21/2007	0	1	0.515	0.306	0.179	0.133	0.112	NaN
S3929		CBC	03/22/2007	0	1	0.362	0.373	0.079	0.124	0.115	0.097
S3929	6x	CBC	03/22/2007	0	1	0.545	0.399	0.056	0.103	0.098	NaN
S3929	7x	CBC	03/22/2007	0	1	0.593	0.344	0.064	0.106	0.100	NaN
S3930		CBS	03/23/2007	0	1	0.551	0.370	0.265	0.152	0.116	0.087
S3930	4x	CBS	03/23/2007	0	1	0.369	0.340	0.291	0.163	0.121	NaN
S3930	7x	CBS	03/23/2007	0	1	0.444	0.433	0.123	0.117	0.104	NaN
S3931		GP	04/18/2007	0	1	0.360	0.297	0.342	0.167	0.117	0.058
S3931	6x	GP	04/18/2007	0	1	0.347	0.415	0.238	0.150	0.119	NaN
S3931	10x	GP	04/18/2007	0	1	0.374	0.428	0.198	0.141	0.116	NaN

Site #	Sample	Site Name	Date	Min Depth	Max Depth	Clay	Silt	Sand	ϕ_{stot}	ϕ_{sm}	Organic
S3932		CBC	04/19/2007	0	1	0.310	0.667	0.024	0.120	0.117	0.088
S3932	10x	CBC	04/19/2007	0	1	0.464	0.477	0.059	0.129	0.122	NaN
S3932	11x	CBC	04/19/2007	0	1	0.573	0.401	0.027	0.101	0.099	NaN
S3933		CBS	04/20/2007	0	1	0.454	0.446	0.100	0.136	0.124	0.080
S3933	9x	CBS	04/20/2007	0	1	0.537	0.360	0.104	0.116	0.106	NaN
S3933	10x	CBS	04/20/2007	0	1	0.488	0.371	0.134	0.085	0.075	NaN
S3937		GP	05/21/2007	0	1	0.385	0.292	0.316	0.153	0.110	0.069
S3937	5x	GP	05/21/2007	0	1	0.563	0.282	0.155	0.097	0.083	NaN
S3937	6x	GP	05/21/2007	0	1	0.557	0.260	0.183	0.109	0.091	NaN
S3938		CBS	05/22/2007	0	1	0.380	0.423	0.197	0.165	0.137	0.117
S3938	5x	CBS	05/22/2007	0	1	0.428	0.316	0.256	0.145	0.112	NaN
S3938	7x	CBS	05/22/2007	0	1	0.298	0.300	0.402	0.176	0.113	NaN
S3939		CBC	05/23/2007	0	1	0.640	0.337	0.023	0.130	0.127	0.083
S3939	12x	CBC	05/23/2007	0	1	0.538	0.411	0.052	0.128	0.122	NaN
S3939	9x	CBC	05/23/2007	0	1	0.515	0.439	0.046	0.143	0.137	NaN
S3940		GP	06/25/2007	0	1	0.504	0.268	0.222	0.119	0.095	0.064
S3940	5x	GP	06/25/2007	0	1	0.373	0.245	0.382	0.147	0.097	NaN
S3940	4x	GP	06/25/2007	0	1	0.404	0.291	0.305	0.160	0.117	NaN
S3941		CBS	06/26/2007	0	1	0.430	0.512	0.058	0.199	0.189	0.046
S3941	6x	CBS	06/26/2007	0	1	0.542	0.380	0.078	0.134	0.125	NaN

Site #	Sample	Site Name	Date	Min Depth	Max Depth	Clay	Silt	Sand	ϕ_{stot}	ϕ_{sm}	Organic
S3941	7x	CBS	06/26/2007	0	1	0.481	0.429	0.090	0.127	0.117	NaN
S3942		CBC	06/27/2007	0	1	0.639	0.353	0.008	0.095	0.095	0.082
S3942	7x	CBC	06/27/2007	0	1	0.547	0.442	0.011	0.088	0.087	NaN
S3942	10x	CBC	06/27/2007	0	1	0.668	0.327	0.006	0.080	0.080	NaN
S3943		CBC	08/08/2007	0	1	0.571	0.381	0.047	0.125	0.120	0.071
S3944		CBS	08/09/2007	0	1	0.388	0.368	0.244	0.153	0.120	0.063
S3945		GP	08/10/2007	0	1	0.678	0.311	0.010	0.081	0.081	0.099
S3946		CBC	10/15/2007	0	1	0.540	0.417	0.035	0.112	0.108	0.091
S3947		GP	10/16/2007	0	1	0.581	0.313	0.106	0.121	0.110	0.088
S3948		CBS	10/17/2007	0	1	0.489	0.323	0.188	0.160	0.134	0.069

Appendix III

Physical sediment profile data *

Site #	Site Name	Date	Min Depth	Max Depth	Clay	Silt	Sand	ϕ_{stot}	ϕ_{sm}	Organic
S3905	GP	04/18/2006	0	1	0.310	0.278	0.412	0.160	0.100	0.056
S3905	GP	04/18/2006	1	2	0.277	0.243	0.481	0.197	0.113	0.051
S3905	GP	04/18/2006	2	3	0.304	0.279	0.374	0.201	0.136	0.051
S3905	GP	04/18/2006	3	4	0.330	0.338	0.331	0.204	0.146	0.053
S3905	GP	04/18/2006	4	5	0.347	0.335	0.318	0.212	0.155	0.051
S3905	GP	04/18/2006	5	6	0.376	0.328	0.293	0.215	0.162	0.052
S3905	GP	04/18/2006	6	7	0.391	0.335	0.268	0.210	0.163	0.051
S3905	GP	04/18/2006	7	8	0.434	0.333	0.228	0.209	0.169	0.055
S3905	GP	04/18/2006	8	9	0.455	0.306	0.235	0.213	0.172	0.053
S3905	GP	04/18/2006	9	10	0.504	0.267	0.229	0.220	0.179	0.053
S3907	CBS	05/02/2006	0	1	0.360	0.325	0.316	0.158	0.114	0.061
S3907	CBS	05/02/2006	1	2	0.300	0.328	0.373	0.174	0.117	0.063
S3907	CBS	05/02/2006	2	3	0.380	0.375	0.245	0.182	0.144	0.063
S3907	CBS	05/02/2006	3	4	0.438	0.241	0.309	0.182	0.134	0.067
S3907	CBS	05/02/2006	4	5	0.396	0.382	0.222	0.184	0.149	0.066
S3907	CBS	05/02/2006	5	6	0.370	0.433	0.197	0.182	0.152	0.066
S3907	CBS	05/02/2006	6	7	0.413	0.404	0.184	0.188	0.159	0.067
S3907	CBS	05/02/2006	7	8	0.393	0.426	0.181	0.188	0.160	0.065
S3907	CBS	05/02/2006	8	9	0.389	0.399	0.212	0.187	0.153	0.067
S3907	CBS	05/02/2006	9	10	0.287	0.418	0.244	0.186	0.148	0.067

Site #	Site Name	Date	Min Depth	Max Depth	Clay	Silt	Sand	ϕ_{stot}	ϕ_{sm}	Organic
S3908	CBC	05/03/2006	0	1	0.560	0.395	0.045	0.123	0.118	0.086
S3908	CBC	05/03/2006	1	2	0.579	0.368	0.051	0.120	0.115	0.087
S3908	CBC	05/03/2006	2	3	0.610	0.356	0.034	0.126	0.122	0.088
S3908	CBC	05/03/2006	3	4	0.629	0.350	0.021	0.129	0.127	0.090
S3908	CBC	05/03/2006	4	5	0.630	0.347	0.023	0.138	0.135	0.088
S3908	CBC	05/03/2006	5	6	0.597	0.375	0.027	0.145	0.141	0.088
S3908	CBC	05/03/2006	6	7	0.522	0.446	0.033	0.147	0.143	0.086
S3908	CBC	05/03/2006	7	8	0.555	0.424	0.021	0.154	0.151	0.083
S3908	CBC	05/03/2006	8	9	0.533	0.419	0.043	0.153	0.147	0.083
S3908	CBC	05/03/2006	9	10	0.526	0.423	0.051	0.165	0.158	0.078
S3911	GP	07/14/2006	0	1	0.573	0.411	0.016	0.107	0.106	0.100
S3911	GP	07/14/2006	1	2	0.592	0.374	0.034	0.113	0.109	0.096
S3911	GP	07/14/2006	2	3	0.617	0.342	0.041	0.121	0.117	0.096
S3911	GP	07/14/2006	3	4	0.535	0.371	0.094	0.131	0.120	0.089
S3911	GP	07/14/2006	4	5	0.515	0.362	0.123	0.149	0.133	0.079
S3912	CBC	07/17/2006	0	1	0.536	0.403	0.061	0.104	0.098	0.096
S3912	CBC	07/17/2006	1	2	0.620	0.359	0.021	0.111	0.109	0.097
S3912	CBC	07/17/2006	2	3	0.604	0.378	0.019	0.120	0.118	0.097
S3912	CBC	07/17/2006	3	4	0.617	0.360	0.023	0.125	0.122	0.096
S3912	CBC	07/17/2006	4	5	0.588	0.389	0.023	0.128	0.125	0.094

Site #	Site Name	Date	Min Depth	Max Depth	Clay	Silt	Sand	ϕ_{stot}	ϕ_{sm}	Organic
S3913	CBS	07/19/2006	0	1	0.422	0.375	0.203	0.163	0.134	0.072
S3913	CBS	07/19/2006	1	2	0.407	0.351	0.242	0.187	0.149	0.068
S3913	CBS	07/19/2006	2	3	0.390	0.362	0.247	0.191	0.151	0.065
S3913	CBS	07/19/2006	3	4	0.412	0.399	0.189	0.187	0.158	0.069
S3913	CBS	07/19/2006	4	5	0.481	0.370	0.149	0.181	0.158	0.072
S3914	GP	08/21/2006	0	1	0.479	0.408	0.113	0.114	0.102	0.086
S3914	GP	08/21/2006	1	2	0.487	0.378	0.135	0.139	0.122	0.078
S3914	GP	08/21/2006	2	3	0.556	0.321	0.122	0.139	0.124	0.082
S3914	GP	08/21/2006	3	4	0.542	0.332	0.126	0.145	0.129	0.078
S3914	GP	08/21/2006	4	5	0.468	0.324	0.208	0.169	0.139	0.068
S3916	CBC	08/22/2006	0	1	0.605	0.342	0.052	0.119	0.114	0.087
S3916	CBC	08/22/2006	1	2	0.573	0.392	0.036	0.124	0.120	0.085
S3916	CBC	08/22/2006	2	3	0.570	0.405	0.025	0.133	0.130	0.086
S3916	CBC	08/22/2006	3	4	0.548	0.406	0.046	0.138	0.133	0.084
S3916	CBC	08/22/2006	4	5	0.536	0.460	0.004	0.143	0.142	0.083
S3917	CBS	08/23/2006	0	1	0.511	0.387	0.102	0.140	0.127	0.080
S3917	CBS	08/23/2006	1	2	0.522	0.394	0.083	0.129	0.120	0.088
S3917	CBS	08/23/2006	2	3	0.549	0.392	0.059	0.129	0.123	0.088
S3917	CBS	08/23/2006	3	4	0.595	0.343	0.062	0.130	0.123	0.087
S3917	CBS	08/23/2006	4	5	0.431	0.360	0.209	0.163	0.134	0.072

Site #	Site Name	Date	Min Depth	Max Depth	Clay	Silt	Sand	ϕ_{stot}	ϕ_{sm}	Organic
S3918	GP	09/25/2006	0	1	0.549	0.225	0.225	0.137	0.110	0.069
S3918	GP	09/25/2006	1	2	0.588	0.232	0.179	0.154	0.130	0.061
S3918	GP	09/25/2006	2	3	0.536	0.216	0.234	0.152	0.121	0.066
S3918	GP	09/25/2006	3	4	0.508	0.195	0.297	0.155	0.114	0.063
S3918	GP	09/25/2006	4	5	0.482	0.186	0.323	0.162	0.115	0.060
S3920	CBS	09/25/2006	0	1	0.704	0.235	0.061	0.169	0.160	0.058
S3920	CBS	09/25/2006	1	2	0.576	0.253	0.171	0.162	0.138	0.062
S3920	CBS	09/25/2006	2	3	0.586	0.288	0.126	0.174	0.156	0.057
S3920	CBS	09/25/2006	3	4	0.628	0.251	0.121	0.204	0.183	0.049
S3920	CBS	09/25/2006	4	5	0.607	0.234	0.160	0.221	0.192	0.048
S3921	CBC	09/29/2006	0	1	0.689	0.298	0.012	0.111	0.110	0.087
S3921	CBC	09/29/2006	1	2	0.681	0.293	0.022	0.123	0.120	0.081
S3921	CBC	09/29/2006	2	3	0.761	0.218	0.021	0.134	0.132	0.079
S3921	CBC	09/29/2006	3	4	0.631	0.332	0.038	0.134	0.130	0.079
S3921	CBC	09/29/2006	4	5	0.660	0.295	0.045	0.138	0.133	0.078
S3922	CBC	11/15/2006	0	1	0.654	0.336	0.010	0.097	0.096	0.097
S3922	CBC	11/15/2006	1	2	0.559	0.416	0.025	0.132	0.129	0.085
S3922	CBC	11/15/2006	2	3	0.610	0.381	0.009	0.125	0.124	0.087
S3922	CBC	11/15/2006	3	4	0.648	0.346	0.006	0.124	0.123	0.090
S3922	CBC	11/15/2006	4	5	0.610	0.376	0.013	0.127	0.125	0.091

Site #	Site Name	Date	Min Depth	Max Depth	Clay	Silt	Sand	ϕ_{stot}	ϕ_{sm}	Organic
S3922	CBC	11/15/2006	5	6	0.609	0.369	0.022	0.127	0.124	0.090
S3922	CBC	11/15/2006	6	7	0.647	0.343	0.009	0.130	0.129	0.088
S3922	CBC	11/15/2006	7	8	0.622	0.368	0.010	0.133	0.132	0.086
S3922	CBC	11/15/2006	8	9	0.590	0.394	0.016	0.138	0.136	0.084
S3922	CBC	11/15/2006	9	10	0.622	0.372	0.006	0.143	0.142	0.082
S3923	CBS	11/17/2006	0	1	0.549	0.286	0.164	0.113	0.097	0.082
S3923	CBS	11/17/2006	1	2	0.368	0.282	0.342	0.176	0.123	0.061
S3923	CBS	11/17/2006	2	3	0.365	0.275	0.360	0.218	0.152	0.052
S3923	CBS	11/17/2006	3	4	0.295	0.225	0.469	0.228	0.136	0.048
S3923	CBS	11/17/2006	4	5	0.242	0.208	0.541	0.274	0.148	0.040
S3923	CBS	11/17/2006	5	6	0.256	0.240	0.497	0.262	0.152	0.045
S3923	CBS	11/17/2006	6	7	0.282	0.228	0.488	0.265	0.156	0.048
S3923	CBS	11/17/2006	7	8	0.271	0.226	0.480	0.256	0.151	0.049
S3923	CBS	11/17/2006	8	9	0.322	0.235	0.423	0.254	0.164	0.051
S3923	CBS	11/17/2006	9	10	0.352	0.319	0.325	0.233	0.170	0.057
S3924	GP	11/20/2006	0	1	0.527	0.353	0.119	0.143	0.128	0.078
S3924	GP	11/20/2006	1	2	0.539	0.366	0.096	0.144	0.132	0.079
S3924	GP	11/20/2006	2	3	0.508	0.363	0.129	0.160	0.142	0.073
S3924	GP	11/20/2006	3	4	0.480	0.368	0.151	0.168	0.146	0.070
S3924	GP	11/20/2006	4	5	0.472	0.380	0.149	0.162	0.141	0.073

Site #	Site Name	Date	Min Depth	Max Depth	Clay	Silt	Sand	ϕ_{stot}	ϕ_{sm}	Organic
S3924	GP	11/20/2006	5	6	0.503	0.343	0.154	0.160	0.139	0.072
S3924	GP	11/20/2006	6	7	0.399	0.303	0.298	0.194	0.144	0.062
S3924	GP	11/20/2006	7	8	0.386	0.285	0.330	0.207	0.149	0.055
S3924	GP	11/20/2006	8	9	0.393	0.308	0.299	0.207	0.155	0.056
S3924	GP	11/20/2006	9	10	0.458	0.326	0.213	0.200	0.164	0.056
S3925	GP	01/09/2007	0	1	0.523	0.293	0.184	0.153	0.129	0.074
S3925	GP	01/09/2007	1	2	0.495	0.354	0.150	0.154	0.134	0.074
S3925	GP	01/09/2007	2	3	0.519	0.342	0.139	0.159	0.140	0.075
S3925	GP	01/09/2007	3	4	0.490	0.369	0.139	0.159	0.140	0.071
S3925	GP	01/09/2007	4	5	0.461	0.309	0.230	0.171	0.137	0.068
S3925	GP	01/09/2007	5	6	0.488	0.301	0.210	0.172	0.141	0.068
S3925	GP	01/09/2007	6	7	0.484	0.299	0.217	0.183	0.149	0.069
S3925	GP	01/09/2007	7	8	0.341	0.442	0.218	0.189	0.154	0.060
S3925	GP	01/09/2007	8	9	0.525	0.292	0.183	0.192	0.163	0.060
S3925	GP	01/09/2007	9	10	0.440	0.333	0.227	0.201	0.163	0.059
S3926	CBC	01/11/2007	0	1	0.473	0.324	0.203	0.154	0.127	0.070
S3926	CBC	01/11/2007	1	2	0.488	0.369	0.142	0.148	0.129	0.080
S3926	CBC	01/11/2007	2	3	0.477	0.377	0.146	0.152	0.133	0.079
S3926	CBC	01/11/2007	3	4	0.500	0.340	0.159	0.157	0.135	0.079
S3926	CBC	01/11/2007	4	5	0.450	0.333	0.217	0.150	0.122	0.081

Site #	Site Name	Date	Min Depth	Max Depth	Clay	Silt	Sand	ϕ_{stot}	ϕ_{sm}	Organic
S3926	CBC	01/11/2007	5	6	0.506	0.305	0.189	0.141	0.117	0.085
S3926	CBC	01/11/2007	6	7	0.451	0.323	0.226	0.145	0.116	0.085
S3926	CBC	01/11/2007	7	8	0.475	0.325	0.200	0.143	0.118	0.085
S3926	CBC	01/11/2007	8	9	0.487	0.321	0.187	0.146	0.122	0.082
S3926	CBC	01/11/2007	9	10	0.449	0.314	0.237	0.148	0.117	0.080
S3927	CBS	01/12/2007	0	1	0.608	0.292	0.099	0.104	0.095	0.090
S3927	CBS	01/12/2007	1	2	0.406	0.259	0.335	0.182	0.129	0.060
S3927	CBS	01/12/2007	2	3	0.335	0.265	0.393	0.222	0.148	0.051
S3927	CBS	01/12/2007	3	4	0.318	0.242	0.422	0.223	0.142	0.053
S3927	CBS	01/12/2007	4	5	0.348	0.248	0.384	0.212	0.142	0.054
S3927	CBS	01/12/2007	5	6	0.284	0.234	0.445	0.251	0.157	0.046
S3927	CBS	01/12/2007	6	7	0.272	0.250	0.467	0.252	0.152	0.047
S3927	CBS	01/12/2007	7	8	0.281	0.240	0.472	0.252	0.151	0.047
S3927	CBS	01/12/2007	8	9	0.306	0.250	0.415	0.267	0.176	0.045
S3927	CBS	01/12/2007	9	10	0.346	0.293	0.356	0.271	0.193	0.049
S3928	GP	03/21/2007	0	1	0.468	0.296	0.236	0.141	0.111	0.073
S3928	GP	03/21/2007	1	2	0.467	0.343	0.190	0.155	0.129	0.070
S3928	GP	03/21/2007	2	3	0.534	0.163	0.302	0.183	0.135	0.062
S3928	GP	03/21/2007	3	4	0.379	0.267	0.354	0.200	0.139	0.054
S3928	GP	03/21/2007	4	5	0.407	0.038	0.555	0.212	0.107	0.053

Site #	Site Name	Date	Min Depth	Max Depth	Clay	Silt	Sand	ϕ_{stot}	ϕ_{sm}	Organic
S3928	GP	03/21/2007	5	6	0.416	0.272	0.312	0.206	0.152	0.054
S3928	GP	03/21/2007	6	7	0.458	0.322	0.220	0.207	0.169	0.057
S3928	GP	03/21/2007	7	8	0.505	0.324	0.171	0.196	0.169	0.059
S3928	GP	03/21/2007	8	9	0.511	0.330	0.159	0.186	0.161	0.063
S3928	GP	03/21/2007	9	10	0.545	0.322	0.134	0.198	0.176	0.059
S3929	CBC	03/22/2007	0	1	0.362	0.373	0.079	0.124	0.115	0.097
S3929	CBC	03/22/2007	1	2	0.346	0.300	0.080	0.122	0.113	0.094
S3929	CBC	03/22/2007	2	3	0.341	0.266	0.073	0.109	0.102	0.104
S3929	CBC	03/22/2007	3	4	0.300	0.255	0.071	0.124	0.116	0.098
S3929	CBC	03/22/2007	4	5	0.291	0.240	0.126	0.146	0.130	0.086
S3929	CBC	03/22/2007	5	6	0.525	0.392	0.084	0.139	0.129	0.087
S3929	CBC	03/22/2007	6	7	0.534	0.394	0.071	0.157	0.147	0.083
S3929	CBC	03/22/2007	7	8	0.514	0.415	0.068	0.157	0.148	0.083
S3929	CBC	03/22/2007	8	9	0.529	0.425	0.046	0.148	0.142	0.086
S3929	CBC	03/22/2007	9	10	0.617	0.337	0.046	0.145	0.139	0.085
S3930	CBS	03/23/2007	0	1	0.551	0.370	0.265	0.152	0.116	0.087
S3930	CBS	03/23/2007	1	2	0.537	0.383	0.354	0.198	0.137	0.076
S3930	CBS	03/23/2007	2	3	0.581	0.345	0.375	0.219	0.149	0.062
S3930	CBS	03/23/2007	3	4	0.541	0.388	0.445	0.230	0.142	0.058
S3930	CBS	03/23/2007	4	5	0.476	0.398	0.448	0.233	0.143	0.053

Site #	Site Name	Date	Min Depth	Max Depth	Clay	Silt	Sand	ϕ_{stot}	ϕ_{sm}	Organic
S3930	CBS	03/23/2007	5	6	0.332	0.245	0.414	0.217	0.140	0.054
S3930	CBS	03/23/2007	6	7	0.347	0.269	0.369	0.213	0.146	0.058
S3930	CBS	03/23/2007	7	8	0.365	0.308	0.321	0.231	0.169	0.060
S3930	CBS	03/23/2007	8	9	0.374	0.273	0.342	0.224	0.160	0.054
S3930	CBS	03/23/2007	9	10	0.345	0.302	0.339	0.235	0.169	0.057
S3931	GP	04/18/2007	0	1	0.360	0.297	0.342	0.167	0.117	0.058
S3931	GP	04/18/2007	1	2	0.372	0.313	0.315	0.170	0.123	0.060
S3931	GP	04/18/2007	2	3	0.414	0.311	0.270	0.170	0.130	0.060
S3931	GP	04/18/2007	3	4	0.370	0.309	0.321	0.184	0.133	0.056
S3931	GP	04/18/2007	4	5	0.445	0.312	0.243	0.195	0.155	0.052
S3931	GP	04/18/2007	5	6	0.063	0.912	0.026	0.179	0.176	0.056
S3931	GP	04/18/2007	6	7	0.495	0.349	0.156	0.186	0.162	0.054
S3931	GP	04/18/2007	7	8	0.482	0.356	0.162	0.182	0.157	0.059
S3931	GP	04/18/2007	8	9	0.602	0.267	0.109	0.184	0.167	0.059
S3931	GP	04/18/2007	9	10	0.664	0.221	0.115	0.178	0.161	0.060
S3932	CBC	04/19/2007	0	1	0.310	0.667	0.024	0.120	0.117	0.088
S3932	CBC	04/19/2007	1	2	0.575	0.413	0.012	0.123	0.122	0.093
S3932	CBC	04/19/2007	2	3	0.503	0.475	0.021	0.140	0.138	0.086
S3932	CBC	04/19/2007	3	4	0.463	0.496	0.041	0.146	0.141	0.084
S3932	CBC	04/19/2007	4	5	0.454	0.479	0.067	0.136	0.128	0.089

Site #	Site Name	Date	Min Depth	Max Depth	Clay	Silt	Sand	ϕ_{stot}	ϕ_{sm}	Organic
S3932	CBC	04/19/2007	5	6	0.566	0.411	0.023	0.133	0.131	0.089
S3932	CBC	04/19/2007	6	7	0.512	0.468	0.019	0.146	0.143	0.082
S3932	CBC	04/19/2007	7	8	0.463	0.492	0.045	0.166	0.159	0.074
S3932	CBC	04/19/2007	8	9	0.485	0.494	0.020	0.159	0.156	0.079
S3932	CBC	04/19/2007	9	10	0.531	0.441	0.028	0.159	0.155	0.080
S3933	CBS	04/20/2007	0	1	0.454	0.446	0.100	0.136	0.124	0.080
S3933	CBS	04/20/2007	1	2	0.465	0.409	0.126	0.120	0.107	0.089
S3933	CBS	04/20/2007	2	3	0.543	0.431	0.027	0.114	0.112	0.091
S3933	CBS	04/20/2007	3	4	0.579	0.400	0.020	0.113	0.111	0.094
S3933	CBS	04/20/2007	4	5	0.545	0.428	0.027	0.111	0.109	0.097
S3933	CBS	04/20/2007	5	6	0.468	0.458	0.074	0.136	0.127	0.085
S3933	CBS	04/20/2007	6	7	0.342	0.423	0.235	0.158	0.126	0.075
S3933	CBS	04/20/2007	7	8	0.343	0.372	0.285	0.183	0.138	0.064
S3933	CBS	04/20/2007	8	9	0.450	0.321	0.229	0.178	0.143	0.065
S3933	CBS	04/20/2007	9	10	0.462	0.322	0.216	0.176	0.143	0.066
S3937	GP	05/21/2007	0	1	0.385	0.292	0.316	0.153	0.110	0.069
S3937	GP	05/21/2007	1	2	0.254	0.453	0.291	0.189	0.142	0.058
S3937	GP	05/21/2007	2	3	0.363	0.328	0.308	0.199	0.147	0.046
S3937	GP	05/21/2007	3	4	0.398	0.303	0.297	0.217	0.163	0.052
S3937	GP	05/21/2007	4	5	0.412	0.347	0.224	0.206	0.168	0.060

Site #	Site Name	Date	Min Depth	Max Depth	Clay	Silt	Sand	ϕ_{stot}	ϕ_{sm}	Organic
S3937	GP	05/21/2007	5	6	0.441	0.307	0.252	0.215	0.170	0.047
S3937	GP	05/21/2007	6	7	0.446	0.369	0.185	0.207	0.175	0.045
S3937	GP	05/21/2007	7	8	0.722	0.043	0.235	0.205	0.165	0.045
S3937	GP	05/21/2007	8	9	0.521	0.320	0.159	0.210	0.183	0.044
S3937	GP	05/21/2007	9	10	0.513	0.329	0.158	0.205	0.179	0.051
S3938	CBS	05/22/2007	0	1	0.380	0.423	0.197	0.165	0.137	0.117
S3938	CBS	05/22/2007	1	2	0.425	0.411	0.164	0.172	0.148	0.068
S3938	CBS	05/22/2007	2	3	0.427	0.481	0.092	0.165	0.152	0.066
S3938	CBS	05/22/2007	3	4	0.604	0.355	0.041	0.145	0.140	0.076
S3938	CBS	05/22/2007	4	5	0.595	0.360	0.045	0.145	0.140	0.075
S3938	CBS	05/22/2007	5	6	0.272	0.700	0.027	0.156	0.152	0.072
S3938	CBS	05/22/2007	6	7	0.513	0.434	0.053	0.156	0.149	0.070
S3938	CBS	05/22/2007	7	8	0.420	0.514	0.066	0.166	0.157	0.068
S3938	CBS	05/22/2007	8	9	0.496	0.412	0.092	0.171	0.158	0.068
S3938	CBS	05/22/2007	9	10	0.359	0.437	0.203	0.198	0.164	0.059
S3939	CBC	05/23/2007	0	1	0.640	0.337	0.023	0.130	0.127	0.083
S3939	CBC	05/23/2007	1	2	0.661	0.306	0.033	0.144	0.140	0.075
S3939	CBC	05/23/2007	2	3	0.581	0.349	0.069	0.151	0.142	0.074
S3939	CBC	05/23/2007	3	4	0.544	0.396	0.059	0.157	0.149	0.073
S3939	CBC	05/23/2007	4	5	0.549	0.413	0.038	0.167	0.162	0.069

Site #	Site Name	Date	Min Depth	Max Depth	Clay	Silt	Sand	ϕ_{stot}	ϕ_{sm}	Organic
S3939	CBC	05/23/2007	5	6	0.686	0.303	0.010	0.146	0.145	0.077
S3939	CBC	05/23/2007	6	7	0.840	0.141	0.019	0.155	0.153	0.072
S3939	CBC	05/23/2007	7	8	0.578	0.419	0.003	0.145	0.145	0.078
S3939	CBC	05/23/2007	8	9	0.668	0.329	0.003	0.149	0.149	0.079
S3939	CBC	05/23/2007	9	10	0.689	0.310	0.001	0.153	0.152	0.079
S3940	GP	06/25/2007	0	1	0.504	0.268	0.222	0.119	0.095	0.064
S3940	GP	06/25/2007	1	2	0.409	0.280	0.311	0.182	0.133	0.047
S3940	GP	06/25/2007	2	3	0.385	0.270	0.345	0.205	0.144	0.044
S3940	GP	06/25/2007	3	4	0.426	0.297	0.277	0.211	0.162	0.044
S3940	GP	06/25/2007	4	5	0.428	0.319	0.253	0.205	0.161	0.043
S3940	GP	06/25/2007	5	6	0.546	0.281	0.174	0.188	0.160	0.045
S3940	GP	06/25/2007	6	7	0.497	0.312	0.190	0.198	0.167	0.047
S3940	GP	06/25/2007	7	8	0.509	0.346	0.143	0.199	0.176	0.048
S3940	GP	06/25/2007	8	9	0.501	0.326	0.173	0.211	0.181	0.046
S3940	GP	06/25/2007	9	10	0.504	0.313	0.181	0.217	0.185	0.044
S3941	CBS	06/26/2007	0	1	0.430	0.512	0.058	0.199	0.189	0.046
S3941	CBS	06/26/2007	1	2	0.363	0.307	0.317	0.188	0.136	0.050
S3941	CBS	06/26/2007	2	3	0.445	0.324	0.231	0.192	0.155	0.054
S3941	CBS	06/26/2007	3	4	0.389	0.321	0.290	0.210	0.159	0.052
S3941	CBS	06/26/2007	4	5	0.435	0.227	0.321	0.225	0.165	0.047

Site #	Site Name	Date	Min Depth	Max Depth	Clay	Silt	Sand	ϕ_{stot}	ϕ_{sm}	Organic
S3941	CBS	06/26/2007	5	6	0.402	0.182	0.408	0.240	0.158	0.046
S3941	CBS	06/26/2007	6	7	0.420	0.137	0.438	0.253	0.160	0.041
S3941	CBS	06/26/2007	7	8	0.000	0.260	0.738	0.253	0.082	0.039
S3941	CBS	06/26/2007	8	9	0.362	0.358	0.257	0.262	0.209	0.041
S3941	CBS	06/26/2007	9	10	0.208	0.247	0.392	0.264	0.179	0.039
S3942	CBC	06/27/2007	0	1	0.639	0.353	0.008	0.095	0.095	0.082
S3942	CBC	06/27/2007	1	2	0.615	0.378	0.008	0.121	0.120	0.073
S3942	CBC	06/27/2007	2	3	0.628	0.362	0.010	0.139	0.138	0.069
S3942	CBC	06/27/2007	3	4	0.568	0.410	0.022	0.144	0.141	0.070
S3942	CBC	06/27/2007	4	5	0.632	0.361	0.007	0.150	0.149	0.071
S3942	CBC	06/27/2007	5	6	0.584	0.401	0.014	0.148	0.146	0.077
S3942	CBC	06/27/2007	6	7	0.627	0.357	0.017	0.146	0.143	0.078
S3942	CBC	06/27/2007	7	8	0.592	0.389	0.018	0.146	0.144	0.076
S3942	CBC	06/27/2007	8	9	0.619	0.359	0.022	0.150	0.147	0.073
S3942	CBC	06/27/2007	9	10	0.623	0.358	0.020	0.155	0.153	0.069
S3943	CBC	08/08/2007	0	1	0.571	0.381	0.047	0.125	0.120	0.071
S3943	CBC	08/08/2007	1	2	0.646	0.318	0.035	0.149	0.144	0.068
S3943	CBC	08/08/2007	2	3	0.608	0.358	0.033	0.153	0.148	0.065
S3943	CBC	08/08/2007	3	4	0.588	0.345	0.066	0.160	0.151	0.061
S3943	CBC	08/08/2007	4	5	0.578	0.366	0.056	0.161	0.153	0.060

Site #	Site Name	Date	Min Depth	Max Depth	Clay	Silt	Sand	ϕ_{stot}	ϕ_{sm}	Organic
S3943	CBC	08/08/2007	5	6	0.557	0.371	0.072	0.168	0.158	0.058
S3943	CBC	08/08/2007	6	7	0.548	0.390	0.063	0.171	0.162	0.056
S3943	CBC	08/08/2007	7	8	0.542	0.374	0.084	0.168	0.156	0.059
S3943	CBC	08/08/2007	8	9	0.584	0.336	0.080	0.180	0.168	0.058
S3943	CBC	08/08/2007	9	10	0.543	0.350	0.107	0.184	0.168	0.055
S3944	CBS	08/09/2007	0	1	0.388	0.368	0.244	0.153	0.120	0.063
S3944	CBS	08/09/2007	1	2	0.381	0.455	0.164	0.191	0.165	0.053
S3944	CBS	08/09/2007	2	3	0.423	0.457	0.120	0.190	0.171	0.056
S3944	CBS	08/09/2007	3	4	0.442	0.444	0.114	0.180	0.163	0.060
S3944	CBS	08/09/2007	4	5	0.581	0.375	0.044	0.159	0.153	0.070
S3944	CBS	08/09/2007	5	6	0.581	0.376	0.043	0.156	0.150	0.074
S3944	CBS	08/09/2007	6	7	0.591	0.368	0.041	0.151	0.146	0.075
S3944	CBS	08/09/2007	7	8	0.581	0.371	0.048	0.155	0.149	0.073
S3944	CBS	08/09/2007	8	9	0.509	0.404	0.087	0.176	0.163	0.066
S3944	CBS	08/09/2007	9	10	0.495	0.439	0.066	0.181	0.171	0.065
S3945	GP	08/10/2007	0	1	0.678	0.311	0.010	0.081	0.081	0.099
S3945	GP	08/10/2007	1	2	0.680	0.306	0.014	0.101	0.100	0.085
S3945	GP	08/10/2007	2	3	0.622	0.354	0.024	0.120	0.117	0.080
S3945	GP	08/10/2007	3	4	0.629	0.341	0.030	0.128	0.124	0.072
S3945	GP	08/10/2007	4	5	0.595	0.375	0.030	0.132	0.128	0.073

Site #	Site Name	Date	Min Depth	Max Depth	Clay	Silt	Sand	ϕ_{stot}	ϕ_{sm}	Organic
S3945	GP	08/10/2007	5	6	0.656	0.308	0.036	0.135	0.131	0.071
S3945	GP	08/10/2007	6	7	0.598	0.320	0.082	0.148	0.137	0.066
S3945	GP	08/10/2007	7	8	0.521	0.270	0.209	0.169	0.139	0.058
S3945	GP	08/10/2007	8	9	0.457	0.312	0.229	0.179	0.144	0.052
S3945	GP	08/10/2007	9	10	0.445	0.311	0.244	0.194	0.154	0.048
S3946	CBC	10/15/2007	0	1	0.540	0.417	0.035	0.112	0.108	0.091
S3946	CBC	10/15/2007	1	2	0.606	0.379	0.015	0.130	0.128	0.089
S3946	CBC	10/15/2007	2	3	0.610	0.372	0.018	0.132	0.130	0.088
S3946	CBC	10/15/2007	3	4	0.616	0.369	0.015	0.138	0.136	0.087
S3946	CBC	10/15/2007	4	5	0.623	0.357	0.020	0.141	0.139	0.084
S3946	CBC	10/15/2007	5	6	0.618	0.361	0.021	0.147	0.144	0.084
S3946	CBC	10/15/2007	6	7	0.609	0.356	0.036	0.149	0.145	0.079
S3946	CBC	10/15/2007	7	8	0.591	0.367	0.041	0.150	0.145	0.080
S3946	CBC	10/15/2007	8	9	0.625	0.329	0.046	0.147	0.141	0.080
S3946	CBC	10/15/2007	9	10	0.659	0.404	0.067	0.144	0.136	0.081
S3947	GP	10/16/2007	0	1	0.581	0.313	0.106	0.121	0.110	0.088
S3947	GP	10/16/2007	1	2	0.559	0.337	0.105	0.138	0.126	0.076
S3947	GP	10/16/2007	2	3	0.556	0.335	0.109	0.146	0.132	0.076
S3947	GP	10/16/2007	3	4	0.537	0.341	0.122	0.155	0.139	0.074
S3947	GP	10/16/2007	4	5	0.607	0.297	0.096	0.149	0.137	0.077

Site #	Site Name	Date	Min Depth	Max Depth	Clay	Silt	Sand	ϕ_{stot}	ϕ_{sm}	Organic
S3947	GP	10/16/2007	5	6	0.603	0.326	0.071	0.142	0.133	0.080
S3947	GP	10/16/2007	6	7	0.626	0.288	0.053	0.141	0.134	0.079
S3947	GP	10/16/2007	7	8	0.581	0.319	0.101	0.150	0.137	0.075
S3947	GP	10/16/2007	8	9	0.498	0.258	0.235	0.176	0.141	0.064
S3947	GP	10/16/2007	9	10	0.435	0.226	0.285	0.193	0.146	0.058
S3948	CBS	10/17/2007	0	1	0.489	0.323	0.188	0.160	0.134	0.069
S3948	CBS	10/17/2007	1	2	0.415	0.386	0.199	0.177	0.147	0.067
S3948	CBS	10/17/2007	2	3	0.438	0.394	0.168	0.181	0.156	0.067
S3948	CBS	10/17/2007	3	4	0.441	0.426	0.133	0.179	0.159	0.070
S3948	CBS	10/17/2007	4	5	0.442	0.450	0.108	0.180	0.164	0.070
S3948	CBS	10/17/2007	5	6	0.506	0.429	0.065	0.167	0.158	0.081
S3948	CBS	10/17/2007	6	7	0.556	0.384	0.059	0.152	0.145	0.092
S3948	CBS	10/17/2007	7	8	0.615	0.350	0.035	0.152	0.147	0.093
S3948	CBS	10/17/2007	8	9	0.562	0.392	0.046	0.155	0.149	0.088
S3948	CBS	10/17/2007	9	10	0.474	0.410	0.116	0.174	0.157	0.080

Appendix IV

Gust erosion microcosm time-series plots and stepwise data tables

Explanation of Appendix IV data table headings

Step – Consecutive step number.

τ_b – Applied shear stress (Pa).

τ_{ce} – Critical erosion stress at end of step (Pa)*. If $\tau_{ce} > \tau_b$ no erosion occurred.

m – Mass eroded during current step (kg m^{-2}).

M – Erosion rate "constant" (kg m^{-2} s^{-1} Pa^{-1})*.

$\mathbf{E_0}$ – Initial erosion rate (kg m^{-2} s^{-1})*. Erosion rate at beginning of each step as determined by fit to erosion rate time series.

λ - Erosion rate decay rate parameter (s^{-1})*.

* Parameters determined following methods described in Sanford and Maa (2001).

s3905-1e
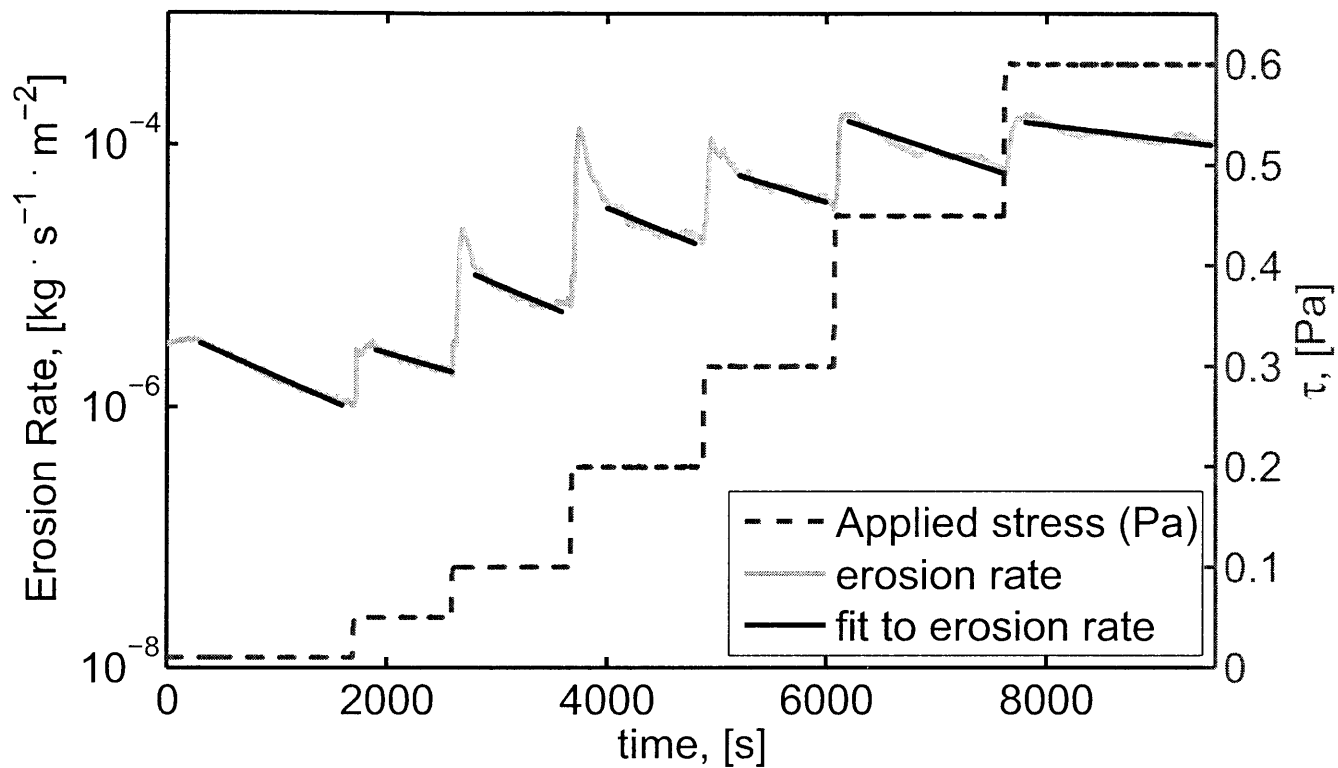
Step	τ_b (Pa)	τ_{ce} (Pa)	m (kg m^{-2})	M (kg m^{-2} s^{-1} Pa^{-1})	E_0 (kg m^{-2} s^{-1})	λ (s^{-1})	length (s)	organic fraction
1	0.0104	0.0300	0.00352	NaN	NaN	8.576e−04	1.719e+03	0.0600
2	0.0504	0.0380	0.00210	3.007e−06	1.472e−04	5.617e−04	8.840e+02	0.0410
3	0.1005	0.0747	0.00929	1.297e−05	2.075e−04	8.210e−04	1.079e+03	0.0490
4	0.2001	0.1512	0.04173	5.395e−05	4.303e−04	7.888e−04	1.194e+03	0.0637
5	0.3003	0.2265	0.06502	7.549e−05	5.066e−04	5.861e−04	1.199e+03	0.0541
6	0.4500	0.3679	0.15696	1.615e−04	7.223e−04	6.511e−04	1.539e+03	0.0534
7	0.5996	0.4527	0.23695	1.529e−04	6.602e−04	2.362e−04	1.929e+03	0.0474

s3905-3e
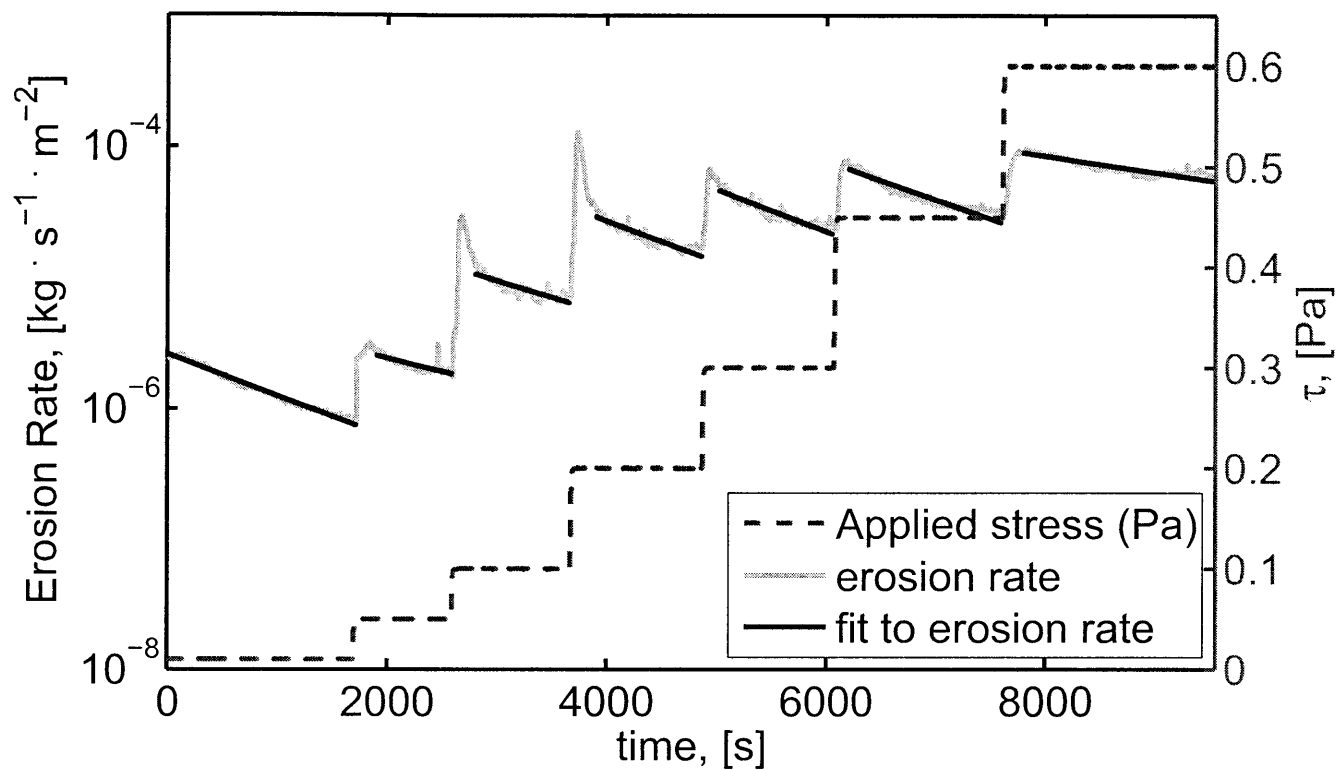
Step	τ_b (Pa)	τ_{ce} (Pa)	m (kg m^{-2})	M (kg m^{-2} s^{-1} Pa^{-1})	E_0 (kg m^{-2} s^{-1})	λ (s^{-1})	length (s)	organic fraction
1	0.0103	0.0300	0.00257	NaN	NaN	7.392e-04	1.719e+03	0.0557
2	0.0504	0.0371	0.00202	2.818e-06	1.382e-04	4.879e-04	8.840e+02	0.0683
3	0.1005	0.0672	0.01083	1.360e-05	2.148e-04	5.958e-04	1.079e+03	0.0505
4	0.2001	0.1444	0.03369	4.225e-05	3.179e-04	7.290e-04	1.194e+03	0.0524
5	0.3002	0.2364	0.04156	5.242e-05	3.365e-04	7.450e-04	1.199e+03	0.0517
6	0.4500	0.3744	0.06934	7.241e-05	3.391e-04	6.745e-04	1.539e+03	0.0732
7	0.5995	0.4705	0.13660	9.235e-05	4.101e-04	2.886e-04	1.929e+03	0.0644

s3907-1e
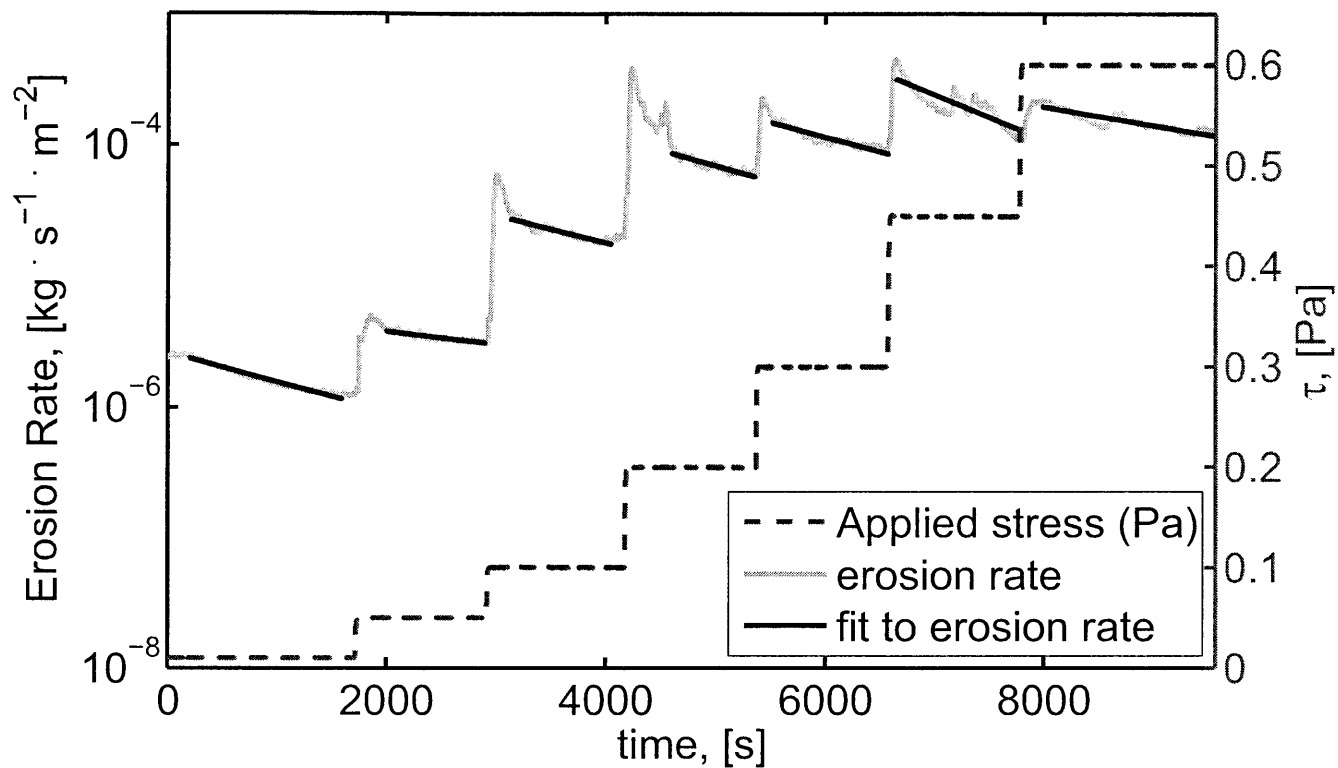
Step	τ_b (Pa)	τ_{ce} (Pa)	m (kg m^{-2})	M (kg m^{-2} s^{-1} Pa^{-1})	E_0 (kg m^{-2} s^{-1})	λ (s^{-1})	length (s)	organic fraction
1	0.0106	0.0300	0.00306	NaN	NaN	5.177e−04	1.749e+03	0.1134
2	0.0502	0.0349	0.00423	4.121e−06	2.036e−04	2.335e−04	1.174e+03	0.0870
3	0.1000	0.0645	0.03043	3.235e−05	4.962e−04	4.827e−04	1.254e+03	0.0842
4	0.2001	0.1288	0.13261	1.500e−04	1.106e−03	5.367e−04	1.199e+03	0.0850
5	0.3002	0.2078	0.14607	1.633e−04	9.531e−04	5.155e−04	1.199e+03	0.0561
6	0.4500	0.3555	0.26000	3.347e−04	1.382e−03	7.850e−04	1.199e+03	0.0499
7	0.5992	0.4633	0.28055	2.071e−04	8.494e−04	3.265e−04	1.789e+03	0.0470

s3907-4e
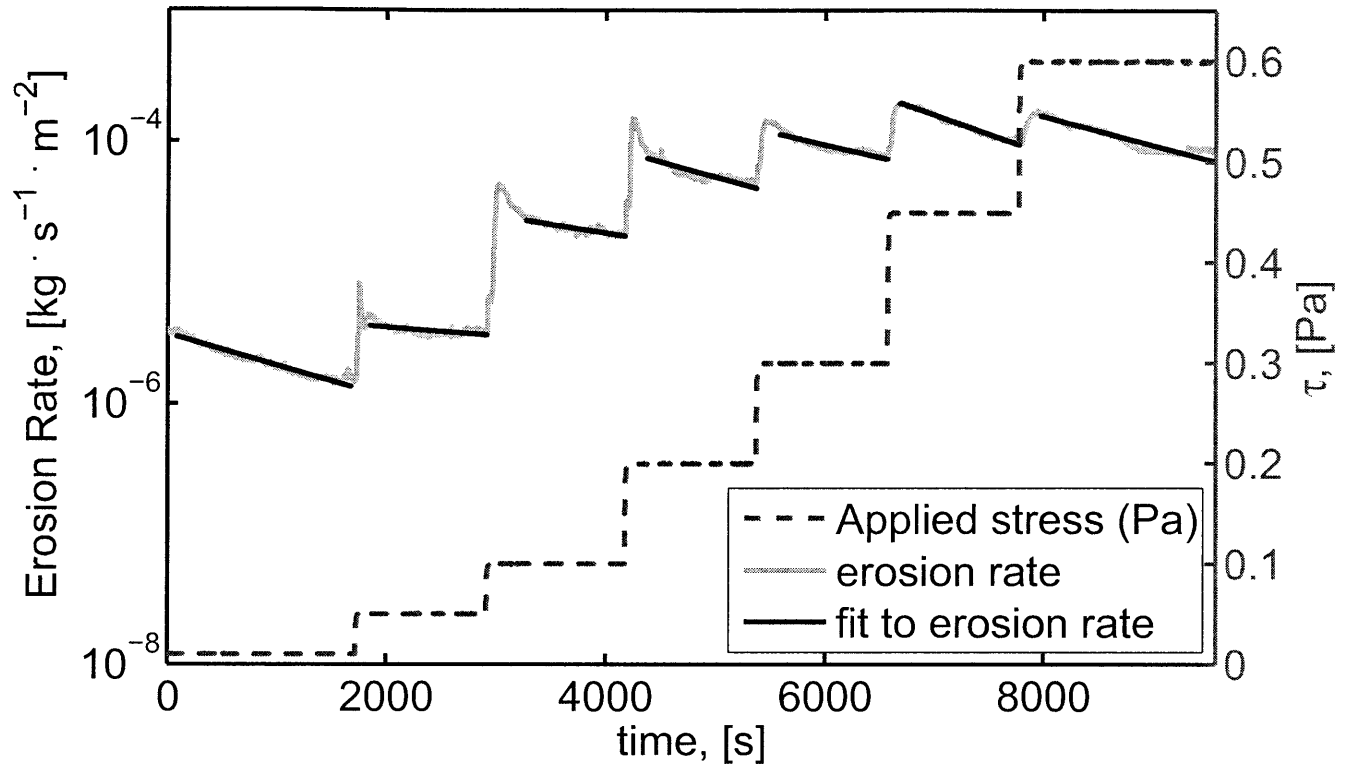
Step	τ_b (Pa)	τ_{ce} (Pa)	m (kg m^{-2})	M (kg m^{-2} s^{-1} Pa^{-1})	E_0 (kg m^{-2} s^{-1})	λ (s^{-1})	length (s)	organic fraction
1	0.0105	0.0300	0.00390	NaN	NaN	5.562e-04	1.749e+03	0.1148
2	0.0503	0.0334	0.00438	4.080e-06	2.010e-04	1.558e-04	1.174e+03	0.0967
3	0.1001	0.0547	0.03052	2.932e-05	4.392e-04	3.065e-04	1.254e+03	0.0697
4	0.2000	0.1228	0.07765	8.738e-05	6.013e-04	5.274e-04	1.199e+03	0.0618
5	0.3000	0.1957	0.11720	1.259e-04	7.106e-04	4.418e-04	1.199e+03	0.0525
6	0.4499	0.3367	0.16959	2.063e-04	8.116e-04	6.748e-04	1.199e+03	0.0464
7	0.5992	0.4933	0.20117	1.711e-04	6.519e-04	5.077e-04	1.789e+03	0.0501

s3908-1e
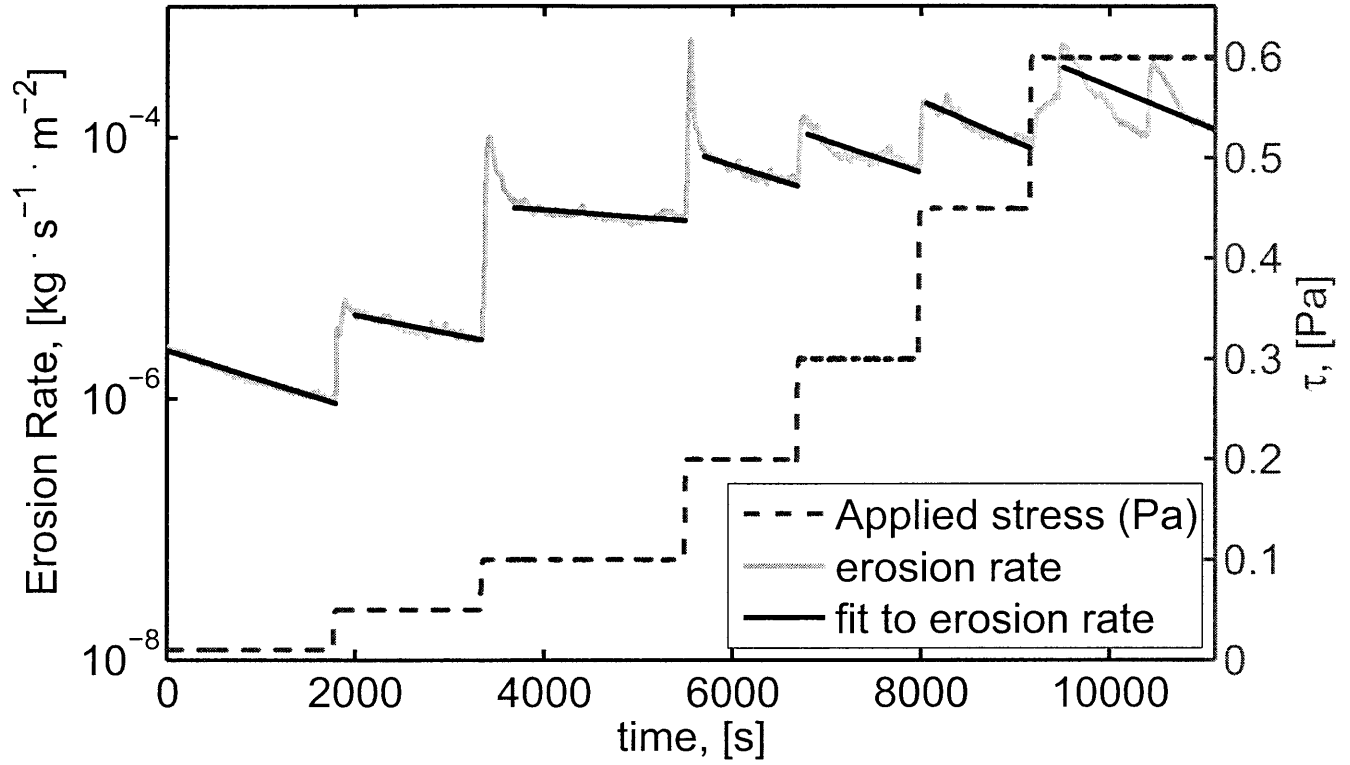
Step	τ_b (Pa)	τ_{ce} (Pa)	m (kg m^{-2})	M (kg m^{-2} s^{-1} Pa^{-1})	E_0 (kg m^{-2} s^{-1})	λ (s^{-1})	length (s)	organic fraction
1	0.0105	0.0300	0.00273	NaN	NaN	5.243e-04	1.799e+03	0.0928
2	0.0500	0.0379	0.00561	4.626e-06	2.310e-04	3.263e-04	1.544e+03	0.1003
3	0.1001	0.0521	0.06406	3.367e-05	5.415e-04	1.197e-04	2.159e+03	0.0695
4	0.2002	0.1213	0.08865	1.001e-04	6.756e-04	5.276e-04	1.194e+03	0.0484
5	0.2999	0.2127	0.10225	1.120e-04	6.272e-04	5.608e-04	1.279e+03	0.0626
6	0.4497	0.3475	0.14964	1.877e-04	7.922e-04	7.134e-04	1.179e+03	0.0541
7	0.5989	0.5324	0.40856	3.752e-04	1.492e-03	6.754e-04	1.969e+03	0.0531

137

s3908-7e
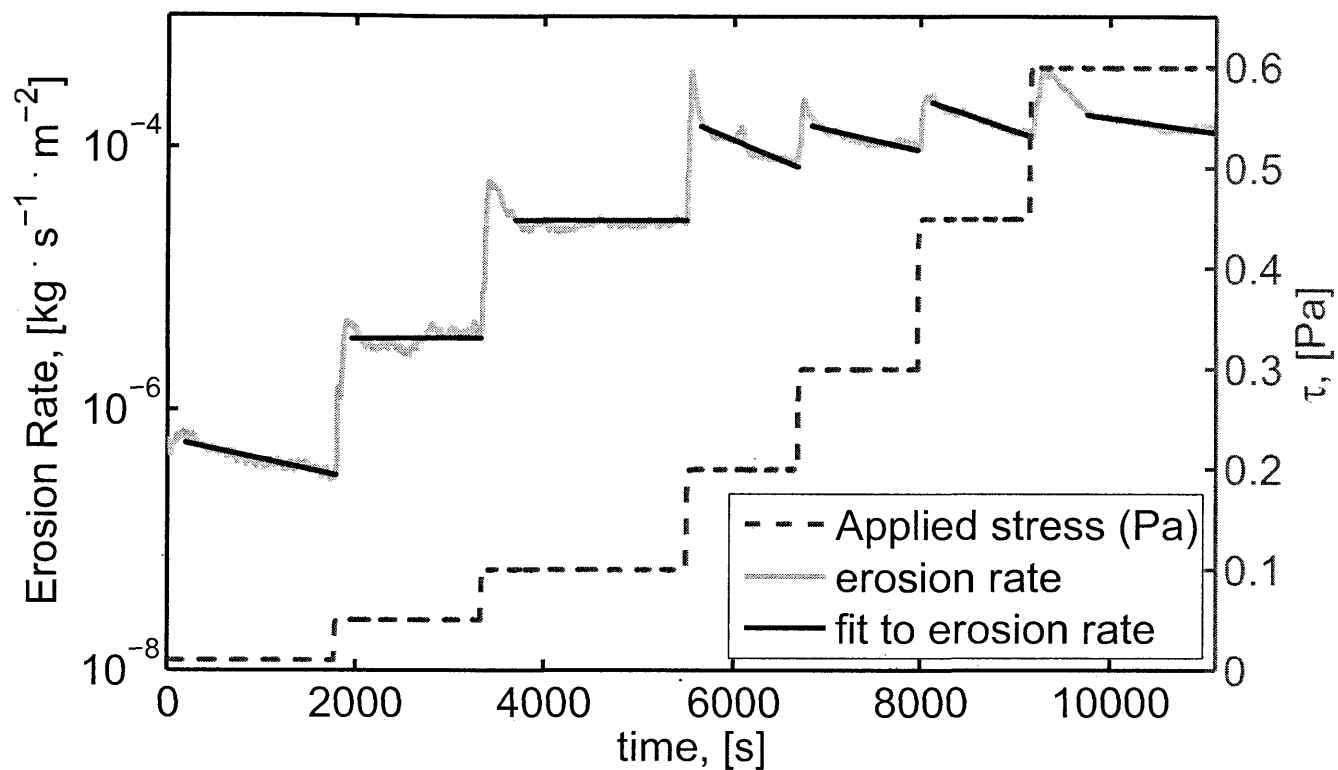
Step	τ_b (Pa)	τ_{ce} (Pa)	m (kg m^{-2})	M (kg m^{-2} s^{-1} Pa^{-1})	E_0 (kg m^{-2} s^{-1})	λ (s^{-1})	length (s)	organic fraction
1	0.0105	0.0300	0.00079	NaN	NaN	3.580e−04	1.799e+03	0.1254
2	0.0501	0.0300	0.00535	3.465e−06	1.721e−04	1.000e−09	1.544e+03	0.1152
3	0.1000	0.0300	0.06013	2.785e−05	3.976e−04	1.000e−09	2.159e+03	0.0758
4	0.2001	0.1250	0.14182	1.739e−04	1.023e−03	6.854e−04	1.194e+03	0.0486
5	0.2998	0.1919	0.16126	1.590e−04	9.097e−04	3.774e−04	1.279e+03	0.0418
6	0.4496	0.3188	0.20163	2.355e−04	9.139e−04	5.750e−04	1.179e+03	0.0381
7	0.5988	0.4209	0.37207	2.350e−04	8.394e−04	2.303e−04	1.969e+03	0.0412

s3911-1e
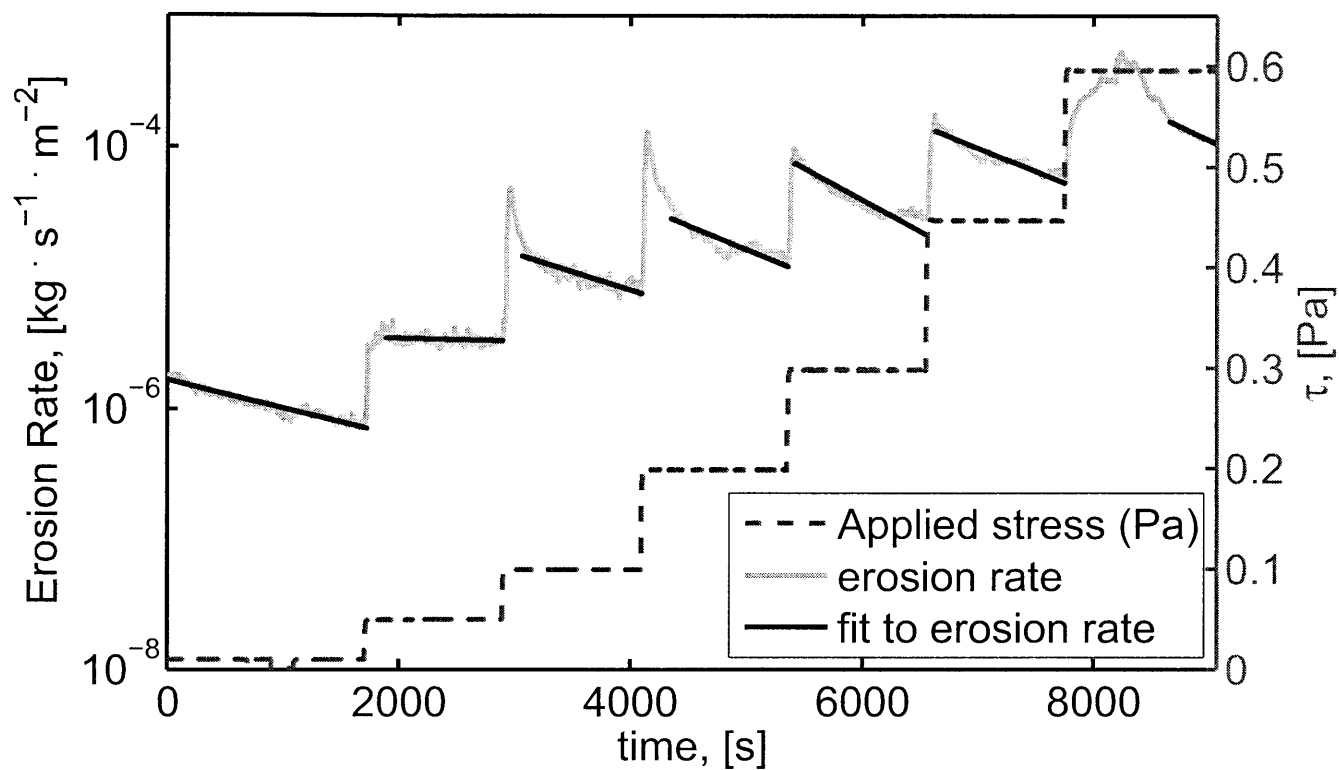
Step	τ_b (Pa)	τ_{ce} (Pa)	m (kg m^{-2})	M (kg m^{-2} s^{-1} Pa^{-1})	E_0 (kg m^{-2} s^{-1})	λ (s^{-1})	length (s)	organic fraction
1	0.0094	0.0300	0.00195	NaN	NaN	5.001e-04	1.734e+03	0.3775
2	0.0500	0.0313	0.00396	3.502e-06	1.752e-04	5.604e-05	1.169e+03	0.2955
3	0.1000	0.0684	0.01553	1.863e-05	2.709e-04	6.484e-04	1.199e+03	0.2514
4	0.1992	0.1542	0.03464	4.475e-05	3.421e-04	8.470e-04	1.259e+03	0.1465
5	0.2985	0.2601	0.05226	7.898e-05	5.473e-04	1.109e-03	1.194e+03	0.1241
6	0.4473	0.3765	0.10529	1.373e-04	7.339e-04	8.113e-04	1.199e+03	0.0907
7	0.5956	0.5349	0.31456	4.264e-04	1.946e-03	9.795e-04	1.309e+03	0.0840

139

s3911-6e
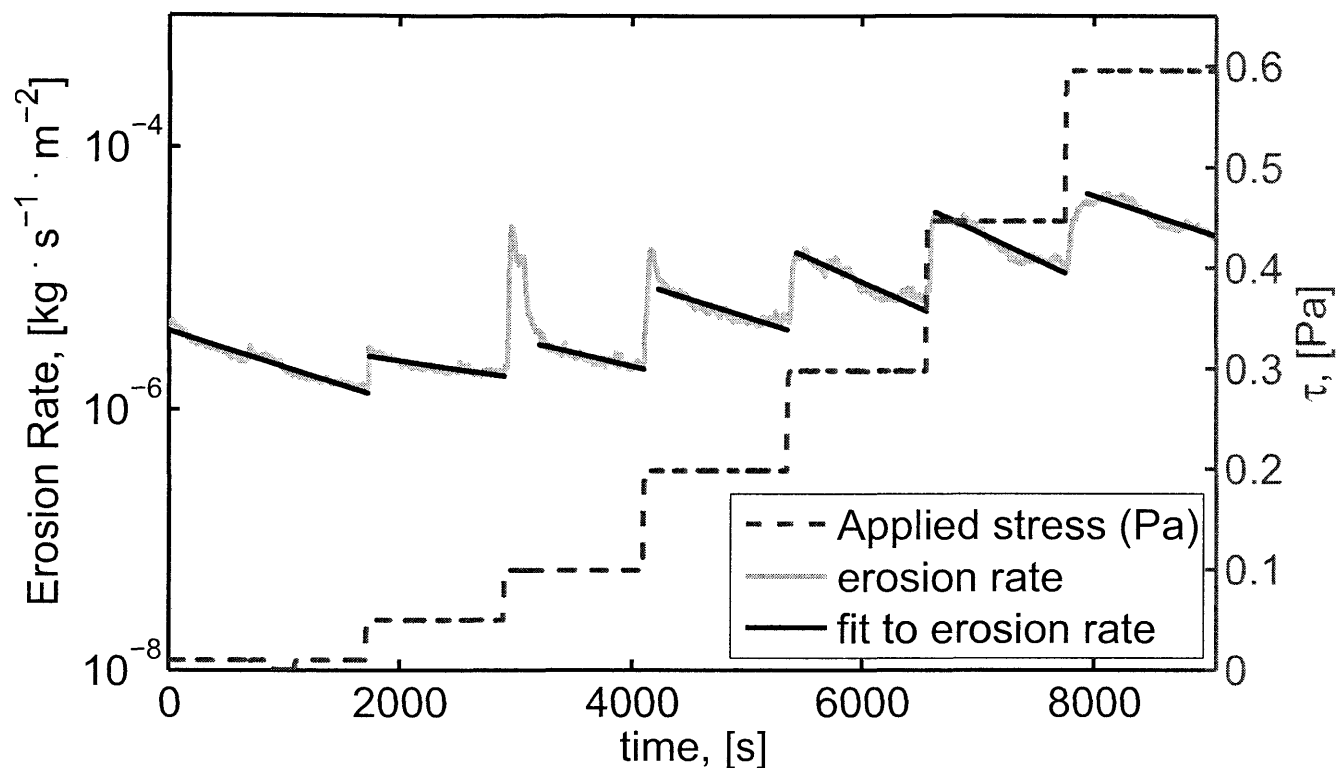
Step	τ_b (Pa)	τ_{ce} (Pa)	m (kg m^{-2})	M (kg m^{-2} s^{-1} Pa^{-1})	E_0 (kg m^{-2} s^{-1})	λ (s^{-1})	length (s)	organic fraction
1	0.0093	0.0300	0.00420	NaN	NaN	6.465e−04	1.734e+03	0.2648
2	0.0499	0.0360	0.00250	2.537e−06	1.273e−04	3.039e−04	1.169e+03	0.3929
3	0.1000	0.0641	0.00526	5.776e−06	9.022e−05	4.823e−04	1.199e+03	0.3037
4	0.1991	0.1381	0.00808	9.299e−06	6.885e−05	6.311e−04	1.259e+03	0.2458
5	0.2985	0.2452	0.01185	1.638e−05	1.021e−04	9.234e−04	1.194e+03	0.2189
6	0.4472	0.3827	0.02354	3.294e−05	1.631e−04	9.530e−04	1.199e+03	0.1822
7	0.5956	0.5060	0.04050	4.623e−05	2.172e−04	6.609e−04	1.309e+03	0.1643

s3912-4e
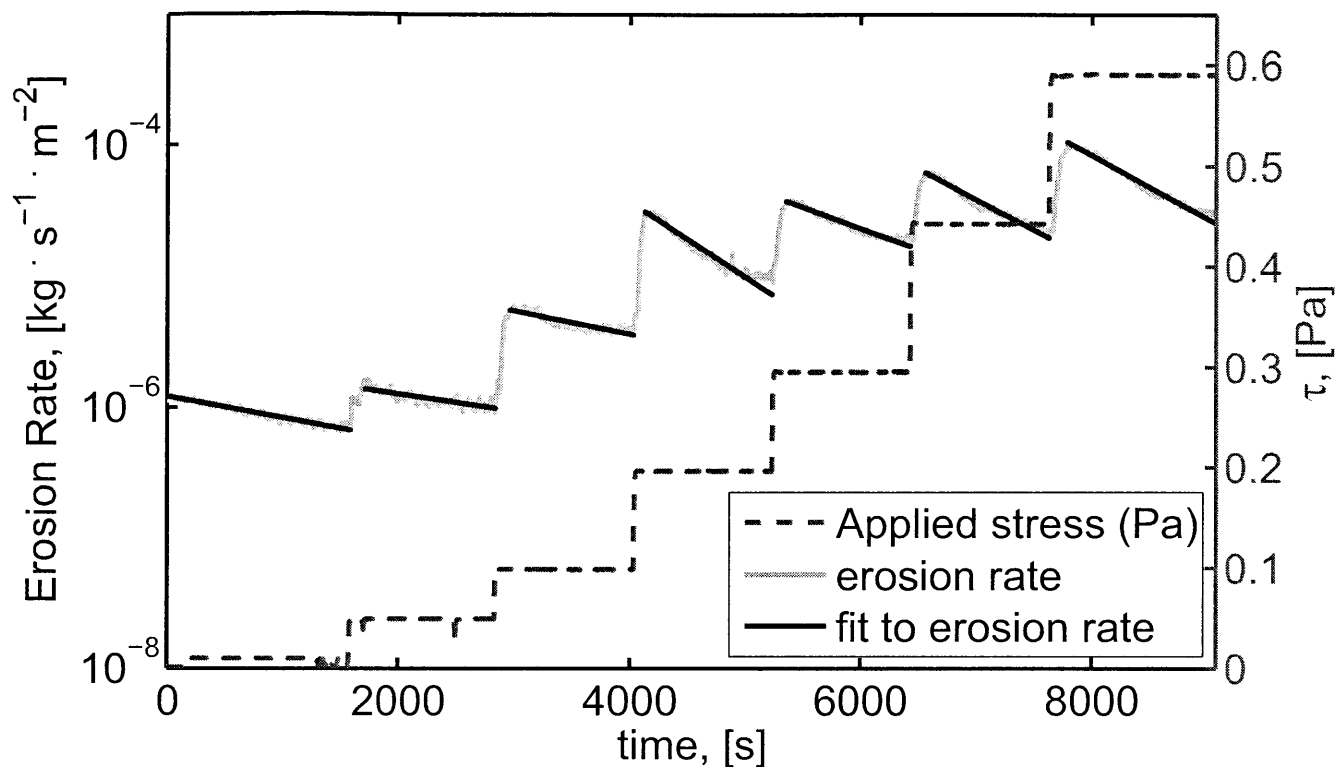
Step	τ_b (Pa)	τ_{ce} (Pa)	m (kg m^{-2})	M (kg m^{-2} s^{-1} Pa^{-1})	E_0 (kg m^{-2} s^{-1})	λ (s^{-1})	length (s)	organic fraction
1	0.0087	0.0700	0.00146	NaN	NaN	3.762e−04	1.589e+03	0.3425
2	0.0492	0.0634	0.00149	1.425e−06	−6.864e−05	3.029e−04	1.254e+03	0.3415
3	0.0988	0.0772	0.00526	5.585e−06	1.580e−04	4.148e−04	1.194e+03	0.2545
4	0.1971	0.1727	0.01983	3.310e−05	2.762e−04	1.330e−03	1.199e+03	0.1572
5	0.2957	0.2448	0.03111	3.904e−05	3.176e−04	7.352e−04	1.199e+03	0.1341
6	0.4432	0.3885	0.04519	6.702e−05	3.377e−04	1.074e−03	1.199e+03	0.1193
7	0.5903	0.5495	0.08274	1.153e−04	5.713e−04	1.112e−03	1.439e+03	0.1085

s3912-13e
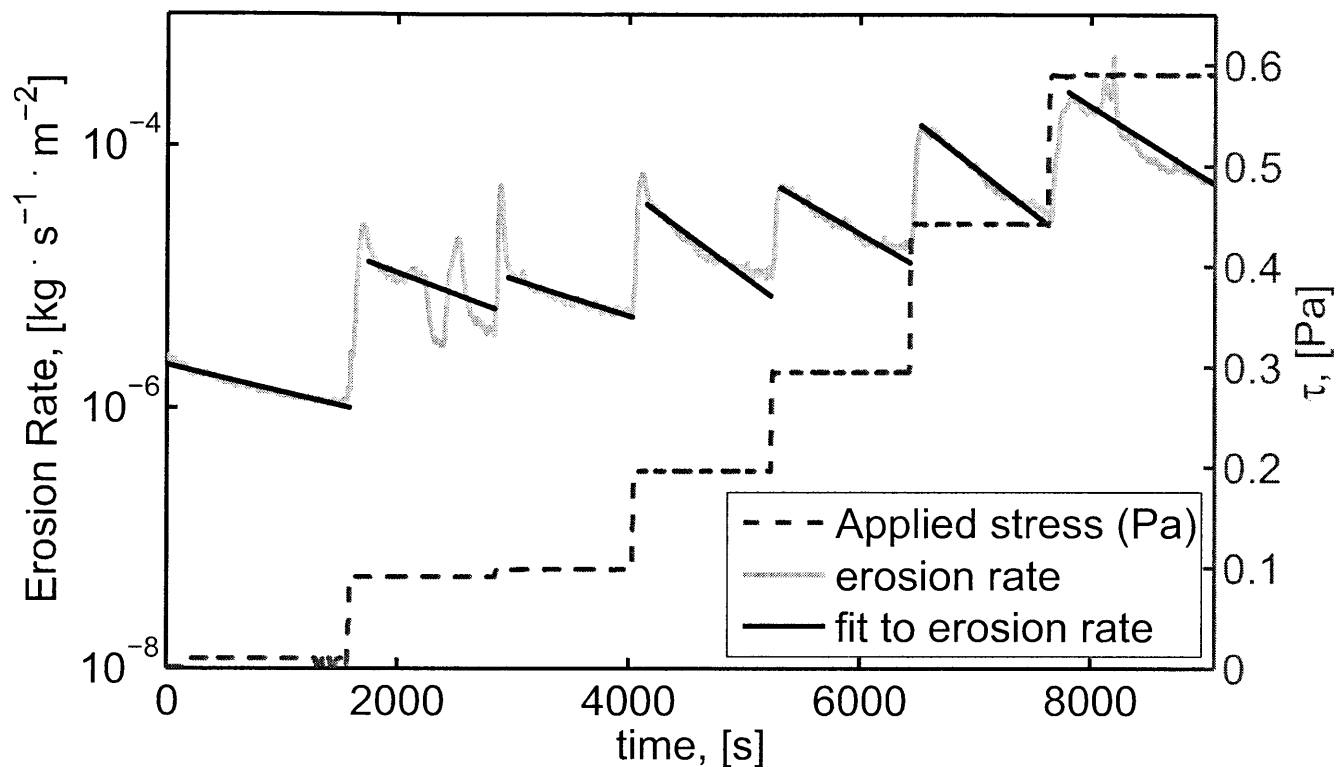
Step	τ_b (Pa)	τ_{ce} (Pa)	m (kg m⁻²)	M (kg m⁻² s⁻¹ Pa⁻¹)	E_0 (kg m⁻² s⁻¹)	λ (s⁻¹)	length (s)	organic fraction
1	0.0087	0.0700	0.00238	NaN	NaN	4.827e-04	1.589e+03	0.3529
2	0.0914	0.0831	0.01189	1.470e-05	6.882e-04	7.590e-04	1.254e+03	0.1681
3	0.0987	0.0915	0.01033	1.243e-05	7.971e-04	6.490e-04	1.194e+03	0.1849
4	0.1970	0.1795	0.02419	4.345e-05	4.119e-04	1.498e-03	1.199e+03	0.1339
5	0.2956	0.2671	0.03246	5.040e-05	4.340e-04	1.172e-03	1.199e+03	0.1489
6	0.4431	0.4168	0.08238	1.535e-04	8.722e-04	1.584e-03	1.199e+03	0.1142
7	0.5902	0.5623	0.18019	2.728e-04	1.573e-03	1.271e-03	1.439e+03	0.1197

142

s3913-1e
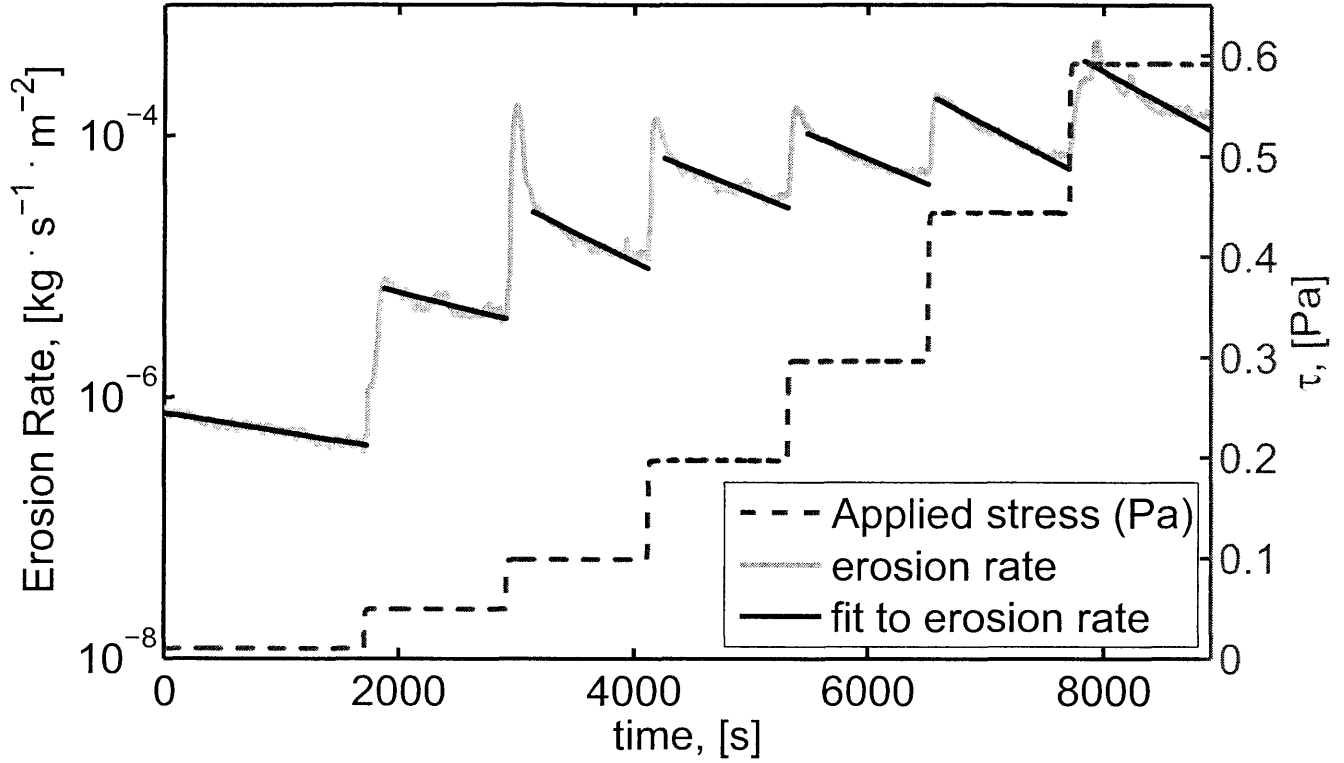
Step	τ_b (Pa)	τ_{ce} (Pa)	m (kg m^{-2})	M (kg m^{-2} s^{-1} Pa^{-1})	E_0 (kg m^{-2} s^{-1})	λ (s^{-1})	length (s)	organic fraction
1	0.0104	0.0300	0.00100	NaN	NaN	3.284e-04	1.739e+03	0.4085
2	0.0496	0.0389	0.00591	6.651e-06	3.394e-04	5.096e-04	1.184e+03	0.1983
3	0.0989	0.0810	0.03349	4.838e-05	8.060e-04	1.014e-03	1.194e+03	0.1154
4	0.1975	0.1544	0.06127	8.065e-05	6.925e-04	8.292e-04	1.199e+03	0.1103
5	0.2963	0.2458	0.09223	1.234e-04	8.700e-04	8.625e-04	1.199e+03	0.0908
6	0.4441	0.3904	0.13397	2.002e-04	1.010e-03	1.090e-03	1.199e+03	0.0865
7	0.5915	0.5399	0.25765	3.932e-04	1.956e-03	1.135e-03	1.199e+03	0.0785

143
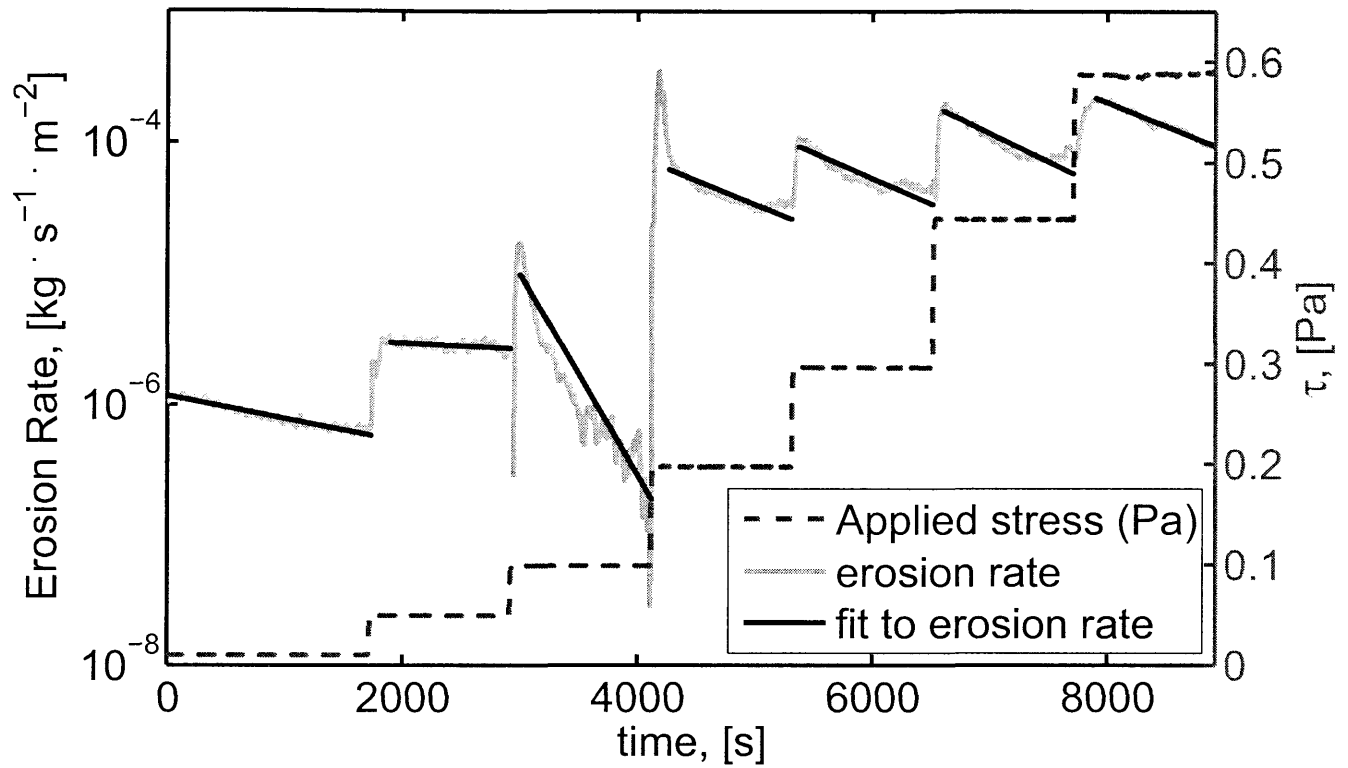
Step	τ_b (Pa)	τ_{ce} (Pa)	m (kg m^{-2})	M (kg m^{-2} s^{-1} Pa^{-1})	E_0 (kg m^{-2} s^{-1})	λ (s^{-1})	length (s)	organic fraction
1	0.0104	0.0300	0.00146	NaN	NaN	4.083e−04	1.739e+03	0.3456
2	0.0497	0.0323	0.00329	2.954e−06	1.503e−04	1.051e−04	1.184e+03	0.3185
3	0.0990	0.0981	0.00290	1.048e−05	1.571e−04	3.559e−03	1.194e+03	0.0026
4	0.1976	0.1613	0.06788	8.990e−05	9.030e−04	8.415e−04	1.199e+03	0.0906
5	0.2964	0.2505	0.07112	9.699e−05	7.182e−04	9.004e−04	1.199e+03	0.0922
6	0.4442	0.3852	0.12768	1.820e−04	9.397e−04	9.915e−04	1.199e+03	0.0830
7	0.5872	0.5131	0.17900	2.364e−04	1.170e−03	8.359e−04	1.199e+03	0.0717

s3914-1e
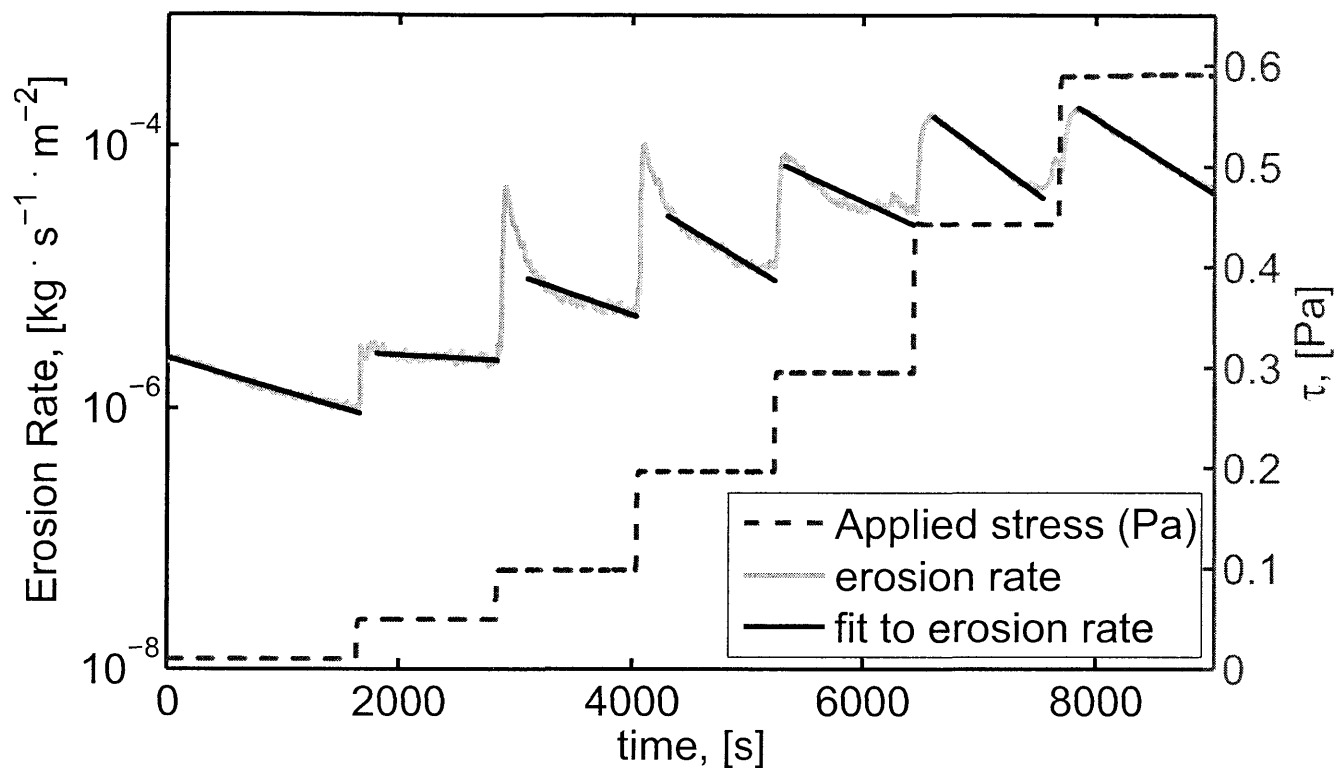
Step	τ_b (Pa)	τ_{ce} (Pa)	m (kg m^{-2})	M (kg m^{-2} s^{-1} Pa^{-1})	E_0 (kg m^{-2} s^{-1})	λ (s^{-1})	length (s)	organic fraction
1	0.0103	0.0400	0.00259	NaN	NaN	5.922e−04	1.664e+03	0.3268
2	0.0495	0.0412	0.00296	2.672e−06	2.798e−04	1.119e−04	1.184e+03	0.3589
3	0.0990	0.0746	0.01257	1.563e−05	2.701e−04	7.169e−04	1.199e+03	0.1777
4	0.1975	0.1689	0.03127	4.955e−05	4.031e−04	1.216e−03	1.199e+03	0.1265
5	0.2956	0.2542	0.05407	7.523e−05	5.934e−04	9.366e−04	1.194e+03	0.1211
6	0.4432	0.4147	0.11359	2.035e−04	1.077e−03	1.521e−03	1.244e+03	0.0938
7	0.5902	0.5589	0.14397	2.248e−04	1.281e−03	1.283e−03	1.344e+03	0.0848

s3914-2e
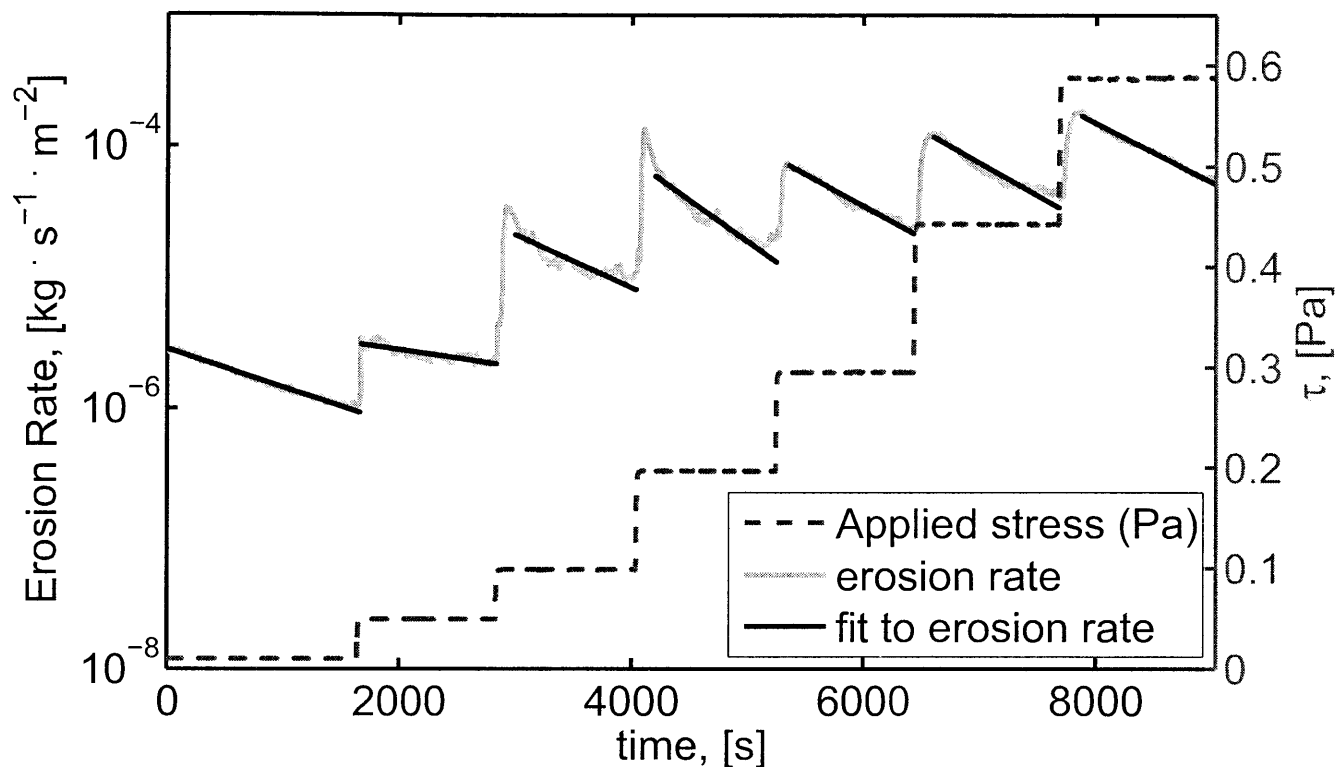
Step	τ_b (Pa)	τ_{ce} (Pa)	m (kg m^{-2})	M (kg m^{-2} s^{-1} Pa^{-1})	E_0 (kg m^{-2} s^{-1})	λ (s^{-1})	length (s)	organic fraction
1	0.0104	0.0400	0.00285	NaN	NaN	6.842e−04	1.664e+03	0.2611
2	0.0496	0.0429	0.00306	3.082e−06	3.213e−04	3.098e−04	1.184e+03	0.3610
3	0.0991	0.0809	0.01756	2.443e−05	4.351e−04	9.404e−04	1.199e+03	0.2051
4	0.1974	0.1772	0.04482	7.923e−05	6.803e−04	1.461e−03	1.199e+03	0.1187
5	0.2955	0.2640	0.05091	7.685e−05	6.493e−04	1.107e−03	1.194e+03	0.1711
6	0.4431	0.4005	0.08733	1.323e−04	7.389e−04	1.155e−03	1.244e+03	0.1306
7	0.5875	0.5415	0.13973	1.934e−04	1.034e−03	1.043e−03	1.344e+03	0.1032

146

s3916-5e
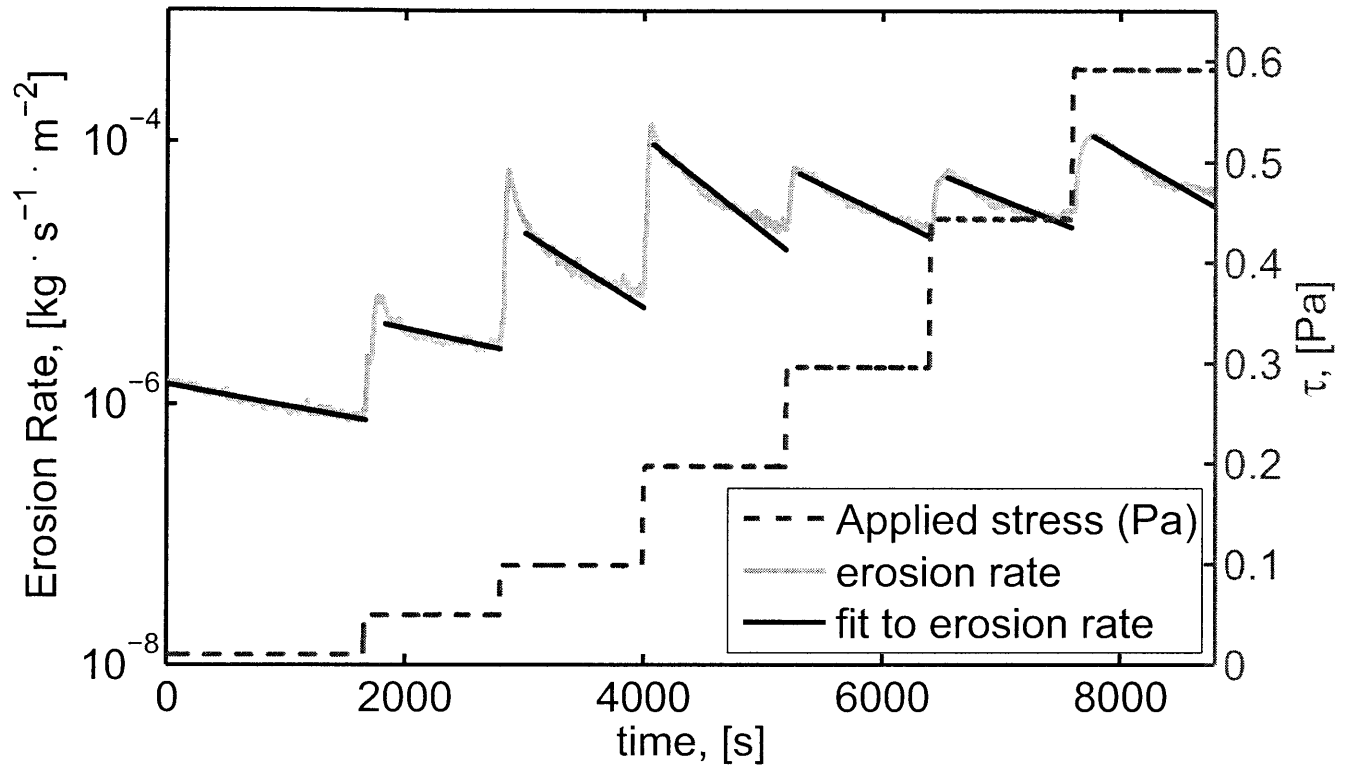
Step	τ_b (Pa)	τ_{ce} (Pa)	m (kg m^{-2})	M (kg m^{-2} s^{-1} Pa^{-1})	E_0 (kg m^{-2} s^{-1})	λ (s^{-1})	length (s)	organic fraction
1	0.0103	0.0300	0.00176	NaN	NaN	3.843e−04	1.679e+03	0.2587
2	0.0496	0.0380	0.00388	4.429e−06	2.262e−04	4.661e−04	1.124e+03	0.2445
3	0.0994	0.0867	0.01789	2.969e−05	4.838e−04	1.317e−03	1.199e+03	0.1522
4	0.1976	0.1825	0.05540	1.070e−04	9.645e−04	1.667e−03	1.194e+03	0.1170
5	0.2964	0.2629	0.04327	6.261e−05	5.497e−04	1.022e−03	1.199e+03	0.1279
6	0.4442	0.3778	0.04423	5.846e−05	3.225e−04	8.375e−04	1.199e+03	0.1272
7	0.5915	0.5419	0.07979	1.265e−04	5.919e−04	1.217e−03	1.199e+03	0.1132

147

s3916-6e
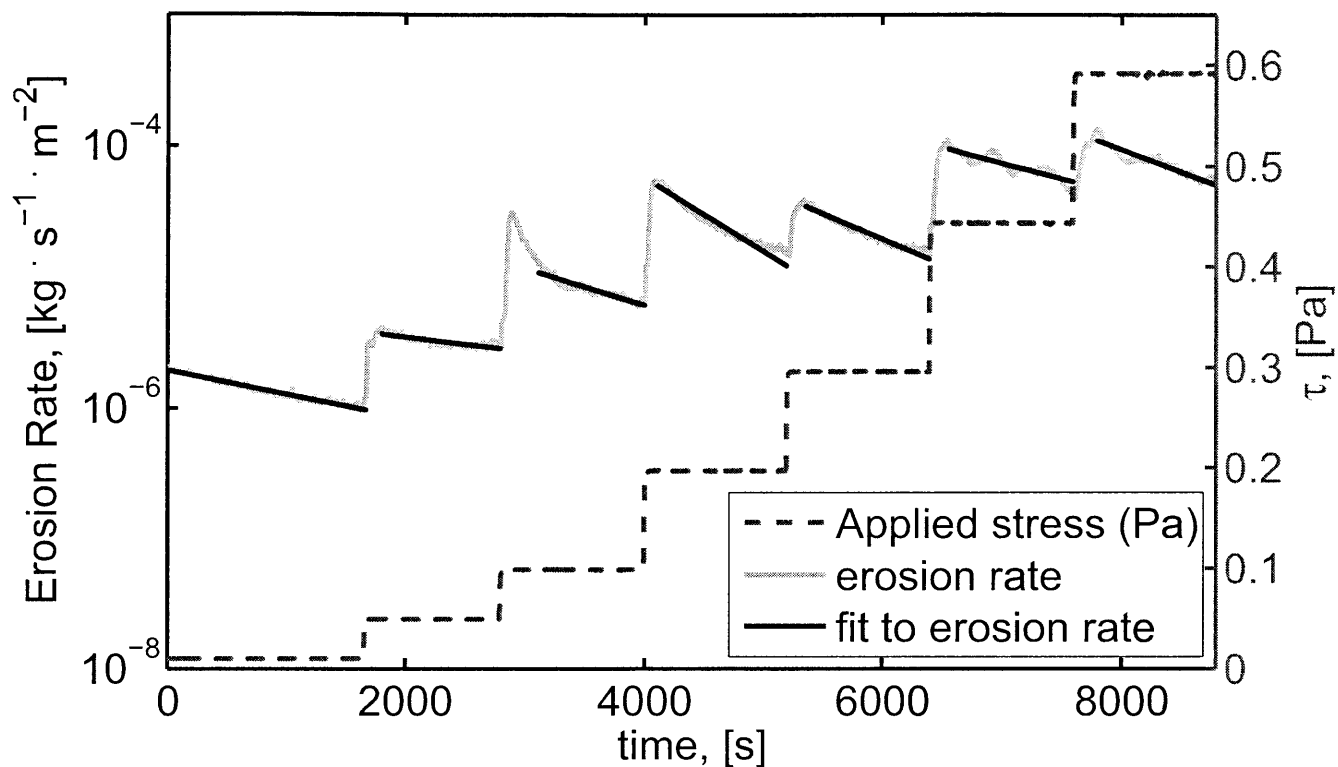
Step	τ_b (Pa)	τ_{ce} (Pa)	m (kg m^{-2})	M (kg m^{-2} s^{-1} Pa^{-1})	E_0 (kg m^{-2} s^{-1})	λ (s^{-1})	length (s)	organic fraction
1	0.0103	0.0300	0.00235	NaN	NaN	4.223e−04	1.679e+03	0.2129
2	0.0496	0.0350	0.00367	3.763e−06	1.920e−04	2.591e−04	1.124e+03	0.2281
3	0.0992	0.0698	0.01302	1.565e−05	2.435e−04	6.522e−04	1.199e+03	0.1850
4	0.1975	0.1705	0.03330	5.494e−05	4.304e−04	1.301e−03	1.194e+03	0.1442
5	0.2963	0.2531	0.02817	3.823e−05	3.039e−04	8.912e−04	1.199e+03	0.2435
6	0.4441	0.3448	0.08716	9.906e−05	5.185e−04	5.459e−04	1.199e+03	0.1134
7	0.5914	0.4957	0.09430	1.217e−04	4.936e−04	7.900e−04	1.199e+03	0.0963

s3917−5e
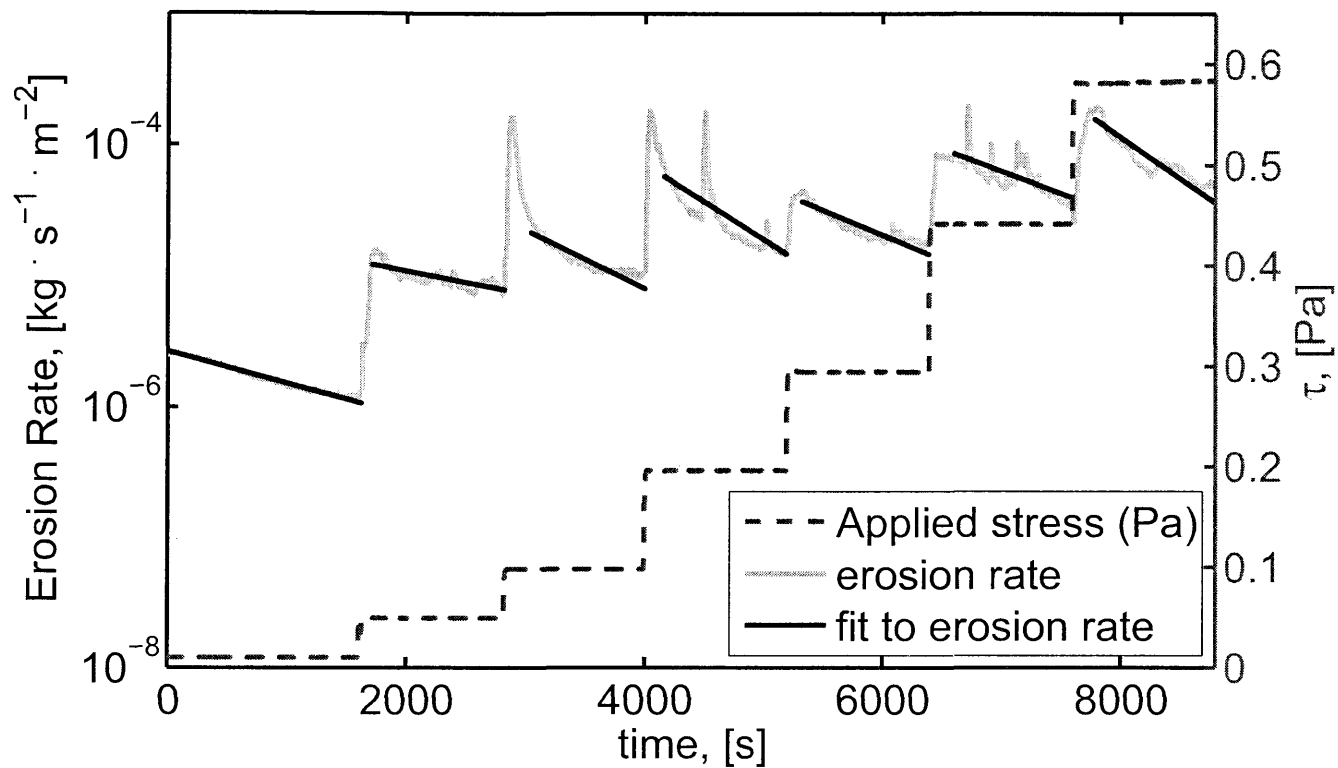
Step	τ_b (Pa)	τ_{ce} (Pa)	m (kg m^{-2})	M (kg m^{-2} s^{-1} Pa^{-1})	E_0 (kg m^{-2} s^{-1})	λ (s^{-1})	length (s)	organic fraction
1	0.0104	0.0300	0.00286	NaN	NaN	5.671e−04	1.629e+03	0.2811
2	0.0493	0.0375	0.01158	1.216e−05	6.302e−04	4.068e−04	1.204e+03	0.1748
3	0.0989	0.0807	0.02830	4.186e−05	6.819e−04	1.041e−03	1.169e+03	0.1274
4	0.1967	0.1727	0.04899	8.151e−05	7.027e−04	1.320e−03	1.194e+03	0.1650
5	0.2950	0.2518	0.03054	4.100e−05	3.351e−04	8.683e−04	1.199e+03	0.1386
6	0.4419	0.3675	0.07437	9.560e−05	5.030e−04	7.824e−04	1.199e+03	0.0929
7	0.5820	0.5443	0.10556	1.858e−04	8.663e−04	1.451e−03	1.199e+03	0.1019

s3917-6e
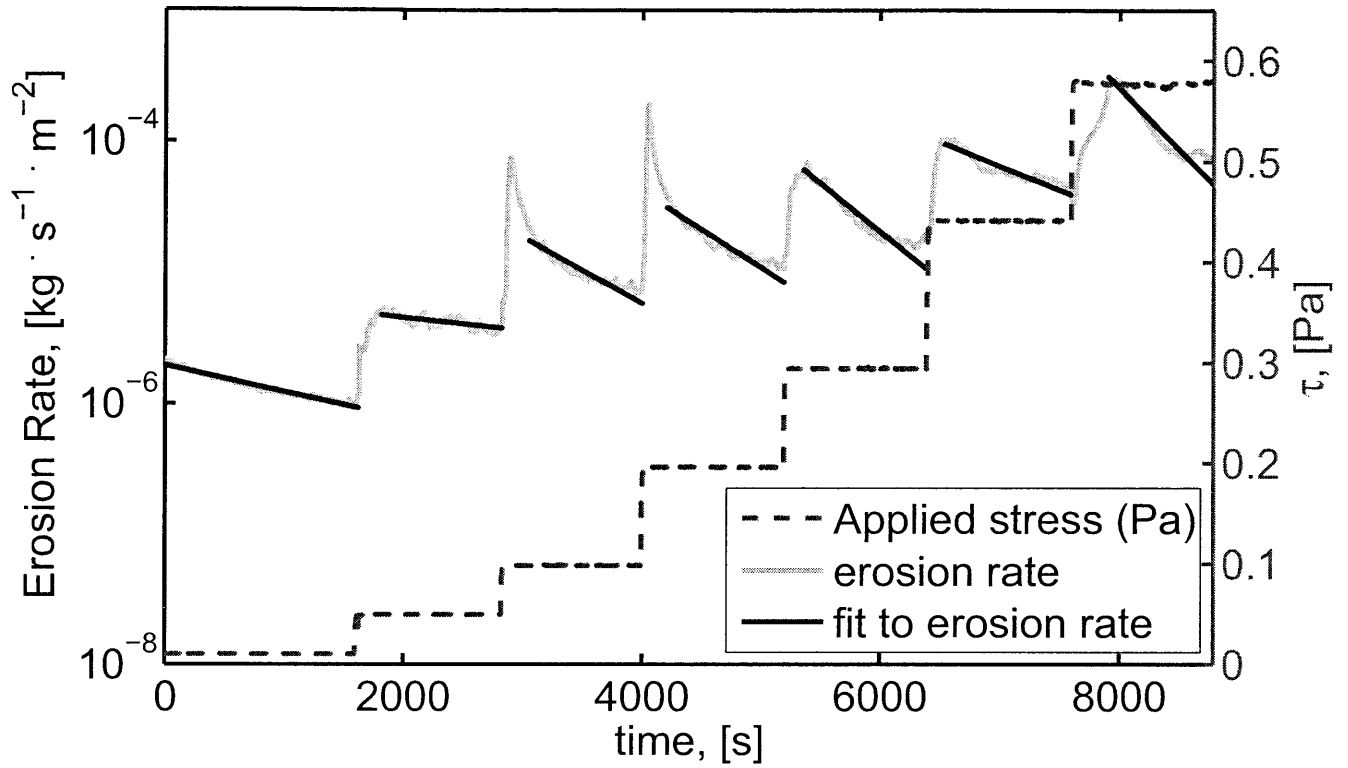
Step	τ_b (Pa)	τ_{ce} (Pa)	m (kg m^{-2})	M (kg m^{-2} s^{-1} Pa^{-1})	E_0 (kg m^{-2} s^{-1})	λ (s^{-1})	length (s)	organic fraction
1	0.0105	0.0300	0.00225	NaN	NaN	4.667e−04	1.629e+03	0.2471
2	0.0493	0.0347	0.00501	4.764e−06	2.465e−04	2.299e−04	1.204e+03	0.2031
3	0.0989	0.0825	0.01825	2.864e−05	4.461e−04	1.169e−03	1.169e+03	0.1558
4	0.1967	0.1736	0.03232	5.422e−05	4.749e−04	1.338e−03	1.194e+03	0.1368
5	0.2950	0.2790	0.03700	7.214e−05	5.941e−04	1.694e−03	1.199e+03	0.1413
6	0.4418	0.3825	0.07693	1.019e−04	6.261e−04	8.420e−04	1.199e+03	0.0976
7	0.5772	0.5620	0.16117	3.715e−04	1.908e−03	2.124e−03	1.199e+03	0.0861

s3918-2e
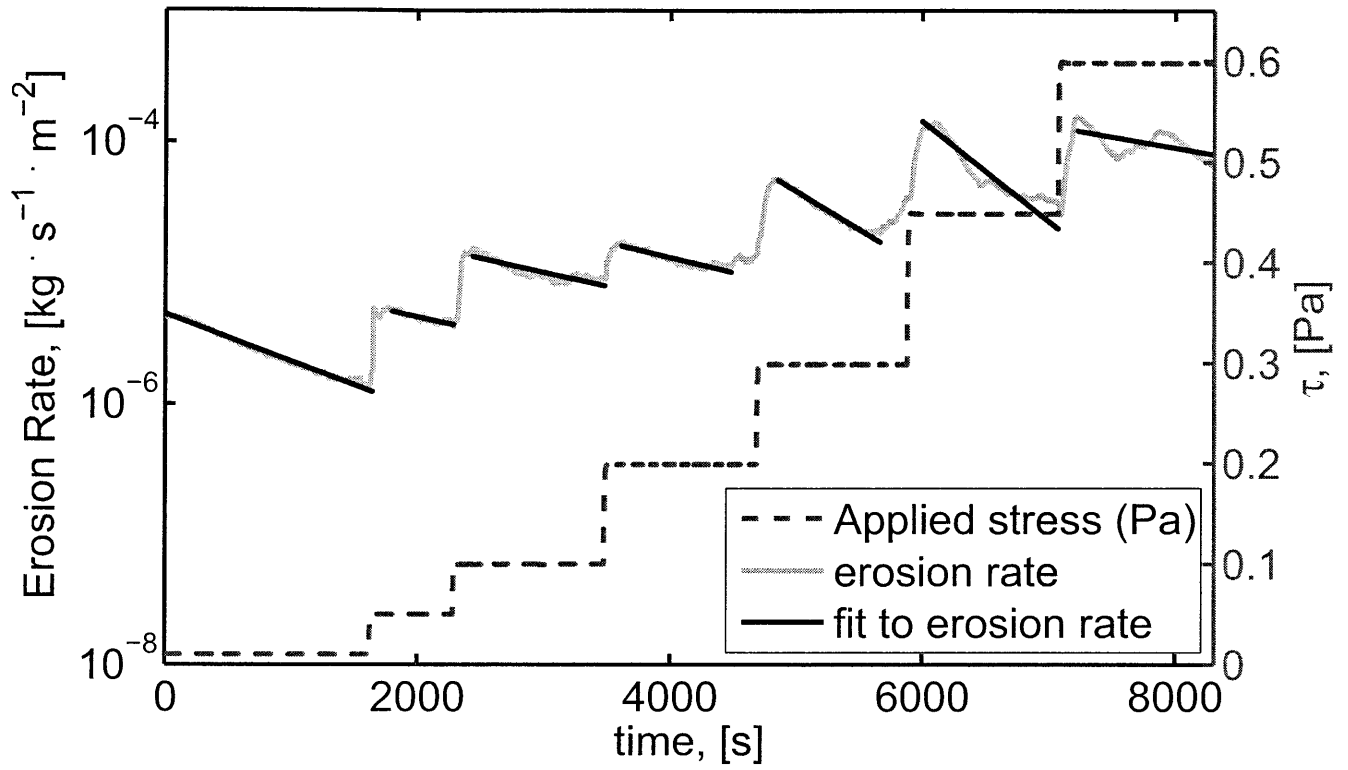
Step	τ_b (Pa)	τ_{ce} (Pa)	m (kg m^{-2})	M (kg m^{-2} s^{-1} Pa^{-1})	E_0 (kg m^{-2} s^{-1})	λ (s^{-1})	length (s)	organic fraction
1	0.0105	0.0400	0.00439	NaN	NaN	8.408e-04	1.649e+03	0.2329
2	0.0505	0.0428	0.00300	5.439e-06	5.202e-04	4.916e-04	6.440e+02	0.2598
3	0.1004	0.0685	0.01258	1.388e-05	2.412e-04	4.912e-04	1.199e+03	0.2122
4	0.1995	0.1303	0.01565	1.772e-05	1.352e-04	5.340e-04	1.194e+03	0.1753
5	0.2994	0.2655	0.03764	6.313e-05	3.733e-04	1.341e-03	1.199e+03	0.1444
6	0.4492	0.4266	0.07933	1.581e-04	8.610e-04	1.748e-03	1.199e+03	0.1166
7	0.5979	0.4911	0.11893	1.225e-04	7.147e-04	3.881e-04	1.219e+03	0.1098

151

s3918-4e
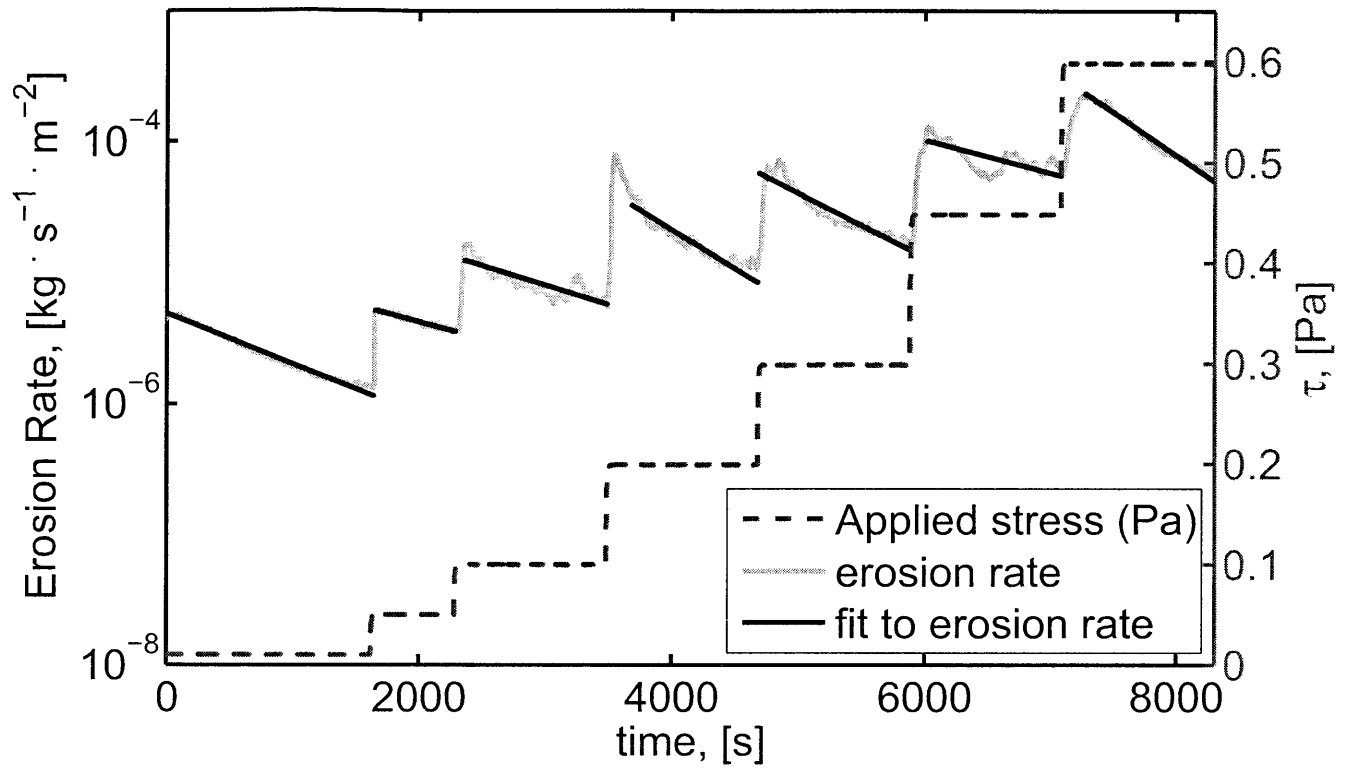
Step	τ_b (Pa)	τ_{ce} (Pa)	m (kg m^{-2})	M (kg m^{-2} s^{-1} Pa^{-1})	E_0 (kg m^{-2} s^{-1})	λ (s^{-1})	length (s)	organic fraction
1	0.0105	0.0400	0.00429	NaN	NaN	8.854e−04	1.649e+03	0.2282
2	0.0505	0.0434	0.00282	5.272e−06	5.026e−04	5.995e−04	6.440e+02	0.2790
3	0.1004	0.0753	0.01035	1.267e−05	2.223e−04	6.866e−04	1.199e+03	0.2069
4	0.1995	0.1750	0.02807	4.755e−05	3.829e−04	1.360e−03	1.194e+03	0.1567
5	0.2993	0.2675	0.03836	5.858e−05	4.714e−04	1.136e−03	1.199e+03	0.1469
6	0.4489	0.3586	0.09109	1.055e−04	5.815e−04	5.815e−04	1.199e+03	0.1150
7	0.5978	0.5594	0.15309	2.738e−04	1.145e−03	1.502e−03	1.219e+03	0.1067

s3920-1e
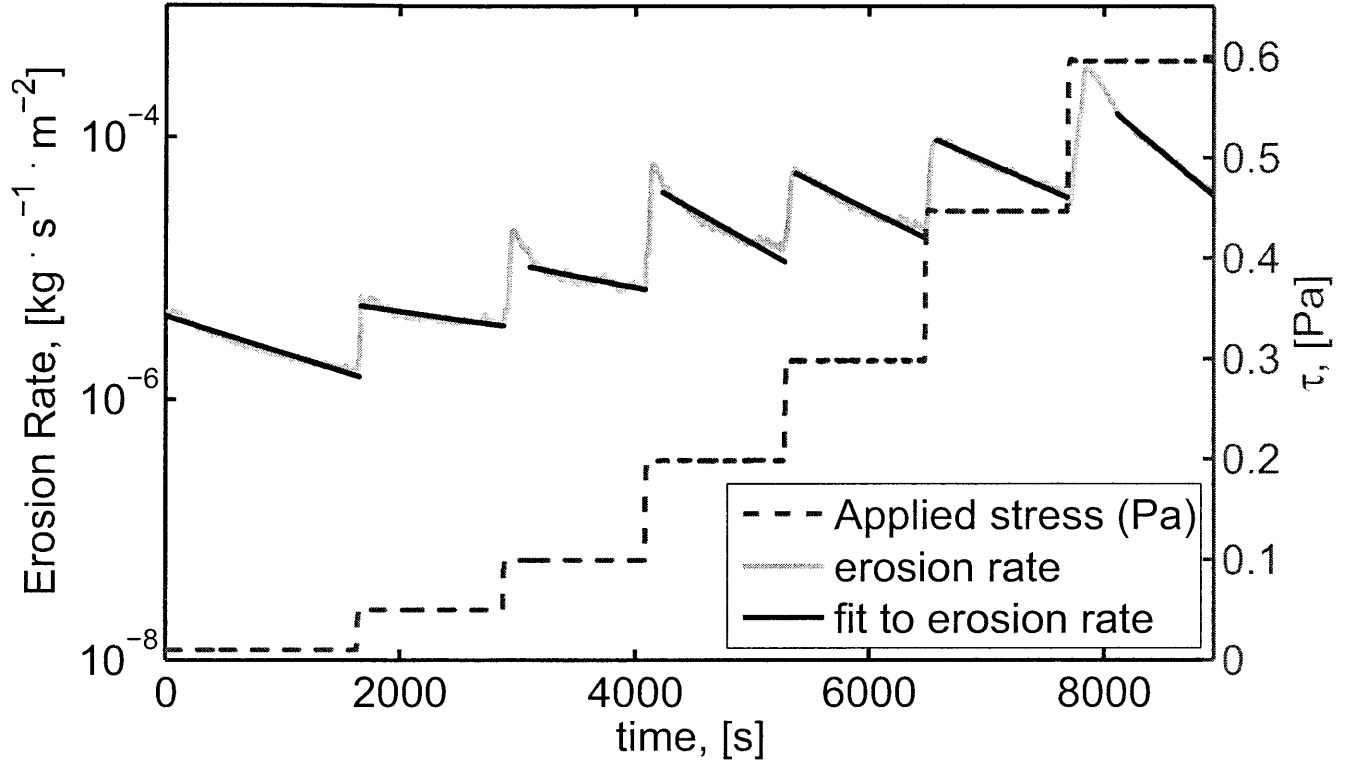
Step	τ_b (Pa)	τ_{ce} (Pa)	m (kg m^{-2})	M (kg m^{-2} s^{-1} Pa^{-1})	E_0 (kg m^{-2} s^{-1})	λ (s^{-1})	length (s)	organic fraction
1	0.0105	0.0400	0.00442	NaN	NaN	6.499e−04	1.664e+03	0.1664
2	0.0501	0.0431	0.00535	5.193e−06	5.160e−04	2.945e−04	1.229e+03	0.1762
3	0.0997	0.0647	0.01124	1.186e−05	2.093e−04	4.039e−04	1.194e+03	0.1285
4	0.1989	0.1656	0.02963	4.577e−05	3.411e−04	1.160e−03	1.199e+03	0.0971
5	0.2984	0.2598	0.03888	5.646e−05	4.249e−04	1.030e−03	1.199e+03	0.0888
6	0.4469	0.3845	0.07297	9.988e−05	5.337e−04	9.127e−04	1.204e+03	0.0757
7	0.5956	0.5713	0.15300	2.980e−04	1.412e−03	1.723e−03	1.254e+03	0.0720

153

s3920-2e
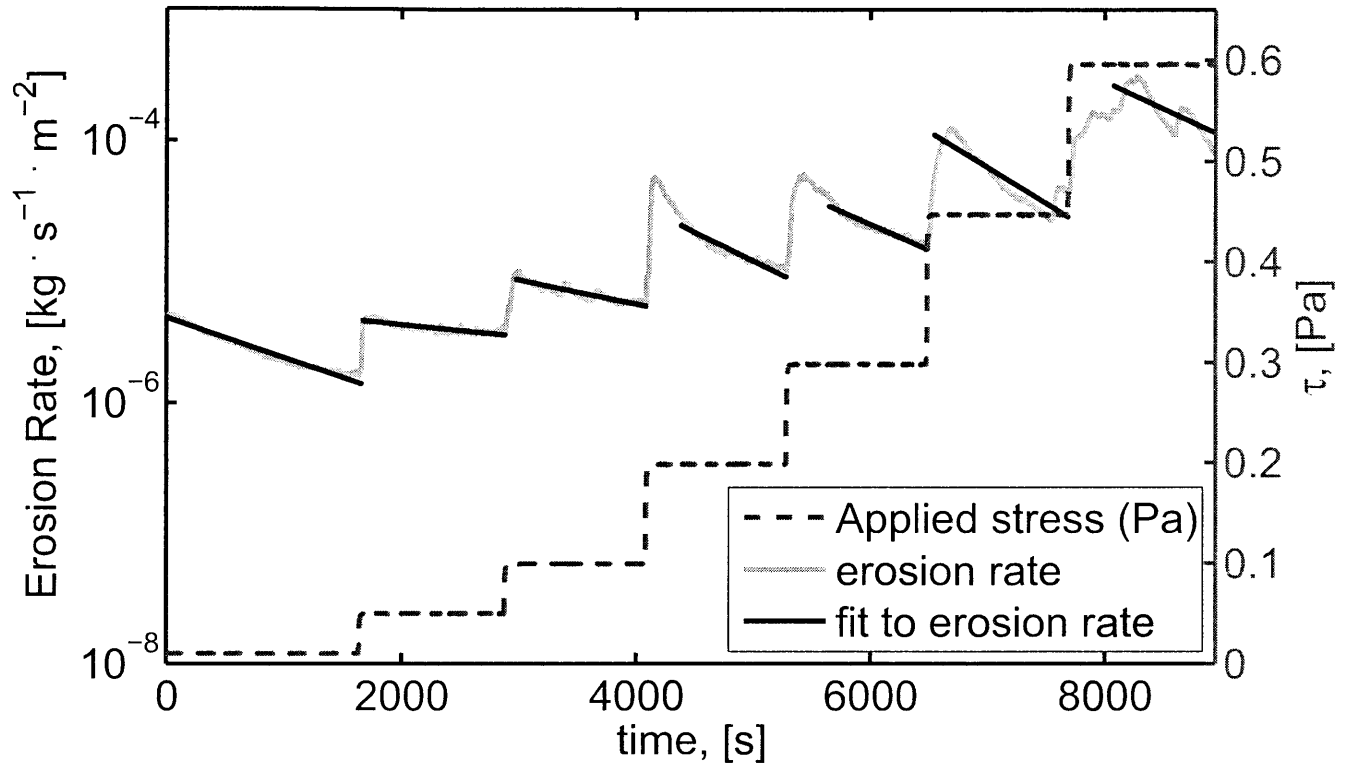
Step	τ_b (Pa)	τ_{ce} (Pa)	m (kg m^{-2})	M (kg m^{-2} s^{-1} Pa^{-1})	E_0 (kg m^{-2} s^{-1})	λ (s^{-1})	length (s)	organic fraction
1	0.0105	0.0400	0.00441	NaN	NaN	7.075e−04	1.664e+03	0.1394
2	0.0499	0.0423	0.00461	4.263e−06	4.300e−04	2.116e−04	1.229e+03	0.1705
3	0.0996	0.0651	0.00834	8.904e−06	1.553e−04	4.250e−04	1.194e+03	0.1569
4	0.1988	0.1591	0.02404	3.463e−05	2.590e−04	1.013e−03	1.199e+03	0.1203
5	0.2983	0.2515	0.03391	4.645e−05	3.336e−04	9.091e−04	1.199e+03	0.1049
6	0.4469	0.4042	0.06932	1.120e−04	5.736e−04	1.263e−03	1.204e+03	0.0876
7	0.5955	0.5374	0.20632	2.816e−04	1.472e−03	9.504e−04	1.254e+03	0.0689

154

s3921-1e
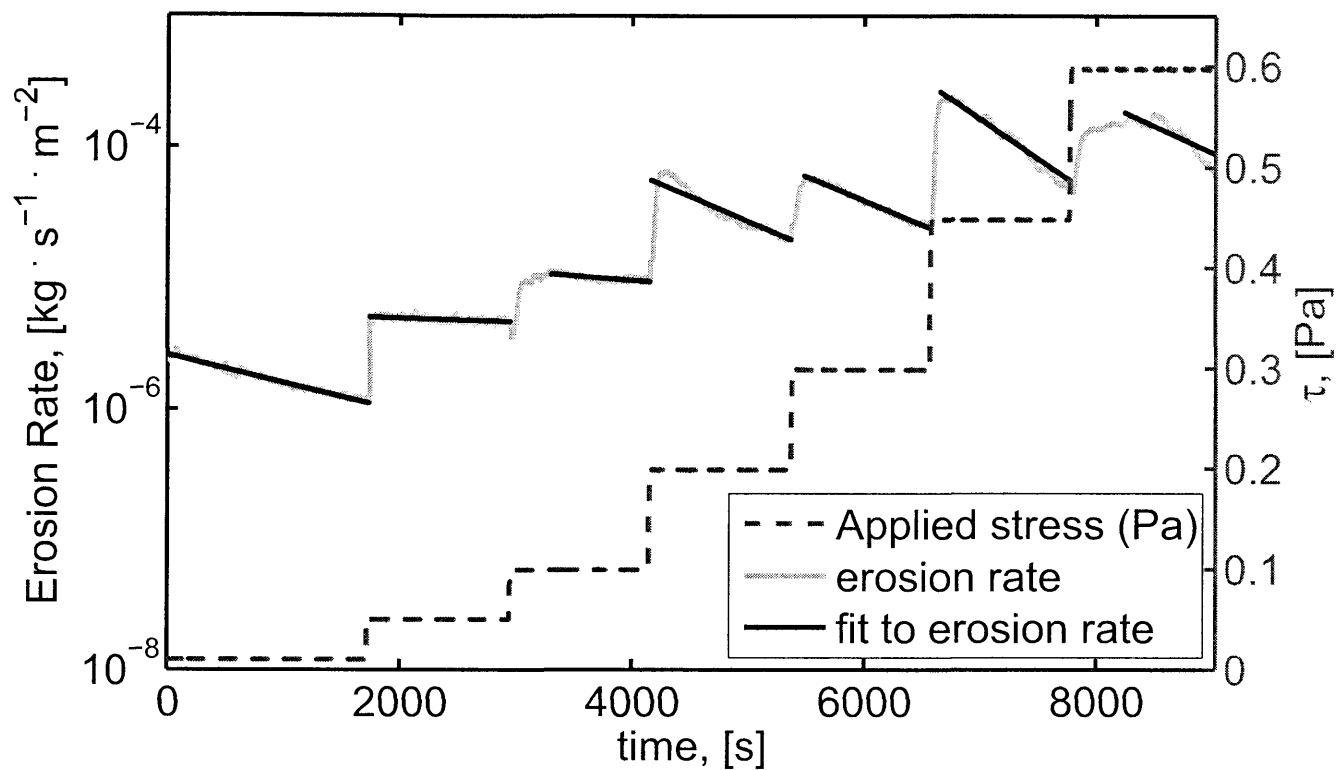
Step	τ_b (Pa)	τ_{ce} (Pa)	m (kg m^{-2})	M (kg m^{-2} s^{-1} Pa^{-1})	E_0 (kg m^{-2} s^{-1})	λ (s^{-1})	length (s)	organic fraction
1	0.0105	0.0400	0.00304	NaN	NaN	4.983e−04	1.739e+03	0.1595
2	0.0501	0.0408	0.00589	5.051e−06	5.006e−04	6.678e−05	1.214e+03	0.1515
3	0.1002	0.0512	0.01163	1.066e−05	1.794e−04	1.605e−04	1.199e+03	0.1541
4	0.1994	0.1481	0.04250	5.632e−05	3.800e−04	8.665e−04	1.224e+03	0.1088
5	0.2991	0.2443	0.04747	6.299e−05	4.170e−04	8.453e−04	1.199e+03	0.1045
6	0.4485	0.4100	0.15953	2.737e−04	1.340e−03	1.392e−03	1.199e+03	0.0784
7	0.5972	0.5391	0.16098	2.187e−04	1.168e−03	9.368e−04	1.249e+03	0.0784

155

s3921-2e
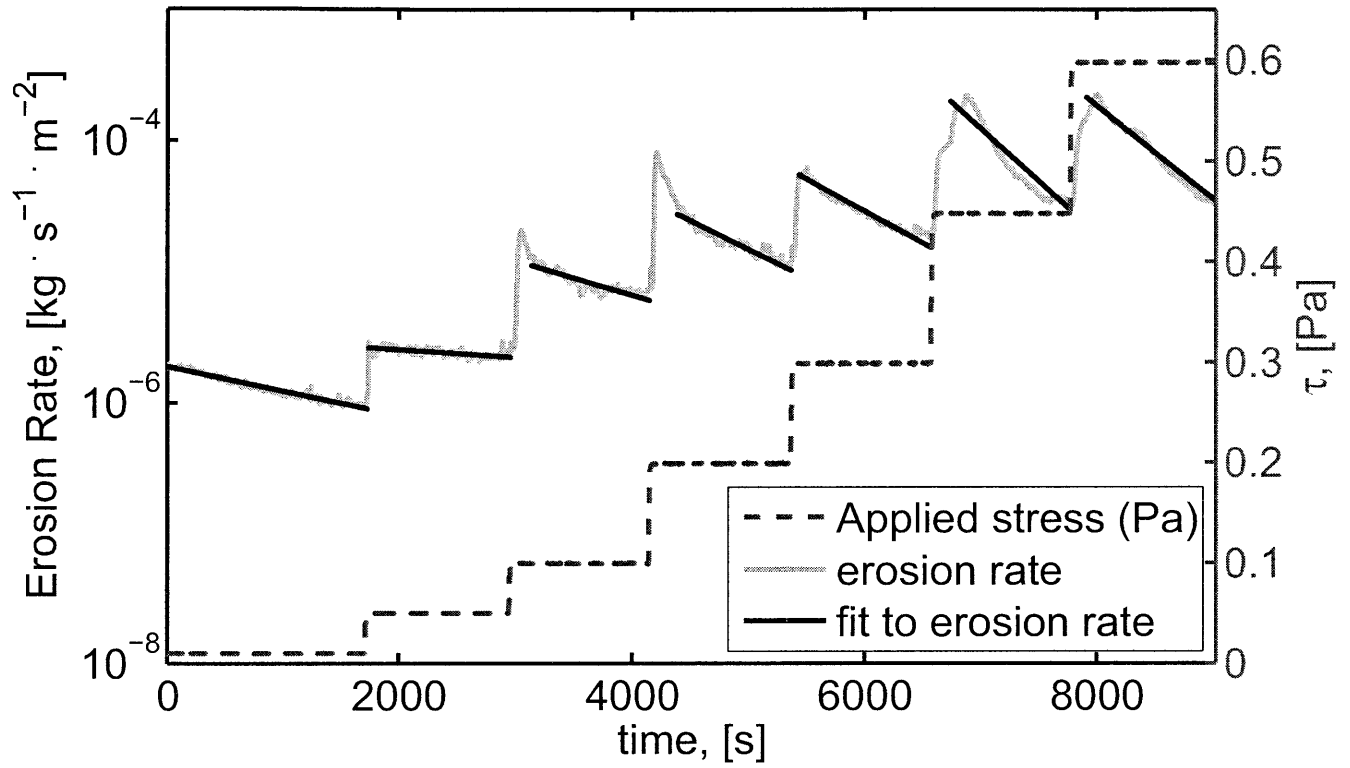
Step	τ_b (Pa)	τ_{ce} (Pa)	m (kg m^{-2})	M (kg m^{-2} s^{-1} Pa^{-1})	E_0 (kg m^{-2} s^{-1})	λ (s^{-1})	length (s)	organic fraction
1	0.0105	0.0400	0.00232	NaN	NaN	4.322e−04	1.739e+03	0.1746
2	0.0500	0.0416	0.00295	2.645e−06	2.642e−04	1.405e−04	1.214e+03	0.1754
3	0.1002	0.0719	0.01075	1.262e−05	2.153e−04	6.072e−04	1.199e+03	0.1436
4	0.1993	0.1623	0.02839	4.041e−05	3.171e−04	1.009e−03	1.224e+03	0.0980
5	0.2991	0.2638	0.03705	5.640e−05	4.123e−04	1.129e−03	1.199e+03	0.0985
6	0.4484	0.4281	0.10340	2.138e−04	1.158e−03	1.840e−03	1.199e+03	0.0822
7	0.5971	0.5752	0.12223	2.295e−04	1.357e−03	1.633e−03	1.249e+03	0.0800

s3922-2e

Step	τ_b (Pa)	τ_{ce} (Pa)	m (kg m^{-2})	M (kg m^{-2} s^{-1} Pa^{-1})	E_0 (kg m^{-2} s^{-1})	λ (s^{-1})	length (s)	organic fraction
1	0.0105	0.0400	0.00256	NaN	NaN	1.091e−03	1.649e+03	0.2419
2	0.0506	0.0451	0.00097	2.261e−06	2.125e−04	1.127e−03	5.840e+02	0.5467
3	0.1008	0.0688	0.01380	1.500e−05	2.694e−04	4.629e−04	1.199e+03	0.2090
4	0.2002	0.1590	0.05281	7.471e−05	5.687e−04	9.710e−04	1.194e+03	0.1102
5	0.3005	0.2778	0.09085	1.651e−04	1.167e−03	1.526e−03	1.199e+03	0.0930
6	0.4499	0.4370	0.11626	2.737e−04	1.590e−03	2.178e−03	1.189e+03	0.0961
7	0.5994	0.5825	0.17024	2.850e−04	1.755e−03	1.500e−03	1.509e+03	0.0928

s3922-3e
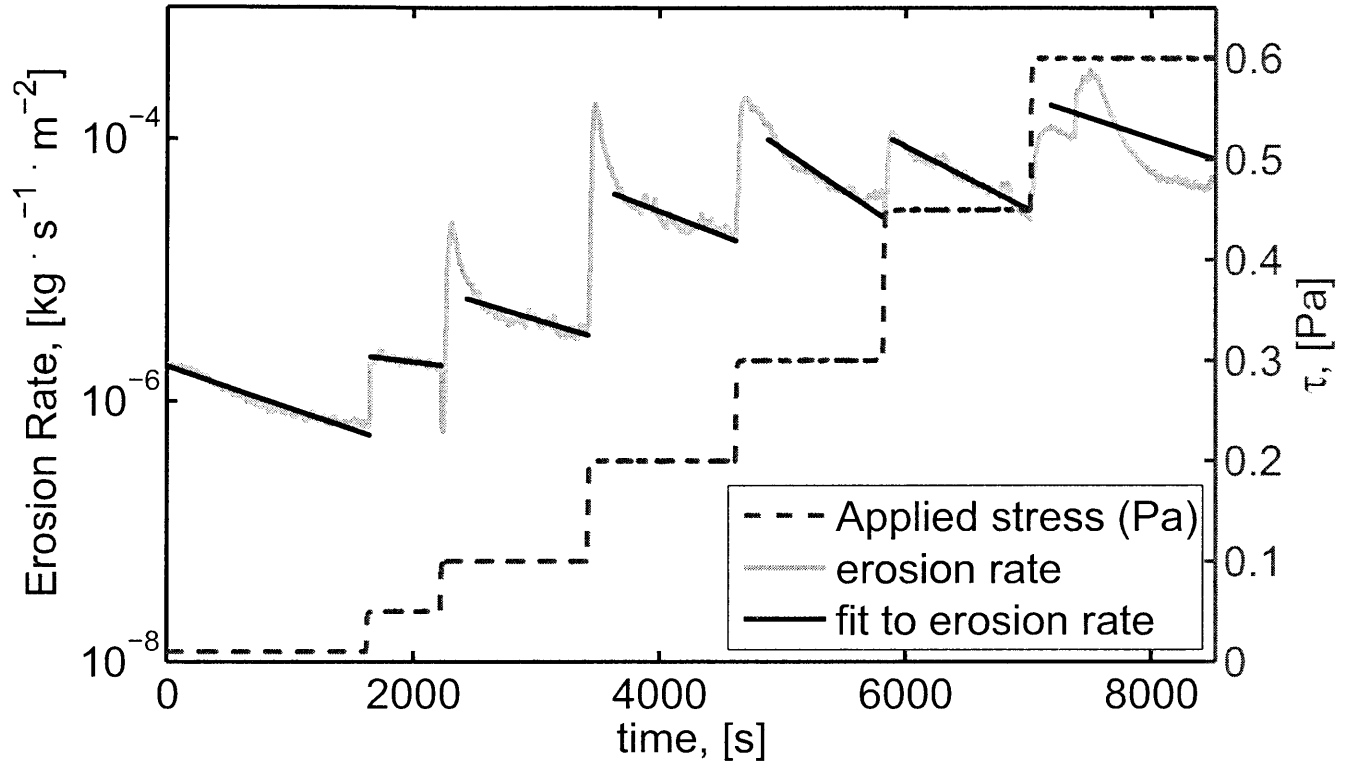
Step	τ_b (Pa)	τ_{ce} (Pa)	m (kg m^{-2})	M (kg m^{-2} s^{-1} Pa^{-1})	E_0 (kg m^{-2} s^{-1})	λ (s^{-1})	length (s)	organic fraction
1	0.0105	0.0400	0.00176	NaN	NaN	7.451e−04	1.649e+03	0.2800
2	0.0506	0.0416	0.00118	2.185e−06	2.060e−04	2.707e−04	5.840e+02	0.4279
3	0.1006	0.0736	0.00682	8.202e−06	1.390e−04	6.531e−04	1.199e+03	0.2088
4	0.2001	0.1536	0.04523	5.993e−05	4.735e−04	8.377e−04	1.194e+03	0.1116
5	0.3003	0.2749	0.09059	1.601e−04	1.091e−03	1.460e−03	1.199e+03	0.1015
6	0.4497	0.4028	0.06857	1.037e−04	5.930e−04	1.107e−03	1.189e+03	0.1194
7	0.5993	0.5323	0.16562	1.791e−04	9.116e−04	7.126e−04	1.509e+03	0.0991

s3923-1e
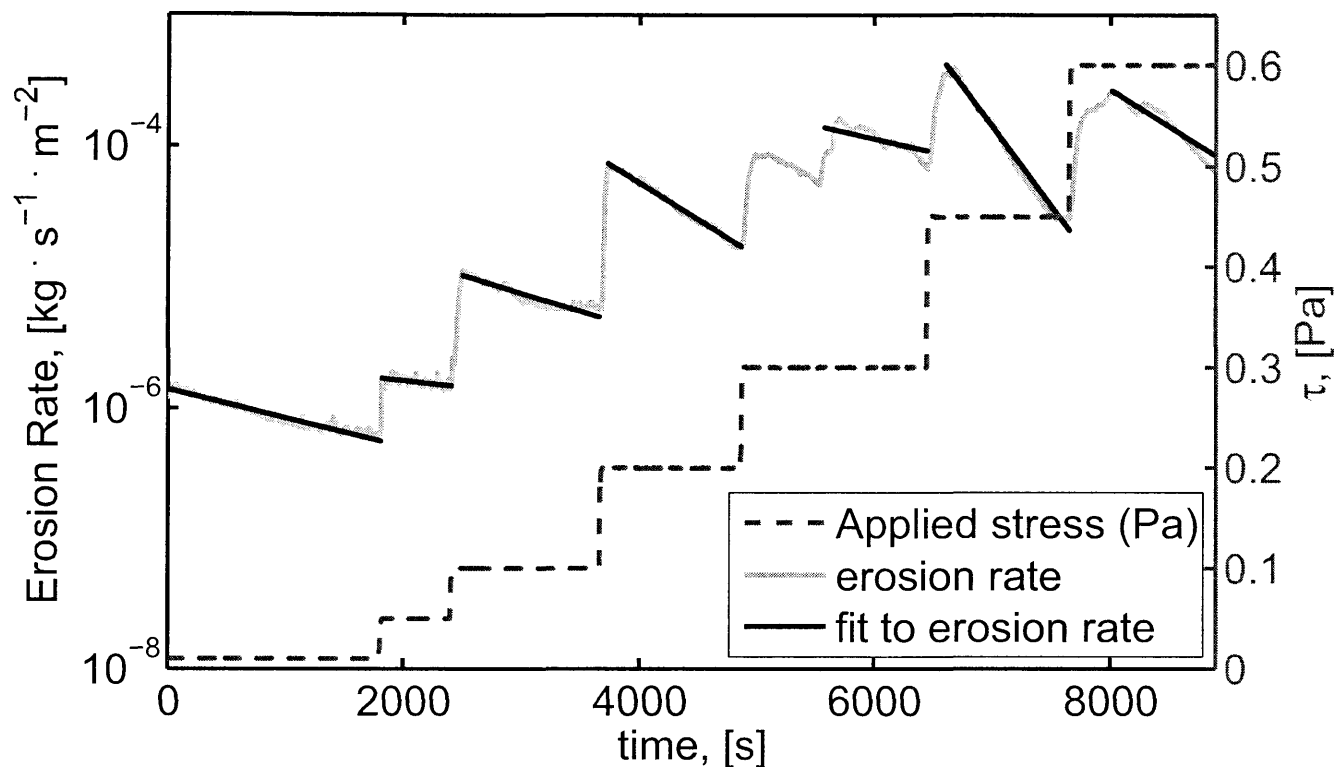
Step	τ_b (Pa)	τ_{ce} (Pa)	m (kg m^{-2})	M (kg m^{-2} s^{-1} Pa^{-1})	E_0 (kg m^{-2} s^{-1})	λ (s^{-1})	length (s)	organic fraction
1	0.0102	0.0400	0.00166	NaN	NaN	5.081e−04	1.814e+03	0.1264
2	0.0506	0.0414	0.00095	1.698e−06	1.602e−04	2.306e−04	5.990e+02	0.1348
3	0.1002	0.0737	0.00903	1.045e−05	1.775e−04	6.354e−04	1.254e+03	0.1826
4	0.2003	0.1735	0.04616	7.581e−05	5.987e−04	1.295e−03	1.199e+03	0.0980
5	0.3005	0.2397	0.14933	1.328e−04	1.045e−03	4.631e−04	1.589e+03	0.0946
6	0.4507	0.4433	0.17353	5.024e−04	2.381e−03	2.794e−03	1.199e+03	0.0837
7	0.6000	0.5685	0.19958	3.233e−04	2.062e−03	1.294e−03	1.239e+03	0.0780

159

s3923-3e
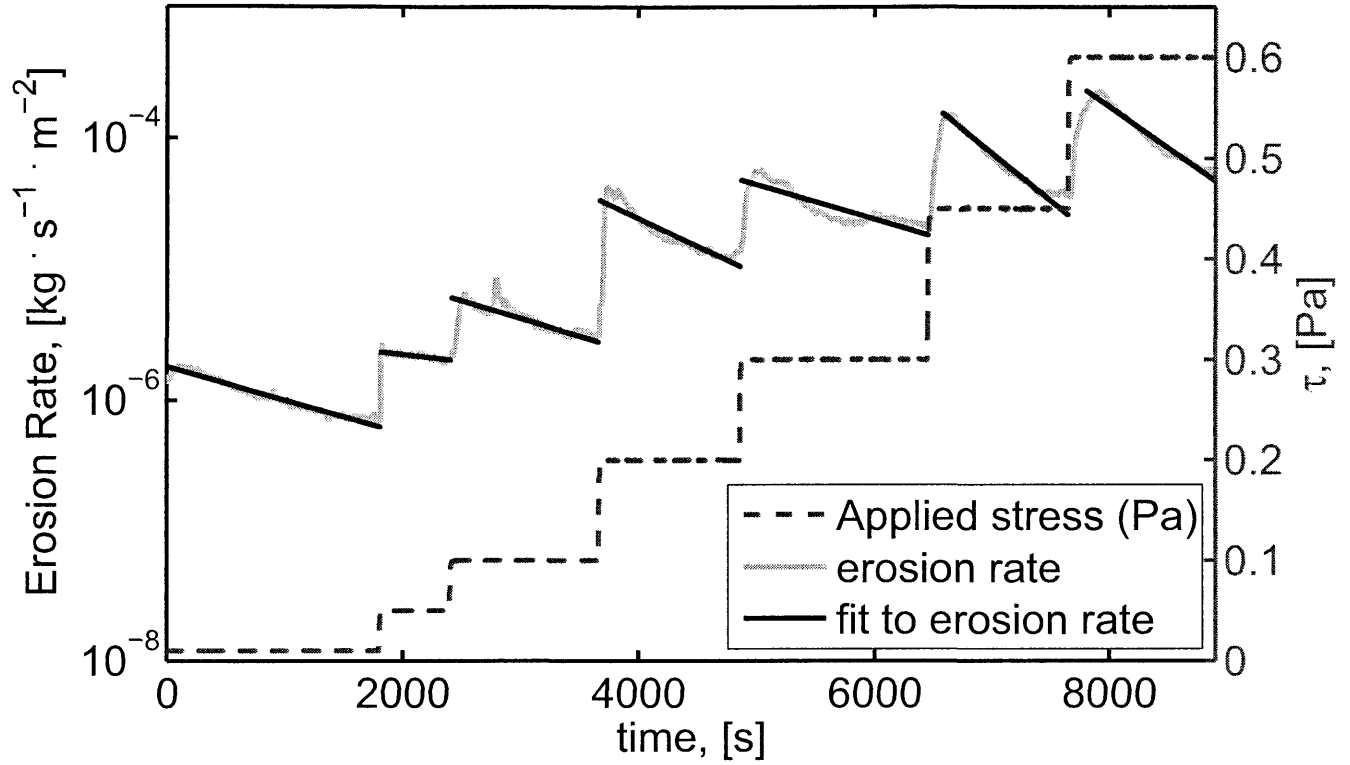
Step	τ_b (Pa)	τ_{ce} (Pa)	m (kg m^{-2})	M (kg m^{-2} s^{-1} Pa^{-1})	E_0 (kg m^{-2} s^{-1})	λ (s^{-1})	length (s)	organic fraction
1	0.0102	0.0400	0.00202	NaN	NaN	5.940e−04	1.814e+03	0.0943
2	0.0506	0.0414	0.00130	2.341e−06	2.210e−04	2.455e−04	5.990e+02	0.1064
3	0.1003	0.0734	0.00534	6.147e−06	1.044e−04	6.248e−04	1.254e+03	0.1308
4	0.2002	0.1611	0.02392	3.391e−05	2.675e−04	9.801e−04	1.199e+03	0.0902
5	0.3004	0.2479	0.04893	4.824e−05	3.462e−04	6.144e−04	1.589e+03	0.0920
6	0.4505	0.4230	0.08655	1.667e−04	8.228e−04	1.665e−03	1.199e+03	0.0842
7	0.5999	0.5708	0.14205	2.476e−04	1.400e−03	1.457e−03	1.239e+03	0.0821

160

s3924-2e
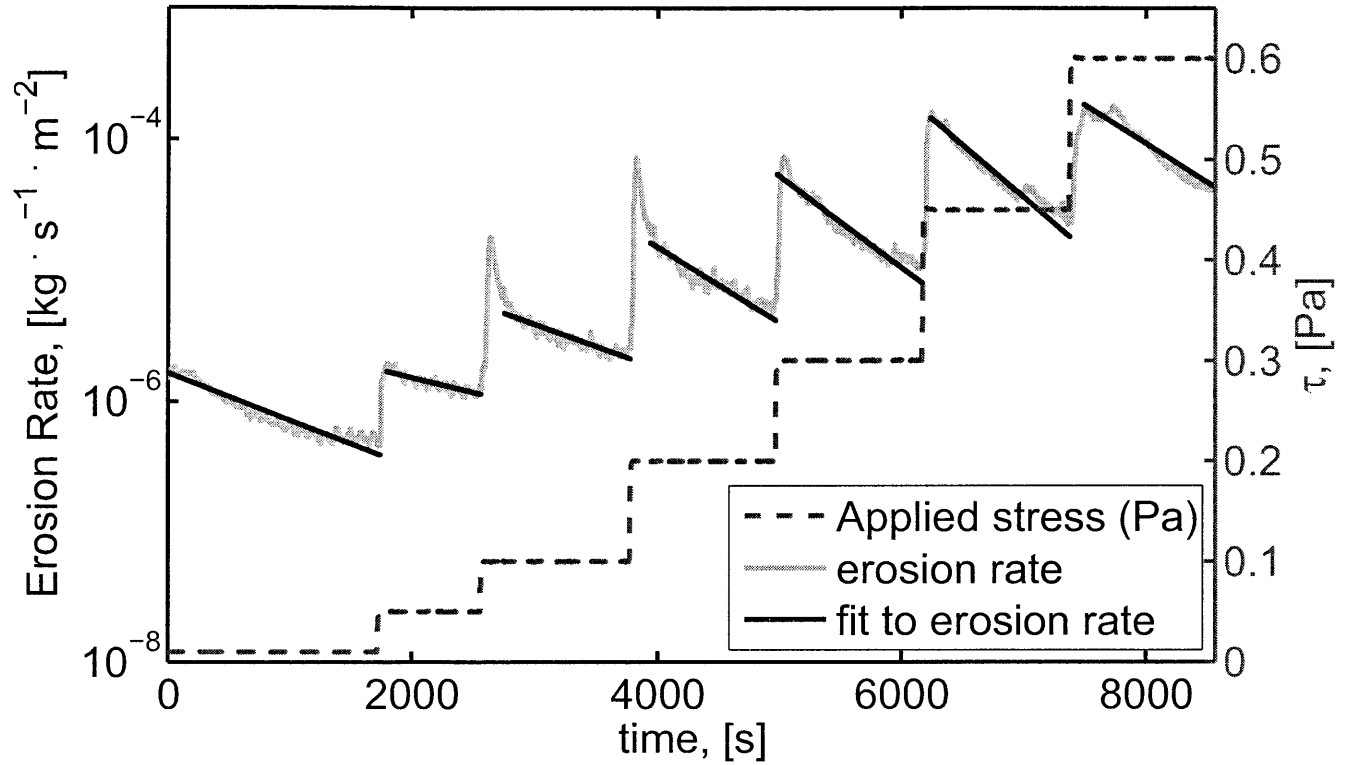
Step	τ_b (Pa)	τ_{ce} (Pa)	m (kg m^{-2})	M (kg m^{-2} s^{-1} Pa^{-1})	E_0 (kg m^{-2} s^{-1})	λ (s^{-1})	length (s)	organic fraction
1	0.0105	0.0400	0.00151	NaN	NaN	8.359e−04	1.744e+03	0.0939
2	0.0506	0.0438	0.00115	1.730e−06	1.633e−04	5.306e−04	8.240e+02	0.1206
3	0.1007	0.0787	0.00492	6.276e−06	1.103e−04	7.831e−04	1.214e+03	0.1211
4	0.2003	0.1753	0.01460	2.434e−05	2.001e−04	1.324e−03	1.194e+03	0.0958
5	0.3008	0.2826	0.02900	5.468e−05	4.358e−04	1.613e−03	1.199e+03	0.0718
6	0.4505	0.4320	0.07518	1.554e−04	9.257e−04	1.839e−03	1.199e+03	0.0562
7	0.5999	0.5662	0.11513	1.930e−04	1.149e−03	1.340e−03	1.199e+03	0.0537

161

s3924-3e
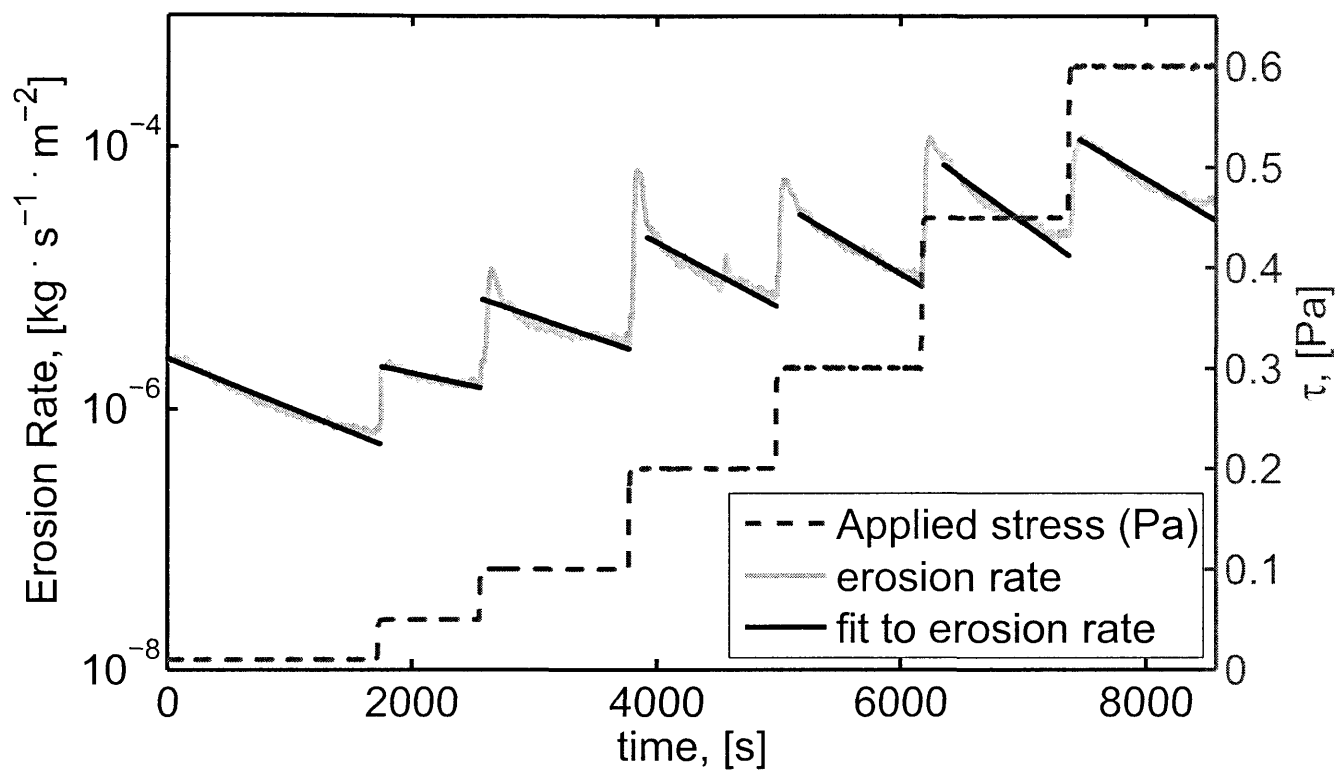
Step	τ_b (Pa)	τ_{ce} (Pa)	m (kg m^{-2})	M (kg m^{-2} s^{-1} Pa^{-1})	E_0 (kg m^{-2} s^{-1})	λ (s^{-1})	length (s)	organic fraction
1	0.0105	0.0400	0.00219	NaN	NaN	8.756e−04	1.744e+03	0.1788
2	0.0504	0.0434	0.00144	2.111e−06	2.022e−04	4.730e−04	8.240e+02	0.2391
3	0.1006	0.0772	0.00552	6.875e−06	1.202e−04	7.359e−04	1.214e+03	0.1309
4	0.2003	0.1694	0.01811	2.798e−05	2.272e−04	1.157e−03	1.194e+03	0.0939
5	0.3005	0.2714	0.02512	4.053e−05	3.091e−04	1.256e−03	1.199e+03	0.0826
6	0.4503	0.4229	0.05288	9.766e−05	5.458e−04	1.563e−03	1.199e+03	0.0611
7	0.5998	0.5619	0.07406	1.211e−04	6.845e−04	1.285e−03	1.199e+03	0.0609

S3925-1e
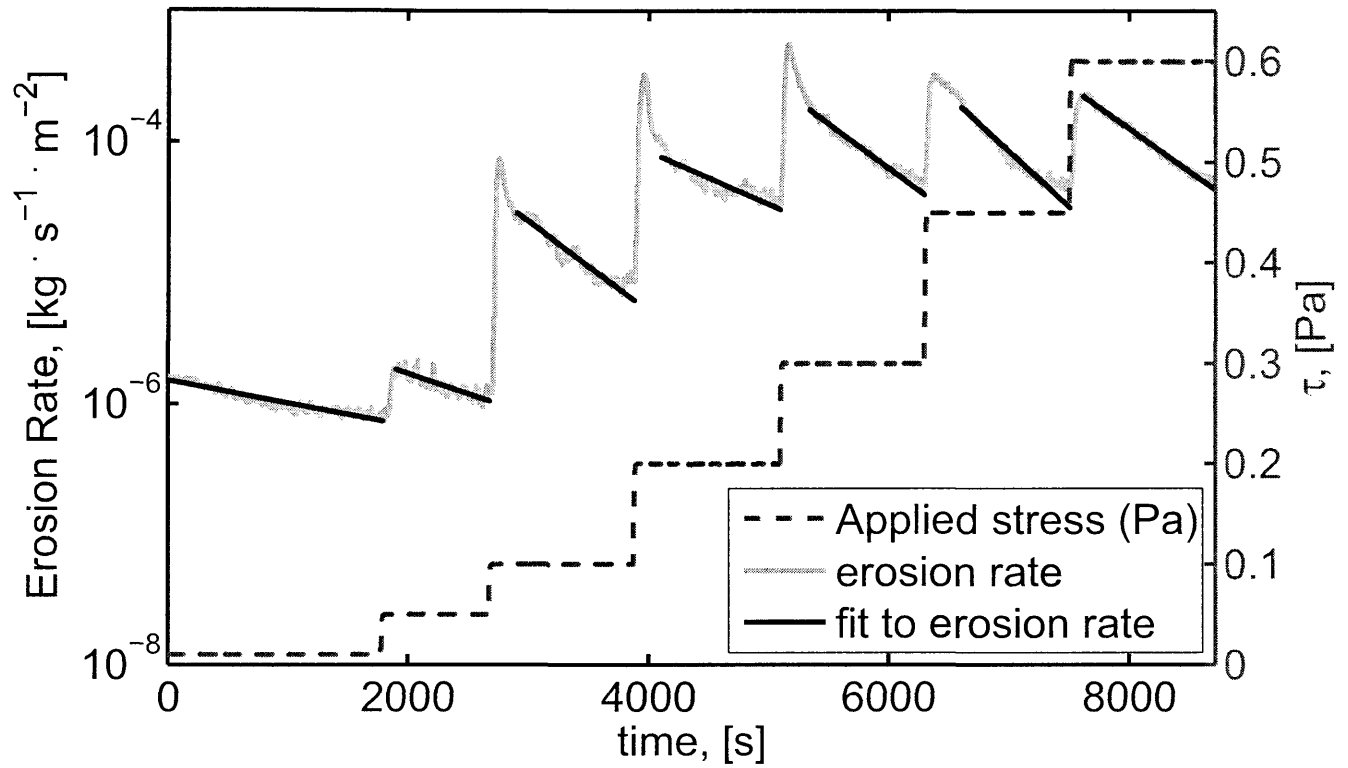
Step	τ_b (Pa)	τ_{ce} (Pa)	m (kg m^{-2})	M (kg m^{-2} s^{-1} Pa^{-1})	E_0 (kg m^{-2} s^{-1})	λ (s^{-1})	length (s)	organic fraction
1	0.0104	0.0400	0.00195	NaN	NaN	4.041e−04	1.799e+03	0.1498
2	0.0504	0.0449	0.00123	1.879e−06	1.804e−04	7.229e−04	8.840e+02	0.1875
3	0.1005	0.0922	0.02274	4.237e−05	7.618e−04	1.585e−03	1.199e+03	0.1000
4	0.2003	0.1652	0.08568	1.166e−04	1.080e−03	9.199e−04	1.224e+03	0.0811
5	0.3003	0.2796	0.16324	3.014e−04	2.231e−03	1.563e−03	1.199e+03	0.0714
6	0.4504	0.4341	0.15400	3.339e−04	1.955e−03	1.962e−03	1.199e+03	0.0659
7	0.5996	0.5724	0.13836	2.464e−04	1.489e−03	1.489e−03	1.214e+03	0.0674

S3925-3e
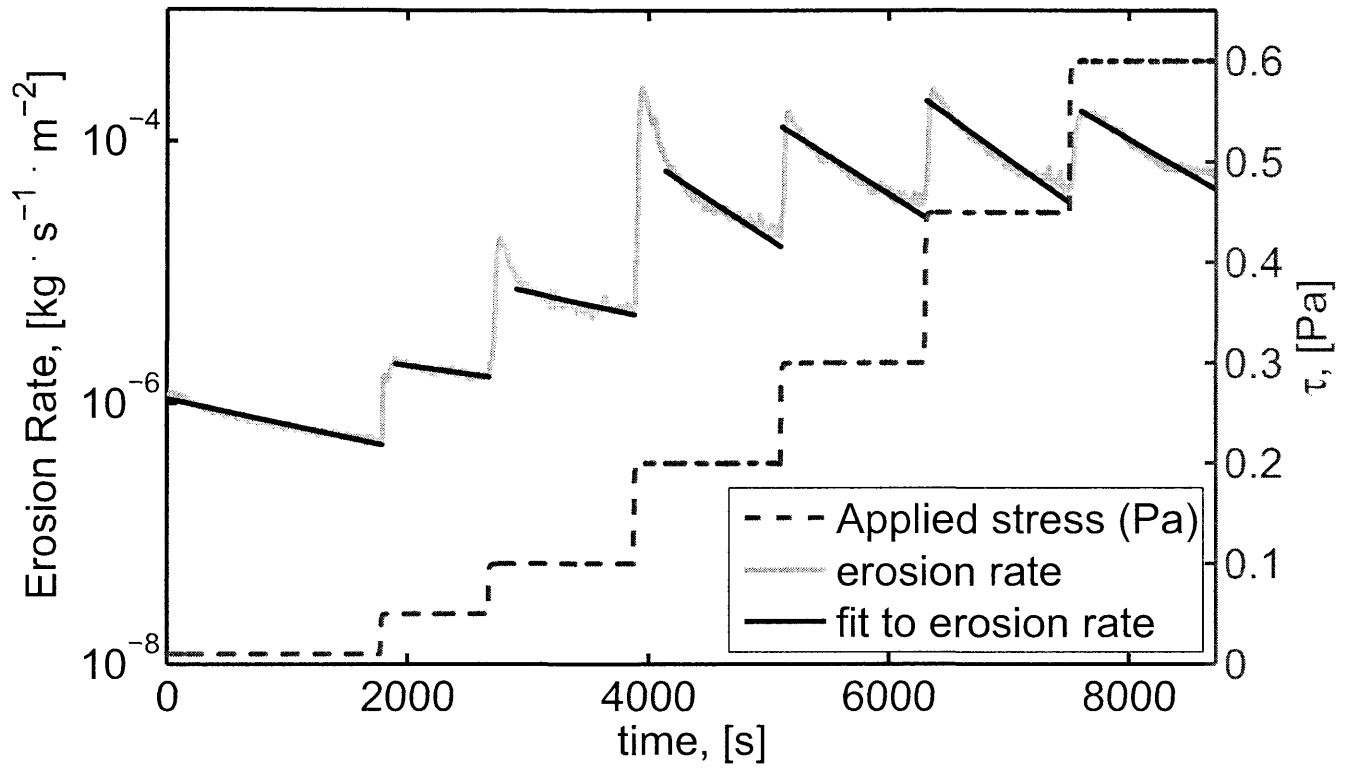
Step	τ_b (Pa)	τ_{ce} (Pa)	m (kg m^{-2})	M (kg m^{-2} s^{-1} Pa^{-1})	E_0 (kg m^{-2} s^{-1})	λ (s^{-1})	length (s)	organic fraction
1	0.0104	0.0400	0.00133	NaN	NaN	4.576e−04	1.799e+03	0.1799
2	0.0503	0.0424	0.00158	2.029e−06	1.972e−04	2.999e−04	8.840e+02	0.1963
3	0.1005	0.0670	0.00834	9.057e−06	1.560e−04	4.607e−04	1.199e+03	0.1234
4	0.2001	0.1758	0.06714	1.141e−04	8.569e−04	1.388e−03	1.224e+03	0.0852
5	0.3003	0.2750	0.07795	1.299e−04	1.043e−03	1.327e−03	1.199e+03	0.0832
6	0.4502	0.4215	0.11516	2.077e−04	1.186e−03	1.508e−03	1.199e+03	0.0749
7	0.5995	0.5593	0.11448	1.812e−04	1.018e−03	1.226e−03	1.214e+03	0.0695

S3926-1e
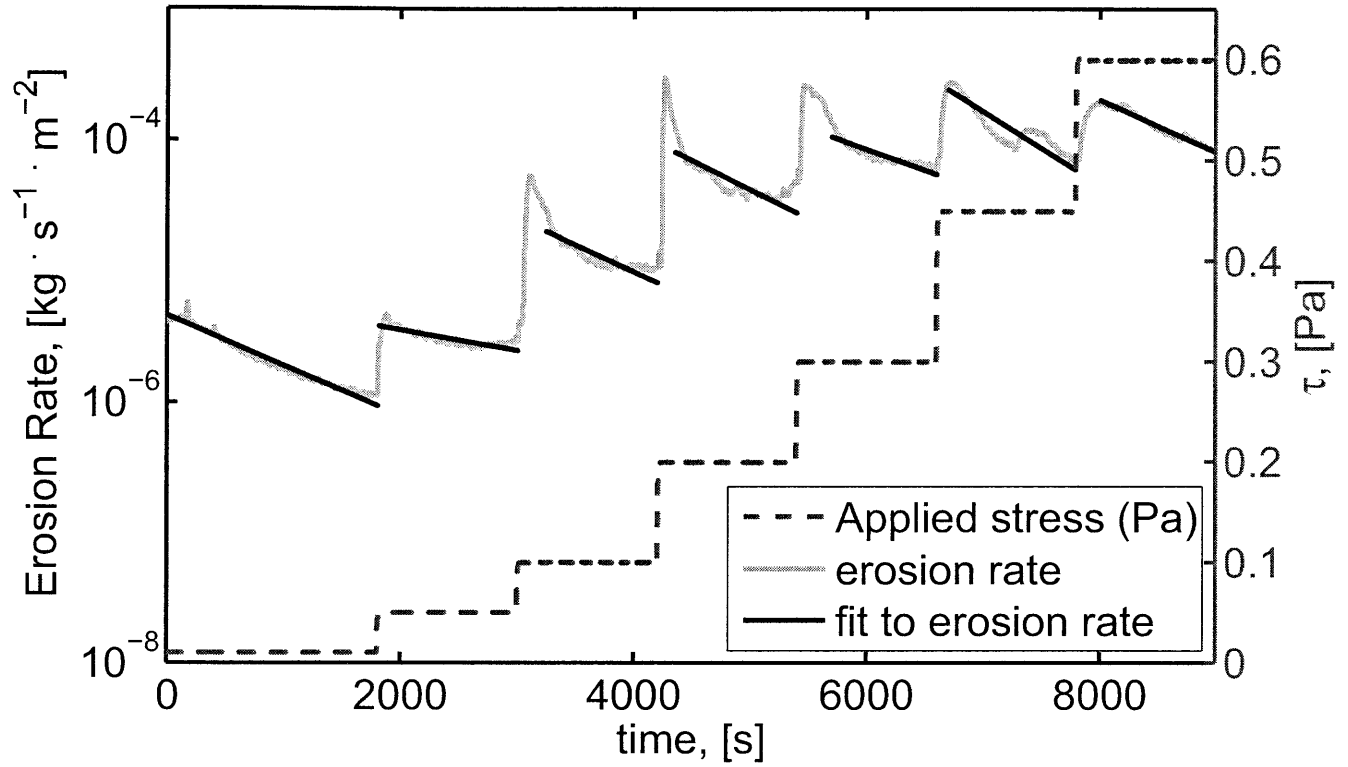
Step	τ_b (Pa)	τ_{ce} (Pa)	m (kg m^{-2})	M (kg m^{-2} s^{-1} Pa^{-1})	E_0 (kg m^{-2} s^{-1})	λ (s^{-1})	length (s)	organic fraction
1	0.0102	0.0400	0.00418	NaN	NaN	8.872e−04	1.814e+03	0.3072
2	0.0503	0.0436	0.00371	3.825e−06	3.727e−04	3.661e−04	1.199e+03	0.3713
3	0.1000	0.0819	0.02026	2.842e−05	5.047e−04	9.537e−04	1.194e+03	0.1950
4	0.1999	0.1651	0.07584	1.095e−04	9.283e−04	1.018e−03	1.199e+03	0.1167
5	0.3000	0.2440	0.12738	1.597e−04	1.184e−03	7.329e−04	1.199e+03	0.0984
6	0.4498	0.4054	0.15927	2.618e−04	1.272e−03	1.289e−03	1.189e+03	0.0863
7	0.5989	0.5346	0.16298	2.243e−04	1.159e−03	9.190e−04	1.199e+03	0.0746

165

S3926-2e
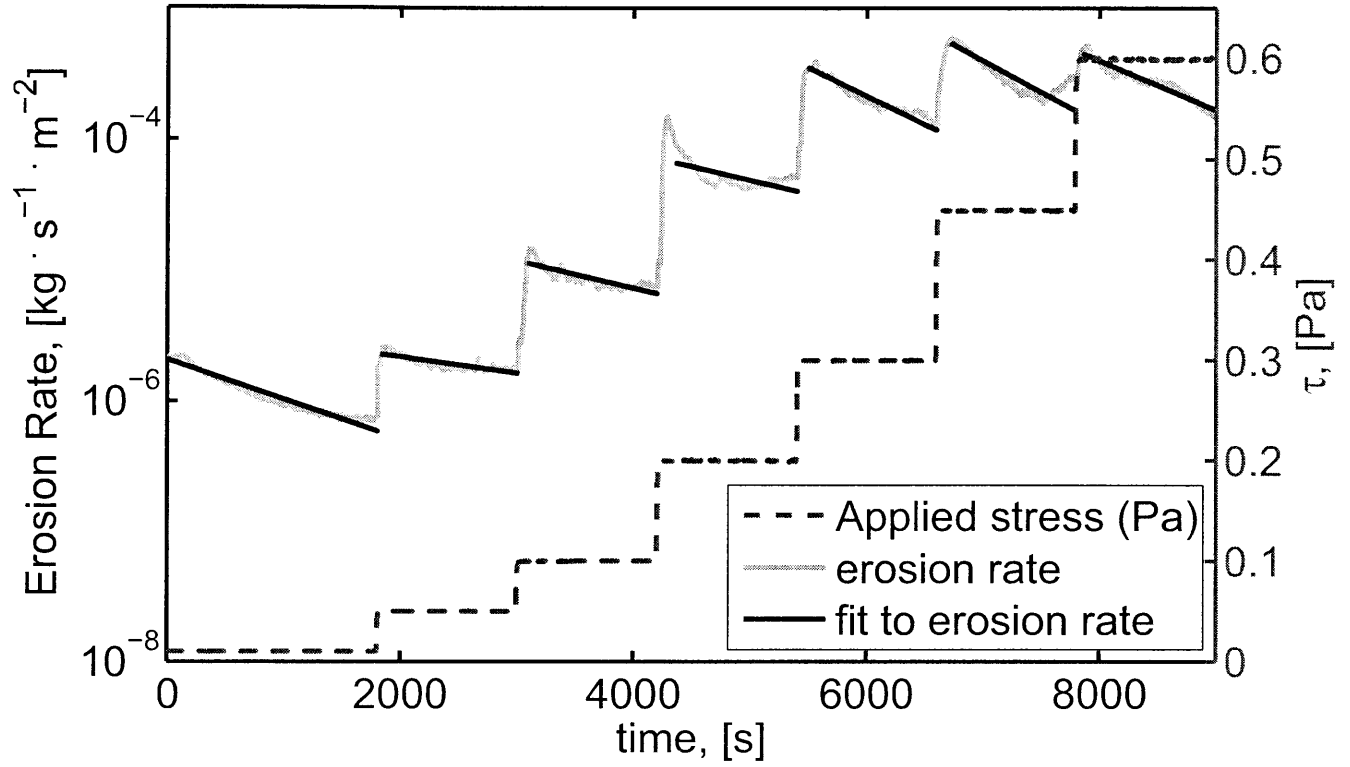
Step	τ_b (Pa)	τ_{ce} (Pa)	m (kg m^{-2})	M (kg m^{-2} s^{-1} Pa^{-1})	E_0 (kg m^{-2} s^{-1})	λ (s^{-1})	length (s)	organic fraction
1	0.0101	0.0400	0.00213	NaN	NaN	7.053e−04	1.814e+03	0.3297
2	0.0502	0.0431	0.00230	2.275e−06	2.224e−04	2.957e−04	1.199e+03	0.3864
3	0.1001	0.0684	0.01012	1.120e−05	1.964e−04	4.920e−04	1.194e+03	0.3197
4	0.1998	0.1260	0.06838	7.506e−05	5.710e−04	4.813e−04	1.199e+03	0.1128
5	0.2999	0.2470	0.25733	3.670e−04	2.111e−03	9.922e−04	1.199e+03	0.0746
6	0.4496	0.3951	0.38899	5.878e−04	2.901e−03	1.105e−03	1.189e+03	0.0647
7	0.5988	0.5272	0.34734	4.672e−04	2.294e−03	8.724e−04	1.199e+03	0.0538

166

S3927-5e
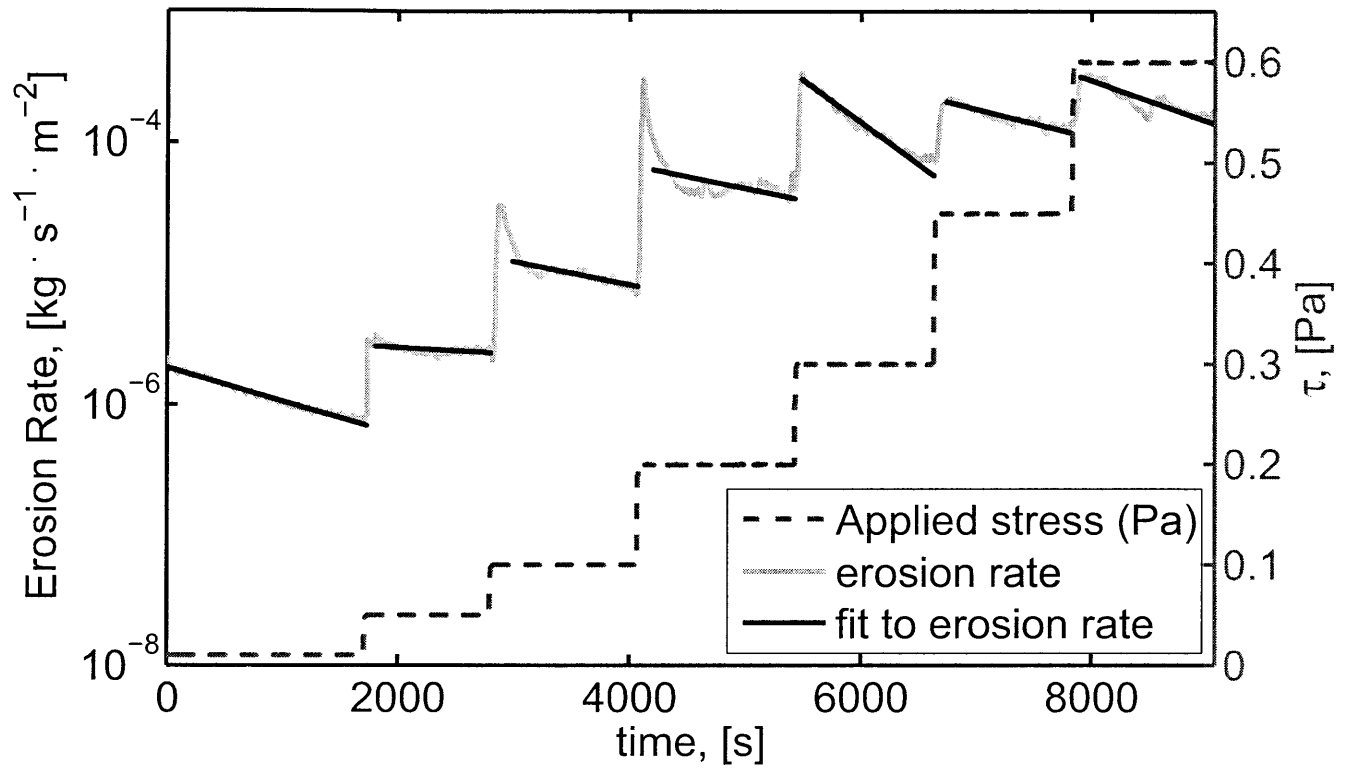
Step	τ_b (Pa)	τ_{ce} (Pa)	m (kg m^{-2})	M (kg m^{-2} s^{-1} Pa^{-1})	E_0 (kg m^{-2} s^{-1})	λ (s^{-1})	length (s)	organic fraction
1	0.0105	0.0400	0.00210	NaN	NaN	5.918e−04	1.739e+03	0.3254
2	0.0502	0.0412	0.00283	2.830e−06	2.764e−04	1.181e−04	1.064e+03	0.2686
3	0.1005	0.0651	0.01461	1.467e−05	2.473e−04	4.040e−04	1.274e+03	0.1589
4	0.2000	0.1234	0.07947	7.660e−05	5.675e−04	4.169e−04	1.359e+03	0.1042
5	0.3001	0.2702	0.17770	3.168e−04	1.793e−03	1.481e−03	1.199e+03	0.0945
6	0.4501	0.3520	0.18797	2.090e−04	1.162e−03	5.054e−04	1.199e+03	0.0910
7	0.5992	0.4969	0.26454	3.227e−04	1.305e−03	7.150e−04	1.234e+03	0.0832

S3927-6e
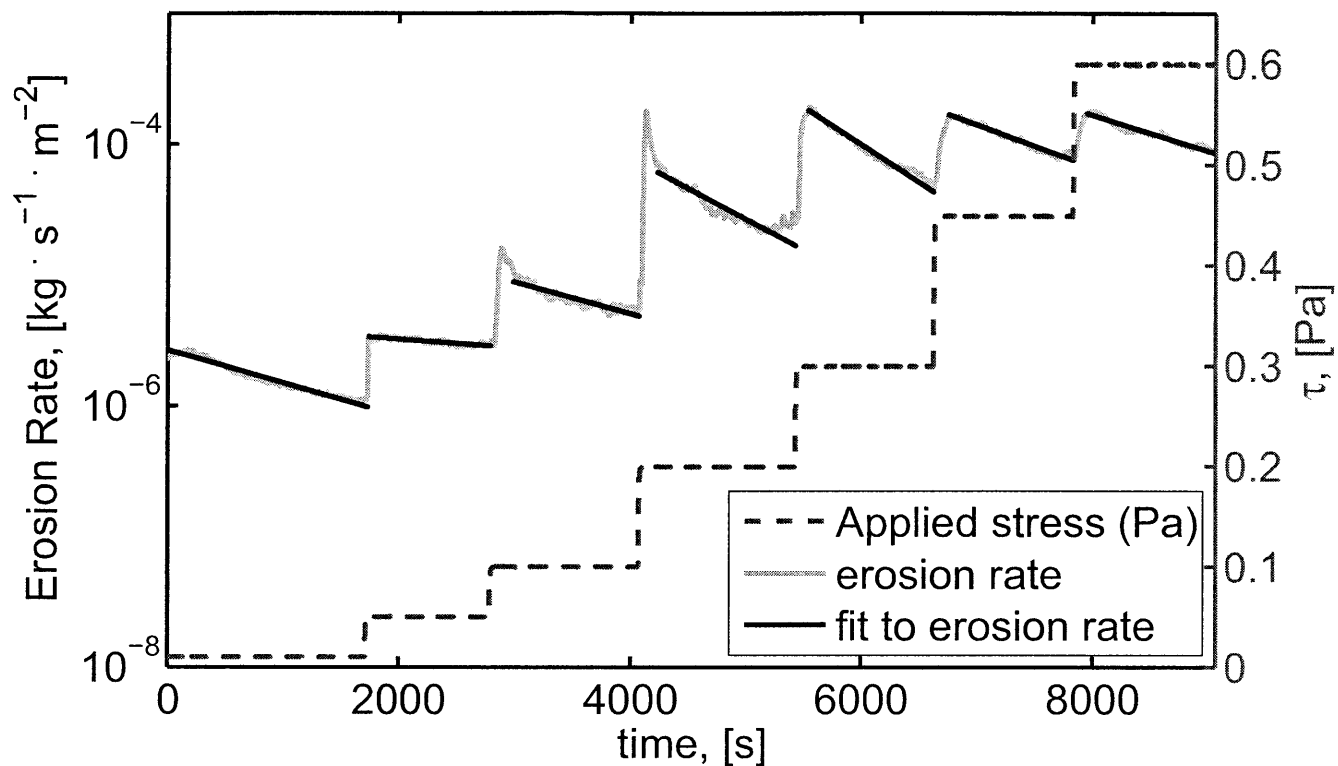
Step	τ_b (Pa)	τ_{ce} (Pa)	m (kg m^{-2})	M (kg m^{-2} s^{-1} Pa^{-1})	E_0 (kg m^{-2} s^{-1})	λ (s^{-1})	length (s)	organic fraction
1	0.0104	0.0400	0.00293	NaN	NaN	5.799e−04	1.739e+03	0.2093
2	0.0503	0.0415	0.00330	3.359e−06	3.255e−04	1.494e−04	1.064e+03	0.3528
3	0.1004	0.0713	0.00917	1.003e−05	1.702e−04	5.535e−04	1.274e+03	0.2421
4	0.1999	0.1700	0.05550	7.764e−05	6.039e−04	1.074e−03	1.359e+03	0.1262
5	0.3001	0.2730	0.11866	1.960e−04	1.507e−03	1.307e−03	1.199e+03	0.1102
6	0.4499	0.3771	0.13896	1.749e−04	9.885e−04	7.406e−04	1.199e+03	0.0958
7	0.5992	0.4964	0.15425	1.793e−04	8.072e−04	6.247e−04	1.234e+03	0.0932

S3928-6e
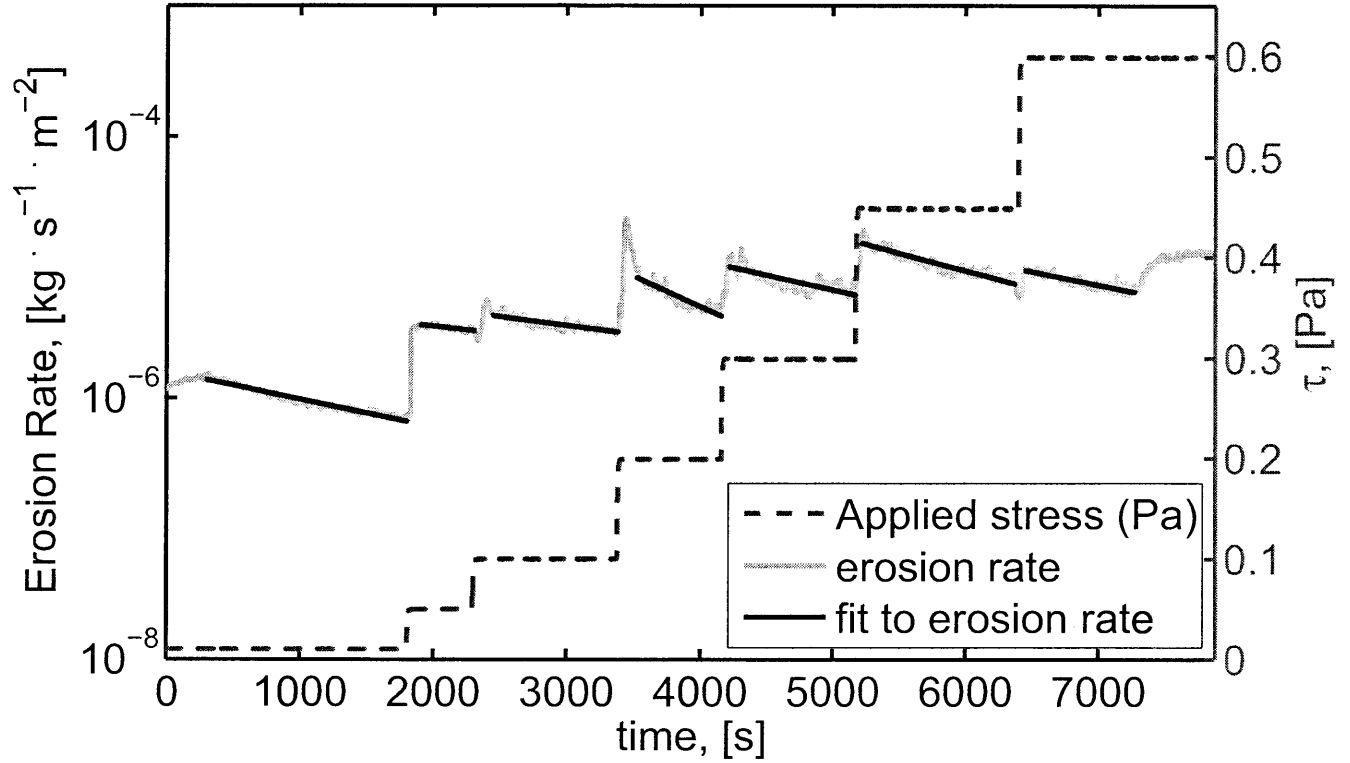
Step	τ_b (Pa)	τ_{ce} (Pa)	m (kg m^{-2})	M (kg m^{-2} s^{-1} Pa^{-1})	E_0 (kg m^{-2} s^{-1})	λ (s^{-1})	length (s)	organic fraction
1	0.0105	0.0600	0.00188	NaN	NaN	4.864e−04	1.829e+03	0.1798
2	0.0507	0.0589	0.00167	3.661e−06	−3.935e−04	2.587e−04	4.840e+02	0.2109
3	0.1006	0.0705	0.00407	4.419e−06	1.061e−04	3.032e−04	1.079e+03	0.2159
4	0.2001	0.1436	0.00570	1.084e−05	8.366e−05	1.073e−03	7.740e+02	0.1926
5	0.2998	0.2074	0.00806	1.027e−05	6.576e−05	5.197e−04	1.009e+03	0.2265
6	0.4488	0.3339	0.01322	1.562e−05	6.470e−05	6.191e−04	1.199e+03	0.1770
7	0.5960	0.4667	0.01407	1.309e−05	4.996e−05	4.717e−04	1.499e+03	0.1993

169

S3928-8e
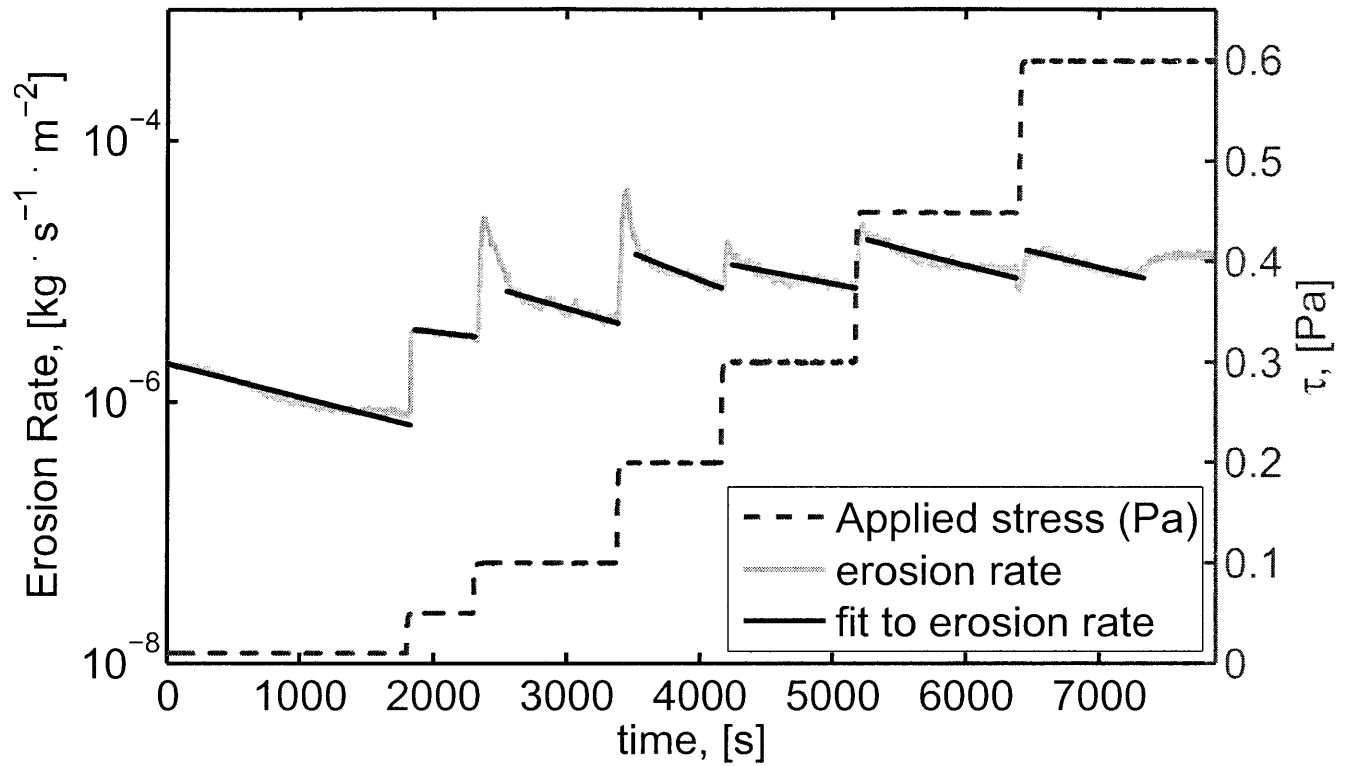
Step	τ_b (Pa)	τ_{ce} (Pa)	m (kg m^{-2})	M (kg m^{-2} s^{-1} Pa^{-1})	E_0 (kg m^{-2} s^{-1})	λ (s^{-1})	length (s)	organic fraction
1	0.0104	0.0600	0.00219	NaN	NaN	5.932e−04	1.829e+03	0.2217
2	0.0508	0.0589	0.00162	3.573e−06	−3.879e−04	2.696e−04	4.840e+02	0.2852
3	0.1005	0.0804	0.00789	1.030e−05	2.475e−04	6.769e−04	1.079e+03	0.1884
4	0.2001	0.1409	0.00964	1.736e−05	1.451e−04	9.103e−04	7.740e+02	0.1576
5	0.2998	0.1983	0.00949	1.167e−05	7.348e−05	4.444e−04	1.009e+03	0.1885
6	0.4486	0.3257	0.01562	1.821e−05	7.275e−05	5.933e−04	1.199e+03	0.1581
7	0.5959	0.4788	0.01794	1.765e−05	6.535e−05	5.575e−04	1.499e+03	0.1335

170

S3929-6e
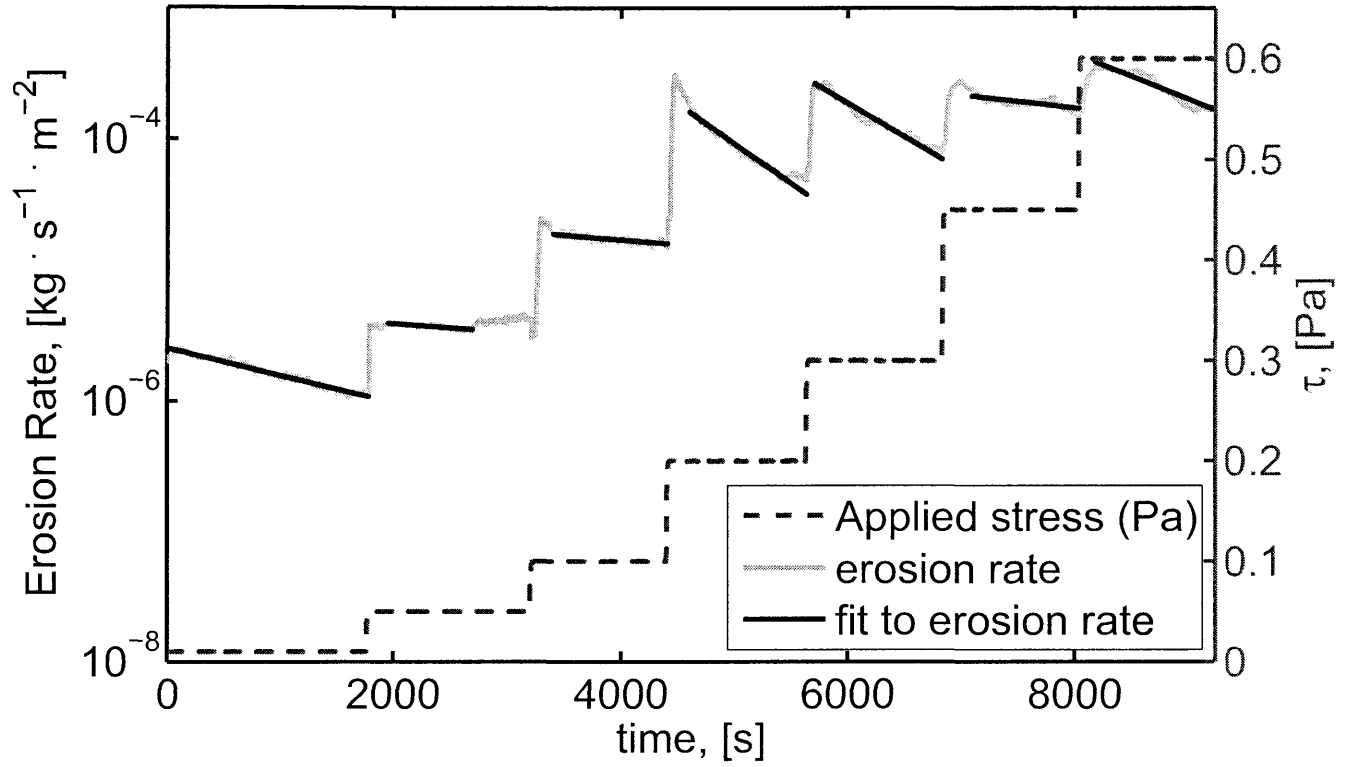
Step	τ_b (Pa)	τ_{ce} (Pa)	m (kg m^{-2})	M (kg m^{-2} s^{-1} Pa^{-1})	E_0 (kg m^{-2} s^{-1})	λ (s^{-1})	length (s)	organic fraction
1	0.0105	0.0450	0.00307	NaN	NaN	4.853e-04	1.789e+03	0.2193
2	0.0503	0.0460	0.00550	4.300e-06	8.181e-04	1.540e-04	1.424e+03	0.1743
3	0.1007	0.0559	0.02058	1.893e-05	3.465e-04	1.663e-04	1.199e+03	0.1335
4	0.2002	0.1744	0.12695	2.174e-04	1.507e-03	1.407e-03	1.224e+03	0.1104
5	0.3004	0.2697	0.17666	2.753e-04	2.185e-03	1.179e-03	1.199e+03	0.1054
6	0.4503	0.3120	0.23824	2.264e-04	1.254e-03	2.223e-04	1.199e+03	0.1061
7	0.5996	0.4892	0.31533	4.087e-04	1.421e-03	7.986e-04	1.199e+03	0.0992

171

S3929-7e
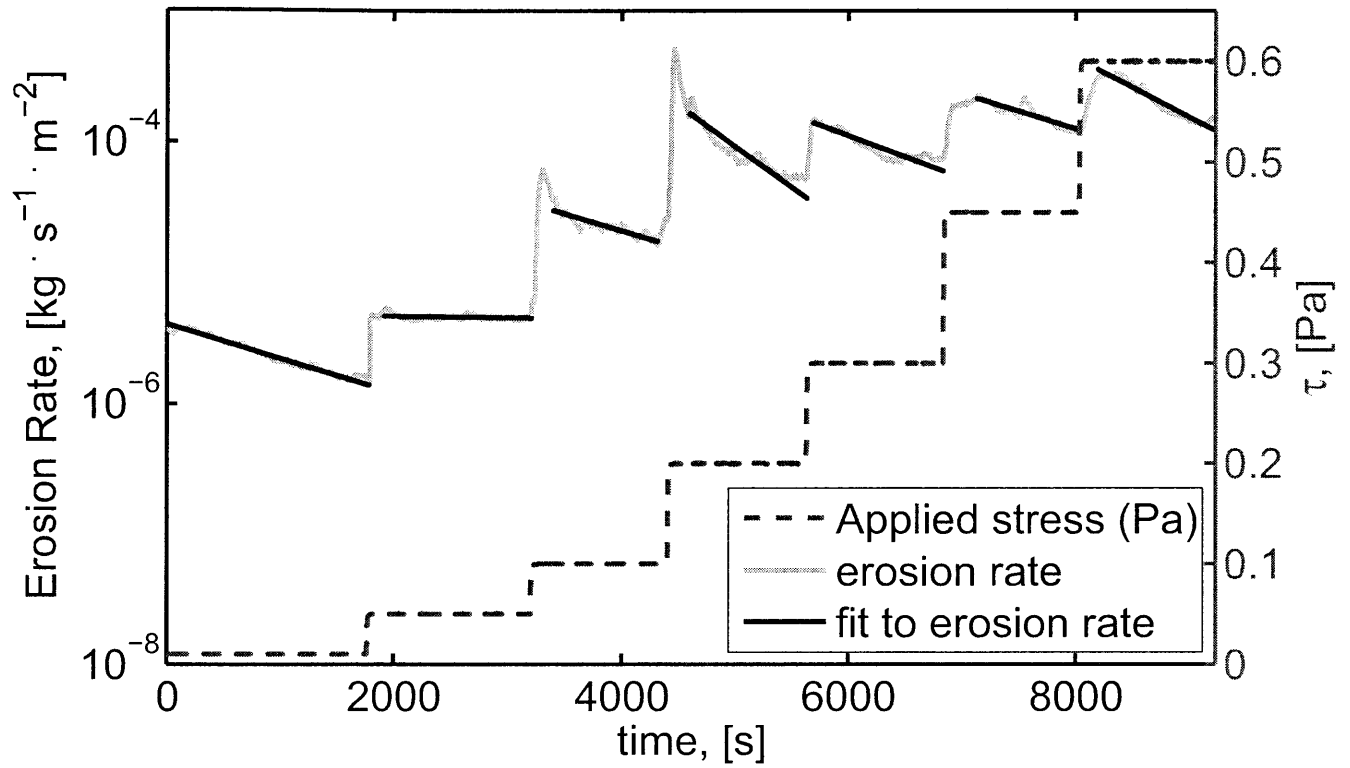
Step	τ_b (Pa)	τ_{ce} (Pa)	m (kg m^{-2})	M (kg m^{-2} s^{-1} Pa^{-1})	E_0 (kg m^{-2} s^{-1})	λ (s^{-1})	length (s)	organic fraction
1	0.0104	0.0450	0.00447	NaN	NaN	6.104e−04	1.789e+03	0.1655
2	0.0502	0.0452	0.00652	4.675e−06	8.957e−04	2.969e−05	1.424e+03	0.1508
3	0.1007	0.0737	0.03052	3.570e−05	6.438e−04	6.001e−04	1.199e+03	0.1347
4	0.2003	0.1784	0.13813	2.397e−04	1.893e−03	1.436e−03	1.224e+03	0.1041
5	0.3002	0.2503	0.11368	1.432e−04	1.176e−03	7.431e−04	1.199e+03	0.1035
6	0.4503	0.3541	0.20156	2.371e−04	1.185e−03	6.108e−04	1.199e+03	0.1017
7	0.5995	0.5285	0.26060	3.793e−04	1.546e−03	1.034e−03	1.199e+03	0.0689

172

S3930-4e
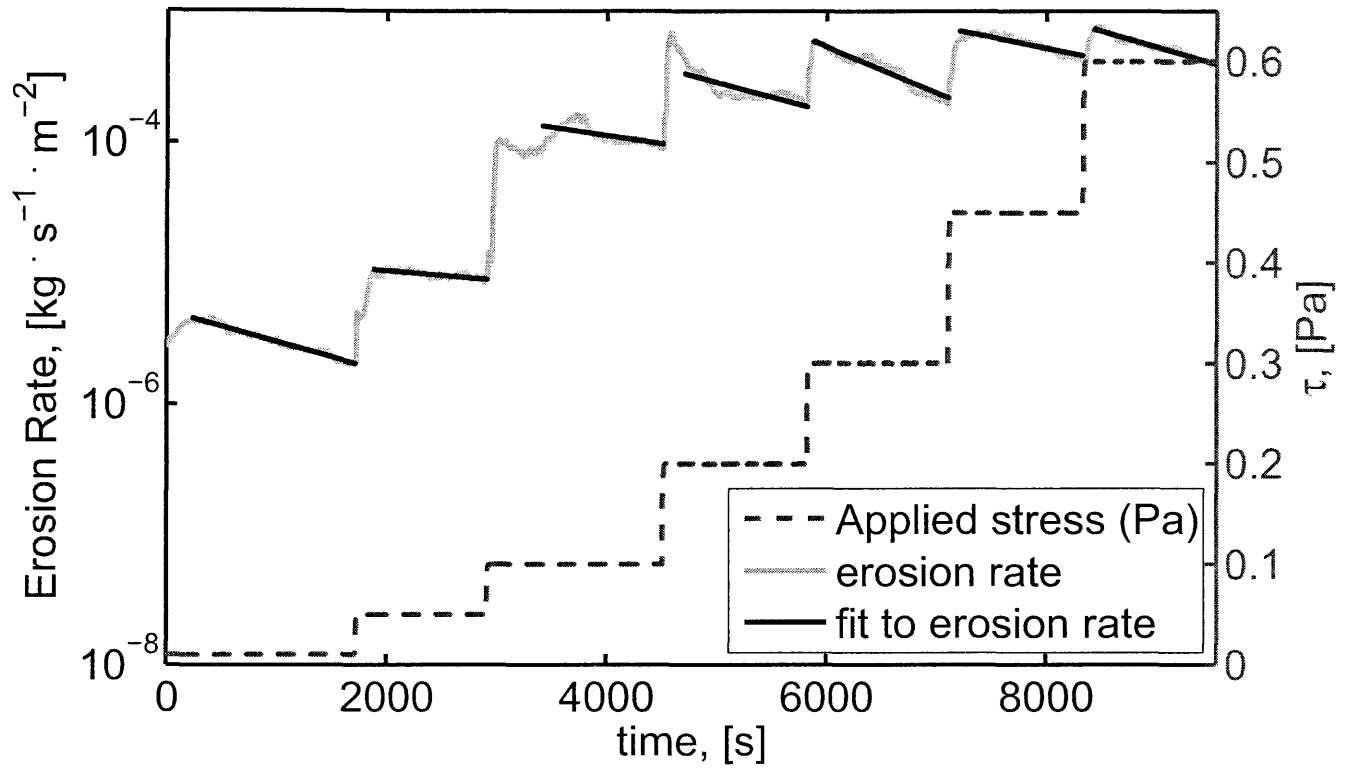
Step	τ_b (Pa)	τ_{ce} (Pa)	m (kg m^{-2})	M (kg m^{-2} s^{-1} Pa^{-1})	E_0 (kg m^{-2} s^{-1})	λ (s^{-1})	length (s)	organic fraction
1	0.0102	0.0400	0.00553	NaN	NaN	5.453e−04	1.724e+03	0.2470
2	0.0502	0.0419	0.01127	1.037e−05	1.013e−03	1.671e−04	1.199e+03	0.1427
3	0.1003	0.0633	0.16574	1.300e−04	2.223e−03	2.880e−04	1.589e+03	0.0687
4	0.2002	0.1308	0.37676	3.951e−04	2.887e−03	5.171e−04	1.314e+03	0.0601
5	0.3004	0.2406	0.48315	6.033e−04	3.558e−03	8.081e−04	1.289e+03	0.0466
6	0.4502	0.3191	0.68603	7.082e−04	3.378e−03	3.869e−04	1.214e+03	0.0351
7	0.5997	0.4554	0.66160	7.461e−04	2.659e−03	5.477e−04	1.214e+03	0.0349

173

S3930-5e
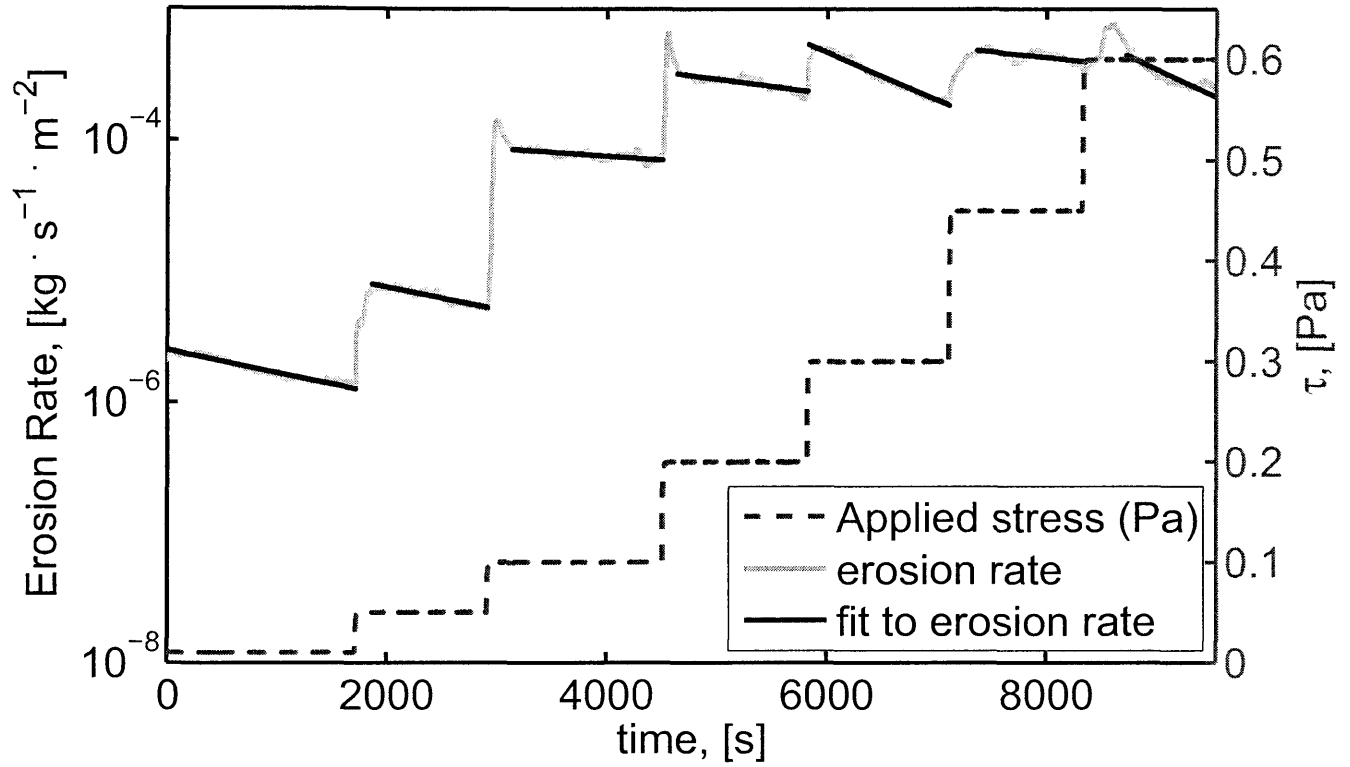
Step	τ_b (Pa)	τ_{ce} (Pa)	m (kg m^{-2})	M (kg m^{-2} s^{-1} Pa^{-1})	E_0 (kg m^{-2} s^{-1})	λ (s^{-1})	length (s)	organic fraction
1	0.0101	0.0400	0.00314	NaN	NaN	4.049e−04	1.724e+03	0.2340
2	0.0503	0.0439	0.00767	8.043e−06	7.803e−04	3.975e−04	1.199e+03	0.2017
3	0.1003	0.0549	0.12700	8.893e−05	1.577e−03	1.368e−04	1.589e+03	0.0718
4	0.2001	0.0970	0.38169	3.430e−04	2.362e−03	2.604e−04	1.314e+03	0.0627
5	0.3002	0.2307	0.42443	5.368e−04	2.641e−03	8.319e−04	1.289e+03	0.0442
6	0.4500	0.2775	0.52018	4.820e−04	2.198e−03	1.979e−04	1.214e+03	0.0377
7	0.5996	0.4912	0.47205	6.384e−04	1.982e−03	8.974e−04	1.214e+03	0.0444

S3931-8e
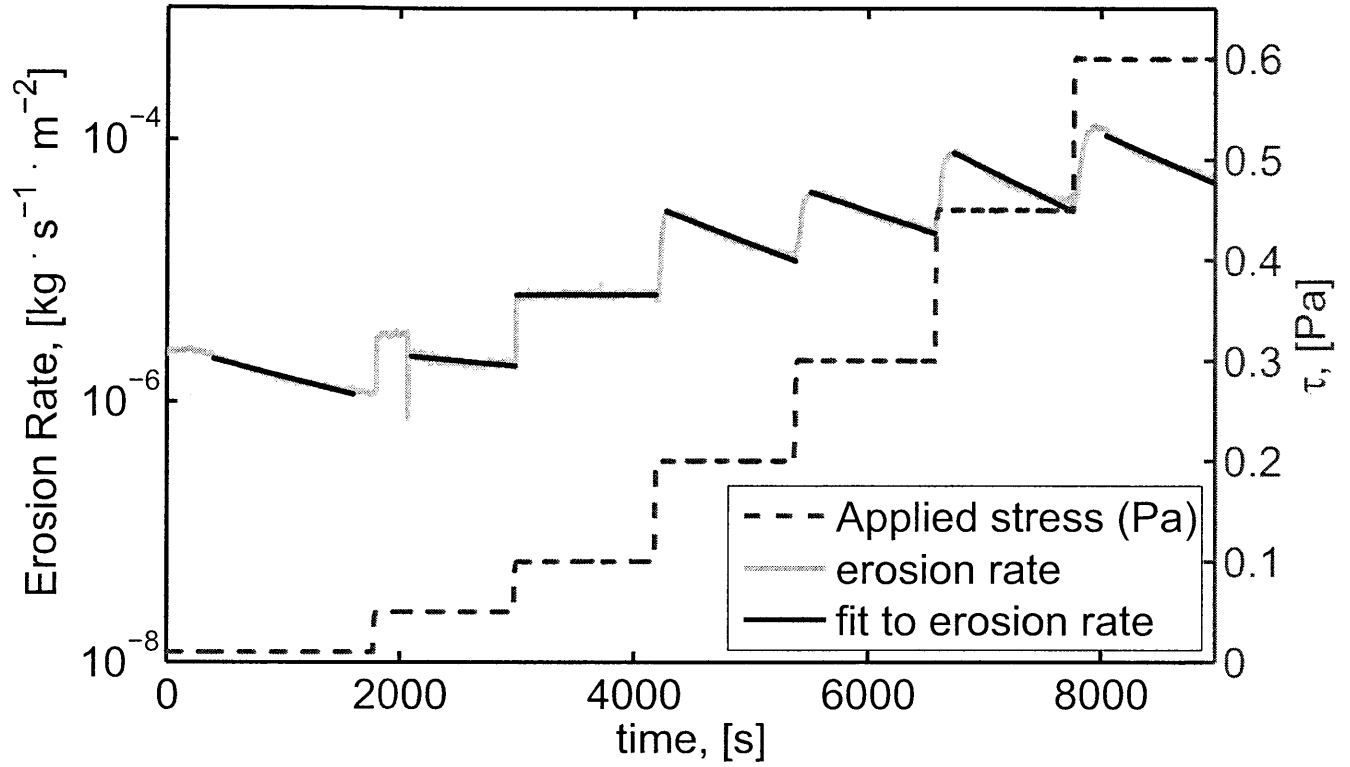
Step	τ_b (Pa)	τ_{ce} (Pa)	m (kg m^{-2})	M (kg m^{-2} s^{-1} Pa^{-1})	E_0 (kg m^{-2} s^{-1})	λ (s^{-1})	length (s)	organic fraction
1	0.0105	0.0800	0.00309	NaN	NaN	5.330e-04	1.799e+03	0.1813
2	0.0502	0.0740	0.00269	2.538e-06	-8.521e-05	1.913e-04	1.184e+03	0.2327
3	0.1006	0.0740	0.00778	6.487e-06	2.433e-04	1.000e-09	1.199e+03	0.1509
4	0.2006	0.1519	0.02238	2.898e-05	2.289e-04	7.967e-04	1.199e+03	0.1341
5	0.2999	0.2348	0.03389	4.161e-05	2.811e-04	6.874e-04	1.194e+03	0.1217
6	0.4501	0.3850	0.06047	8.717e-05	4.048e-04	1.005e-03	1.189e+03	0.0924
7	0.5997	0.5272	0.09531	1.292e-04	6.017e-04	8.983e-04	1.209e+03	0.0829

175

S3931-10e
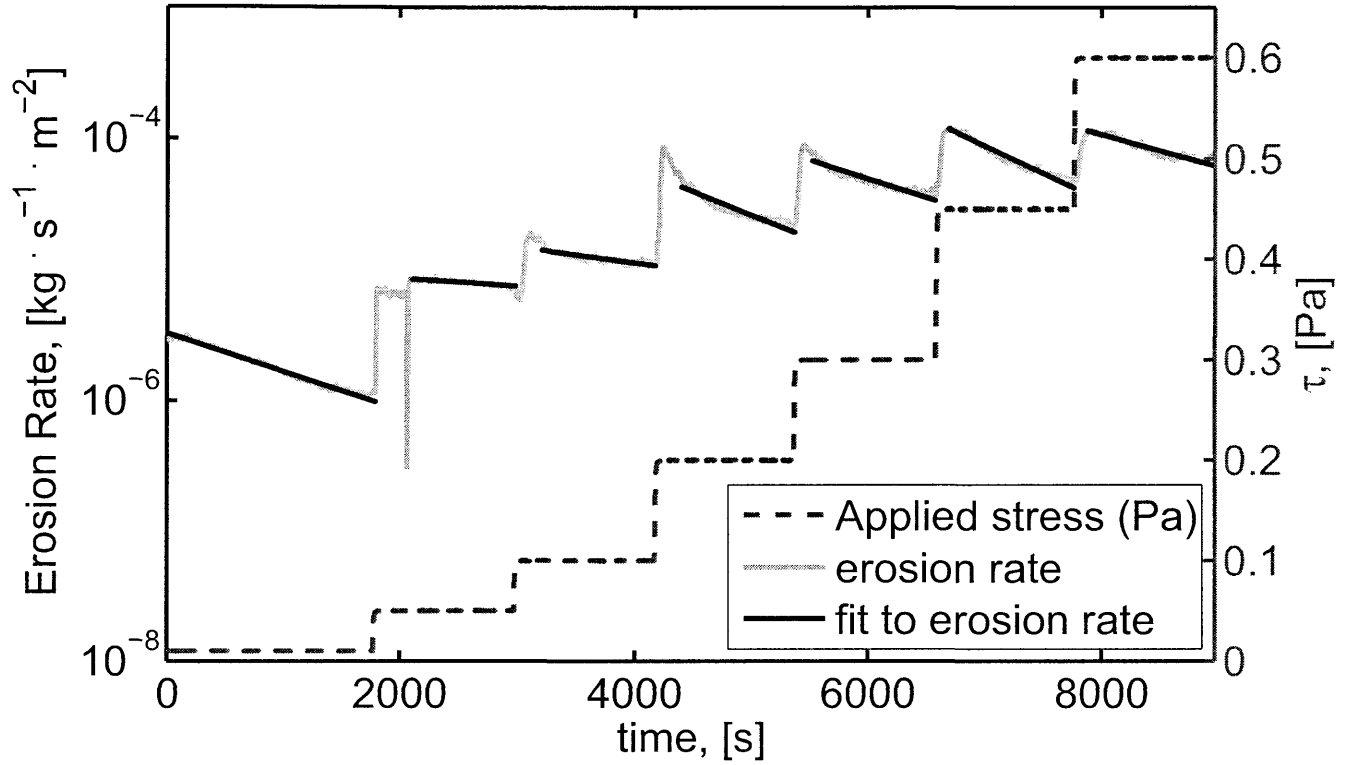
Step	τ_b (Pa)	τ_{ce} (Pa)	m (kg m^{-2})	M (kg m^{-2} s^{-1} Pa^{-1})	E_0 (kg m^{-2} s^{-1})	λ (s^{-1})	length (s)	organic fraction
1	0.0104	0.0450	0.00344	NaN	NaN	6.804e−04	1.799e+03	0.2077
2	0.0503	0.0458	0.00901	8.268e−06	1.549e−03	1.430e−04	1.184e+03	0.1190
3	0.1007	0.0618	0.01507	1.485e−05	2.708e−04	2.862e−04	1.199e+03	0.1189
4	0.2006	0.1488	0.04149	5.444e−05	3.922e−04	8.230e−04	1.199e+03	0.1051
5	0.3000	0.2316	0.06137	7.445e−05	4.926e−04	6.644e−04	1.194e+03	0.0942
6	0.4499	0.3809	0.08913	1.262e−04	5.782e−04	9.686e−04	1.189e+03	0.0732
7	0.5997	0.4889	0.10295	1.174e−04	5.366e−04	5.628e−04	1.209e+03	0.0699

S3932-8e
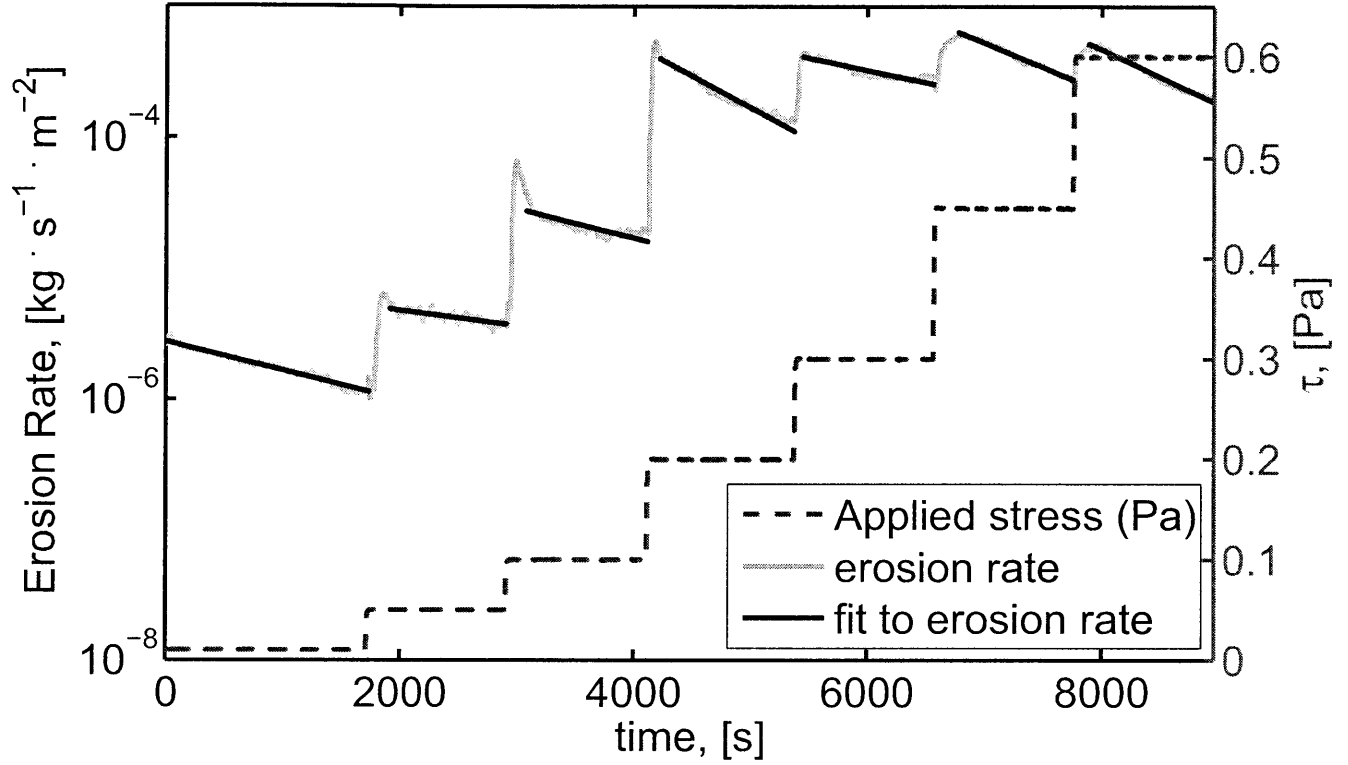
Step	τ_b (Pa)	τ_{ce} (Pa)	m (kg m^{-2})	M (kg m^{-2} s^{-1} Pa^{-1})	E_0 (kg m^{-2} s^{-1})	λ (s^{-1})	length (s)	organic fraction
1	0.0105	0.0300	0.00320	NaN	NaN	5.104e−04	1.739e+03	0.2256
2	0.0503	0.0355	0.00506	4.991e−06	2.464e−04	2.690e−04	1.184e+03	0.2263
3	0.1006	0.0657	0.02833	3.175e−05	4.876e−04	5.198e−04	1.199e+03	0.0882
4	0.2002	0.1664	0.29752	4.376e−04	3.254e−03	1.101e−03	1.254e+03	0.0469
5	0.3004	0.2200	0.39086	4.164e−04	3.108e−03	4.263e−04	1.199e+03	0.0379
6	0.4504	0.3668	0.52103	6.973e−04	3.026e−03	8.528e−04	1.189e+03	0.0429
7	0.5998	0.5260	0.40406	5.671e−04	2.435e−03	9.592e−04	1.199e+03	0.0474

177

S3932-10e
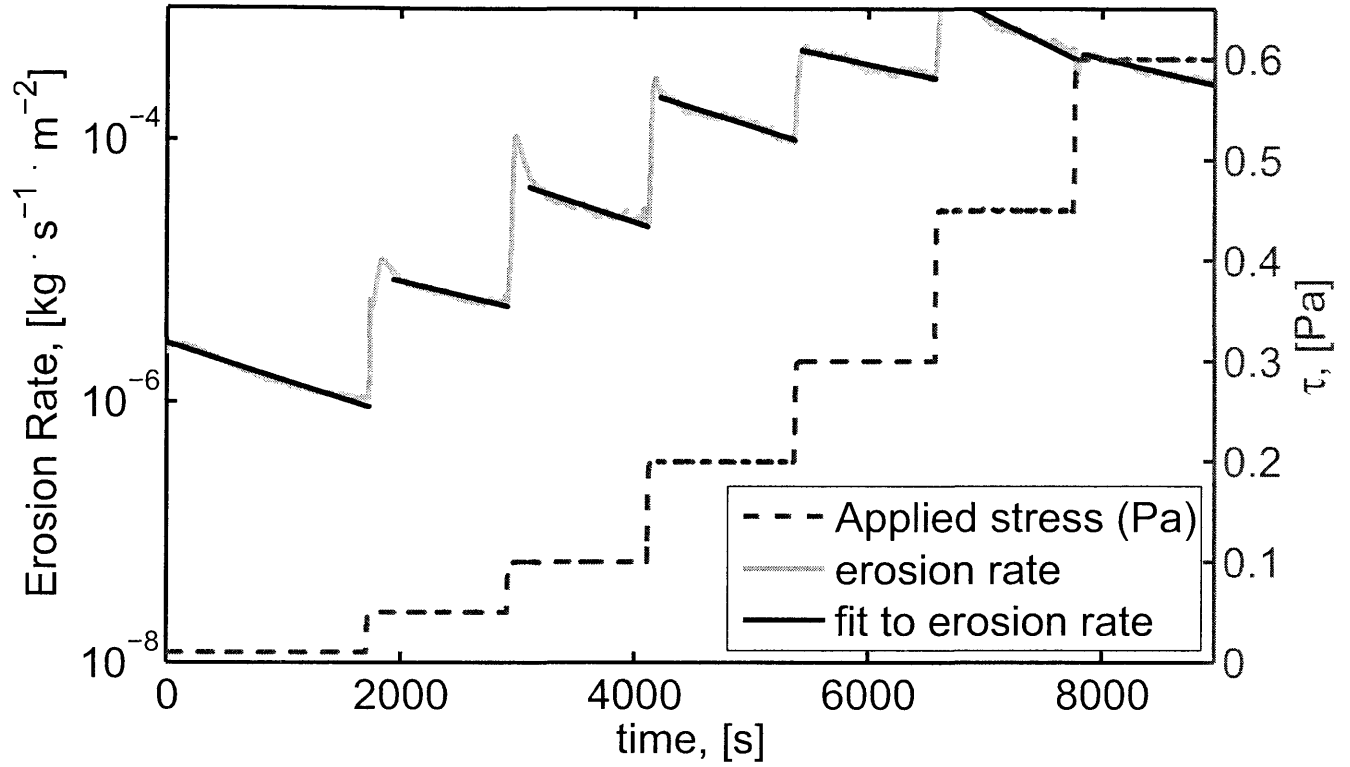
Step	τ_b (Pa)	τ_{ce} (Pa)	m (kg m^{-2})	M (kg m^{-2} s^{-1} Pa^{-1})	E_0 (kg m^{-2} s^{-1})	λ (s^{-1})	length (s)	organic fraction
1	0.0104	0.0300	0.00295	NaN	NaN	6.600e−04	1.739e+03	0.2295
2	0.0504	0.0389	0.00864	9.603e−06	4.715e−04	4.874e−04	1.184e+03	0.1800
3	0.1007	0.0734	0.04379	5.346e−05	8.650e−04	6.818e−04	1.199e+03	0.0767
4	0.2001	0.1434	0.19251	2.233e−04	1.762e−03	6.404e−04	1.254e+03	0.0548
5	0.3003	0.2074	0.45313	4.855e−04	3.094e−03	4.369e−04	1.199e+03	0.0354
6	0.4503	0.3772	0.93138	1.346e−03	5.541e−03	1.010e−03	1.189e+03	0.0335
7	0.5997	0.4747	0.41869	4.596e−04	2.066e−03	4.812e−04	1.199e+03	0.0447

S3933-10e
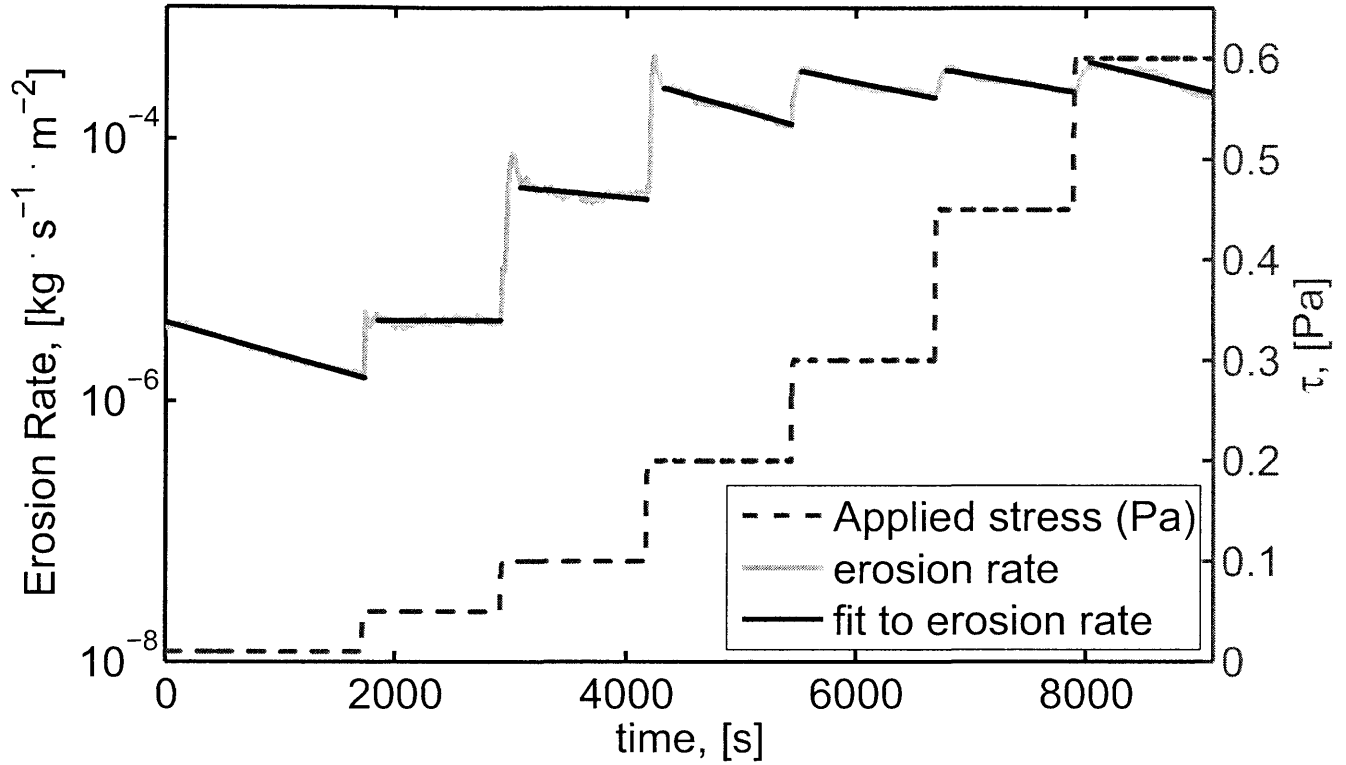
Step	τ_b (Pa)	τ_{ce} (Pa)	m (kg m^{-2})	M (kg m^{-2} s^{-1} Pa^{-1})	E_0 (kg m^{-2} s^{-1})	λ (s^{-1})	length (s)	organic fraction
1	0.0105	0.0400	0.00445	NaN	NaN	5.730e-04	1.739e+03	0.1743
2	0.0503	0.0400	0.00486	4.102e-06	3.987e-04	1.000e-09	1.184e+03	0.1806
3	0.1005	0.0532	0.04998	4.477e-05	7.397e-04	1.948e-04	1.259e+03	0.1676
4	0.2002	0.1285	0.24206	2.683e-04	1.825e-03	5.675e-04	1.264e+03	0.0618
5	0.3004	0.1969	0.32803	3.349e-04	1.947e-03	4.062e-04	1.249e+03	0.0559
6	0.4504	0.2831	0.33367	3.402e-04	1.342e-03	3.469e-04	1.199e+03	0.0612
7	0.5997	0.4276	0.36070	3.984e-04	1.259e-03	5.039e-04	1.209e+03	0.0631

179

S3933-11e
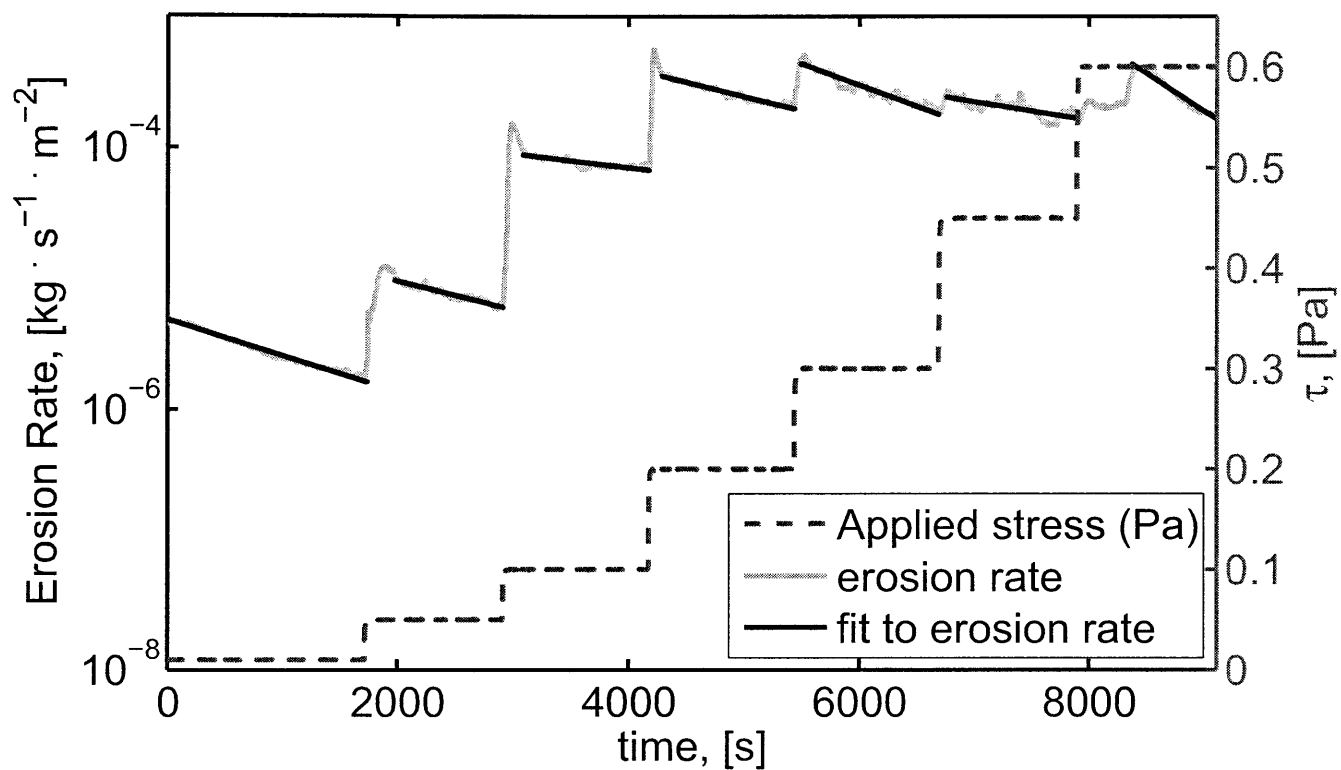
Step	τ_b (Pa)	τ_{ce} (Pa)	m (kg m^{-2})	M (kg m^{-2} s^{-1} Pa^{-1})	E_0 (kg m^{-2} s^{-1})	λ (s^{-1})	length (s)	organic fraction
1	0.0105	0.0400	0.00515	NaN	NaN	6.412e−04	1.739e+03	0.1763
2	0.0503	0.0447	0.00958	1.079e−05	1.045e−03	5.135e−04	1.184e+03	0.1583
3	0.1005	0.0595	0.10108	9.333e−05	1.674e−03	2.455e−04	1.259e+03	0.0767
4	0.2002	0.1255	0.35099	3.749e−04	2.665e−03	5.013e−04	1.264e+03	0.0682
5	0.3003	0.2315	0.36374	4.479e−04	2.563e−03	7.470e−04	1.249e+03	0.0650
6	0.4502	0.3031	0.24257	2.451e−04	1.121e−03	3.308e−04	1.199e+03	0.0647
7	0.5996	0.5400	0.30650	5.091e−04	1.717e−03	1.327e−03	1.209e+03	0.0670

S3937–3e
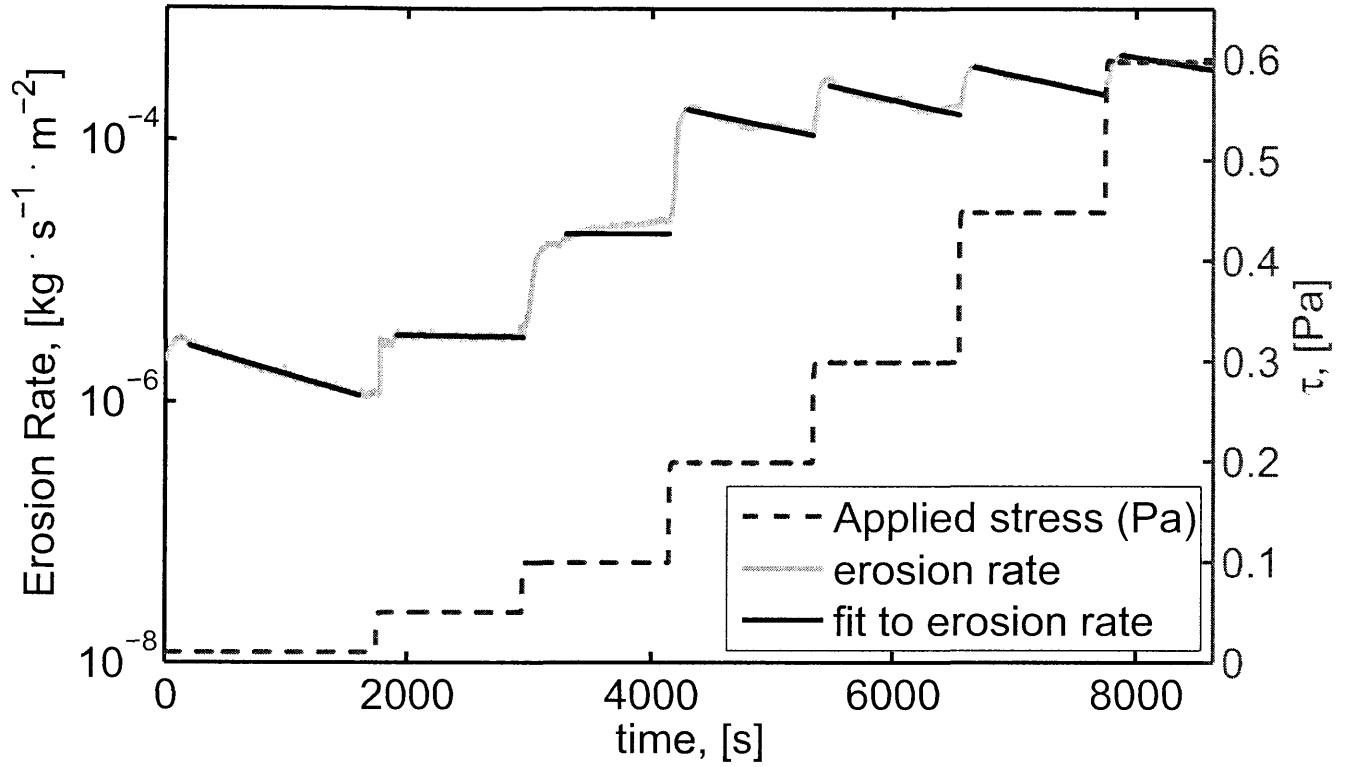
Step	τ_b (Pa)	τ_{ce} (Pa)	m (kg m^{-2})	M (kg m^{-2} s^{-1} Pa^{-1})	E_0 (kg m^{-2} s^{-1})	λ (s^{-1})	length (s)	organic fraction
1	0.0104	0.0400	0.00325	NaN	NaN	6.286e−04	1.769e+03	0.2877
2	0.0502	0.0404	0.00371	3.196e−06	3.146e−04	3.163e−05	1.184e+03	0.3533
3	0.1000	0.0404	0.02305	1.923e−05	3.224e−04	1.000e−09	1.199e+03	0.1062
4	0.1994	0.1040	0.16006	1.712e−04	1.076e−03	4.277e−04	1.194e+03	0.0683
5	0.2992	0.1894	0.24884	2.730e−04	1.399e−03	4.802e−04	1.199e+03	0.0651
6	0.4484	0.2984	0.34254	3.707e−04	1.431e−03	4.553e−04	1.199e+03	0.0636
7	0.5972	0.3780	0.34915	4.516e−04	1.511e−03	3.445e−04	8.990e+02	0.0607

S3937-4e
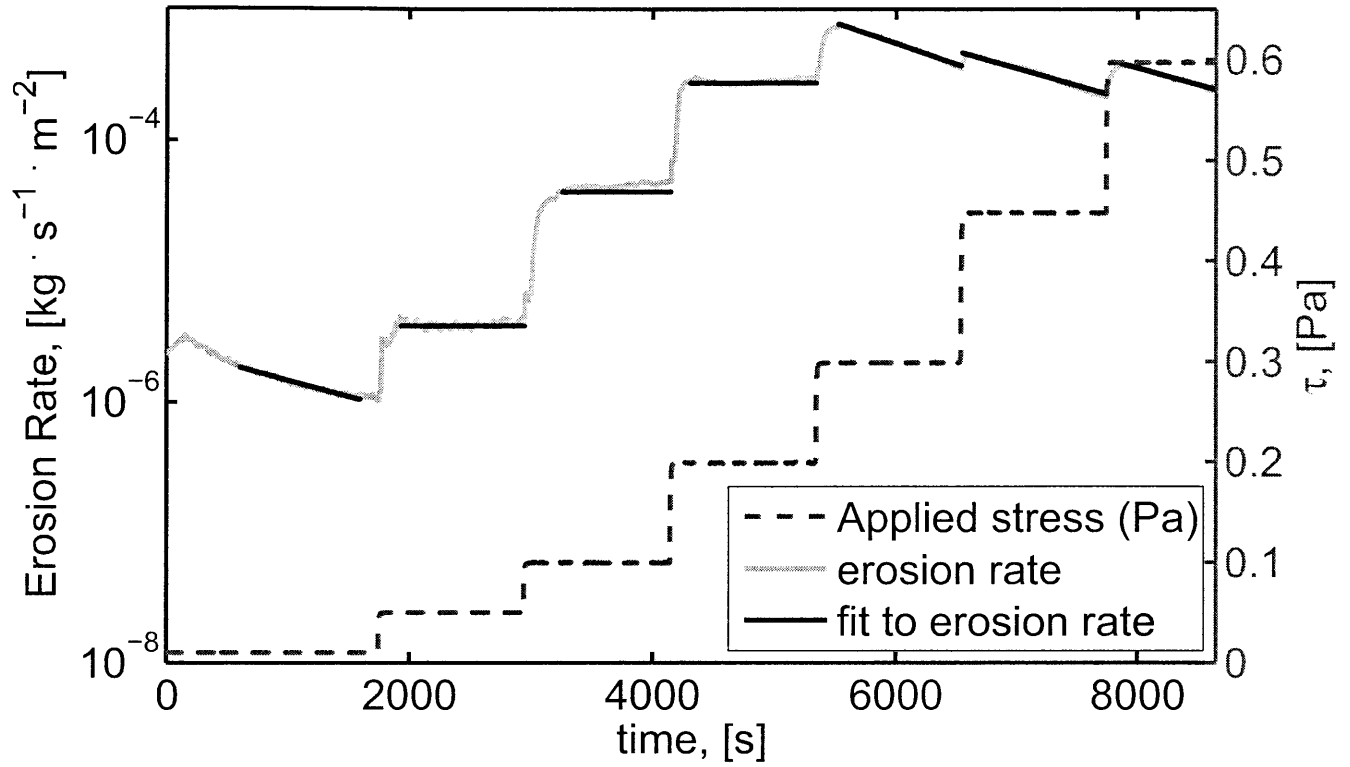
Step	τ_b (Pa)	τ_{ce} (Pa)	m (kg m^{-2})	M (kg m^{-2} s^{-1} Pa^{-1})	E_0 (kg m^{-2} s^{-1})	λ (s^{-1})	length (s)	organic fraction
1	0.0105	0.0400	0.00311	NaN	NaN	5.827e−04	1.769e+03	0.2608
2	0.0500	0.0400	0.00453	3.823e−06	3.812e−04	1.000e−09	1.184e+03	0.3713
3	0.1001	0.0400	0.04845	4.041e−05	6.725e−04	1.000e−09	1.199e+03	0.0909
4	0.1994	0.0400	0.32548	2.726e−04	1.711e−03	1.000e−09	1.194e+03	0.0617
5	0.2991	0.1900	0.66618	8.300e−04	3.203e−03	7.211e−04	1.199e+03	0.0702
6	0.4483	0.3228	0.39656	4.644e−04	1.797e−03	6.022e−04	1.199e+03	0.0594
7	0.5970	0.4360	0.28045	4.022e−04	1.467e−03	5.917e−04	8.990e+02	0.0578

S3938-5e
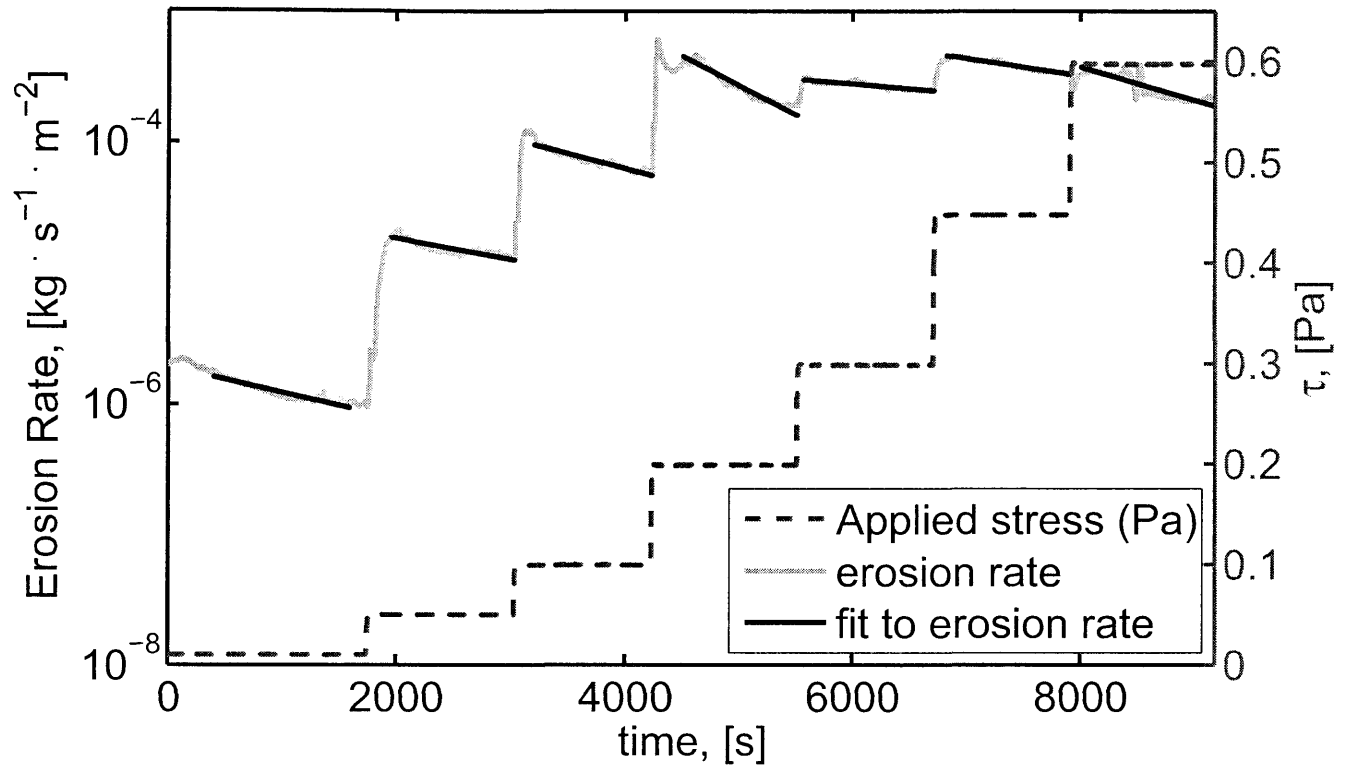
Step	τ_b (Pa)	τ_{ce} (Pa)	m (kg m^{-2})	M (kg m^{-2} s^{-1} Pa^{-1})	E_0 (kg m^{-2} s^{-1})	λ (s^{-1})	length (s)	organic fraction
1	0.0104	0.0400	0.00248	NaN	NaN	4.605e−04	1.769e+03	0.2840
2	0.0502	0.0439	0.01878	1.855e−05	1.823e−03	3.762e−04	1.274e+03	0.2119
3	0.1002	0.0702	0.09188	1.033e−04	1.836e−03	5.264e−04	1.199e+03	0.0767
4	0.1994	0.1645	0.38670	5.442e−04	4.213e−03	1.027e−03	1.274e+03	0.0480
5	0.2990	0.1895	0.32609	3.009e−04	2.237e−03	1.715e−04	1.199e+03	0.0502
6	0.4484	0.2681	0.46773	4.649e−04	1.795e−03	3.015e−04	1.199e+03	0.0477
7	0.5972	0.4391	0.34483	3.835e−04	1.165e−03	5.780e−04	1.269e+03	0.0533

S3938-6e

Step	τ_b (Pa)	τ_{ce} (Pa)	m (kg m^{-2})	M (kg m^{-2} s^{-1} Pa^{-1})	E_0 (kg m^{-2} s^{-1})	λ (s^{-1})	length (s)	organic fraction
1	0.0105	0.0400	0.00212	NaN	NaN	4.319e−04	1.769e+03	0.2772
2	0.0500	0.0475	0.01831	2.665e−05	2.656e−03	1.094e−03	1.274e+03	0.2072
3	0.1002	0.0613	0.09284	8.973e−05	1.703e−03	2.522e−04	1.199e+03	0.0772
4	0.1993	0.1144	0.39918	3.955e−04	2.865e−03	3.809e−04	1.274e+03	0.0518
5	0.2990	0.1547	0.60878	5.729e−04	3.103e−03	2.057e−04	1.199e+03	0.0463
6	0.4484	0.2631	0.68224	7.100e−04	2.418e−03	3.840e−04	1.199e+03	0.0453
7	0.5971	0.3877	0.60173	5.935e−04	1.777e−03	3.680e−04	1.269e+03	0.0525

S3939-8e
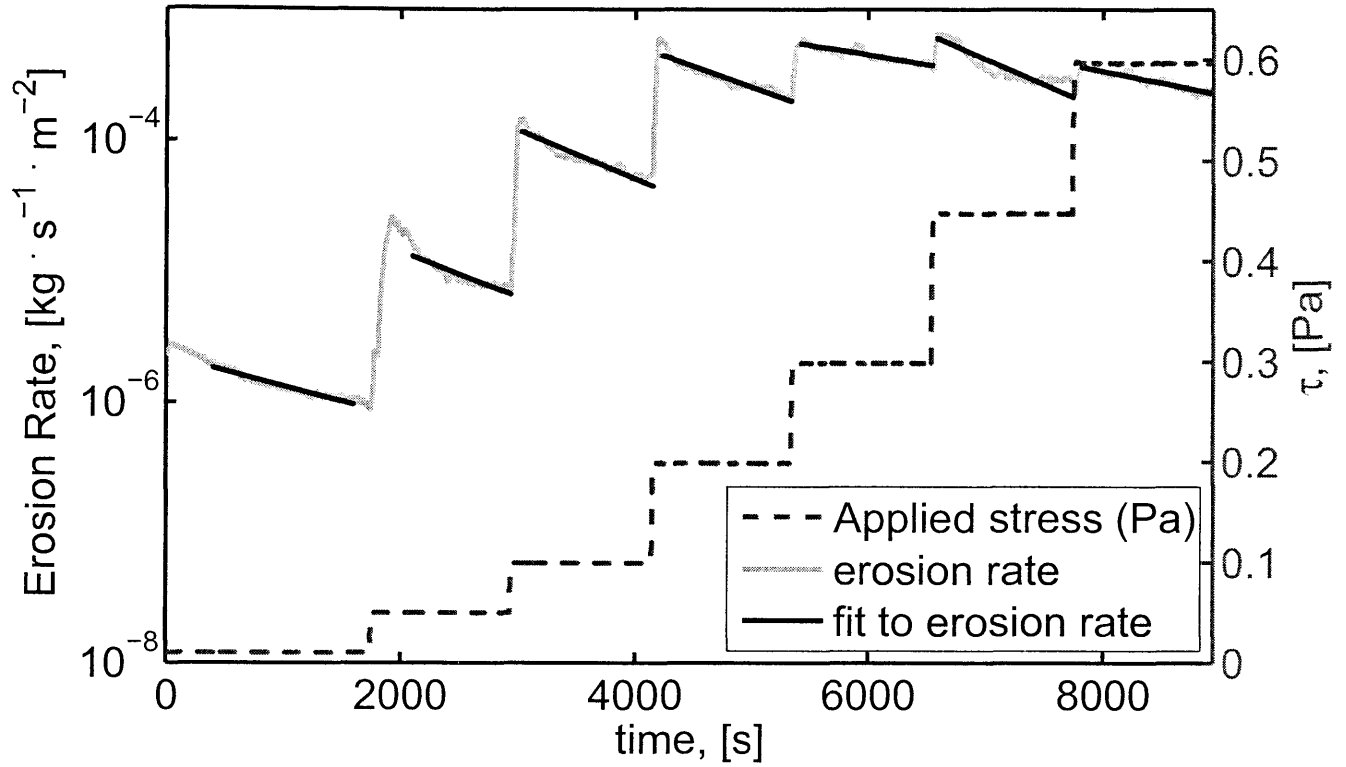
Step	τ_b (Pa)	τ_{ce} (Pa)	m (kg m^{-2})	M (kg m^{-2} s^{-1} Pa^{-1})	E_0 (kg m^{-2} s^{-1})	λ (s^{-1})	length (s)	organic fraction
1	0.0104	0.0400	0.00274	NaN	NaN	5.410e−04	1.769e+03	0.2670
2	0.0500	0.0461	0.01354	1.764e−05	1.764e−03	7.937e−04	1.184e+03	0.2038
3	0.1001	0.0808	0.09097	1.214e−04	2.246e−03	8.564e−04	1.199e+03	0.0785
4	0.1992	0.1494	0.37497	4.695e−04	3.964e−03	7.255e−04	1.194e+03	0.0515
5	0.2988	0.1994	0.54542	5.539e−04	3.708e−03	3.400e−04	1.199e+03	0.0360
6	0.4479	0.3630	0.45438	6.181e−04	2.487e−03	8.954e−04	1.199e+03	0.0416
7	0.5965	0.4536	0.34973	3.692e−04	1.581e−03	4.098e−04	1.199e+03	0.0511

185

S3939-9e
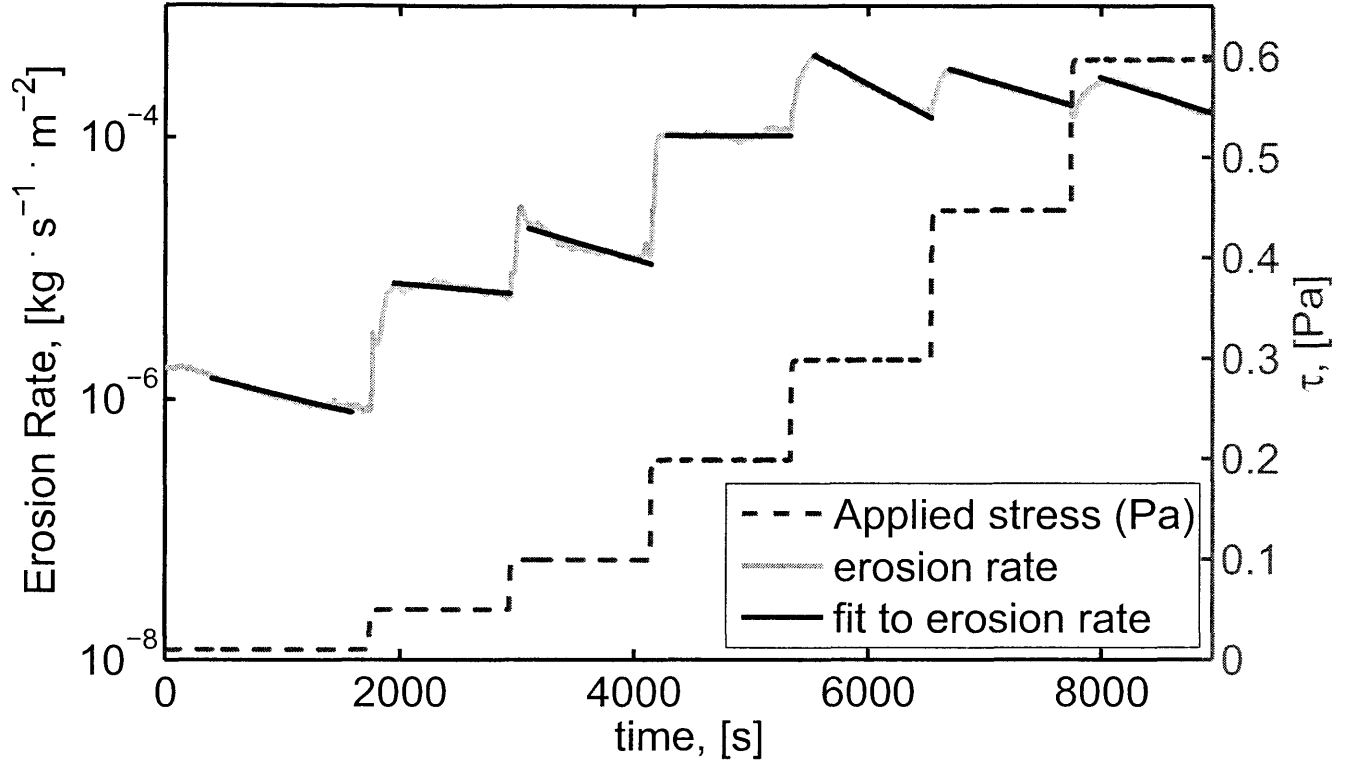
Step	τ_b (Pa)	τ_{ce} (Pa)	m (kg m^{-2})	M (kg m^{-2} s^{-1} Pa^{-1})	E_0 (kg m^{-2} s^{-1})	λ (s^{-1})	length (s)	organic fraction
1	0.0104	0.0400	0.00212	NaN	NaN	5.041e−04	1.769e+03	0.2565
2	0.0501	0.0420	0.00791	7.436e−06	7.371e−04	1.839e−04	1.184e+03	0.2000
3	0.1000	0.0716	0.01875	2.188e−05	3.771e−04	5.959e−04	1.199e+03	0.1164
4	0.1991	0.0716	0.12275	1.028e−04	8.061e−04	1.000e−09	1.194e+03	0.0707
5	0.2987	0.2378	0.31515	4.726e−04	2.081e−03	1.097e−03	1.199e+03	0.0574
6	0.4478	0.3463	0.29564	3.469e−04	1.652e−03	6.062e−04	1.199e+03	0.0570
7	0.5964	0.4833	0.25358	3.064e−04	1.225e−03	6.617e−04	1.199e+03	0.0593

S3940-3e
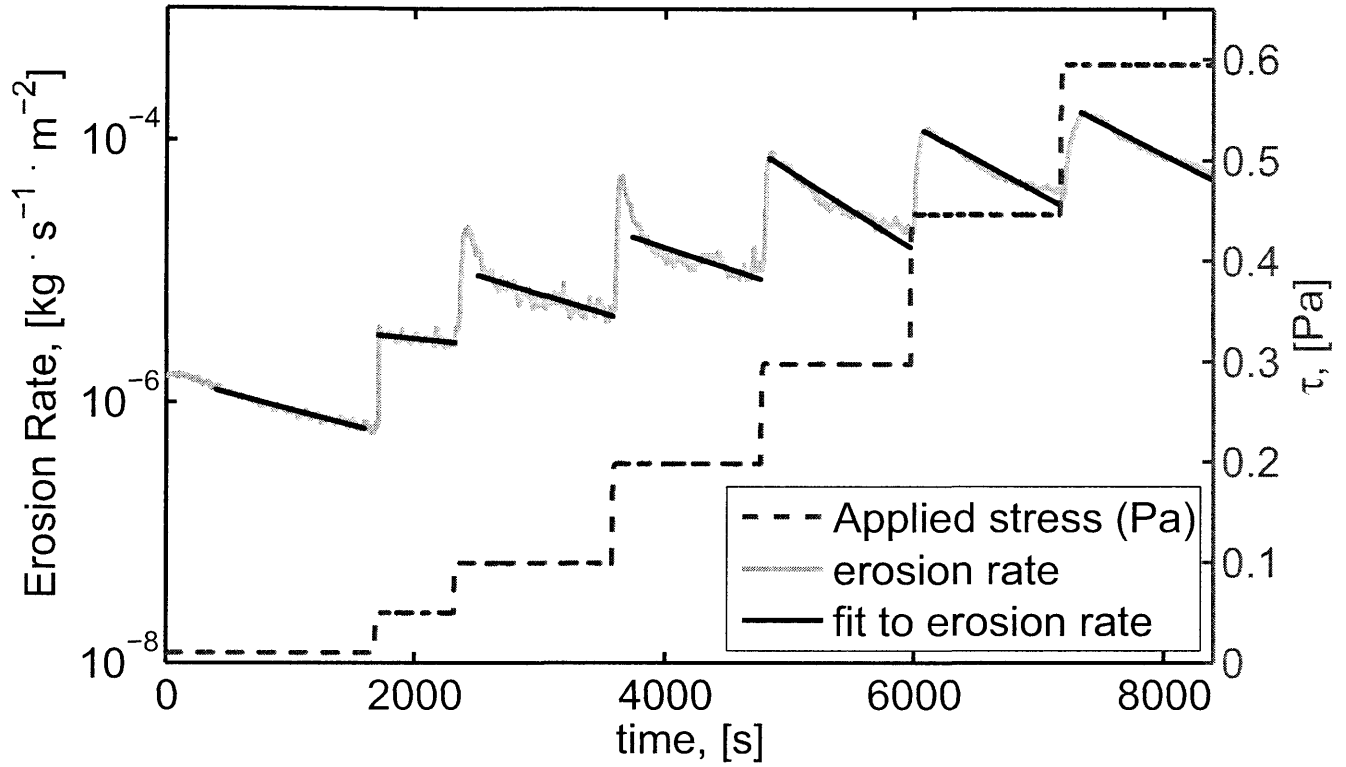
Step	τ_b (Pa)	τ_{ce} (Pa)	m (kg m^{-2})	M (kg m^{-2} s^{-1} Pa^{-1})	E_0 (kg m^{-2} s^{-1})	λ (s^{-1})	length (s)	organic fraction
1	0.0104	0.0700	0.00175	NaN	NaN	5.747e-04	1.709e+03	0.3497
2	0.0502	0.0674	0.00187	3.268e-06	-1.652e-04	2.300e-04	6.140e+02	0.3106
3	0.0998	0.0858	0.00965	1.134e-05	3.498e-04	6.686e-04	1.259e+03	0.2214
4	0.1986	0.1509	0.01858	2.321e-05	2.059e-04	7.212e-04	1.194e+03	0.1689
5	0.2979	0.2701	0.04441	7.610e-05	5.178e-04	1.390e-03	1.199e+03	0.1274
6	0.4467	0.4044	0.07930	1.243e-04	7.041e-04	1.192e-03	1.199e+03	0.1053
7	0.5947	0.5464	0.11650	1.757e-04	9.231e-04	1.125e-03	1.219e+03	0.0962

S3940-6e
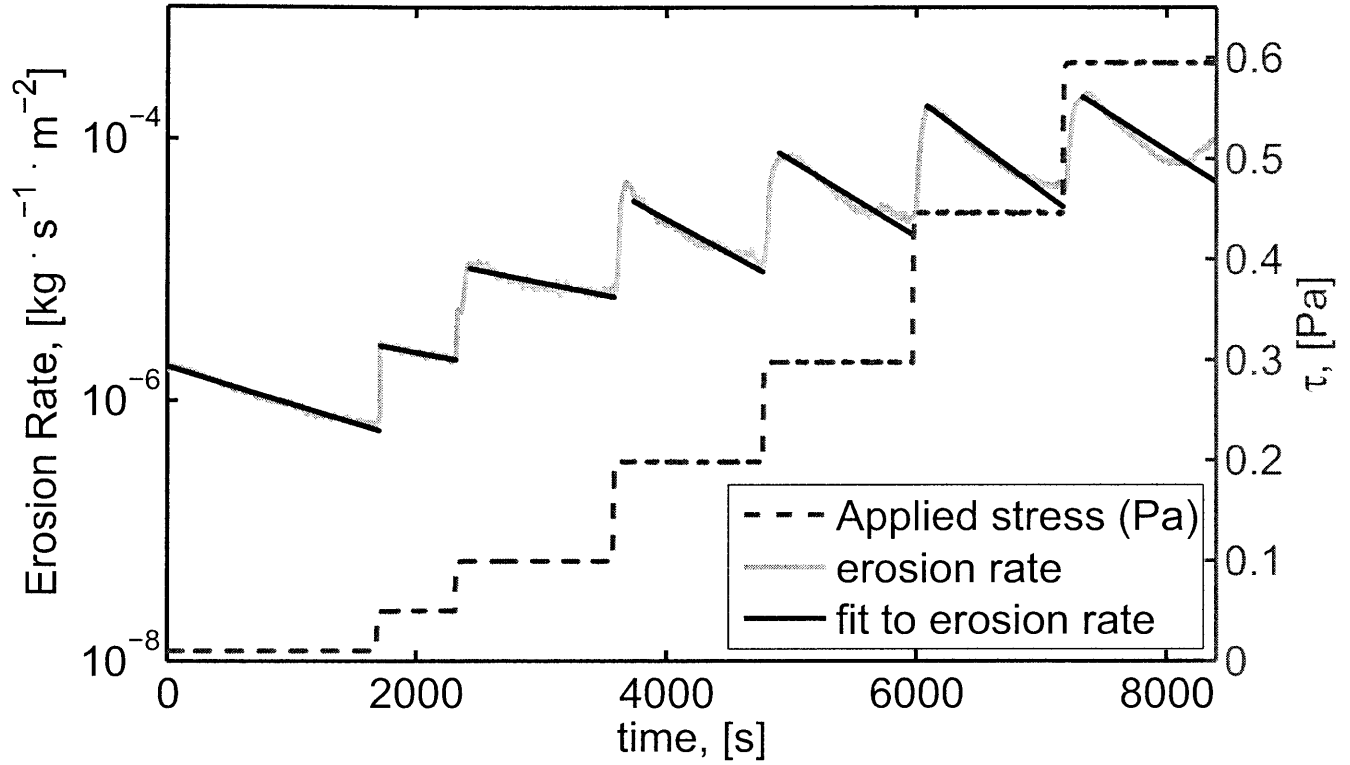
Step	τ_b (Pa)	τ_{ce} (Pa)	m (kg m^{-2})	M (kg m^{-2} s^{-1} Pa^{-1})	E_0 (kg m^{-2} s^{-1})	λ (s^{-1})	length (s)	organic fraction
1	0.0104	0.0700	0.00186	NaN	NaN	6.736e−04	1.709e+03	0.3310
2	0.0502	0.0655	0.00141	2.611e−06	−1.321e−04	4.173e−04	6.140e+02	0.4324
3	0.0998	0.0800	0.00992	1.025e−05	2.989e−04	4.369e−04	1.259e+03	0.2197
4	0.1986	0.1704	0.02472	3.903e−05	3.292e−04	1.204e−03	1.194e+03	0.1397
5	0.2979	0.2724	0.04999	8.395e−05	6.589e−04	1.345e−03	1.199e+03	0.1203
6	0.4465	0.4217	0.10060	1.907e−04	1.096e−03	1.626e−03	1.199e+03	0.0977
7	0.5947	0.5633	0.13638	2.332e−04	1.349e−03	1.399e−03	1.219e+03	0.0946

188

S3941-6e
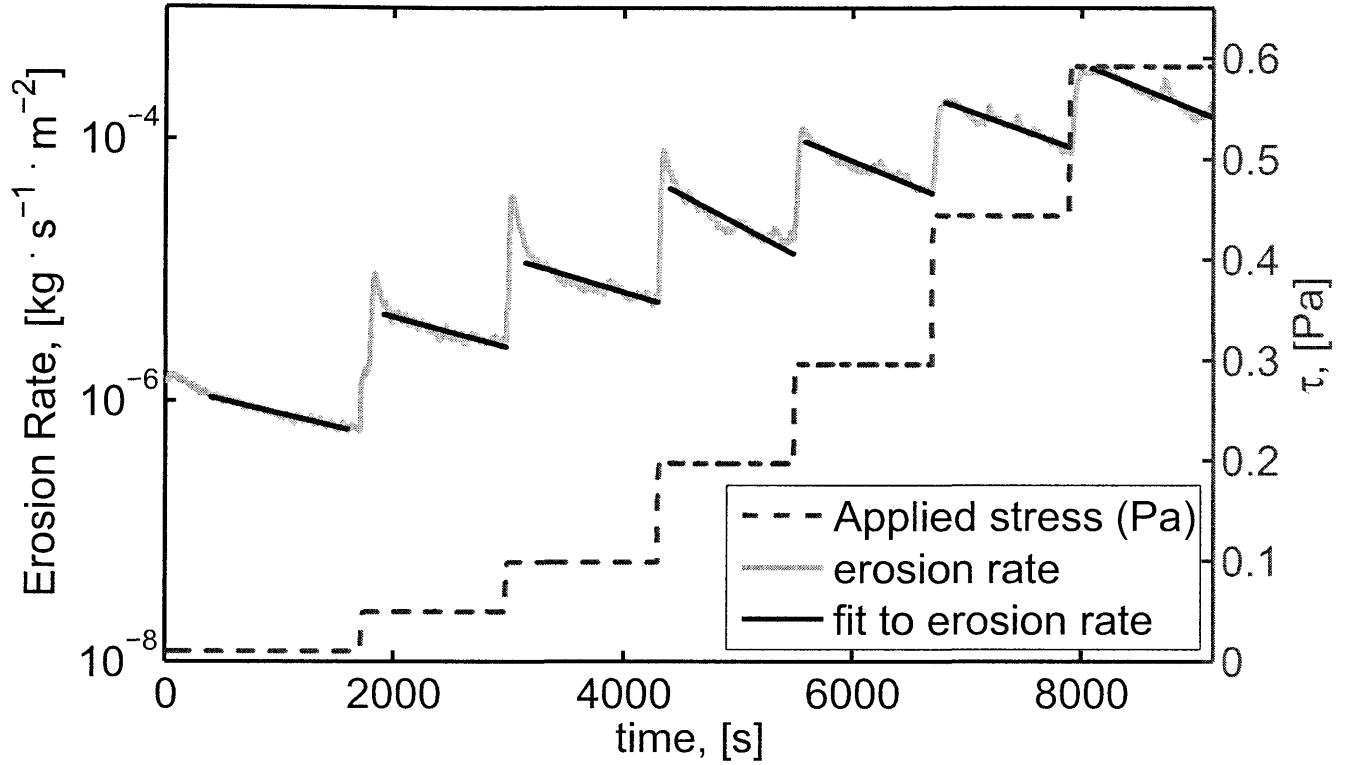
Step	τ_b (Pa)	τ_{ce} (Pa)	m (kg m^{-2})	M (kg m^{-2} s^{-1} Pa^{-1})	E_0 (kg m^{-2} s^{-1})	λ (s^{-1})	length (s)	organic fraction
1	0.0098	0.0400	0.00158	NaN	NaN	4.764e−04	1.709e+03	0.2977
2	0.0493	0.0447	0.00467	5.085e−06	5.447e−04	5.437e−04	1.274e+03	0.2122
3	0.0993	0.0749	0.01300	1.436e−05	2.627e−04	6.105e−04	1.319e+03	0.1439
4	0.1975	0.1629	0.03300	4.870e−05	3.972e−04	1.059e−03	1.194e+03	0.1144
5	0.2963	0.2467	0.07687	1.010e−04	7.572e−04	8.257e−04	1.199e+03	0.0818
6	0.4441	0.3609	0.15823	1.970e−04	9.981e−04	7.202e−04	1.199e+03	0.0594
7	0.5915	0.5087	0.29857	3.790e−04	1.643e−03	8.137e−04	1.259e+03	0.0536

189

S3941-7e
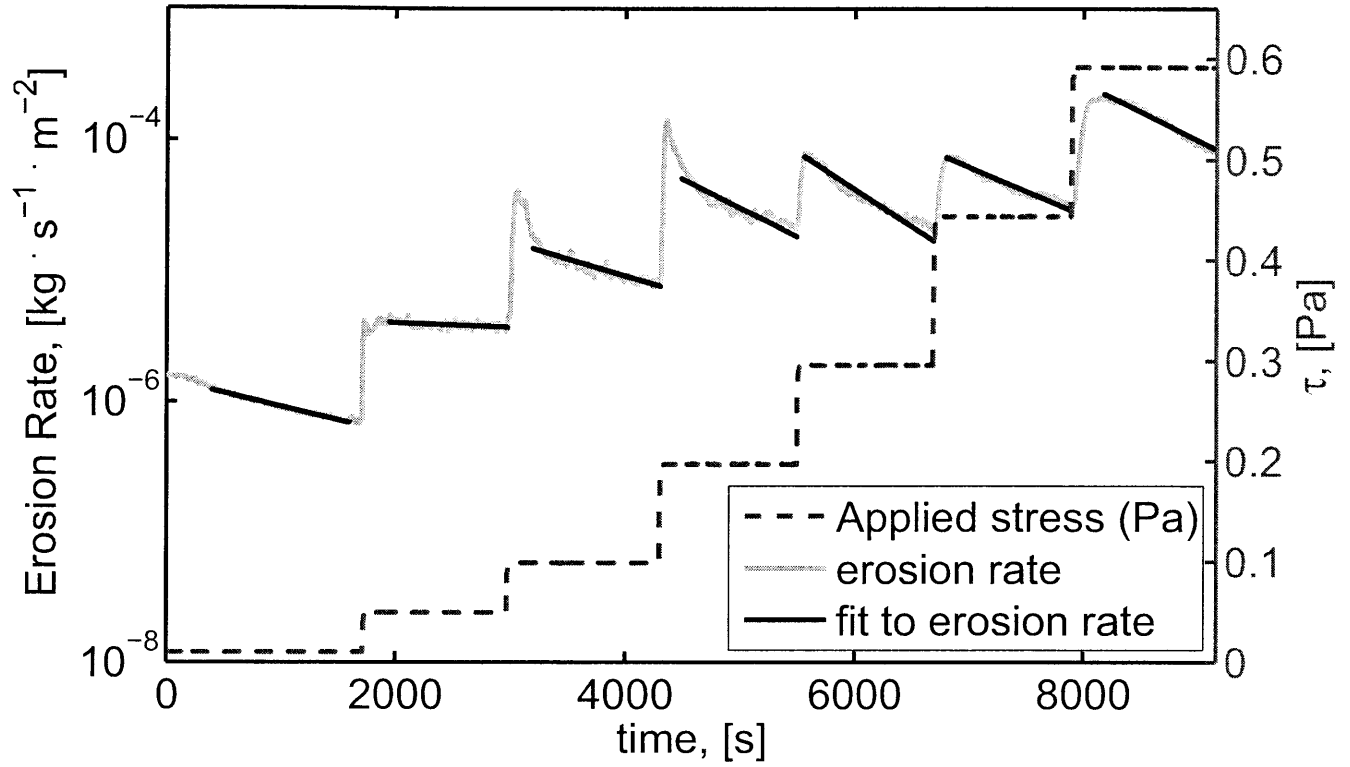
Step	τ_b (Pa)	τ_{ce} (Pa)	m (kg m^{-2})	M (kg m^{-2} s^{-1} Pa^{-1})	E_0 (kg m^{-2} s^{-1})	λ (s^{-1})	length (s)	organic fraction
1	0.0098	0.0400	0.00179	NaN	NaN	4.893e−04	1.709e+03	0.2282
2	0.0493	0.0409	0.00490	4.044e−06	4.339e−04	7.941e−05	1.274e+03	0.1812
3	0.0992	0.0729	0.01749	1.922e−05	3.297e−04	6.028e−04	1.319e+03	0.1236
4	0.1974	0.1601	0.04792	6.910e−05	5.548e−04	1.010e−03	1.194e+03	0.0911
5	0.2961	0.2677	0.04741	7.822e−05	5.753e−04	1.305e−03	1.199e+03	0.0906
6	0.4440	0.3810	0.05695	7.604e−05	4.311e−04	8.578e−04	1.199e+03	0.0847
7	0.5915	0.5320	0.18117	2.535e−04	1.204e−03	1.004e−03	1.259e+03	0.0692

190

S3942-7e
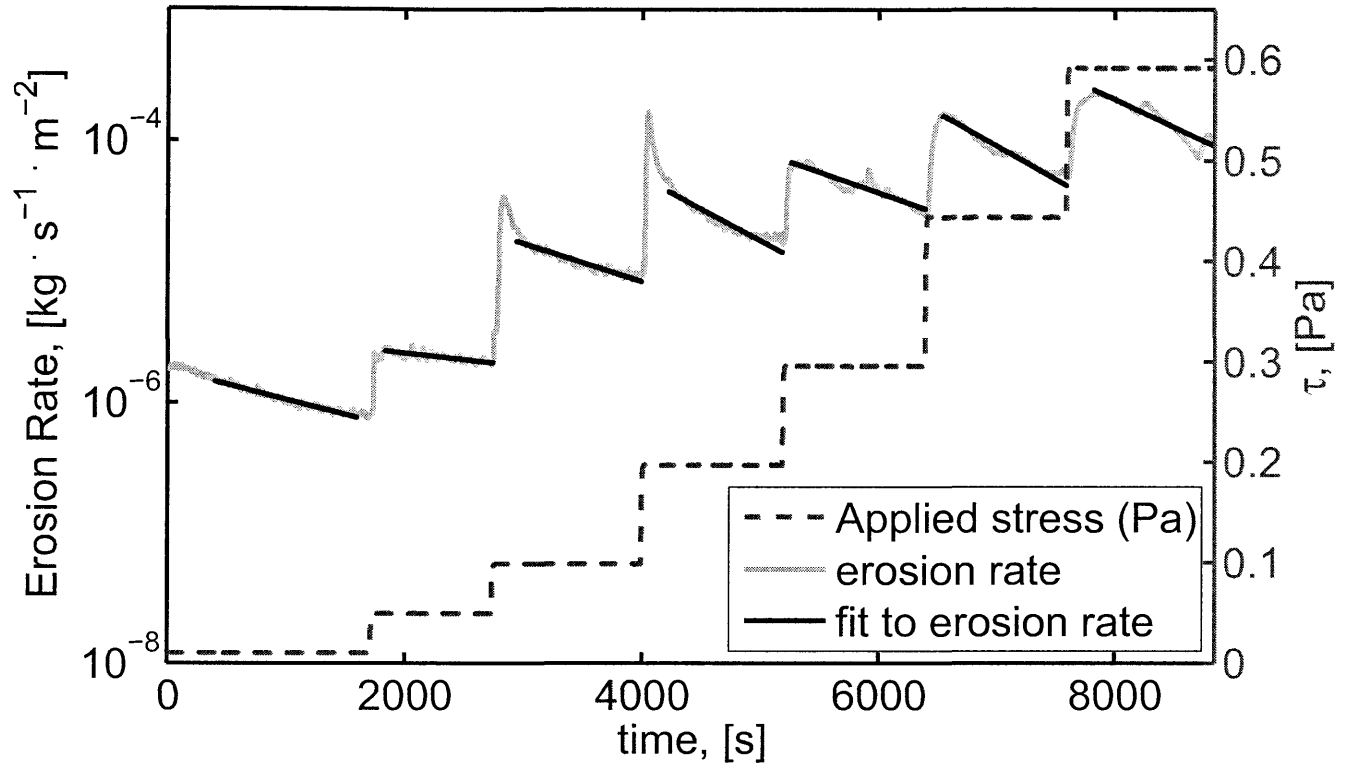
Step	τ_b (Pa)	τ_{ce} (Pa)	m (kg m^{-2})	M (kg m^{-2} s^{-1} Pa^{-1})	E$_0$ (kg m^{-2} s^{-1})	λ (s^{-1})	length (s)	organic fraction
1	0.0103	0.0450	0.00210	NaN	NaN	5.373e−04	1.739e+03	0.3132
2	0.0497	0.0460	0.00225	2.516e−06	5.398e−04	2.361e−04	1.004e+03	0.3056
3	0.0993	0.0764	0.01739	2.047e−05	3.838e−04	6.722e−04	1.259e+03	0.1484
4	0.1976	0.1652	0.04046	6.103e−05	5.038e−04	1.106e−03	1.194e+03	0.0966
5	0.2963	0.2416	0.05552	6.943e−05	5.299e−04	7.285e−04	1.199e+03	0.0885
6	0.4442	0.3944	0.10907	1.692e−04	8.351e−04	1.170e−03	1.199e+03	0.0784
7	0.5915	0.5327	0.19600	2.704e−04	1.372e−03	9.678e−04	1.249e+03	0.0751

S3942-8e
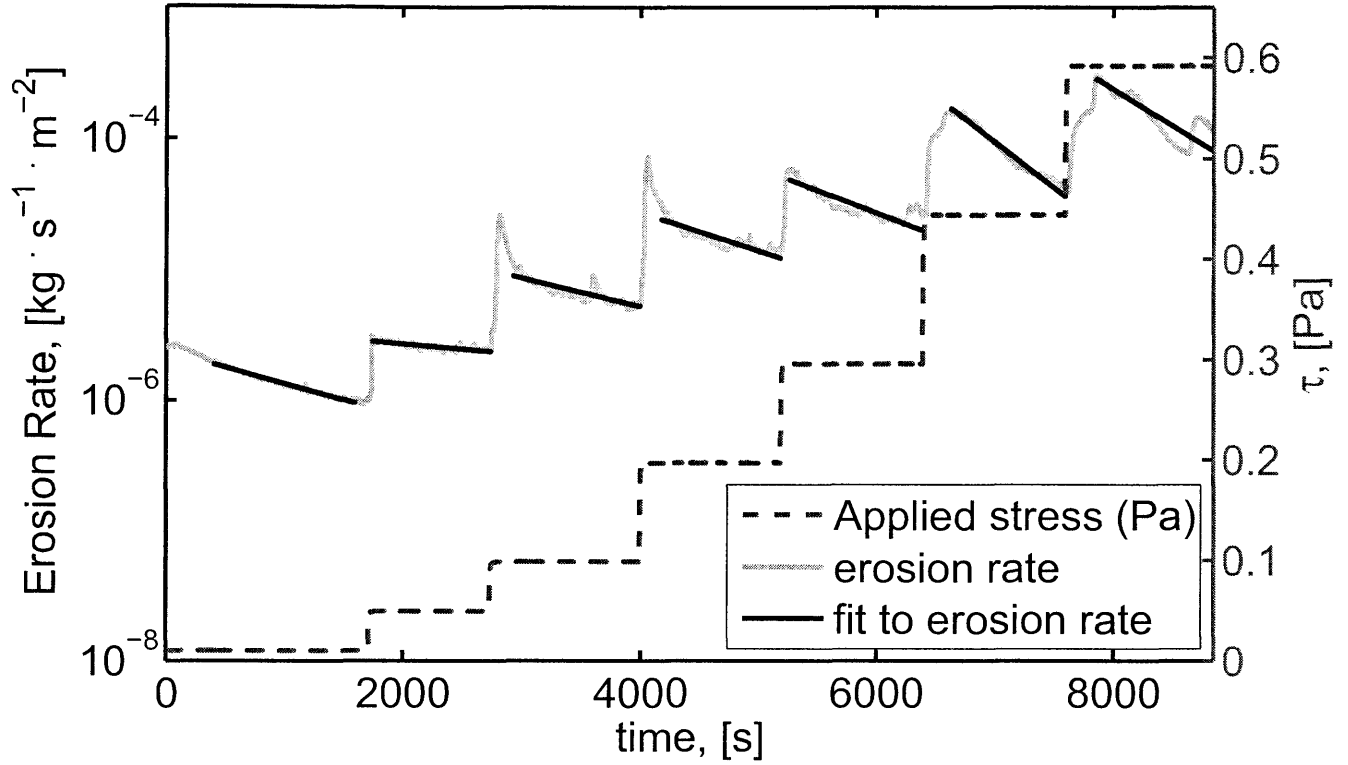
Step	τ_b (Pa)	τ_{ce} (Pa)	m (kg m^{-2})	M (kg m^{-2} s^{-1} Pa^{-1})	E_0 (kg m^{-2} s^{-1})	λ (s^{-1})	length (s)	organic fraction
1	0.0104	0.0450	0.00272	NaN	NaN	5.731e−04	1.739e+03	0.2157
2	0.0496	0.0458	0.00259	2.819e−06	6.101e−04	1.812e−04	1.004e+03	0.2634
3	0.0992	0.0709	0.00998	1.072e−05	2.007e−04	5.048e−04	1.259e+03	0.1509
4	0.1975	0.1406	0.02458	2.990e−05	2.361e−04	6.698e−04	1.194e+03	0.1190
5	0.2961	0.2365	0.03873	5.023e−05	3.230e−04	7.994e−04	1.199e+03	0.0958
6	0.4441	0.4141	0.10825	2.042e−04	9.834e−04	1.614e−03	1.199e+03	0.0765
7	0.5914	0.5555	0.19611	3.142e−04	1.772e−03	1.277e−03	1.249e+03	0.0739

192

S3943-5e
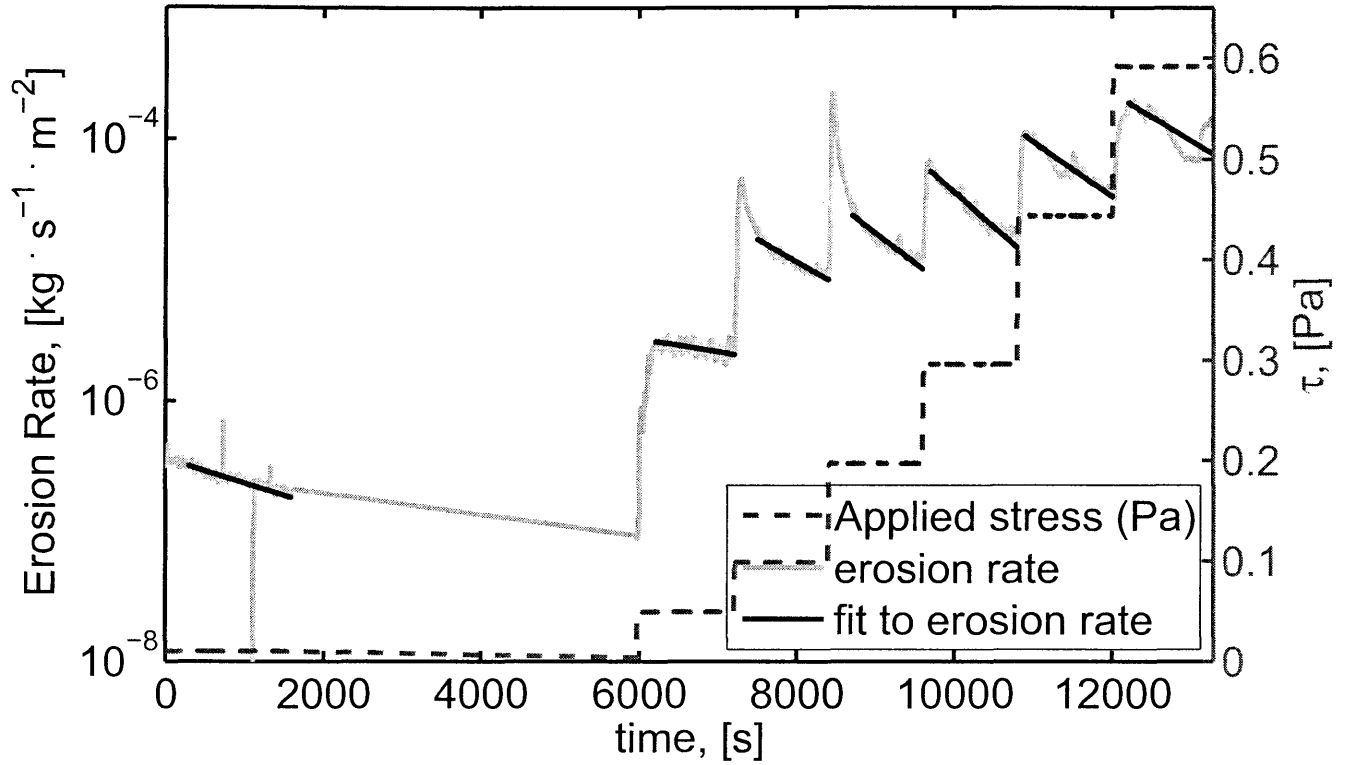
Step	τ_b (Pa)	τ_{ce} (Pa)	m (kg m^{-2})	M (kg m^{-2} s^{-1} Pa^{-1})	E_0 (kg m^{-2} s^{-1})	λ (s^{-1})	length (s)	organic fraction
1	0.0103	0.0300	0.00083	NaN	NaN	4.360e−04	5.999e+03	0.2639
2	0.0496	0.0348	0.00286	2.698e−06	1.377e−04	2.303e−04	1.214e+03	0.2203
3	0.0994	0.0743	0.01946	2.510e−05	3.888e−04	7.888e−04	1.199e+03	0.1112
4	0.1976	0.1626	0.03842	5.655e−05	4.584e−04	1.053e−03	1.194e+03	0.0951
5	0.2964	0.2656	0.03934	6.267e−05	4.683e−04	1.227e−03	1.199e+03	0.0986
6	0.4442	0.3880	0.07828	1.101e−04	6.170e−04	9.643e−04	1.199e+03	0.0877
7	0.5915	0.5215	0.15847	2.015e−04	9.900e−04	8.341e−04	1.279e+03	0.0793

S3943-6e
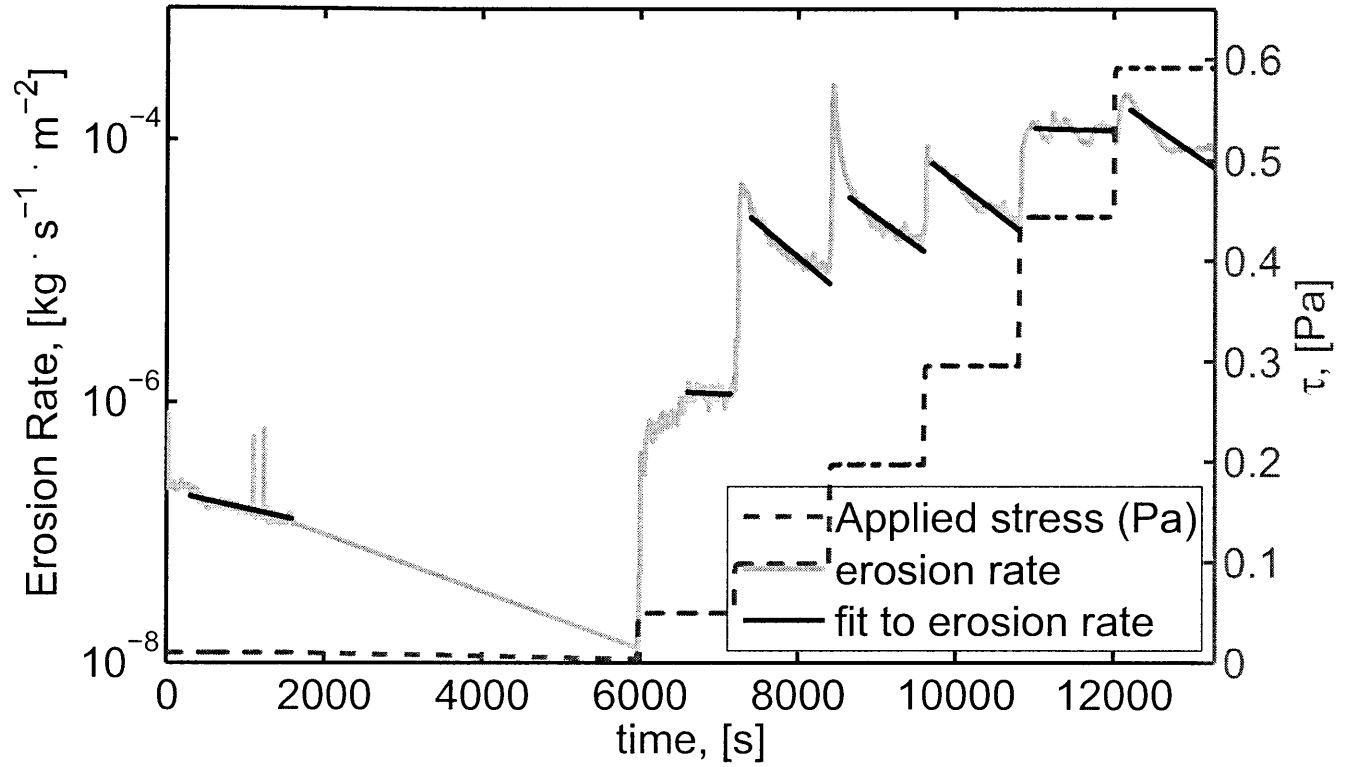
Step	τ_b (Pa)	τ_{ce} (Pa)	m (kg m^{-2})	M (kg m^{-2} s^{-1} Pa^{-1})	E_0 (kg m^{-2} s^{-1})	λ (s^{-1})	length (s)	organic fraction
1	0.0103	0.0300	0.00033	NaN	NaN	3.074e-04	5.999e+03	0.2576
2	0.0496	0.0315	0.00114	9.750e-07	4.980e-05	6.486e-05	1.214e+03	0.2473
3	0.0992	0.0823	0.02141	3.305e-05	4.884e-04	1.159e-03	1.199e+03	0.1090
4	0.1975	0.1627	0.04512	6.480e-05	5.624e-04	1.002e-03	1.194e+03	0.1082
5	0.2962	0.2594	0.04929	7.314e-05	5.480e-04	1.075e-03	1.199e+03	0.1043
6	0.4440	0.2676	0.14166	1.209e-04	6.546e-04	3.820e-05	1.199e+03	0.0795
7	0.5915	0.4959	0.15112	2.045e-04	6.316e-04	9.538e-04	1.279e+03	0.0812

S3944-5e
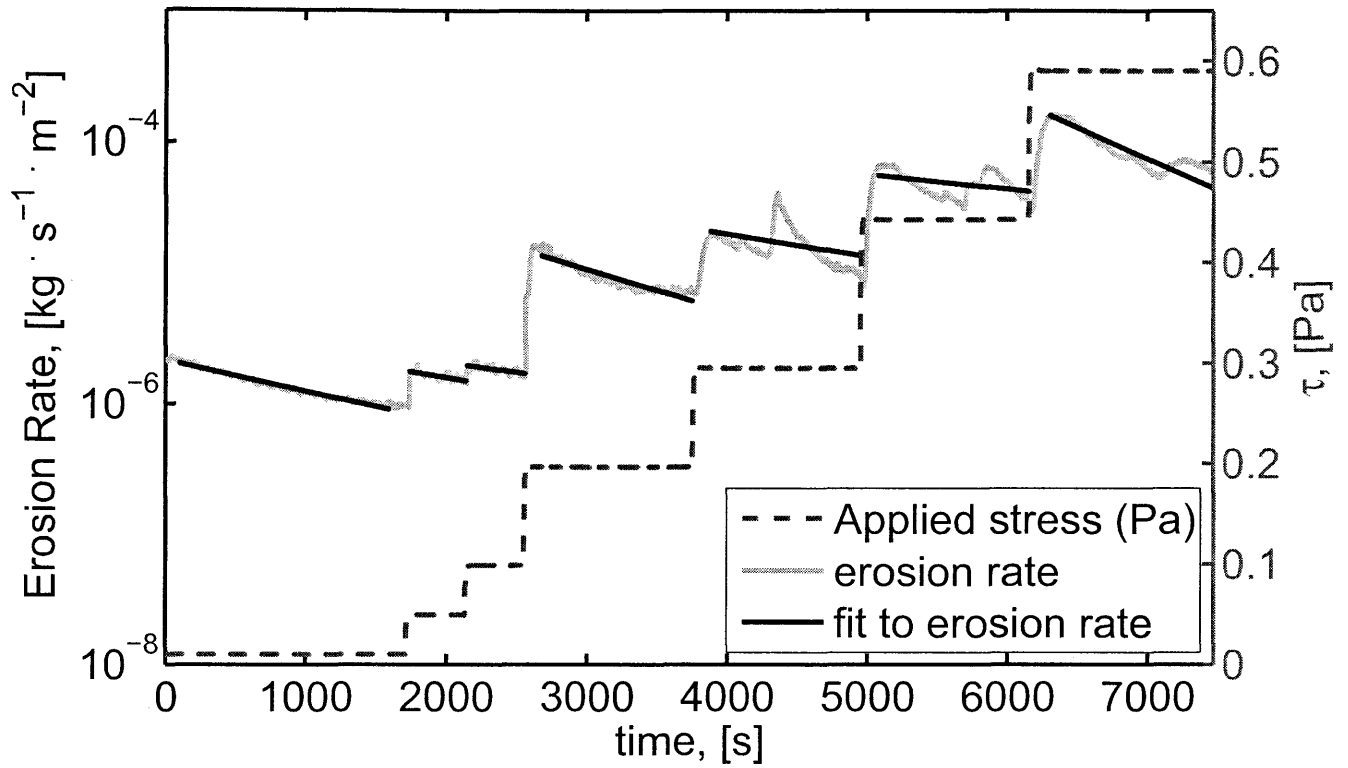
Step	τ_b (Pa)	τ_{ce} (Pa)	m (kg m^{-2})	M (kg m^{-2} s^{-1} Pa^{-1})	E_0 (kg m^{-2} s^{-1})	λ (s^{-1})	length (s)	organic fraction
1	0.0103	0.1500	0.00245	NaN	NaN	5.461e−04	1.739e+03	0.2659
2	0.0501	0.1347	0.00066	1.771e−06	−1.773e−05	4.123e−04	4.040e+02	0.4000
3	0.1004	0.1299	0.00077	1.975e−06	−5.767e−05	3.610e−04	4.190e+02	0.3152
4	0.1970	0.1693	0.01152	1.454e−05	2.164e−04	7.403e−04	1.194e+03	0.1500
5	0.2957	0.2171	0.01972	2.067e−05	1.635e−04	3.964e−04	1.199e+03	0.1312
6	0.4434	0.2778	0.05642	5.479e−05	2.421e−04	2.607e−04	1.199e+03	0.1043
7	0.5902	0.5157	0.11836	1.702e−04	5.448e−04	1.095e−03	1.309e+03	0.0855

S3944-6e
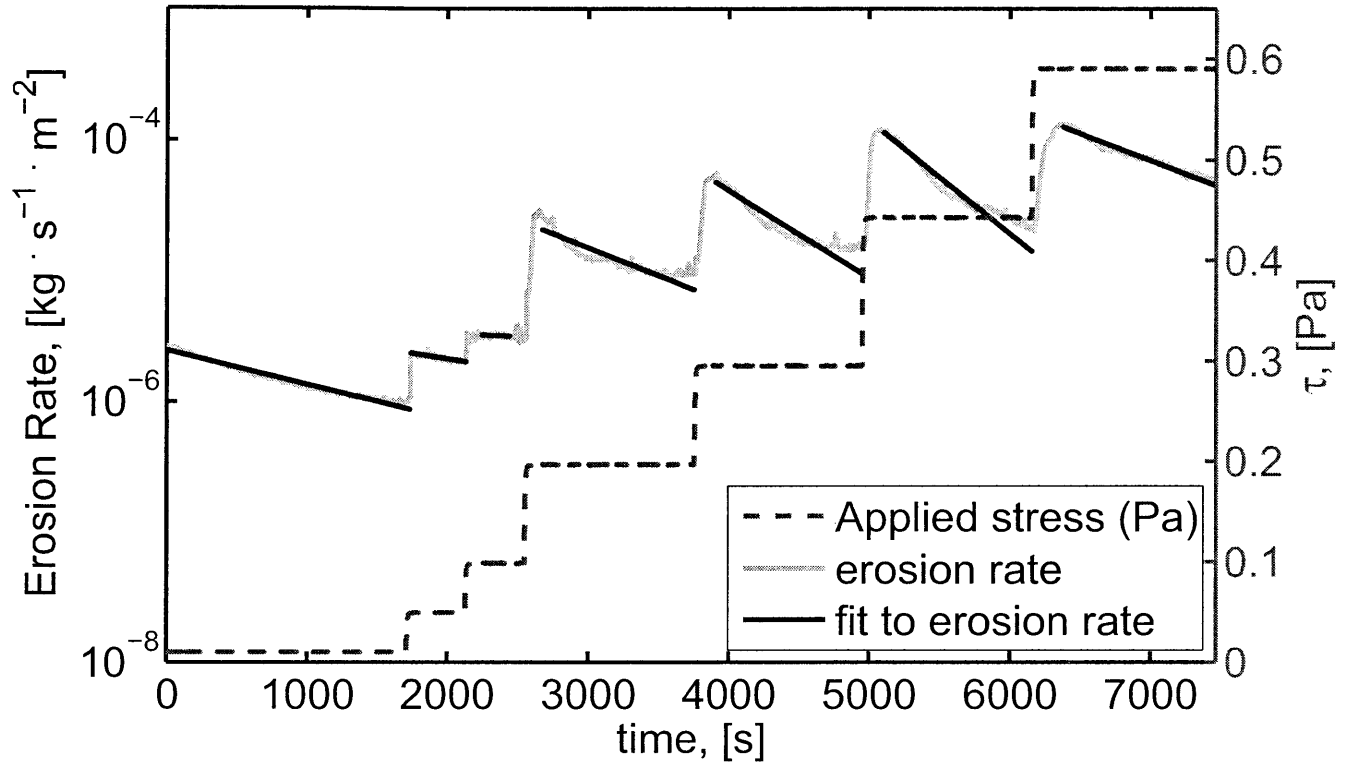
Step	τ_b (Pa)	τ_{ce} (Pa)	m (kg m^{-2})	M (kg m^{-2} s^{-1} Pa^{-1})	E_0 (kg m^{-2} s^{-1})	λ (s^{-1})	length (s)	organic fraction
1	0.0103	0.1500	0.00266	NaN	NaN	6.050e−04	1.739e+03	0.2332
2	0.0501	0.1356	0.00088	2.354e−06	−2.355e−05	3.865e−04	4.040e+02	0.3197
3	0.1002	0.1341	0.00133	3.232e−06	−9.149e−05	9.868e−05	4.190e+02	0.2756
4	0.1970	0.1777	0.01605	2.289e−05	3.640e−04	9.884e−04	1.194e+03	0.1347
5	0.2956	0.2769	0.03037	5.547e−05	4.706e−04	1.537e−03	1.199e+03	0.1156
6	0.4432	0.4279	0.06273	1.377e−04	8.281e−04	1.994e−03	1.199e+03	0.0956
7	0.5902	0.5430	0.10389	1.382e−04	8.514e−04	9.430e−04	1.309e+03	0.0869

S3945-6e
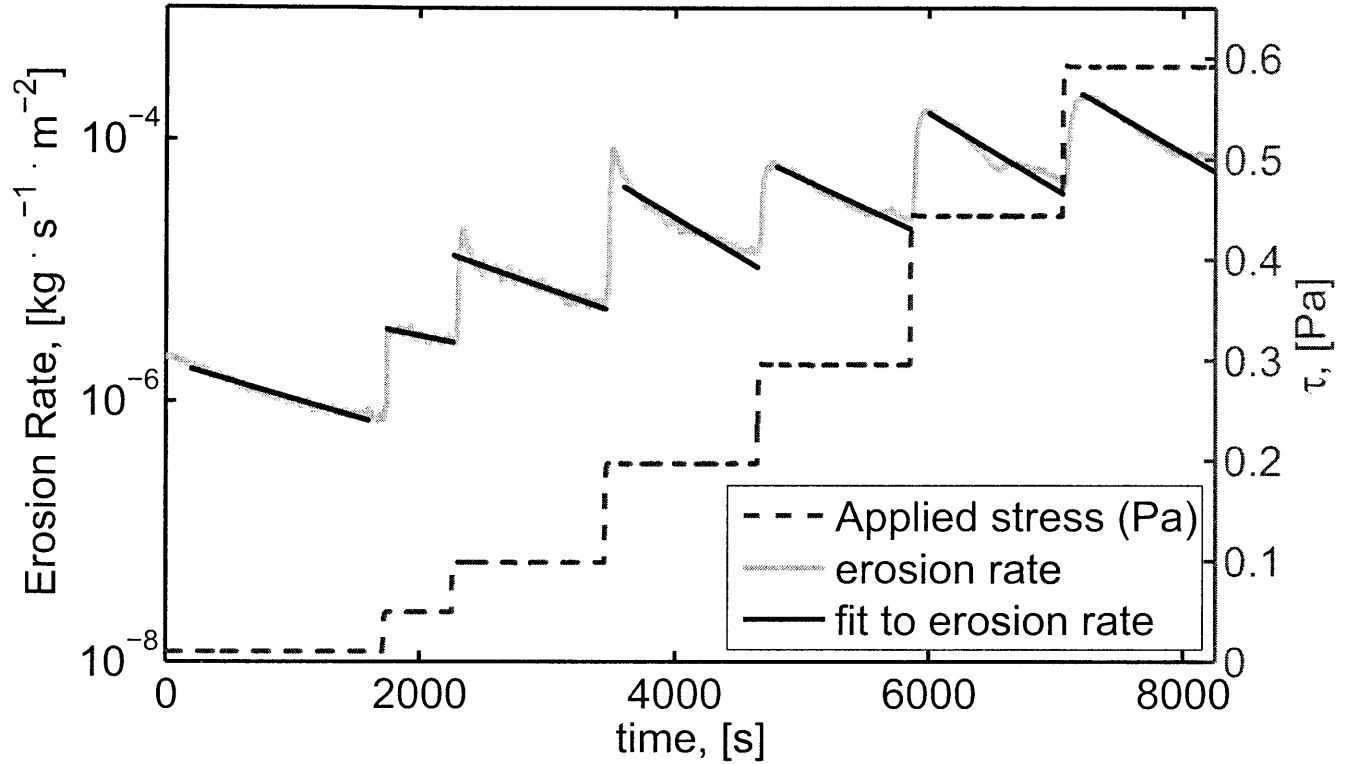
Step	τ_b (Pa)	τ_{ce} (Pa)	m (kg m^{-2})	M (kg m^{-2} s^{-1} Pa^{-1})	E_0 (kg m^{-2} s^{-1})	λ (s^{-1})	length (s)	organic fraction
1	0.0103	0.0750	0.00214	NaN	NaN	6.564e−04	1.739e+03	0.2849
2	0.0500	0.0697	0.00166	3.564e−06	−1.424e−04	4.537e−04	5.240e+02	0.3035
3	0.0994	0.0879	0.01007	1.299e−05	4.379e−04	7.892e−04	1.199e+03	0.1993
4	0.1976	0.1757	0.03220	5.429e−05	4.947e−04	1.350e−03	1.194e+03	0.1009
5	0.2964	0.2616	0.04701	6.852e−05	5.677e−04	1.037e−03	1.199e+03	0.0758
6	0.4443	0.4077	0.10622	1.782e−04	9.751e−04	1.342e−03	1.199e+03	0.0764
7	0.5916	0.5530	0.14816	2.443e−04	1.329e−03	1.303e−03	1.199e+03	0.0708

197

S3945-7e
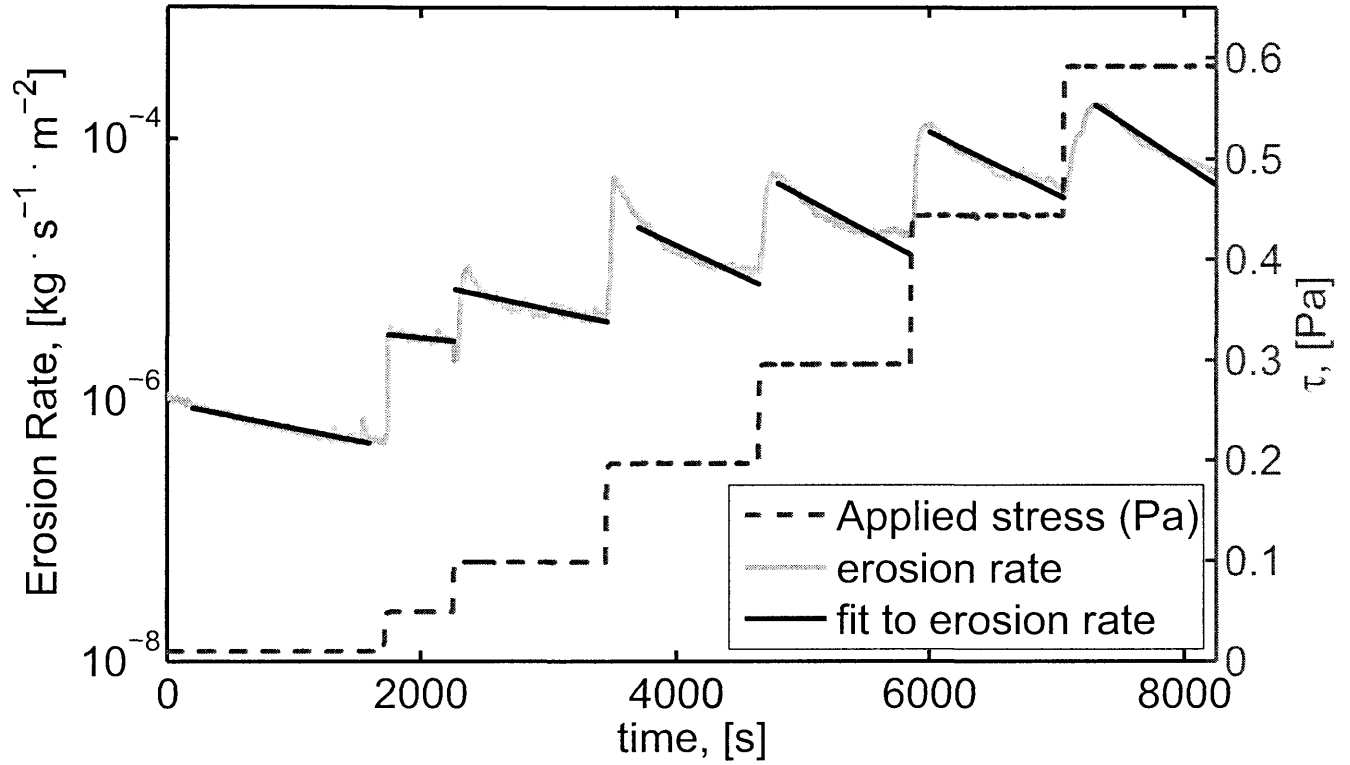
Step	τ_b (Pa)	τ_{ce} (Pa)	m (kg m^{-2})	M (kg m^{-2} s^{-1} Pa^{-1})	E_0 (kg m^{-2} s^{-1})	λ (s^{-1})	length (s)	organic fraction
1	0.0103	0.0750	0.00119	NaN	NaN	4.488e−04	1.739e+03	0.3443
2	0.0500	0.0722	0.00158	3.210e−06	−1.282e−04	2.301e−04	5.240e+02	0.2847
3	0.0992	0.0839	0.00646	7.076e−06	2.616e−04	4.771e−04	1.199e+03	0.1581
4	0.1975	0.1652	0.02069	3.046e−05	2.683e−04	1.054e−03	1.194e+03	0.0460
5	0.2962	0.2652	0.03316	5.219e−05	3.984e−04	1.201e−03	1.199e+03	0.1126
6	0.4441	0.3961	0.08376	1.256e−04	7.018e−04	1.097e−03	1.199e+03	0.0891
7	0.5914	0.5584	0.12020	2.144e−04	1.098e−03	1.482e−03	1.199e+03	0.0854

S3946-6e
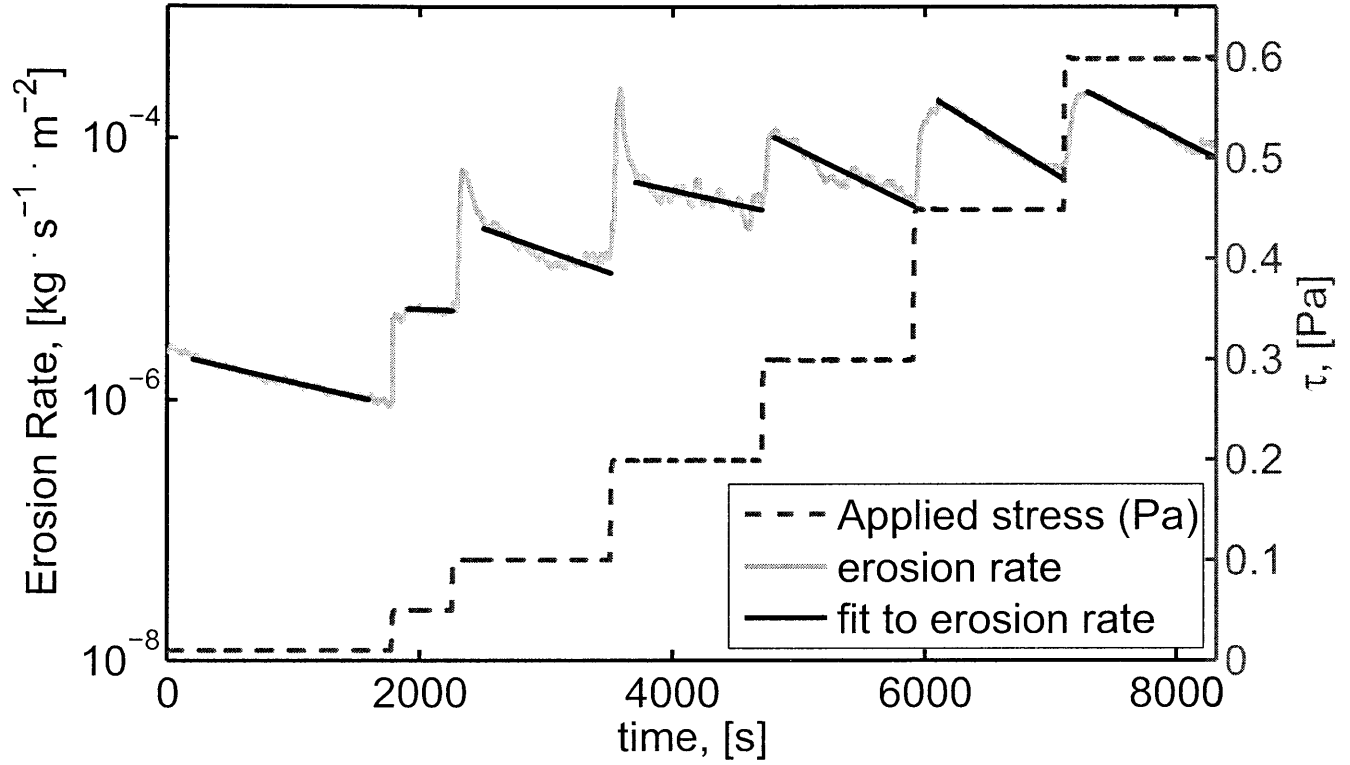
Step	τ_b (Pa)	τ_{ce} (Pa)	m (kg m^{-2})	M (kg m^{-2} s^{-1} Pa^{-1})	E_0 (kg m^{-2} s^{-1})	λ (s^{-1})	length (s)	organic fraction
1	0.0101	0.0750	0.00270	NaN	NaN	5.164e−04	1.784e+03	0.1422
2	0.0504	0.0738	0.00227	4.864e−06	−1.980e−04	1.015e−04	4.790e+02	0.1417
3	0.1005	0.0905	0.02216	2.767e−05	1.038e−03	7.826e−04	1.259e+03	0.1060
4	0.1997	0.1391	0.05621	6.227e−05	5.705e−04	4.926e−04	1.194e+03	0.0879
5	0.2997	0.2563	0.07214	1.079e−04	6.719e−04	1.092e−03	1.199e+03	0.0823
6	0.4488	0.4117	0.12793	2.177e−04	1.131e−03	1.374e−03	1.199e+03	0.0723
7	0.5978	0.5509	0.16408	2.521e−04	1.354e−03	1.149e−03	1.199e+03	0.0694

S3946-8e
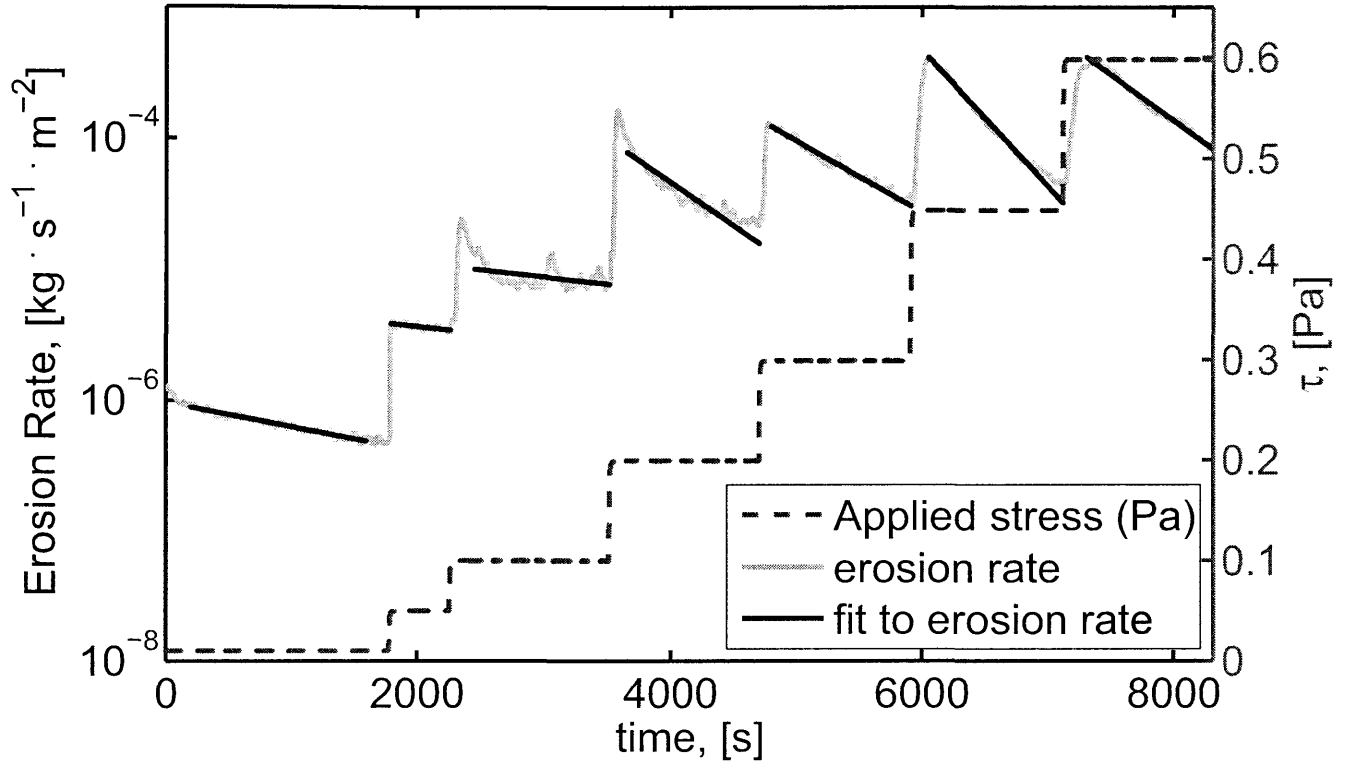
Step	τ_b (Pa)	τ_{ce} (Pa)	m (kg m^{-2})	M (kg m^{-2} s^{-1} Pa^{-1})	E_0 (kg m^{-2} s^{-1})	λ (s^{-1})	length (s)	organic fraction
1	0.0101	0.0750	0.00123	NaN	NaN	4.317e−04	1.784e+03	0.1672
2	0.0504	0.0722	0.00175	3.877e−06	−1.576e−04	2.525e−04	4.790e+02	0.1631
3	0.1003	0.0799	0.01214	1.128e−05	4.012e−04	2.560e−04	1.259e+03	0.1068
4	0.1997	0.1802	0.05494	9.972e−05	8.327e−04	1.519e−03	1.194e+03	0.0835
5	0.2995	0.2734	0.08120	1.317e−04	1.103e−03	1.266e−03	1.199e+03	0.0736
6	0.4488	0.4390	0.18731	4.780e−04	2.725e−03	2.410e−03	1.199e+03	0.0660
7	0.5977	0.5744	0.24632	4.617e−04	2.909e−03	1.599e−03	1.199e+03	0.0657

200

S3947-2e
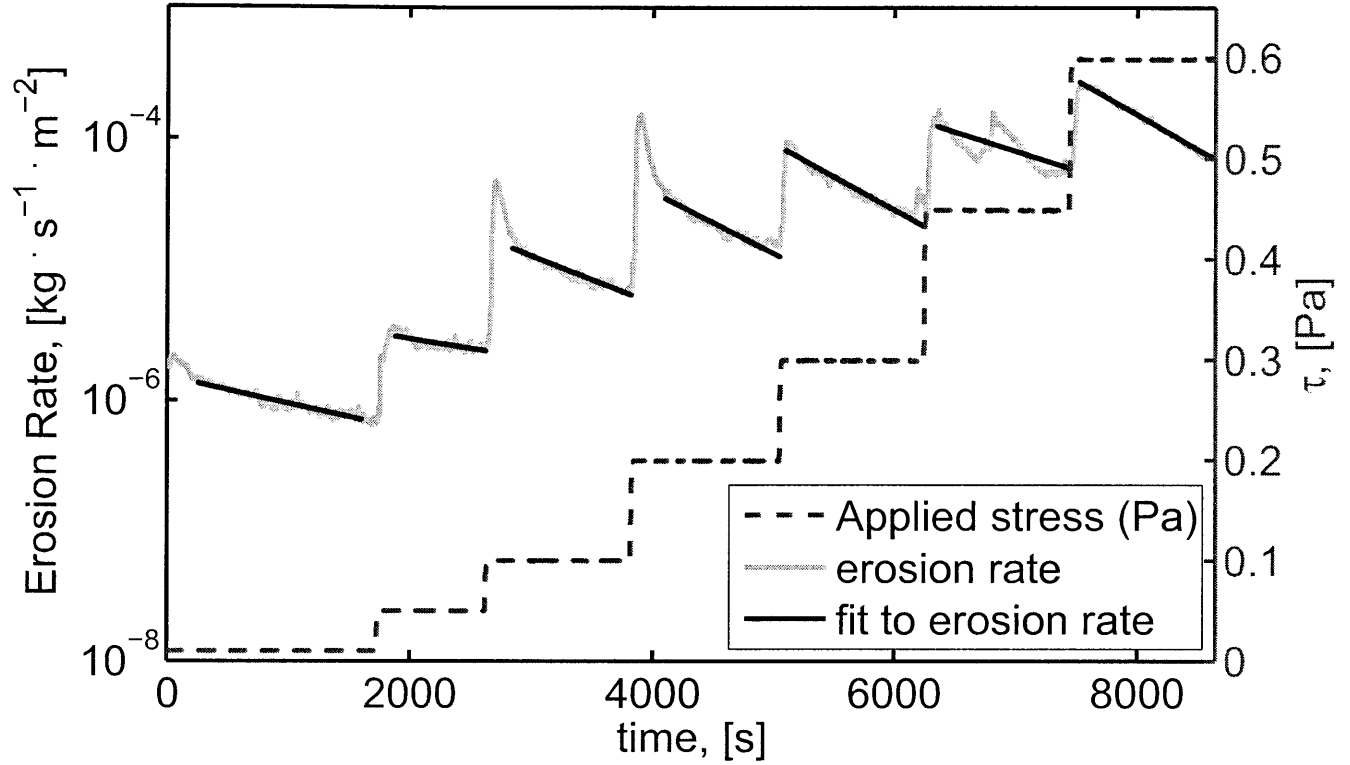
Step	τ_b (Pa)	τ_{ce} (Pa)	m (kg m^{-2})	M (kg m^{-2} s^{-1} Pa^{-1})	E_0 (kg m^{-2} s^{-1})	λ (s^{-1})	length (s)	organic fraction
1	0.0105	0.0400	0.00191	NaN	NaN	4.786e−04	1.749e+03	0.1899
2	0.0503	0.0427	0.00243	3.164e−06	3.074e−04	3.401e−04	8.890e+02	0.1848
3	0.1004	0.0795	0.01514	2.017e−05	3.495e−04	8.492e−04	1.194e+03	0.0959
4	0.1998	0.1677	0.04084	6.035e−05	5.014e−04	1.083e−03	1.219e+03	0.0938
5	0.2997	0.2671	0.05409	8.375e−05	6.343e−04	1.166e−03	1.199e+03	0.0590
6	0.4494	0.3681	0.10618	1.291e−04	7.080e−04	6.735e−04	1.199e+03	0.0581
7	0.5984	0.5446	0.17653	2.795e−04	1.213e−03	1.214e−03	1.199e+03	0.0492

S3947-5e
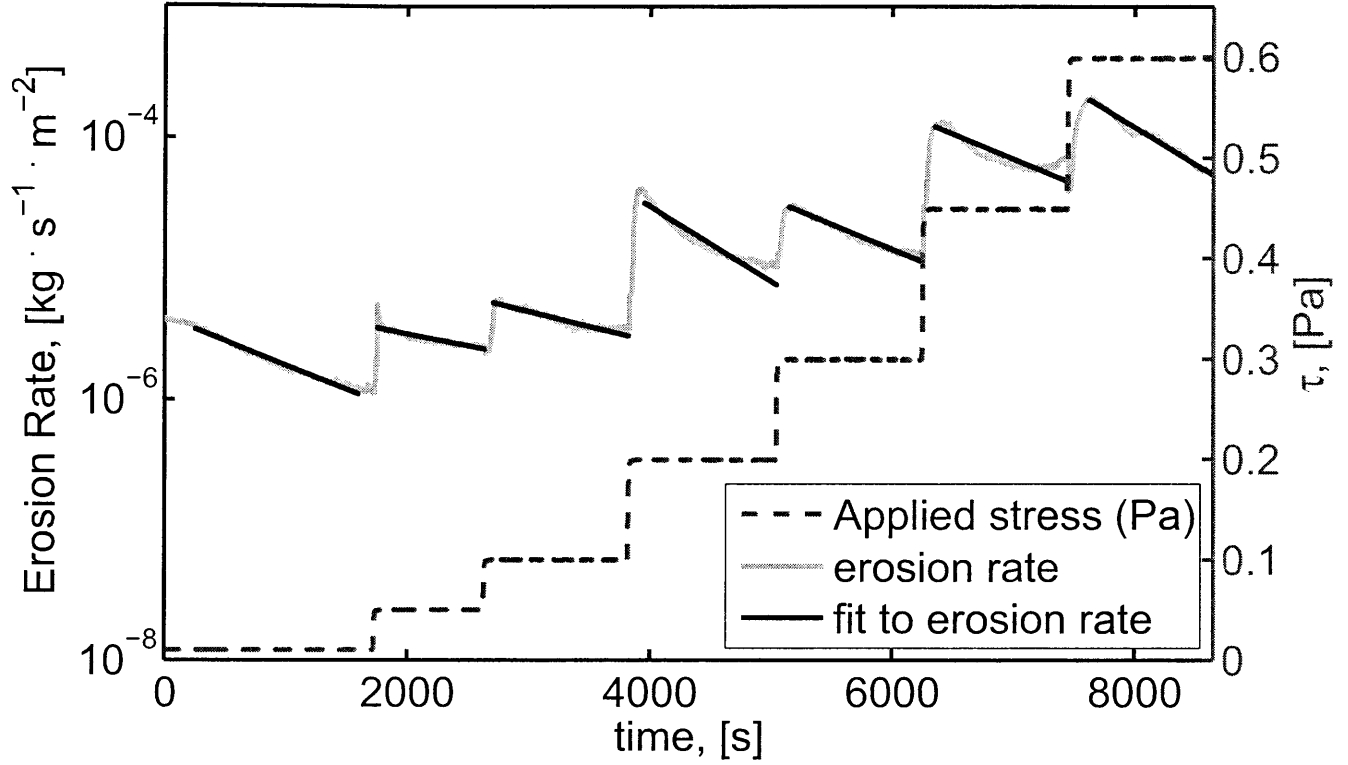
Step	τ_b (Pa)	τ_{ce} (Pa)	m (kg m^{-2})	M (kg m^{-2} s^{-1} Pa^{-1})	E_0 (kg m^{-2} s^{-1})	λ (s^{-1})	length (s)	organic fraction
1	0.0105	0.0400	0.00394	NaN	NaN	8.587e−04	1.749e+03	0.1681
2	0.0503	0.0432	0.00260	3.516e−06	3.425e−04	4.262e−04	8.890e+02	0.1939
3	0.1002	0.0698	0.00484	5.459e−06	9.579e−05	5.254e−04	1.194e+03	0.0956
4	0.1998	0.1737	0.02190	3.613e−05	2.780e−04	1.319e−03	1.219e+03	0.0724
5	0.2996	0.2561	0.02296	3.110e−05	2.470e−04	8.862e−04	1.199e+03	0.0711
6	0.4492	0.3813	0.09339	1.255e−04	6.501e−04	8.713e−04	1.199e+03	0.0529
7	0.5983	0.5522	0.13371	2.194e−04	1.011e−03	1.292e−03	1.199e+03	0.0616

S3948-4e

Step	τ_b (Pa)	τ_{ce} (Pa)	m (kg m^{-2})	M (kg m^{-2} s^{-1} Pa^{-1})	E_0 (kg m^{-2} s^{-1})	λ (s^{-1})	length (s)	organic fraction
1	0.0105	0.0400	0.00256	NaN	NaN	5.280e−04	1.749e+03	0.1981
2	0.0502	0.0443	0.00306	4.810e−06	4.694e−04	6.592e−04	8.240e+02	0.1838
3	0.1004	0.0819	0.01301	1.796e−05	3.198e−04	9.249e−04	1.199e+03	0.0865
4	0.1996	0.1739	0.03244	5.182e−05	4.404e−04	1.249e−03	1.219e+03	0.0741
5	0.2994	0.2523	0.03134	4.099e−05	3.265e−04	8.167e−04	1.199e+03	0.0765
6	0.4489	0.3901	0.09842	1.413e−04	7.188e−04	1.006e−03	1.199e+03	0.0454
7	0.5978	0.5124	0.19905	2.506e−04	1.206e−03	7.412e−04	1.199e+03	0.0444

S3948-6e
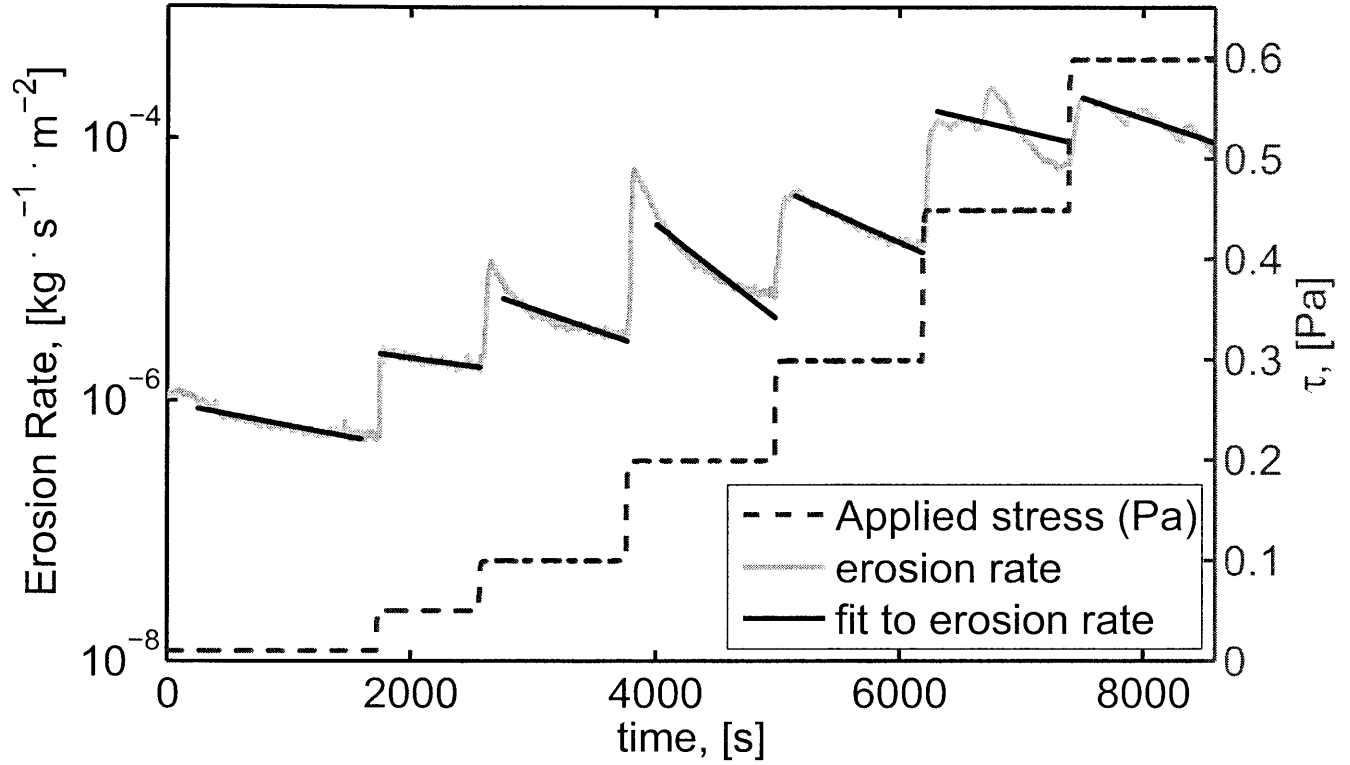
Step	τ_b (Pa)	τ_{ce} (Pa)	m (kg m^{-2})	M (kg m^{-2} s^{-1} Pa^{-1})	E_0 (kg m^{-2} s^{-1})	λ (s^{-1})	length (s)	organic fraction
1	0.0104	0.0400	0.00126	NaN	NaN	4.076e-04	1.749e+03	0.2005
2	0.0503	0.0422	0.00166	2.269e-06	2.210e-04	2.972e-04	8.240e+02	0.1810
3	0.1003	0.0763	0.00565	7.102e-06	1.224e-04	7.390e-04	1.199e+03	0.1087
4	0.1996	0.1835	0.01936	3.721e-05	3.019e-04	1.672e-03	1.219e+03	0.2322
5	0.2994	0.2631	0.02858	4.031e-05	3.480e-04	9.690e-04	1.199e+03	0.1088
6	0.4488	0.3465	0.14427	1.598e-04	8.603e-04	4.974e-04	1.199e+03	0.0588
7	0.5977	0.4922	0.16858	2.103e-04	8.370e-04	7.232e-04	1.199e+03	0.0540

Appendix V

X-radiographs

Gloucester Point X-radiographs
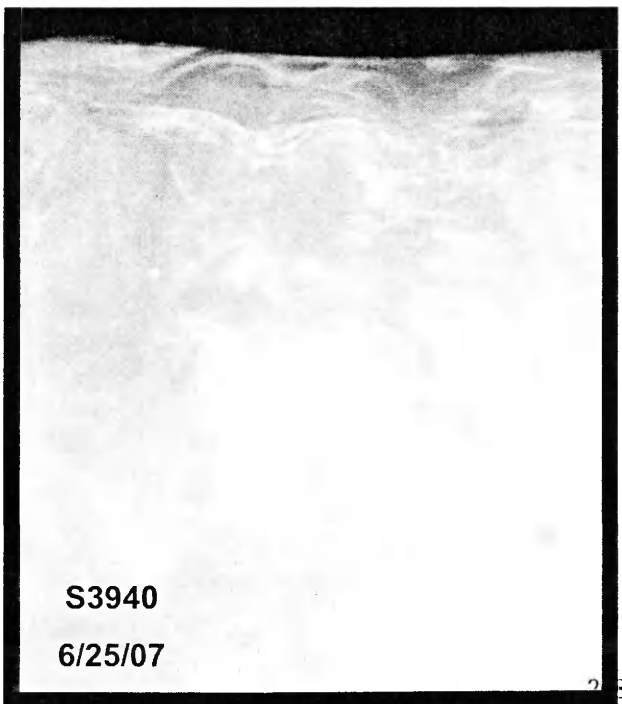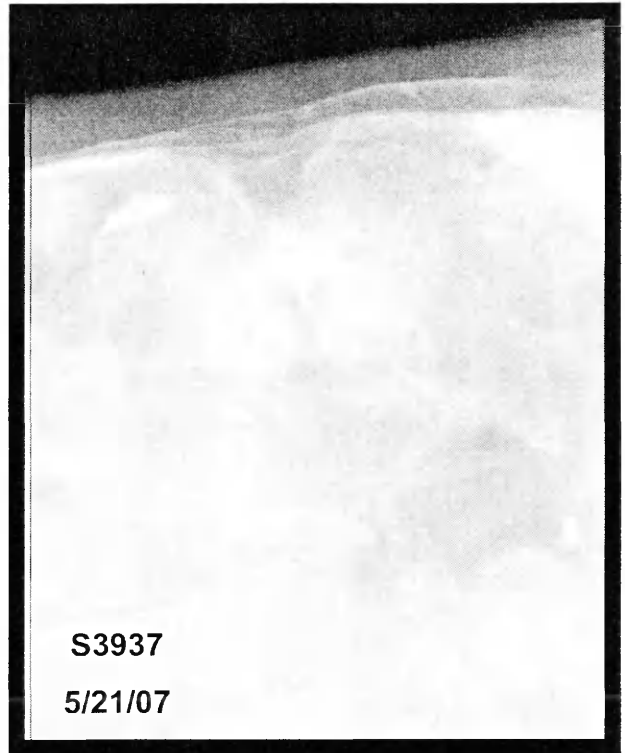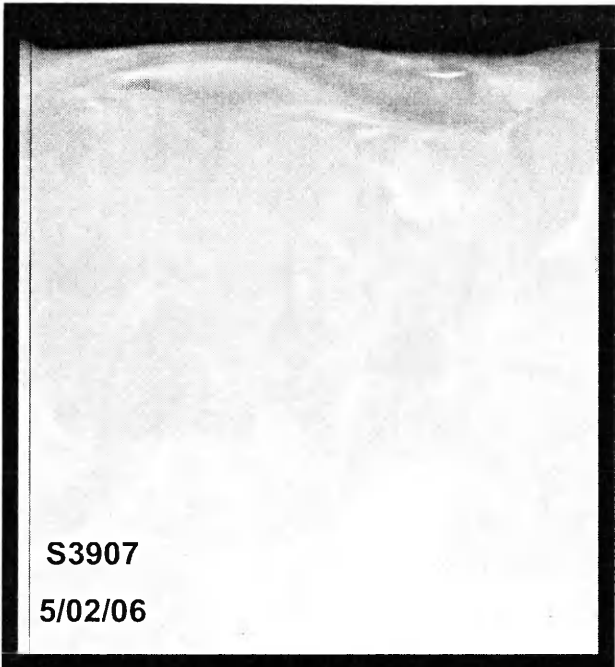
S3905
4/18/06

S3911
7/14/06

S3914
8/2106

S3918
9/25/06

S3924
11/20/06

S3925
1/09/07

S3928
3/21/07

207

S3931
4/18/07

S3937
5/21/07

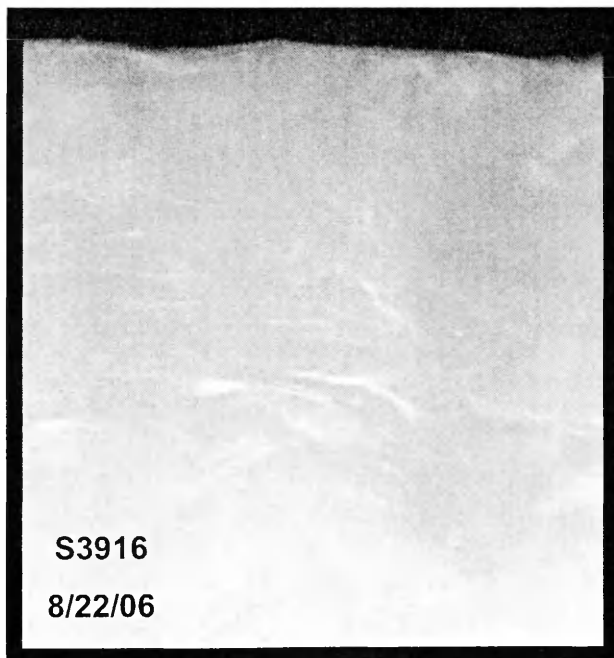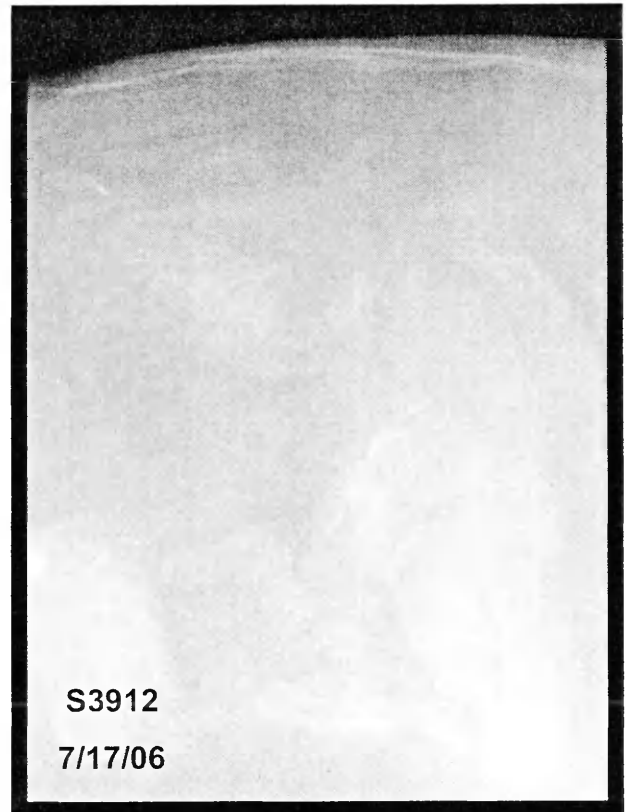S3940
6/25/07

S3947
10/16/07

S3907
5/02/06

S3913
7/19/06

S3917
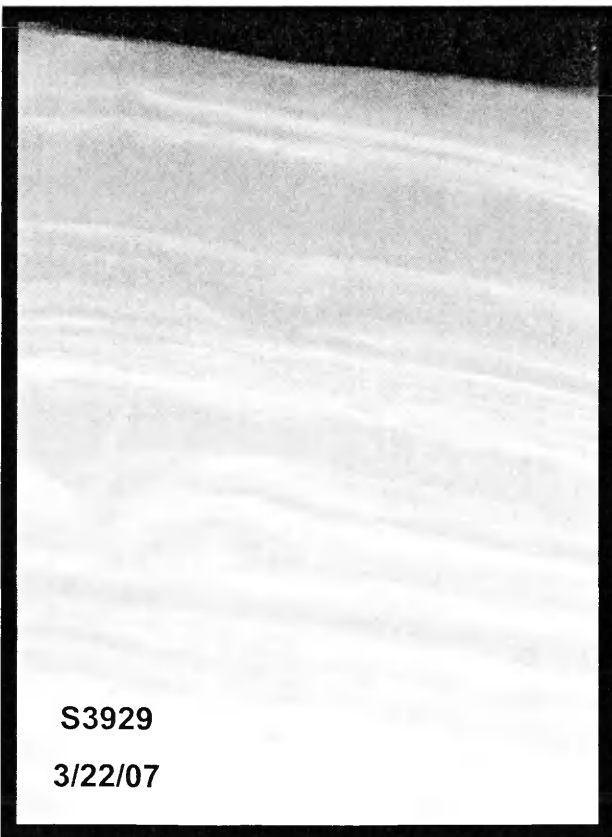8/23/06

S3920
9/28/06

Clay Bank Secondary Channel X-radiographs

S3923
11/17//06

S3927
1/12/07

S3930
3/23/07

S3933
4/20/07

Clay Bank Secondary Channel X-radiographs

S3938
5/22/07

S3941
6/26/07

S3948
10/17/07

Clay Bank Channel X-radiographs

S3908
5/03/06

S3912
7/17/06

S3916
8/22/06

S3921
9/29/06

212

Clay Bank Channel X-radiographs

S3922
11/15/06

S3926
1/11/07

S3929
3/22/07

S3932
4/19/07

S3939
5/23/07

S3942
6/27/07

S3946
10/15/07

214
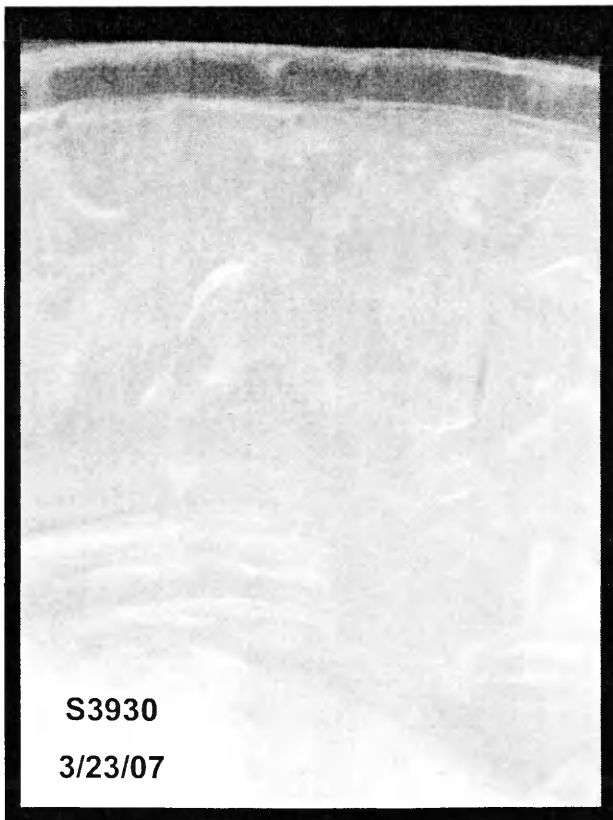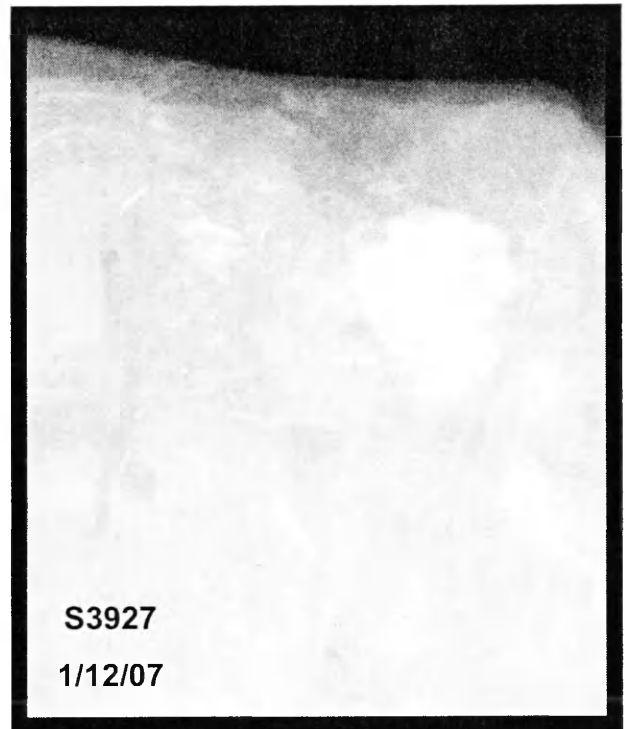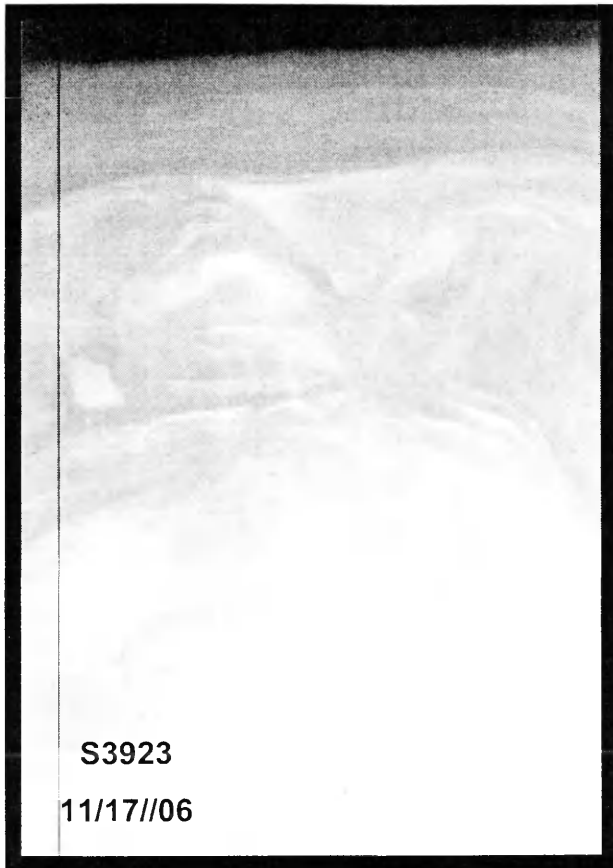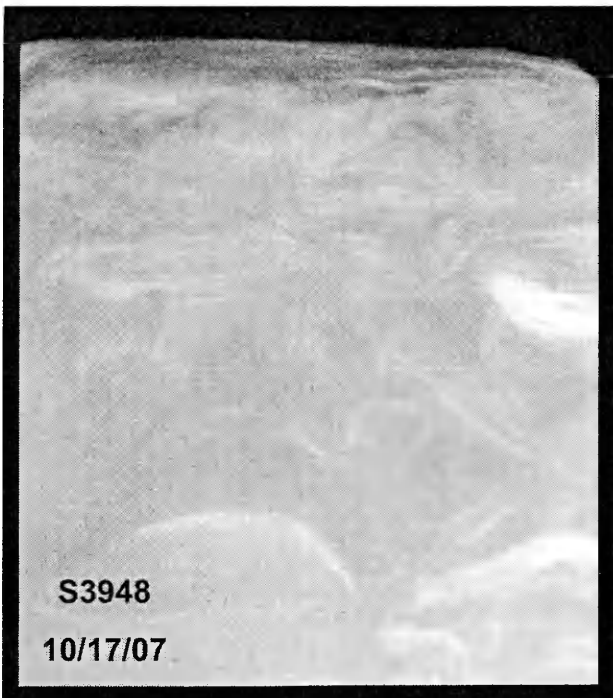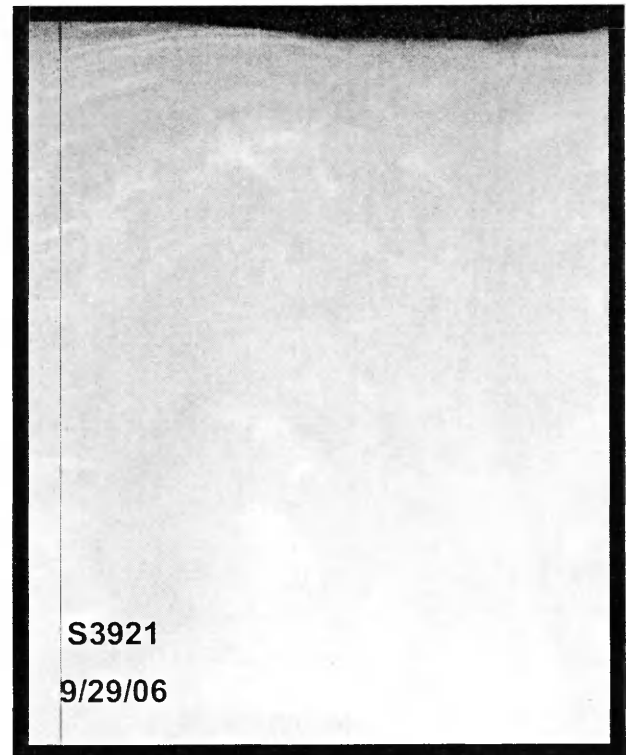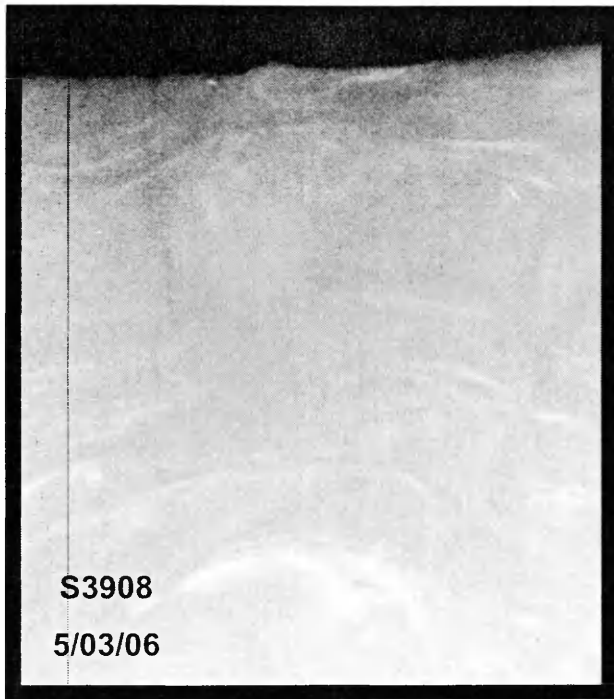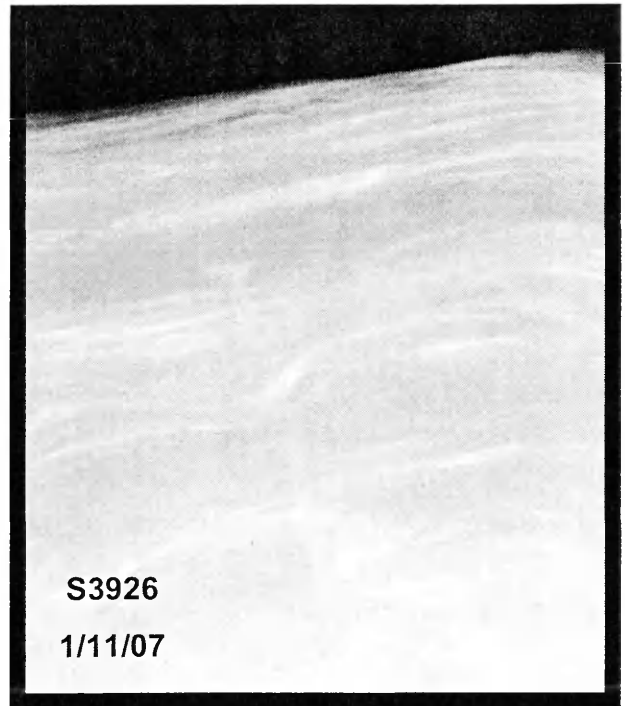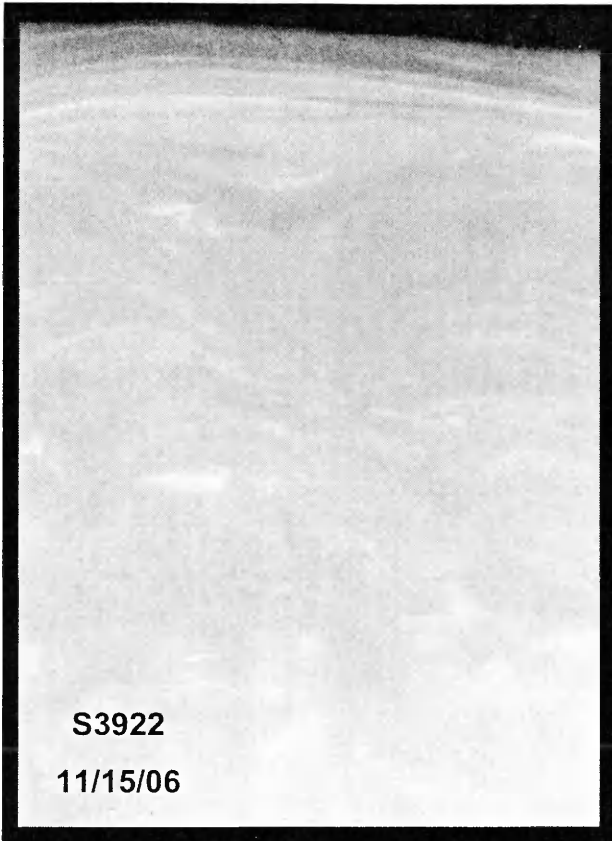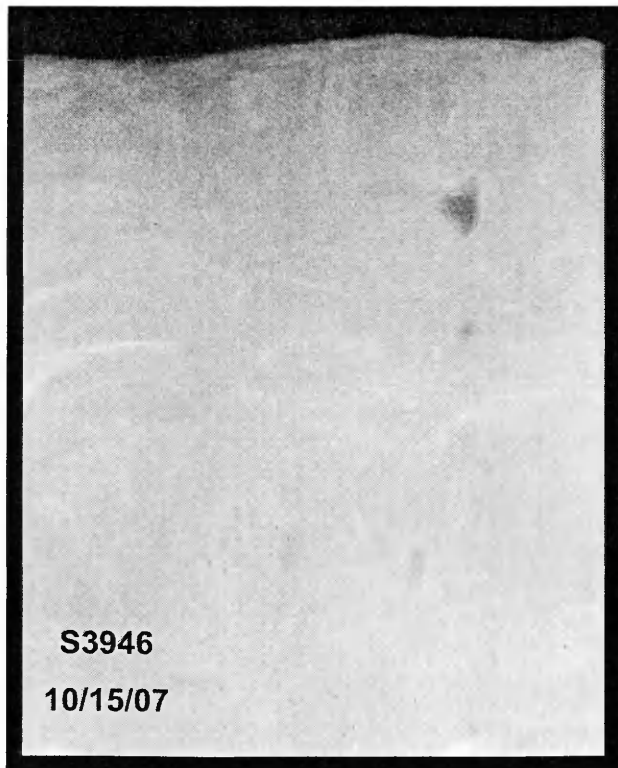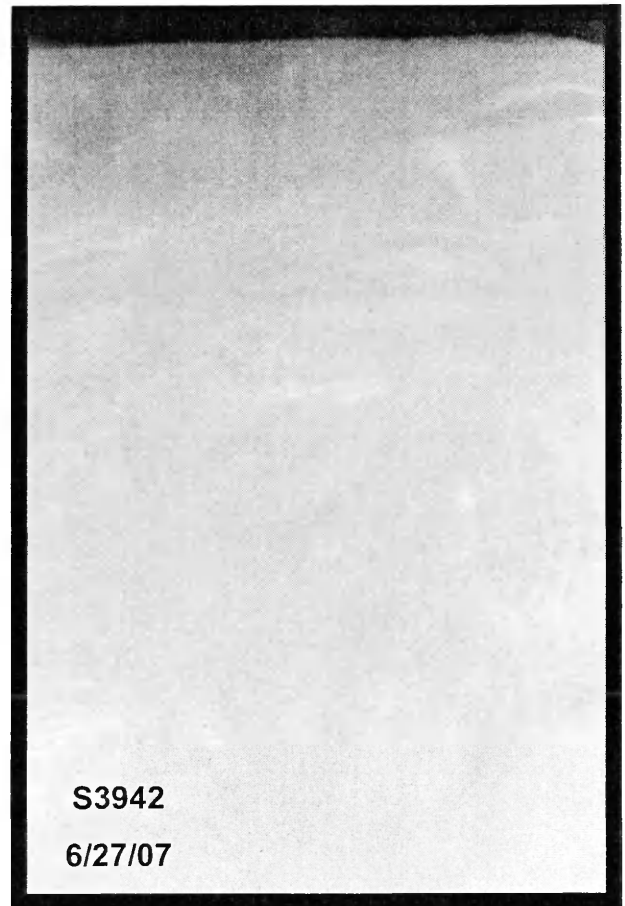
Literature Cited

Amos, C.L., Feeney, T., Sutherland, T.F., and Luternauer, J.L., 1997. The stability of
fine-grained sediments from the Fraser River delta. *Estuarine, Coastal, and Shelf
Science* 45, 507-524.

Andersen, T.J., 2001. Seasonal variation in erodibility of two temperate microtidal
mudflats. *Estuarine, Coastal, and Shelf Science* 53, 1-12.

Andersen, T.J., Lund-Hansen, L.C., Pejrup, M., Jensen, K.T., and Mouritsen. K.N., 2005.
Biologically induced differences in erodibility and aggregation of subtidal and
intertidal sediments: a possible cause for seasonal changes in sediment deposition.
Journal of Marine Systems 55, 123-138.

Bender, K., and W. R. Davis. 1984. The effect of feeding by *Yoldia limatula* on
bioturbation. *Ophelia* 23, 91–100.

Black, K.S., Tolhurst, T.J., Paterson, D.M., and Hagerthey, S.E., 2002. Working with
natural cohesive sediments. *Journal of Hydraulic Engineering* 128(1), 2-8.

Boon, J.D., 1996. Hydrodynamics of sediment suspensions in the littoral zone of the

    lower York River – phase II. Contract report to the Coastal Resources

    Management Program of the Virginia Department of Environmental Quality.

    Virginia Institute of Marine Science, 44 p.

Chapman, P.M. and Wang, F., 2001. Assessing sediment contamination in estuaries.

    Environmental Toxicology and Chemistry 20(1), 3-22.

de Brouwer, J.F.C., Bjelic, S., de Deckere, E.M.G.T., and Stal, L.J., 2000. Interplay

    between biology and sedimentology in a mudflat (Biezelingse Ham,

    Westerschelde, The Netherlands). *Continental Shelf Research* 20, 1159-1177.

de Brouwer, J.F.C., Wolfstein, K., Ruddy, G.K., Jones, T.E.R., and Stal, L.J., 2005.

    Biogenic stabilization of intertidal sediments: The importance of extracellular

    polymeric substances produced by benthic diatoms. *Microbial Ecology* 49, 501-

    512.

Dellapenna, T.M., Kuehl, S.A., and Schaffner, L.C., 1998. Sea-bed mixing and particle

    residence times in biologically and physically dominated estuarine systems: a

    comparison of Lower Chesapeake Bay and the York River subestuary. *Estuarine,*

    Coastal, and Shelf Science 46, 777-795.

216

Dellapenna, T.M., Kuehl, S.A., and Schaffner, L.C., 2003. Ephemeral deposition, seabed

    mixing, and fine-scale strata formation in the York River estuary, Chesapeake

    Bay. *Estuarine, Coastal, and Shelf Science* 58, 621-643.

Dennison, W.C., Orth, R.J., Moore, K.A., Stevenson, J.C., Carter, V., Kollar, S.,

    Bergstrom, P.W., and Batiuk, R.A., 1993. Assessing water quality with

    submersed aquatic vegetation: Habitat requirements as barometers of Chesapeake

    Bay health. Bioscience 43(2), 86-94.

Diaz, R.J. and Cutter, G.R., 2001. In situ measurement of organism–sediment

    interaction: rates of burrow formation/abandonment and sediment

    oxidation/reduction. In: J.Y. Aller, S.A. Woodin and R.C. Aller, Editors,

    Organism–Sediment Interactions, University of South Carolina Press, Columbia

    (2001), pp. 19–32.

Feuillet, J.-P., and Fleisher P., 1980. Estuarine circulation: Controlling factor of clay

    mineral distribution in James River estuary, Virginia. *Journal of Sedimentary*

    Petrology 50(1), 267-279.

Flemming, B.W., and Delafontaine, M.T., 2000. Mass physical properties of muddy

    intertidal sediments: some applications, misapplications, and non-applications.

    Continental Shelf Research 20, 1179-1197.

Friedrichs, C.T., Wright, L.D., Hepworth, D.A., and Kim, S.C., 2000. Bottom-boundary-

    layer processes associated with fine sediment accumulation in coastal seas and

    bays. *Continental Shelf Research* 20, 807-841.

Fugate, D.C., and Friedrichs, C.T., 2003. Controls on suspended aggregate size in

    partially mixed estuaries. *Estuarine, Coastal, and Shelf Science* 58, 389-404.

Gerino, M., Aller, R.C., Lee, C. Cochran, J.K., Aller, J.Y., Green, M.A., and Hirschberg,

    D., 1998. Comparison of different tracers and methods used to quantify

    bioturbation during a spring bloom: 234-Thorium, luminophores, and Chlorophyll

    a. *Estuarine, Coastal, and Shelf Science* 46, 531-547.

Gust, G., and Muller, V., 1997. Interfacial hydrodynamics and entrainment functions of

    currently used erosion devices. In: *Cohesive sediments*, Burt, Parker, and Watts

    (eds), Wallingford, U.K., 149-174.

Hall, M.O., Durako, M.J., Fourqurean, J.W., and Zieman, J.C., 1999. Decadal changes in seagrass distribution and abundance in Florida Bay. Estuaries 22(2B), 445-459.

Houwing, E.-J., 1999. Determination of the critical erosion threshold of cohesive sediments on intertidal mudflats along the Dutch Wadden Sea coast. *Estuarine, Coastal, and Shelf Science* 49, 545-555.

Jassby, A.D., Cloern, J.E., and Cole, B.E., 2002. Annual primary production: Patterns and mechanisms of change in a nutrient-rich tidal ecosystem. Limnology and Oceanography 47(3), 698-712.

Jepsen, R., Roberts, J., and Lick, W., 1997. Effects of bulk density on sediment erosion rates. *Water, Air, and Soil Pollution* 99, 21-31.

Jones, S.E., and Jago, C.F., 1993. In situ assessment of modification of sediment properties by burrowing invertebrates. *Marine Biology* 115, 133-142.

Kamphuis, J.W., and Hall, K.R., 1983. Cohesive material erosion by unidirectional current. *Journal of Hydraulic Engineering* 109(1), 49-61.

Kandiah, A., 1974. Fundamental aspects of surface erosion of cohesive soils. *Ph.D. thesis*, University of California, Davis, 261 p.

Kelly, W. E., and Gularte, R. C., 1981. Erosion resistance of cohesive soils. *Journal of the Hydraulics Division of ASCE* 107(10), 1211-1224.

Kniskern, T.A., and Kuehl, S.A., 2003. Spatial and temporal variability of seabed disturbance in the York River subestuary. *Estuarine, Coastal, and Shelf Science* 58, 37-55.

Koch, E.W., 2001. Beyond light: Physical, geological, and geochemical parameters as possible submersed aquatic vegetation habitat requirements. Estuaries 24(1), 1-17.

Lau, Y.L., 1994. Temperature effect on settling velocity and deposition of cohesive sediments. *Journal of Hydraulic Research* 32((1), 41-51.

Lin, J. and Kuo, A. Y., 2001. Secondary turbidity maximum in a partially mixed microtidal estuary. *Estuaries* 24, 707-720.

Lohrer, A.M., Thrush, S.F., Hewitt, J.E., Berkenbusch, K., Ahrens, M., and Cummins, V.J., 2004. Terrestrially derived sediment: response of marine macrobenthic communities to thin terrigenous deposits. *Marine Ecology Progress Series* 273, 121-138.

Lucas, C.H., Widdows, J., and Wall, L., 2003. Relating spatial and temporal variability in sediment chlorophyll *a* and carbohydrate distribution with erodibility of a tidal flat. *Estuaries* 26(4A), 885-893.

Maa, J.P.-Y., Kim, S.-C., 2002. A constant erosion rate model for fine sediment in the York River, Virginia. *Environmental Fluid Mechanics* 1, 345-360.

Mahatma, L., 2004. The spatial and temporal patterns of erodiblity of an intertidal flat in the East Frisian Wadden Sea, Germany. Ph. D thesis, University of Kiel, Germany, 129 p.

Mcneil, J., Taylor, C., and Lick, W., 1996. Measurements of erosion of undisturbed bottom sediments with depth. *Journal of Hydraulic Engineering* 122 (6), 316 - 324.

Murray, J.M.H., Meadows, A., and Meadows, P.S., 2002. Biogeomorphological implications of microscale interactions between sediment geotechnics and marine benthos: a review. *Geomorphology* 47, 15-30.

Nichols, M.M., S.C. Kim, and C.M. Brouwer, 1991. Sediment characterization of the Chesapeake Bay and its tributaries, Virginian Province. National estuarine inventory: supplement. NOAA Strategic Assessment Branch. 88 p.

Panagiotopoulos, I., Voulgaris, G., and Collins, M.B., 1997. The influence of clay on the threshold of movement of fine sandy beds. *Coastal Engineering* 32, 19-43.

Parchure, T.M., and Mehta, A.J., 1985. Erosion of soft cohesive sediment deposits. *Journal of Hydraulic Engineering* 111 (10), 1308-1326.

Paterson, D.M., Tolhurst, T.J., Kelly, J.A., Honeywell, C., de Deckere, E.M.G.T., Huet, V., Shayler, S.A., Black, K.S., de Brouwer, J., and Davidson, I., 2000. Variations in sediment properties, Skeffling mudflat, Humber Estuary, UK. *Continental Shelf Research* 20, 1373-1396.

Piedra-Cueva, I., and Mory, M., 2001. Erosion of a deposited layer of cohesive sediment. In: *Coastal and Estuarine Fine Sediment Transport Processes*, W. H. McAnally and A. J. Mehta, eds.Elsevier, Amsterdam, 41-51.

Reimers, C.E., 1982. Organic matter in anoxic sediments off central Peru: Relations of porosity, microbial decomposition, and deformation properties. *Marine Geology* 46, 175-197.

Riethmuller, R., Heineke, M., Kuhl, H., and Keuker-Rudiger, R., 2000. Chlorophyll *a* concentration as an index of sediment surface stabilization of microphytobenthos?. *Continental Shelf Research* 20, 1351-1372.

Roberts, J., Jepsen, R., Gotthard, D., and Lick, W., 1998. Effects of particle size and bulk density on erosion of quartz particles. *Journal of Hydraulic Engineering* 124(12), 1261-1268.

Romine, H.M., 2004. Documenting the suspended sediment and bottom sediment dynamics of a two estuarine turbidity maximum system using ^{7}Be and ^{234}Th. Masters Thesis, School of Marine Science, College of William and Mary, 100 p.

Rowden, A.A., Jago, C.F., and Jones, S.E., 1998. Influence of benthic macrofauna on the

geotechnical and geophysical properties of surficial sediment, North Sea.

Continental Shelf Research 18, 1347-1363.

Sanford, L.P., 2006. Uncertainties in sediment erodibility estimates due to lack of

standards for experimental protocols and data interpretation. *Integrated*

Environmental Assessment and Management 2(1), 29-34.

Sanford, L.P., 2008. Modelling a dynamically varying mixed sediment bed with erosion,

deposition, bioturbation, consolidation, and armoring. *Computers and*

Geosciences, in press.

Sanford, L.P., and Maa, J.P.-Y., 2001. A unified erosion formulation for fine sediments.

Marine Geology 179, 9-23.

Schaffner, L.C., Diaz, R.J., and Byrne, R.J., 1987a. Processes affecting recent estuarine

stratigraphy. In N. C. Kraus (ed.), Coastal Sediments '87, Proceedings of a

Specialty Conference on Advances in Understanding of Coastal Sediment

Processes. Vol. I. American Society of Civil Engineers, New York, p. 584-599.

Schaffner, L.C., Diaz, R.J., Olsen, C.R., and Larsen, I.L., 1987b. Faunal characteristics and sediment accumulation processes in the James River estuary, Virginia. *Estuarine, Coastal, and Shelf Science* 25, 211-226.

Schaffner, L.C., Hinchey, E.K., Dellapenna, T.M. , Friedrichs, C.T., Neubauer, M.E., Smith, M.E., and Kuehl, S.A., 2001. Physical energy regimes, sea-bed dynamics and organism-sediment interactions along an estuarine gradient. In: J.Y. Aller, S.A. Woodin and R.C. Aller (eds.), Organism-Sediment Interactions, University of South Carolina Press, Columbia, SC, p. 159-179.

Scully, M.E., and Friedrichs, C.T., 2003. The influence of asymmetries in overlying stratification on near-bed turbulence and sediment suspension in a partially mixed estuary. *Ocean Dynamics* 53, 208-219.

Shields, A. (1936). Anwendung der aehnlichkeitsmechanik und der turbulenzforschung auf die geschiebebewegung. Mitteilungen der Preussischen Versuschsanstalt fur Wasserbau und Schiffbau, 26, 5-24. [English title: Application of similarity principles and turbulence research to bed-load movement. Translation by Ott, W.P. and J.C. van Uchelen, Technical Report, California Institute of Technology, Hydrodynamics Lab, Publication 167].

Smith, D.J. and Underwood, G.J.C., 1998. Exopolymer production by intertidal epipelic diatoms. *Limnology and Oceanography* 43(7), 1578-1591.

Smith, D.J. and Underwood, G.J.C., 2000. The production of extracellular carbohydrates by estuarine benthic diatoms: The effects of growth phase and light and dark treatment. *Journal of Phycology* 36, 321-333.

Stevens, A.W., Wheatcroft, R.A., and Wiberg, P.L., 2007. Seabed Properties and sediment erodibility along the western Adriatic margin, Italy. *Continental Shelf Research* 27(3-4), 400-416.

Thrush, S.F., Hewitt, J.E., Norkko, A., Cummings, V.J., and Funnell, G.A., 2003. Macrobenthic recovery processes following catastrophic sedimentation on estuarine sandflats. *Ecological Applications* 13(5), 1433-1455.

Tolhurst, T.J., Black, K.S., Paterson, D.M., Mitchener, H.J., Termaat, G.R., and Shayler, S.A., 2000. A comparison and measurement standardization of four in situ devices for determining the erosion shear stress of intertidal sediments. *Continental Shelf Research* 20, 1397-1418.

Tolhurst, T.J., Defew, E.C., de Brouwere, J.F.C., Wolfstein, K., Stal, L.J., and Paterson, D.M., 2006. Small-scale temporal and spatial variability in the erosion threshold and properties of cohesive intertidal sediments. *Continental Shelf Research* 26, 351-362.

Tolhurst, T.J., Gust, G., and Paterson, D.M., 2002. The influence of extracellular polymeric substance (EPS) on cohesive sediment stability. In: *Fine Sediment Dynamics in the Marine Environment*, J.C. Winterwerp and C. Kranenburg (eds). Elsevier Science, Amsterdam, p. 409-425.

Torfs, H., Jiang, J., and Mehta, A. J., 2001. Assessment of erodibility of fine/coarse sediment mixtures. In: *Coastal and Estuarine Fine Sediment Transport Processes*, W. H. McAnally and A. J. Mehta, eds., Elsevier, Amsterdam, 109-123.

Underwood, G.J.C., Paterson, D.M., and Parkes, R.J., 1995. The measurement of microbial carbohydrate exopolymers from intertidal sediments. *Limnology and Oceanography* 40(7), 1243-1253.

Valette-Silver, N.J., Bricker, S.B., and Salomons, W., 1993. Historical trends in

    contamination of estuarine and coastal sediments: An introduction to the

    dedicated issue. Estuaries 16(3B), 575-576.

Vandever, J.P., 2007. Acoustic measurement and modeling of waves in estuarine and

    coastal environments. Masters Thesis, School of Marine Science, College of

    William and Mary, 176 p.

Wiberg, P.L., Drake, D.E., and Cacchione, D.A., 1994. Sediment resuspension and bed

    armoring during high bottom stress events on the northern California continental

    shelf: Measurements and predictions. *Continental Shelf Research 14, 1191-1219.*

Widdows, J., Blauw, A., Heip, C.H.R., Herman, P.M.J., Lucas, C.H., Middelburg, J.J.,

    Schmidt, S., Brinsley, M.D., Twisk, F., and Verbeek, H., 2004. Role of physical

    and biological processes in sediment dynamics of a tidal flat in Westerschelde

    Estuary, SW Netherlands. *Marine Ecology Progress Series* 274, 41-56.

Widdows, J. and Brinsley, M., 2002. Impact of biotic and abiotic processes on sediment

    dynamics and the consequences to the structure and functioning of the intertidal

    zone. Journal of Sea Research 48, 143-156.

Widdows, J., Brinsley, M.D., Bowley, N., and Barret, C., 1998. A benthic annular flume for *in situ* measurement of suspension feeding/biodeposition rates and erosion potential of intertidal cohesive sediments. *Estuarine, Coastal, and Shelf Science* 46, 27-38.

Widdows, J., Brown, S., Brinsley, M.D., Salkeld, P.N., and Elliot, M., 2000. Temporal changes in intertidal sediment erodability: influence of biological and climatic factors. *Continental Shelf Research* 20, 1275-1289.

Widdows, J., Friend, P.L., Bale, A.J., Brinsley, M.D., Pope, N.D., and Thompson, C.E.L., 2007. Inter-comparison between five devices for determining erodability of intertidal sediments. *Continental Shelf Research* 27, 1174-1189.

Williamson, H.J., and Ockenden, M.C., 1996. ISIS: An Instrument for measuring erosion Shear stress *In Situ*. *Estuarine, Coastal, and Shelf Science* 42, 1-18.

Wright, L.D., Schaffner, L.C., and Maa, J.P.-Y., 1997. Biological mediation of bottom boundary layer processes and sediment suspension in the lower Chesapeake Bay. *Marine Geology* 141, 27-50.

Vita

Patrick John Dickhudt

Born April 16, 1977 in Olivia, Minnesota. Graduated from Montevideo Senior High School in 1995. Earned a B.S. in Hydrogeology from University of Minnesota – Duluth in 2000. Entered M.S. program at College of William and Mary, School of Marine Science in 2004.